ADSORPTION MODELING OF COALBED GASES AND THE EFFECTS OF WATER ON THEIR ADSORPTION BEHAVIOR

By

SAYEED AHMED MOHAMMAD

Bachelor of Science in Chemical Engineering
Osmania University
Hyderabad, India
2003

Submitted to the Faculty of the
Graduate College of the
Oklahoma State University
in partial fulfillment of
the requirements for
the Degree of
DOCTOR OF PHILOSOPHY
May, 2009

ADSORPTION MODELING OF COALBED GASES

AND THE EFFECTS OF WATER ON THEIR

ADSORPTION BEHAVIOR

Dissertation Approved:

Dr. Khaled A. M. Gasem

Dissertation Adviser

Dr. Robert L. Robinson, Jr.

Dr. Jan Wagner

Dr. William D. Warde

Dr. A. Gordon Emslie

Dean of the Graduate College

ACKNOWLEDGMENTS

I would like to express my gratitude to my adviser, Dr. Khaled Gasem, for giving me the opportunity to work with him on this project. I greatly appreciate his invaluable guidance, support and encouragement for conducting quality research, and for teaching me to be a "truth seeker" as a researcher. Through out my five years of work with him, I have learnt some great lessons in research and life.

I would like to thank my co-adviser, Dr. Robert Robinson, Jr., for his invaluable insight, supervision and thoughtful reviews of this work. I am also grateful to my advisory committee members, Dr. Jan Wagner and Dr. Bill Warde, for their valuable input and helpful suggestions. It has been a great honor for me to have worked with these distinguished members of the OSU Graduate Faculty.

I also express my sincere appreciation and gratitude for my past colleagues in this project, Dr. James Fitzgerald and Ms. Jing Chen, for their support and help with this project. I also thank the many friends and acquaintances I made over the years, whose friendship I truly appreciate.

I also acknowledge the support of the U.S. Department of Energy to our research group that made this project possible.

I thank many of the friends at Stillwater Islamic Center for their good wishes. I would like to thank Dr. Saleh Ashaghathra, Dr. Ahmed Abo Basha, Dr. Mumtaz Hussain and Dr. Qamar Arsalan for their valuable friendship and encouragement.

Finally, I am grateful to my parents, sister, brother and his family for their sacrifices, patience and prayers through out my graduate studies. Their support, understanding and encouragement were most crucial in my continued success away from home.

Sayeed Mohammad
May 8, 2009

TABLE OF CONTENTS

Chapter Page

LIST OF TABLES

Table Page

Table Page

LIST OF FIGURES

Figure Page

Figure Page

Figure Page

Figure Page

Figure Page

Figure Page

CHAPTER 1

INTRODUCTION

1.1 Coalbed Methane and CO_2 Sequestration

Fossil fuels have been the main resource for our increasing demand for energy. They have also been the source of the steady rise in the atmospheric concentration of CO_2, which is hypothesized to be a significant contributor to global warming. Efforts to address climate change issues have culminated in the 1991 Kyoto Protocol, which mandates the signatory nations to reduce their carbon emissions and/or adopt environment-friendly methods of energy usage by 2012. Several methods have been proposed to reduce carbon/CO_2 emissions. These include "geological sequestration" of CO_2, which involves capture and the subsequent storage of CO_2 in saline aquifers, oil and gas shales, depleted oil reservoirs, or deep unmineable coalbeds. The latter is considered particularly attractive because of the potential for sequestering large amounts of CO_2, with the important concomitant recovery of coalbed methane (CBM) gas. The recovery of coalbed methane is expected to (at least partially) offset the costs of CO_2 sequestration and to provide an increased supply of our "cleanest" fossil fuel, natural gas.

Further, the demand for natural gas is expected to rise steeply in the coming years. The Energy Information Administration (EIA) estimated that natural gas demand in the U.S. could be 24.4 trillion cubic feet by the year 2030.[1] This accounts for an annual increase of 1.2% over the next twenty years. Coalbed methane has become

an important resource of natural gas since coalbeds contain an estimated 14% of U.S. natural gas reserves.[2] The production of natural gas from coalbeds increased from 6% in 1997[3] to 10% in 2006.[4] Therefore, this unconventional resource of natural gas has steadily gained in its economic importance. Moreover, the U.S. Department of Energy (DOE) has initiated research and development programs aimed at geologic CO_2 sequestration.[5] In pursuit of this goal, researchers at Oklahoma State University (OSU) have conducted adsorption measurements[6, 7] and modeling studies.[7-12]

In coalbeds, natural gas (methane) resides within the microporous coal structure in an "adsorbed" state. In adsorption, the van der Waals-type gas-coal interactions at the coal-gas interface give rise to increased concentrations of the gas molecules near the coal surface, where the densities become comparable to those of liquids. Thus, coalbeds can actually hold more gas than a conventional gas reservoir of comparable volume. Since most of the coalbed gas is in the adsorbed state, simulations of coalbed methane (CBM) recovery and the design of optimal CO_2 sequestration processes require a suitable model to describe the adsorption phenomena. Specifically, an adsorption model is needed to predict the gas-in-place values as a function of coalbed reservoir temperature and pressure.

1.2 Adsorption Models

As mentioned above, simulations of enhanced coalbed gas recovery require accurate adsorption models capable of *a priori* predictions of gas adsorption behavior in the presence of water. Some of the desired characteristics of a CBM adsorption model include:

- Representing precisely high-pressure pure-gas adsorption

- Facilitating generalized predictions of pure-gas adsorption based on accessible adsorbent and adsorbate properties
- Predicting mixed-gas adsorption based on pure-gas data
- Accounting for the presence of moisture in the coal, since water is present in essentially all coalbeds

Different models, ranging from very simple to complex, can be used to describe the adsorption behavior of CBM gases. These include the Langmuir model[13], Brunauer-Emmett-Teller (BET) model[14], Ideal Adsorbed Solution (IAS) theory[15], two-dimensional equations of state[16-18] (2-D EOS), the Ono-Kondo lattice model[19-21] and the simplified local-density model.[22-27] Although most of these models have good correlative capabilities for existing experimental data, only a few of them appear to be capable of accurate *predictions* of supercritical, high-pressure adsorption systems encountered in CBM-related work. Further, an adsorption model which can describe this effect at water levels that are below, at, and above the equilibrium moisture level will be crucial for reservoir modeling purposes. The CBM industry would benefit greatly from adsorption models which contain rigorous accounting for the effects of water on gas adsorption. Our analysis indicates that the simplified local-density model is amenable to the modeling demands mentioned above.

1.3 Effect of Water on Coalbed Gas Adsorption Behavior

Most coalbeds contain significant amounts of water. The presence of water in a gas-solid adsorption system demands special attention, because water can significantly affect gas adsorption capacity by blocking the porous adsorbent structure and limiting the accessibility of an adsorbing gas like methane.[28] Measurements of adsorption isotherms

on wet coals have also revealed marked effects of water on gas adsorption capacity. Joubert et al.[29] reported adsorption data which showed that moisture can reduce methane adsorption by as much as 40% on Pittsburgh coal and 15% on Pocahontas coal. Clarkson and Bustin[30] showed that 2% moisture can cause 20% reduction of both methane and CO_2 adsorption capacity on a wet coal when compared to the adsorption on the dry coal. Similarly, Levy et al.[31] observed that 4% moisture can reduce the methane adsorption by as much as 60% from that of the dry coal. Our own measurements on wet Illinois coal have shown that 9% moisture can cause 50% reduction of CO_2 adsorption at 3 MPa.[8]

The above results demonstrate the significant effect of moisture on gas adsorption behavior. Thus, proper accounting for moisture effects is critical in experimental data reduction, interpretation and modeling. Current experimental data reduction techniques do not account for the presence and effect of moisture in all three equilibrium phases (gas, aqueous and adsorbed). This inadequacy in data reduction methods may result in significant errors in the estimated gas adsorption capacity, adsorbed phase density and (in gas mixtures) the partitioning of constituents among the equilibrium phases.

The adsorption behavior of water is fundamentally different from other gases like methane.[32] For water, the fluid-fluid interactions are stronger than the fluid-solid interactions, and hydrogen bonding plays a significant role in water adsorption. Thus, the simultaneous, competitive adsorption of water and coalbed gases presents an equilibrium problem which requires accurate description of the different molecular interactions involved in the process.

Accordingly, the present research places a particular emphasis on delineating the fluid-fluid and fluid-solid molecular interactions of water, coalbed gases and

carbonaceous adsorbents, and proposing rigorous accounting procedures for the effects of moisture on the adsorption behavior of coalbed gases and their mixtures at typical reservoir temperatures and pressures. Further, the research included the development of a coal-structure-based generalized adsorption model for facilitating simulations of CBM recovery and CO_2 sequestration. Therefore, the goal of this research addresses two important aspects of CBM adsorption research:

A. Delineate the molecular interactions of adsorbed water with coals and other coalbed gases, and propose rigorous accounting procedures for the effects of water on gas adsorption behavior and
B. Develop a coal-structure-based, predictive generalized adsorption model for CBM simulation purposes.

As such, two tracks of CBM adsorption research were undertaken in parallel. The first addressed the need to incorporate more accurate physics in an adsorption model, whereas the second addressed the need to develop a generalized adsorption model that would be useful in coalbed reservoir simulations. Although the generalized model developed in this work (B) is based on the currently accepted, traditional modeling approach (where adsorbed water is treated as a "pacifier" of the matrix), the parallel development of a rigorous modeling approach for adsorbed water (A) has laid the foundation for further advancement of this method in future works on coalbed gas adsorption.

1.4 Objectives

The basic premise of this research is that *upon modification, the SLD-PR model can describe accurately the equilibrium adsorption of water and coalbed gases on coals*

and account for the effect of water on coalbed gas adsorption. As such, a major focus of this study was modifying the simplified local-density/Peng-Robinson (SLD-PR) model to meet the modeling demands of wet adsorbents. In particular, the SLD-PR model was further developed to (a) include the polar interactions of water with the carbon surface, and (b) account more realistically for the effect of water adsorption by treating water as a separate adsorbed component in equilibrium with the bulk gas phase.

Moreover, for engineering practice purposes, the SLD-PR model was generalized (using the accepted, traditional modeling approach) to render the model suitable for use in simulations of coalbed methane recovery and CO_2 sequestration.

To accomplish the goal discussed above, the following objectives were undertaken:

1. Acquire accurate experimental data for adsorption of methane, carbon dioxide, and nitrogen on wet coals and on activated carbon at reservoir temperatures and pressures.
2. Review existing knowledge regarding pure water adsorption behavior on coals and activated carbons.
3. Use the SLD-PR model to represent precisely the water adsorption capacity on activated carbons and coals.
4. Conduct a Gibbs-energy (or phase-check) analysis for adsorption of CO_2-water mixtures on coals.
5. Generalize the SLD-PR model by correlating the model parameters in terms of assessable coal properties.

In earlier studies[6, 10, 33], the OSU Thermodynamics Group measured pure and mixed-gas adsorption isotherms on wet coals. However, the moisture content of the coals in those measurements was well above the equilibrium moisture content (EMC) of the coals. At moisture contents above the EMC, the additional water does not significantly affect the gas adsorption capacity.[29] Therefore, a need exists for measurements to elucidate the adsorption behavior of coalbed gases at different levels of moisture-above and below the EMC (Objective 1).

Accounting properly for water adsorption behavior on activated carbons and coals and its modeling presents an interesting and challenging problem, due to the unique structure of the water molecule. The adsorption behavior of water on carbons is fundamentally different from that of simple, non-polar fluids like nitrogen, methane and organic vapors. The difference arises mainly because the *fluid-fluid* interactions for water are much more strongly attractive than the *fluid-solid* interactions, and because water forms hydrogen bonds with the oxygenated groups on the surface of the carbon matrix.[32] This is in direct contrast to the adsorption behavior of non-polar molecules. Therefore, a detailed review of water adsorption behavior on activated carbons and coals (Objective 2) was essential to an unambiguous understanding of pure water adsorption and, ultimately, of coalbed gas *mixture* adsorption in the presence of water.

The pre-requisite for the prediction of the water-coalbed gas mixture adsorption is the accurate modeling of the water adsorption capacity. The SLD model was modified to account for interactions of water with the coal surface; and the effect of this new parameterization of the SLD model was investigated by constructing different case studies (Objective 3).

The accurate modeling of water-coalbed gas mixture adsorption requires treating water as a *separate adsorbed component*. Water at reservoir temperatures is a sub-critical component, while the coalbed gases are typically at supercritical conditions. The presence of the sub-critical water may result in the formation of an additional (liquid) phase. The definitive method to determine the number of possible phases present at equilibrium is to conduct a Gibbs free energy or phase-check analysis. Therefore, a phase-check analysis was performed to investigate the phase behavior of this system (Objective 4).

As mentioned in Section 1.2, simulations of coalbed methane recovery require an adsorption model to predict, *a priori*, the amounts adsorbed of coalbed gases. Frequently, this is necessary due to an absence of experimental data on the system of interest. Therefore, the SLD-PR model was generalized in terms of coal characterization information (Objective 5). This facilitates *a priori* predictions of adsorbed amounts of gas and renders the model capable of use in simulations of coalbed methane recovery.

Further, in developing the generalized model, the currently accepted approach for modeling wet adsorbents was adopted. The extension of the new modeling approach for wet adsorbents (developed in Objective 4) to the generalized model is not feasible at this stage for a variety of reasons, which include the unavailability of sufficient adsorption and vapor-liquid equilibrium data for the systems of interest.

1.5 Organization

This dissertation is organized as follows. Chapter 1 gives a brief introduction of coalbed methane and outlines the hypothesis of this research, the objectives undertaken and the ultimate goal of this study. Chapter 2 presents details of the experimental

methods and procedures used in this study and discusses the experimental data acquired in this project. Chapter 3 reviews a number of CBM adsorption models used in the literature and at OSU for modeling of CBM systems. Chapter 4 presents an interpretive review of pure water adsorption on activated carbons and coals. The SLD model for pure- and mixed-gas adsorption is discussed in Chapter 5. Also included in Chapter 5 are the SLD modeling results of CO_2-water *mixture* adsorption and the phase-check analysis for these systems. A coal-structure-based generalized adsorption model is presented in Chapter 6. Finally, Chapter 7 contains the important conclusions and recommendations of this study.

This study was part of a continuing research project dealing with high-pressure gas-adsorption modeling for CBM systems.[8, 12] Therefore, the experimental data presented in Chapter 2 and discussion of the theoretical framework of SLD-PR model presented in Chapter 5 represent a collective effort involving the author, Jing Chen[27] and James Fitzgerald.[25] Further, the OSU CBM adsorption database utilized for the generalized model development was gathered over a period of fifteen years by various authors.[6, 8, 12]

CHAPTER 2

EXPERIMENTAL METHODS, PROCEDURES AND RESULTS

In this chapter, the experimental methods and procedures used to measure adsorption isotherms are discussed. Since this study is a continuation of previous works at OSU, some aspects of the following discussion of experimental methods are similar to previous descriptions.[18, 20, 25, 34] Further, an outline of the various methods that can be used to measure gas adsorption equilibria are given elsewhere[18] and, therefore, they are not discussed here.

In particular, the chapter contains a discussion of the following aspects of this work:

- Adsorption isotherms of pure CO_2 on five wet Argonne coals measured at a temperature of 328.2 K and pressures to 13.8 MPa
- Adsorption isotherms of pure methane, nitrogen and CO_2 on wet and dry activated carbon measured at a temperature of 328.2 K and pressures to 13.8 MPa. In addition, the desorption measurements of CO_2 on dry activated carbon are also discussed.
- An introduction to the OSU adsorption database for coalbed methane gases.[12]
- A Monte Carlo analysis/confirmation of the analytical error analysis technique used to estimate the expected experimental uncertainties of the acquired data.

The following material in Sections 2.1 to 2.10 (Part A) has been reproduced with permission from [Mohammad, S. A.; Chen, J. S.; Fitzgerald, J. E.; Robinson, R. L., Jr.; Gasem, K. A. M., Adsorption of Pure Carbon Dioxide on Wet Argonne Coals at 328.2 K and Pressures up to 13.8 MPa. *Energy & Fuels* **2009,** 23, (2), 1107-1117] Copyright [2008] American Chemical Society.

2.1 Adsorption Isotherm Measurements

The experimental method used in the OSU adsorption laboratory is based on a mass balance principle, which employs precise measurements of pressure, volume and temperature. The experimental apparatus, shown schematically in Figure 2.1, has been used successfully in previous measurements.[6-8] Brief descriptions of the experimental apparatus and procedures are provided below:

The entire apparatus is maintained in a constant temperature air bath. The equilibrium cell (Figure 2.1) is filled with the adsorbent under study, and the cell is placed under vacuum prior to gas injection. The void (gas) volume, V_{void}, in the equilibrium cell is then determined by injecting a known quantity of helium from a calibrated injection pump (Ruska). Since the adsorption of helium is insignificant at the conditions of this study, the void volume can be determined easily from measured values of the temperature, pressure and amount of helium injected into the cell.

The mass balance equation for the measurement of void volume is given as:

$$V_{void} = \frac{\left(\frac{P\Delta V}{ZT}\right)_{pump}}{\left(\frac{P_2}{Z_2 T} - \frac{P_1}{Z_1 T}\right)_{cell}} \tag{2.1}$$

where ΔV is the volume of helium gas injected from the pump, Z is the compressibility factor of helium, T is the temperature, P is the pressure, subscripts "cell" and "pump" refer to conditions in the cell and pump sections of the apparatus, respectively, and "1" and "2" refer to conditions in the cell before and after an injection of gas from the pump, respectively. The helium void volume measurements were performed at the same temperature as the gas adsorption isotherms (328.2 K in this study) and over a range of pressures from atmospheric to about 13.8 MPa (2000 psia) in intervals of 1.4 MPa (200 psia).

The several sequential injections of helium into the cell at different pressures showed consistency in the calculated void volume. Generally, the void volume calculated from sequential injections varied less than 0.3 cm^3 from the average value of approximately 85 cm^3. This helium void volume includes all the volume of the cell section exclusive of the adsorbent volume that is impenetrable to helium gas. The constancy of the calculated void volume from the incremental injections over a range of pressures confirmed the validity of our assumption that adsorption of helium is negligible at the conditions of the measurements and that the adsorbent volume impenetrable to helium remained constant.

The Gibbs adsorption (also known as the excess adsorption) can be calculated directly from experimentally measured quantities. For pure-gas adsorption isotherm measurements, a known quantity, n_{inj}, of gas (e.g., CO_2) is injected from the pump section into the cell section. Some of the injected gas will be adsorbed, and the remainder, n_{unads}^{Gibbs}, will exist in the equilibrium bulk (gas) phase in the cell.

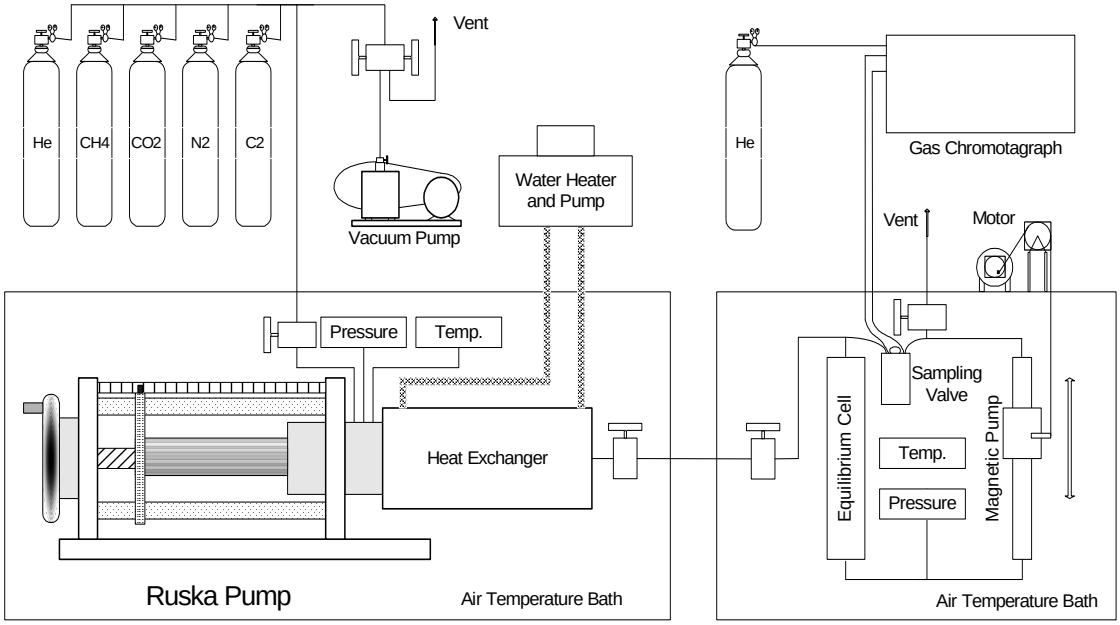

Figure 2.1 Schematic Diagram of the Experimental Apparatus

The mass balance used to calculate the Gibbsian amount adsorbed, n_{ads}^{Gibbs}, is

$$n_{ads}^{Gibbs} = n_{inj} - n_{unads}^{Gibbs} \tag{2.2}$$

where n_{unads}^{Gibbs} is the Gibbsian amount unadsorbed at given pressure and temperature.

The amount injected can be determined from pressure, temperature and volume measurements of the pump section:

$$n_{inj} = \left(\frac{P\Delta V}{ZRT} \right)_{pump} \tag{2.3}$$

The amount of unadsorbed gas (Gibbsian amount unadsorbed) is calculated from conditions at equilibrium in the cell:

$$n_{unads}^{Gibbs} = \left(\frac{PV_{Void}}{ZRT} \right)_{cell} \tag{2.4}$$

where the pressure P is measured after equilibrium is reached in the cell (usually within 6 to 12 hours, depending on the adsorption capacity of the adsorbent), which occurs when

no further change in pressure is observed. In Equations (2.3) and (2.4), Z is the compressibility factor of the gas at the applicable conditions of temperature and pressure.

The above steps are repeated at sequentially higher pressures to yield a complete adsorption isotherm. The amount adsorbed is usually reported as an intensive quantity (mmol adsorbed / g adsorbent, or mmol/g) by dividing n_{ads}^{Gibbs} by the mass of adsorbent in the cell. Equations (2.2)-(2.4) reveal that the amount adsorbed can be calculated in a straightforward manner from the experimental measurements of pressures, temperatures and volumes, coupled with independent knowledge of the gas compressibility factors, Z, from an accurate equation of state.

2.2 Gas Compressibility Factors

As evident from the above discussion, accurate compressibility factors are required for pure methane, nitrogen and CO_2 for proper adsorption data analysis. These compressibility factors were calculated from highly accurate equations of state.[35-37] Further, for void volume determination, the helium compressibility factor was calculated with an expression based on experimental data from the National Bureau of Standards Technical Note 631 for helium.[38]

2.3 Materials

The pure gases used in this work were obtained from Airgas-Pennsylvania with reported purities of about 99.99% and were used as received. The Argonne coal samples were obtained from the Argonne National Laboratory, Argonne, Illinois in ampoules containing 5 grams of 100-mesh material of each coal. The compositional analyses of Argonne coals are presented in Table 2.1. The Illinois #6 coal is a high-volatile bituminous coal from the Illinois #6 or Herrin seam. The Wyodak coal is a sub-

bituminous coal from the Wyodak-Anderson seam. The Upper Freeport coal is a medium-volatile bituminous coal, Pocahontas coal is a low-volatile bituminous coal and Beulah Zap coal is lignite.[39]

The activated carbon used was Filtrasorb 400, 12x40 mesh from Calgon Carbon Company. The compositional analyses of this activated carbon are also presented in Table 2.1. The composition of activated carbons is typically less complex than coals and provides a useful reference material prior to adsorption studies on coals. As evident from Table 2.1, the activated carbon has higher carbon content and significantly less volatile matter than medium-rank coals, which facilitates the modeling of the fluid-solid interactions in an adsorption process. The nitrogen BET surface area at 77 K of this carbon was reported to be 850 m^2/g.[40]

Table 2.1 Compositional Analyses of Adsorbents Used in this Study

Analysis*	**Beulah Zap**	**Wyodak**	**Illinois #6**	**Upper Freeport**	**Pocahontas**	**Activated Carbon**
Ultimate						
Carbon %	72.9	75.0	77.7	85.5	91.1	88.65
Hydrogen %	4.83	5.35	5.00	4.70	4.44	0.74
Oxygen %	20.3	18.0	13.5	7.5	2.5	3.01
Nitrogen	1.15	1.12	1.37	1.55	1.33	0.40
Sulfur %	0.70	0.47	2.38	0.74	0.50	0.73
Ash %	9.7	8.8	15.5	13.2	4.8	6.46
Proximate						
Moisture %	32.2	28.1	8.0	1.1	0.7	-
Vol. Matter %	30.5	32.2	36.9	27. 1	18.5	3.68
Fixed Carbon %	30.7	33.0	40.9	58.7	76.1	89.86
Ash %	6.6	6.3	14.3	13.0	4.7	-

*Analysis of coals provided by Argonne National Laboratory
*Analysis of activated carbon provided by Huffman Laboratories, Inc., Golden, Colorado

2.4 Error Analysis

Frequent instrument calibrations were performed during the course of the experiments. Usually, the calibrations were performed before the adsorption experiments on a new adsorbent sample. The thermocouples and resistance thermometers (RTDs) were calibrated against a Minco platinum reference RTD. Super TJE pressure transducers (range: 0 – 13.8 MPa) were calibrated using helium as the working fluid against a Ruska deadweight tester with a calibration traceable to the National Institute of Standards and Technology. Detailed information on calibration procedure is available elsewhere.[34] The uncertainties in the experimentally measured quantities after calibrations were estimated as follows: temperature, 0.1 K; pressure, 6.9 kPa (1 psia); and injected gas volume, 0.02 cm^3.

A detailed error analysis was performed to estimate the uncertainty associated with each experimental data point by propagating the errors from the primary measurements of pressure, temperature and volume. The detailed error analysis expressions are given elsewhere.[12, 20]

2.5 Equilibrium Moisture of Coals and Activated Carbon

Moisture equilibration of porous adsorbents such as coals is usually carried out using the standard ASTM D1412 method.[41] This method consists of equilibrating the adsorbent samples at 30ºC (303.2 K) in a vacuum desiccator over a saturated solution of K_2SO_4 to maintain the relative humidity at 96-97%. In the standard test method, the desiccator is used to equilibrate a previously "wetted" sample such that only the equilibrium moisture remains in the coal. However, the use of vacuum in a desiccator can often result in condensation problems when the pressure is restored, thus negating the

experiment.[29, 42] Therefore, we used a modified method where the samples were equilibrated under an inert nitrogen atmosphere. The moisture content of the equilibrated sample was then determined by drying a part of the sample under vacuum at a temperature of about 313.2 K for 48-72 hours. The weight of the sample was monitored, and the weight loss after 72 hours was taken as the moisture loss. The expected uncertainty in the measured moisture content is estimated to be about 0.1 wt. %.

The Illinois #6 coal samples were equilibrated using the above method by placing them in a nitrogen atmosphere at 95-100% relativity humidity in a Hot-pack Model 434300 temperature-humidity chamber. This resulted in a gain of only 1.2% moisture over the equilibrium value reported in the literature.[39] Therefore, for the other four Argonne coals, namely, Beulah Zap, Pocahontas, Upper Freeport and Wyodak coals, the as-received coal samples were placed directly in the equilibrium cell under inert atmosphere. This was done under the reasonable assumption that further moistening of the coal in the temperature-humidity chamber would not greatly change the coal moisture content from its as-received moisture. Moreover, the direct use of as-received samples minimizes possible oxidation of the samples that can affect the integrity of the coal sample. Great care has been taken by the Argonne National laboratory to maintain the coal samples at their in-seam conditions.[39] Since the objective of our study was to simulate the conditions of a coalbed reservoir while measuring adsorption isotherms (in terms of pressure, temperature and moisture content), measuring the isotherms at their as-received or in-seam moisture values was considered greatly beneficial. These isotherms can be considered to be measured near or at the equilibrium moisture content of the coals.

In the present context, the term “wet” coal is used to signify saturation of coal with adsorbed moisture.

For adsorption measurements on the dry Argonne coals, the coal samples were dried under vacuum in an equilibrium cell at 353 K for 36 hours following the National Energy Technology Laboratory (NETL) drying protocol before being used in the adsorption measurements. The adsorption data on dry coals were measured in an earlier work.[21]

The activated carbon was equilibrated as explained in the procedure above. Further, the raw activated carbon sample was first washed with deionized water to remove any impurities present in the carbon. This wetted sample was air dried for several days (to remove excess water) and then used for moisture equilibration as discussed above.

For adsorption measurements on the dry activated carbon, drying of the sample was carried out under vacuum at about 313.2 K for 48-72 hours. The lower drying temperature was used to avoid the loss of any volatile organics from the carbon surface and/or possible structural changes of the carbon sample.

2.6 Gas Solubility in Water

In previous studies at OSU on wet adsorbents[6, 8], we included a term in Equation (2.2) to account for the amount of gas, n_{sol}, dissolved in the water.

$$n_{ads}^{Gibbs} = n_{inj} - n_{unads}^{Gibbs} - n_{sol} \tag{2.5}$$

To calculate the amount of gas soluble in water as a function of pressure, an empirical equation obtained from Amoco Corporation was used for temperatures at 318.2 K or 319.3 K.

$$x_{gas} = \frac{P}{a + bP + cP^2} \tag{2.6}$$

Table 2.2 lists the parameter values for each gas. Since the solubilities of methane and nitrogen in water are small; the same equation and parameter values were used at other temperatures (e.g., 328.2 K in this study).

Table 2.2 Parameters for Gas Solubility in Water at 318.2 K or 319.3 K

Constant	Units of Constant	Methane	Nitrogen	CO_2
a	MPa	5302.07	10204.24	274.69
b	---	150.4	127.3	9.452
c	1/MPa	-0.78	-0.09	1.21

In comparison to nitrogen and methane, the solubility of CO_2 is significant at temperatures near 318.2 K. To calculate the gas dissolved in water for use in Equation (2.5), literature data[43-45] were used to construct an empirical relationship for CO_2-water solubility at temperatures from 313.2 K to 348.2 K.[8] In the 0-15 MPa range, the empirical function represents their data with an average absolute deviation of 1.5%. Thus, the mole fraction of CO_2 present in water at temperature T (in K) and pressure P (in MPa) is given as:

$$x_{CO2} = \frac{P}{a + (b_1 + b_0 T)P + (c_1 + c_0 T)P^2} \tag{2.7}$$

Table 2.3 lists the parameter values for this correlation. The amount of CO_2 dissolved in water can be given as

$$n_{sol} = \frac{x_{co_2} n_{water}}{(1 - x_{co_2})} \tag{2.8}$$

The denominator in Equation (2.8) is close to unity and therefore, the amount of gas dissolved in water was taken (approximately) as the product of mole fraction of CO_2 and

the amount of water in moles in the system. Further, the amount of CO_2 dissolved in water per unit mass of coal is expressed as:

$$n_{sol} = \frac{x_{co_2} n_{water}}{m_{coal}} \tag{2.9}$$

where n_{water} is the amount of water in moles and m_{coal} is the mass of coal in the system. The solubility of CO_2 in water calculated with Equation (2.9) is a monotonic increasing function of pressure at a given temperature. Thus, the maximum solubility of CO_2 in water was observed at 13.8 MPa and was about 2 mole percent.

Table 2.3 Parameters for CO_2 Solubility in Water at Multiple Temperatures

Constant	Value	Units of Constant
a	272.21	MPa
b_1	-332.637	---
b_0	1.06683	1/K
c_1	19.18	1/MPa
c_0	-0.05609	1/(MPa K)

As evident from the above discussion (Equation 2.5), accounting for the solubility of gas in water-rich adsorbed phase lowers the calculated Gibbs adsorption values. In the above discussion, we have assumed that all the water present in the system is adsorbed and, therefore, the amount of gas dissolved in water was estimated based on all the water present in the system. In addition, this means that we have assumed that the bulk gas phase was free from water (i.e., that $y_{H2O} = 0$, where y is the gas phase mole fraction).

2.7 Adsorption Measurements on Wet Coals and Activated Carbon

For the adsorption isotherm measurements on wet Argonne coals and wet activated carbon, care was taken to prevent moisture loss during the experiments. The coal samples were handled in a chamber filled with nitrogen. Since the evacuation step during the void volume measurement and at the beginning of the isotherm can result in

moisture loss, the system pressure was not reduced below 21 kPa at 328.2 K. This is slightly above the vapor pressure of water at this temperature, and this minimizes any potential water being removed from the coal or carbon surface. Further, before the start of the gas adsorption experiment, a small amount of the same adsorbing gas (methane, nitrogen or CO_2) was injected into the cell until the pressure was 0.35 MPa to flush any remaining helium gas out. The adsorbing gas was then evacuated until the pressure was again about 21 kPa, and the flushing procedure was performed once more.

To test for any moisture loss during the experiment on wet coals, two additional checks were performed. First, the equilibrium cell/coal sample was weighed before and after the adsorption isotherm. There was no significant mass loss observed from the equilibrium cell at the end of the isotherm. Second, the helium void volume was measured before and after the adsorption isotherm. The helium void volumes measured were within the experimental uncertainty of our void volume measurements (about 0.3%). The constancy in the calculated void volume further indicated that there was no significant moisture loss during the experiment.

Given the size of our volumetric apparatus, any miniscule amount of water leaving the coal surface would introduce an uncertainty in the isotherm measurement, which is well within the reported experimental uncertainty of the isotherm as obtained by multivariate error propagation. These uncertainty estimates for each data point of each isotherm are included with Gibbs adsorption data.

2.8 Coal Swelling

Another aspect of supercritical gas adsorption on coals that deserves consideration is the potential swelling of coal caused by adsorbates such as CO_2. Some investigators

believe that adsorption of CO_2 can significantly alter the porous coal structure and these changes, if left unaccounted for, can result in large errors in the modeling of supercritical CO_2 adsorption on coals. In fact, several researchers have attempted to model the swelling of coal by incorporating volumetric corrections to the adsorption isotherm equations. Ozdemir et al.[46] and Dutta et al.[47] used different adsorption models to study the volumetric effects of CO_2 adsorption on coals. Romanov et al.[48] have also attempted to interpret the volumetric changes in coals under CO_2 pressure. Pan and Connell[49], balancing the change in surface energy due to adsorption to the change in elastic energy of the coal matrix, developed a theoretical model to describe adsorption-induced coal swelling.

Recently, Day et al.[50] measured swelling on coals and corrected their adsorption measurements to account for volumetric changes to the sample. These corrections involved adjusting the void volume to account for an increased volume of coal sample. We have measured helium void volume before and after each adsorption isotherm experiment. The constancy of the calculated void volume within its experimental uncertainty of 0.3% indicated that there was no irreversible change to the volume of the sample. This result is also supported by the findings of Day et al.[50], who found the coal swelling to be entirely reversible. Although they applied a correction to the isotherm, we have used a constant void volume in our data reduction procedures. Thus, the adsorption data reported in this study are under the assumption that there is no appreciable swelling of the coal.

2.9 Gibbs and Absolute Adsorption

Adsorption data are typically reported either in terms of Gibbs or absolute adsorption. Gibbs adsorption is calculated directly from experimentally-measured quantities and this accounts for the fact that there is additional material present near the adsorbent surface due to adsorption phenomenon. This additional material is *in excess* of that which would be present in the same (void) volume if there was no adsorption. This excess material is usually referred to as the Gibbs or excess adsorption. In contrast, the calculation of absolute adsorption requires a value for the adsorbed phase density, ρ_{ads}, which is not readily accessible by experimental measurement.

The exact mathematical expressions that highlight the physical interpretation of Gibbs adsorption and the approximate nature of calculated absolute adsorption have been presented elsewhere.[7] The relationship between the two quantities is given as:

$$n_{ads}^{Abs} = n_{ads}^{Gibbs}\left(\frac{\rho_{ads}}{\rho_{ads} - \rho_{gas}}\right) \tag{2.10}$$

where n_{ads}^{Abs} and n_{ads}^{Gibbs} are the absolute and Gibbs adsorption, respectively, and ρ_{gas} and ρ_{ads} are the gas phase and the adsorbed phase densities, respectively. To calculate absolute adsorption from Equation (2.10), estimates of ρ_{ads} are usually employed. Commonly used approximations are the liquid density at the normal boiling point, as was done by Arri and Yee[51], or the reciprocal of the Van der Waals (VDW) co-volume.[8]

2.10 Experimental Results

A. Adsorption of CO_2 on Wet Argonne Coals

The experimental data from the present work for the CO_2 adsorption on Beulah-Zap, Illinois #6, Pocahontas #3, Upper Freeport and Wyodak coals are listed in Tables

2.4-2.8, respectively. All adsorption amounts are reported on a dry-mass basis. Tables 2.4-2.8 include the pressures (MPa), Gibbs adsorption (mmol/gm) and expected experimental uncertainties "σ" (mmol/gm) in the adsorption values for each datum.

Table 2.4 Gibbs Adsorption of Pure CO_2 on Wet Beulah Zap Coal at 328.2 K

Pressure (MPa)	Gibbs Adsorption (mmol/g)	σ Gibbs (mmol/g)
1.02	0.135	0.053
1.50	0.179	0.053
2.82	0.262	0.052
4.22	0.324	0.052
5.91	0.372	0.051
7.15	0.369	0.051
8.35	0.357	0.053
9.71	0.327	0.068
11.05	0.312	0.094
12.04	0.248	0.107
13.57	0.089	0.120

Table 2.5 Gibbs Adsorption of Pure CO_2 on Wet Illinois #6 Coal at 328.2 K

Pressure (MPa)	Gibbs Adsorption (mmol/g)	σ Gibbs (mmol/g)
0.42	0.146	0.052
0.79	0.231	0.052
1.56	0.356	0.051
2.23	0.440	0.051
2.87	0.511	0.050
4.27	0.634	0.050
5.62	0.701	0.049
7.02	0.765	0.049
8.34	0.791	0.063
9.69	0.800	0.065
11.04	0.777	0.075
12.41	0.716	0.092
13.88	0.644	0.088

Table 2.6 Gibbs Adsorption of Pure CO_2 on Wet Pocahontas #3 Coal at 328.2 K

Pressure (MPa)	Gibbs Adsorption (mmol/g)	σ Gibbs (mmol/g)
0.40	0.281	0.040
.77	0.439	0.040
1.49	0.605	0.040
2.84	0.764	0.039
4.25	0.854	0.038
5.63	0.901	0.038
6.99	0.915	0.037
8.33	0.908	0.038
9.69	0.868	0.048
10.34	0.840	0.050
12.16	0.730	0.068
13.11	0.674	0.075

Table 2.7 Gibbs Adsorption of Pure CO_2 on Wet Upper Freeport Coal at 328.2 K

Pressure (MPa)	Gibbs Adsorption (mmol/g)	σ Gibbs (mmol/g)
0.40	0.239	0.043
0.81	0.363	0.043
1.47	0.482	0.042
2.86	0.624	0.042
4.24	0.698	0.041
5.64	0.739	0.041
7.00	0.756	0.040
8.35	0.758	0.041
9.67	0.742	0.052
10.75	0.737	0.056
12.31	0.667	0.073
13.86	0.593	0.082

Table 2.8 Gibbs Adsorption of Pure CO_2 on Wet Wyodak Coal at 328.2 K

Pressure (MPa)	Gibbs Adsorption (mmol/g)	σ Gibbs (mmol/g)
0.47	0.041	0.048
0.76	0.067	0.048
1.46	0.130	0.048
2.77	0.233	0.048
4.22	0.319	0.048
5.64	0.372	0.048
7.01	0.411	0.049
8.35	0.417	0.063
9.67	0.420	0.074
10.92	0.424	0.084
12.35	0.368	0.099
13.92	0.254	0.101

The decreasing order of Gibbs adsorption among the five coals is: wet Pocahontas, wet Illinois #6, wet Upper Freeport, wet Wyodak and wet Beulah Zap. In comparison, the decreasing order of the rank of these coals was: wet Pocahontas, wet Upper Freeport, wet Illinois #6, wet Wyodak and wet Beulah Zap. Thus, higher rank coals appear to have a larger capacity for CO_2 adsorption; however, the coal moisture contents which vary significantly also play an important role in CO_2 adsorption on these coals.

The Gibbs adsorption data on three of the coals, namely, wet Beulah Zap, Illinois #6 and Pocahontas coals, have been published in an NETL inter-laboratory study.[52] The remaining two coals in this study (wet Pocahontas and upper Freeport coals) have not been published previously. The main objective of the NETL inter-laboratory study[52] was to investigate the reproducibility of CO_2/coal adsorption isotherm measurements among various laboratories. In contrast, the objective of the present study is to investigate the

effect of water content of the coals on the experimental data, the data reduction, and the model analysis of these isotherms.

The adsorption data published earlier[52] did not include accounting for the solubility of CO_2 in adsorbed water and, thus, differ from the results presented here. Neglecting the solubility in the earlier work was part of a specified data reduction procedure provided by NETL, designed to insure consistent data reductions among the participating laboratories in that study. Accounting for the dissolved CO_2 in adsorbed water yields the actual amounts adsorbed on the wet coals, leading to lower values of the calculated Gibbs adsorption than previously published.[52] For the higher moisture containing coals in this study, this correction is significant, and it also affects the subsequent model analysis of these isotherms.

To highlight this difference, Figure 2.2 presents a comparison of CO_2 adsorption data on wet Beulah Zap coal published in Goodman et al.[52] and the data from this study. As evident from the figure, accounting for the gas solubility in adsorbed water can result in quite different calculated values of Gibbs adsorption.

Figures 2.3-2.7 illustrate the Gibbs adsorption of CO_2 on Beulah-Zap, Illinois #6, Pocahontas #3, Upper Freeport and Wyodak coals from this study, respectively. The CO_2 adsorption on each of the dry coals is also illustrated for comparison. The adsorption data on dry coals were measured in an earlier study.[21] For each coal, the CO_2 adsorption on the wet coal was lower than that on the dry coal. Further, the reduction in the gas adsorbed from that on dry coals appears to be correlated positively with the moisture content of the coal. The Pocahontas, Upper Freeport, Illinois #6, Wyodak and Beulah Zap

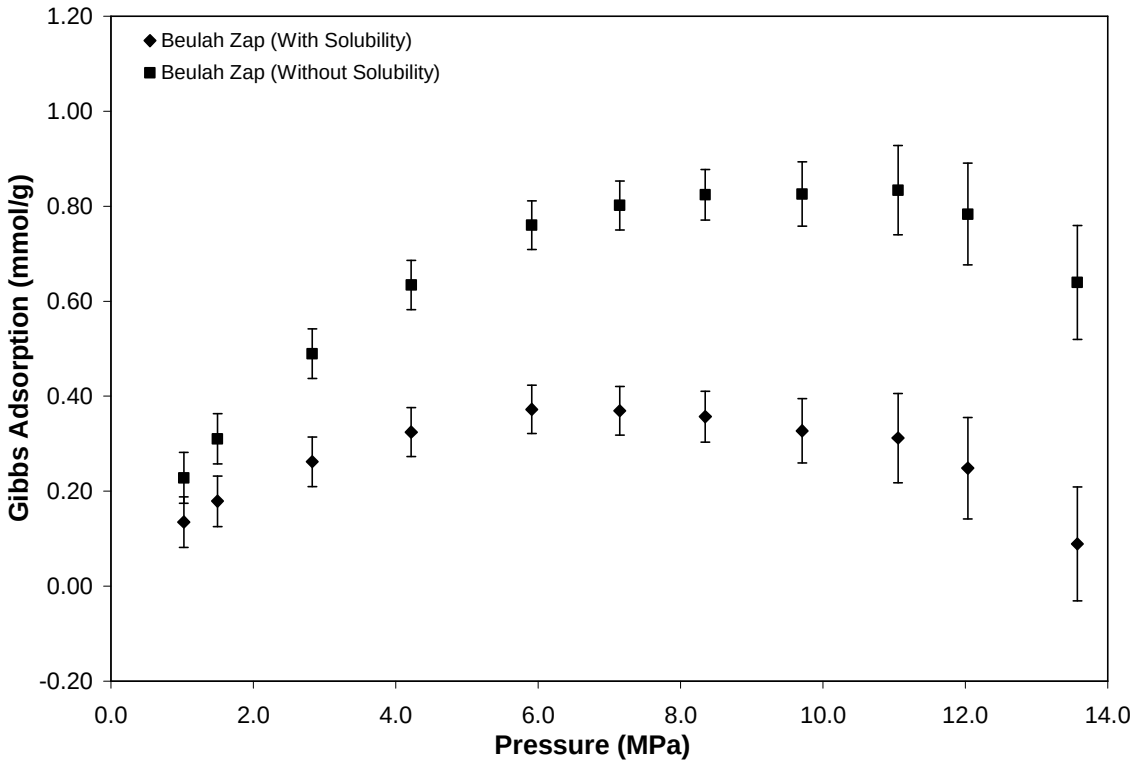

Figure 2.2 Comparison of CO_2 Adsorption Data on Wet Beulah Zap Coal at 328.2 K: Effect of Gas Solubility in Water

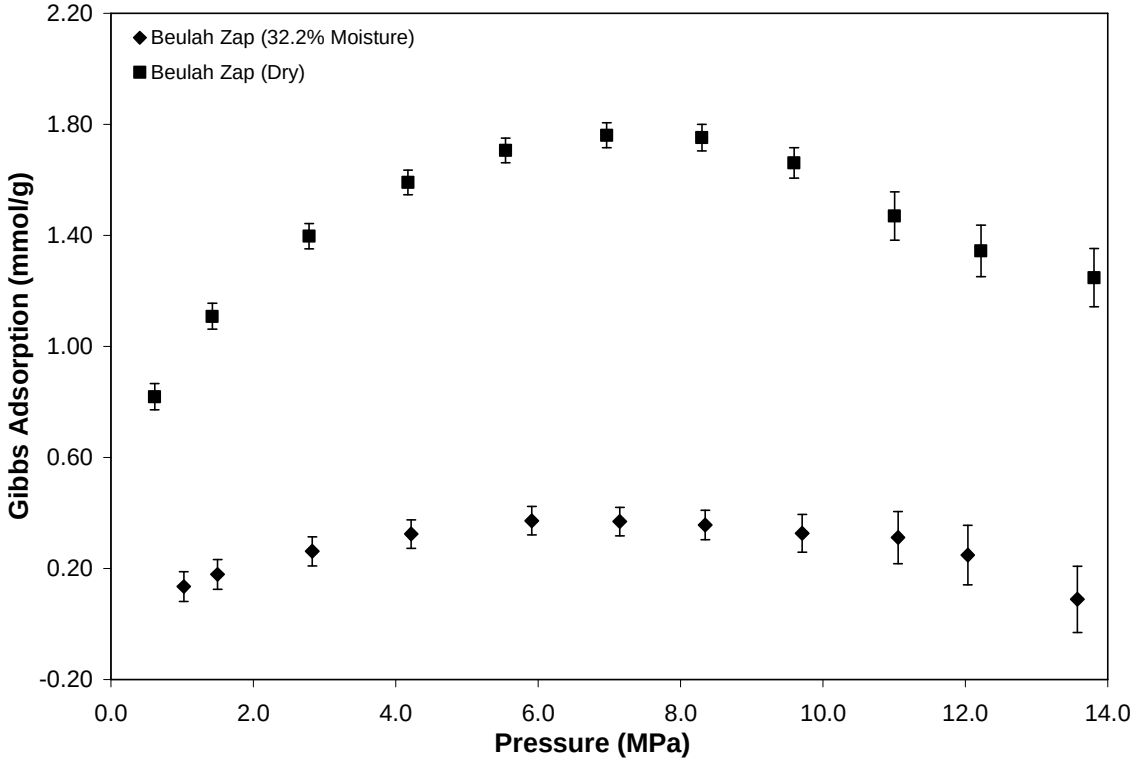

Figure 2.3 CO_2 Adsorption on Wet and Dry Beulah Zap Coal at 328.2 K

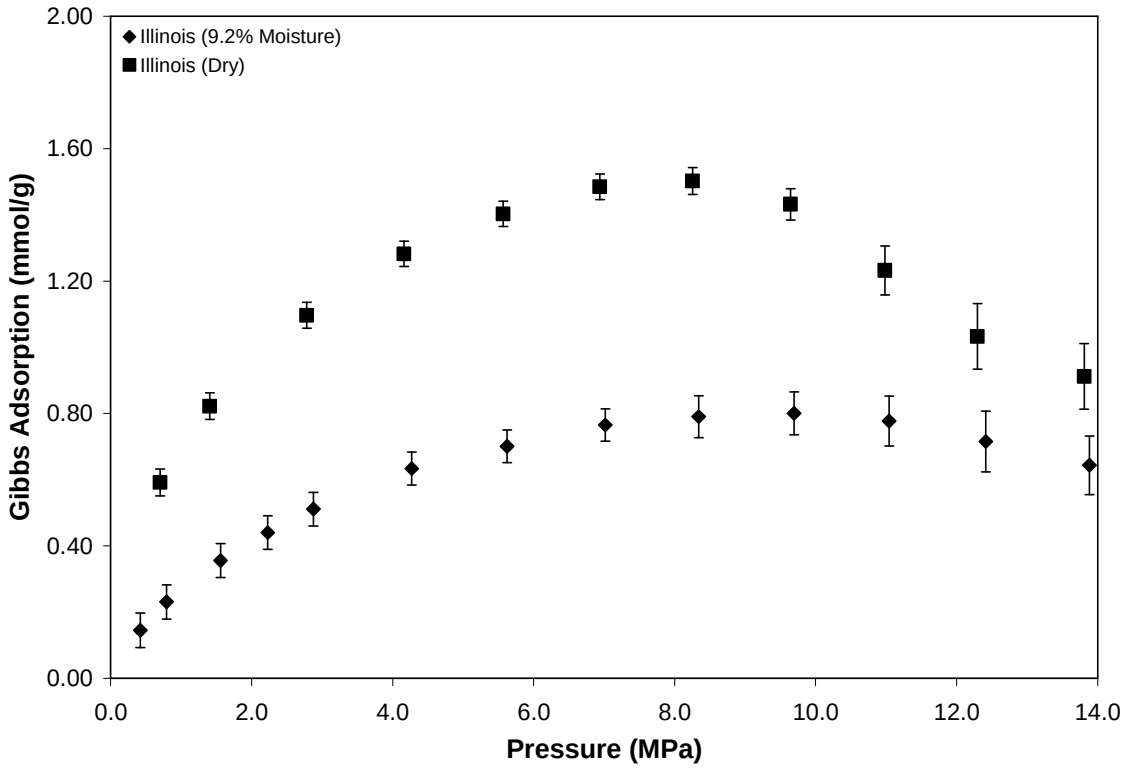

Figure 2.4 CO_2 Adsorption on Wet and Dry Illinois #6 Coal at 328.2 K

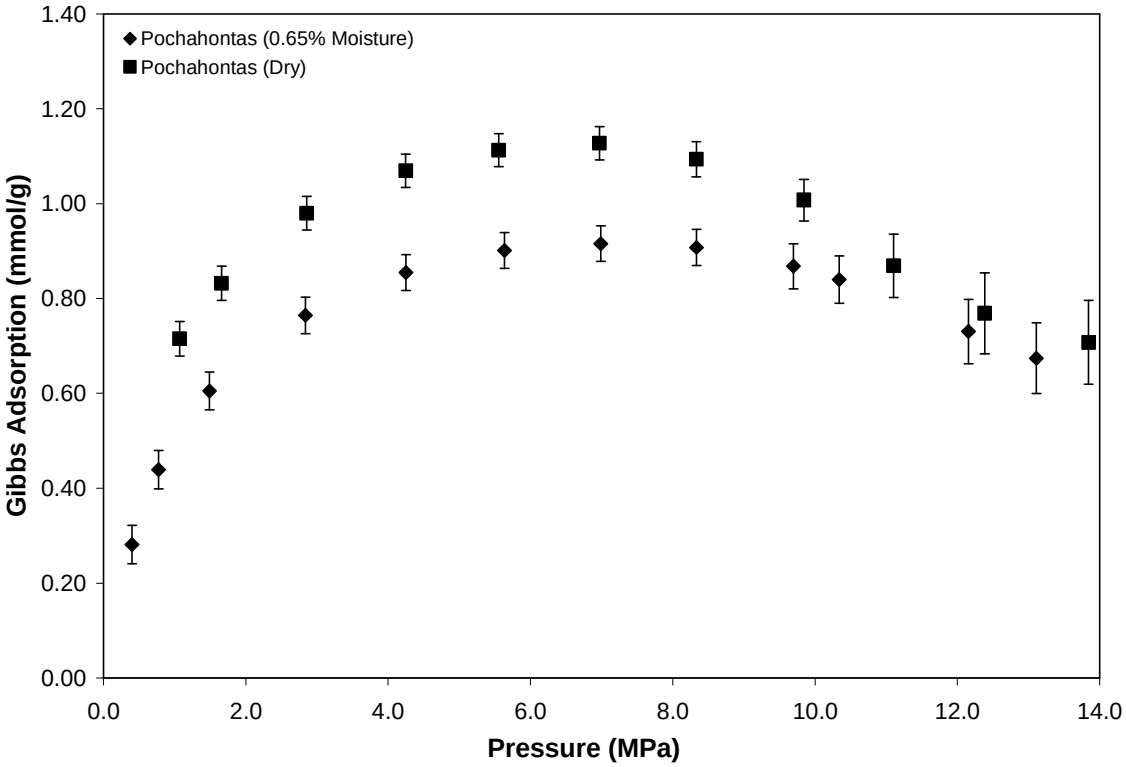

Figure 2.5 CO_2 Adsorption on Wet and Dry Pocahontas Coal at 328.2 K

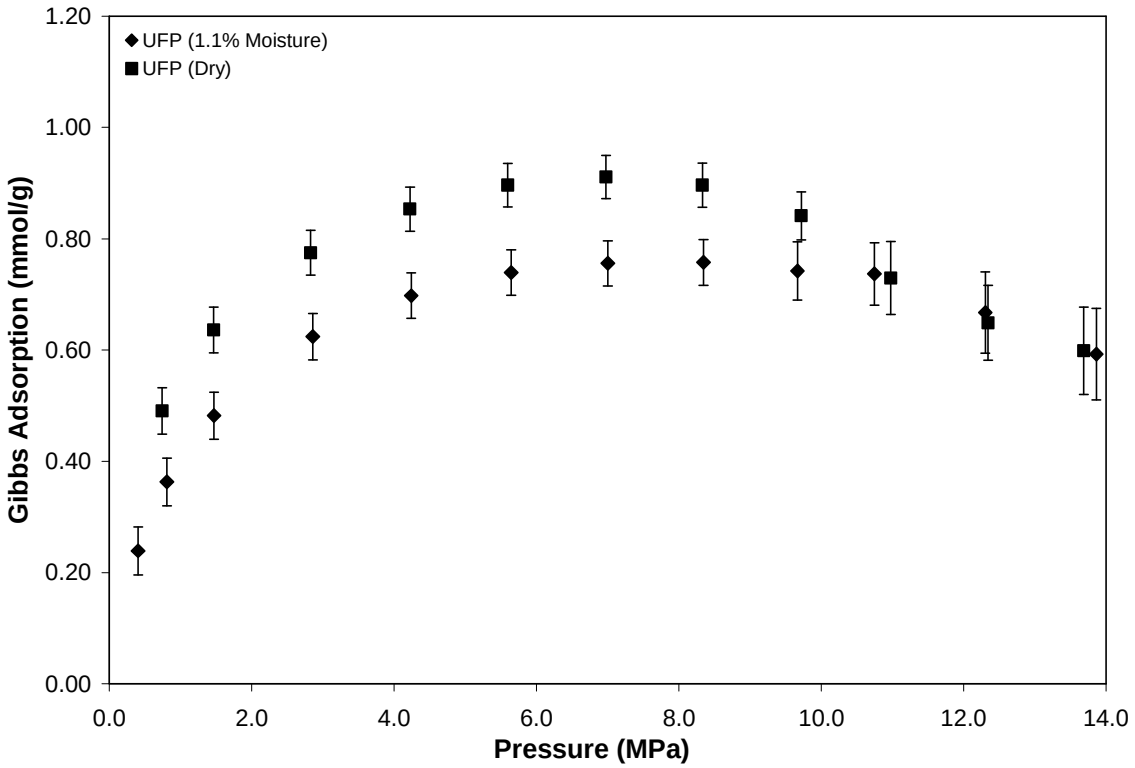

Figure 2.6 CO_2 Adsorption on Wet and Dry Upper Freeport Coal at 328.2 K

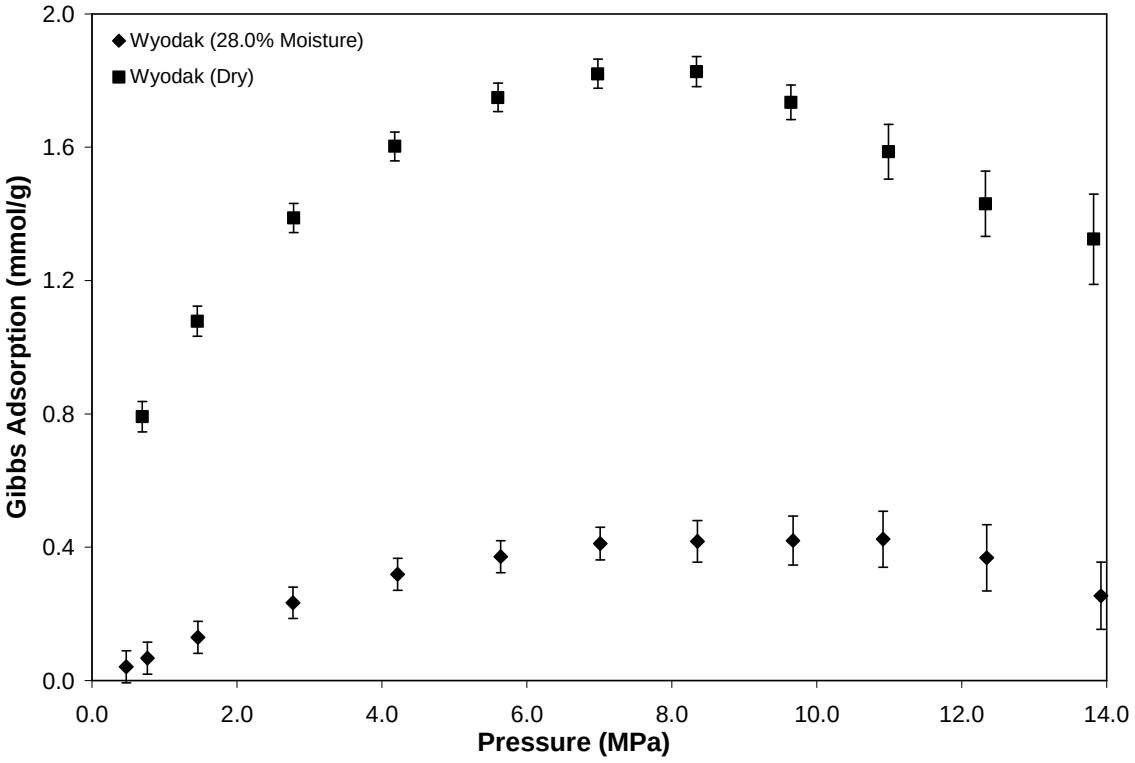

Figure 2.7 CO_2 Adsorption on Wet and Dry Wyodak Coal at 328.2 K

coals exhibited, respectively, about 19%, 17%, 48%, 76% and 79% reductions in the adsorption on the wet coals at 7 MPa when compared to the adsorption on the dry coals.

Figure 2.8 compares the Gibbs adsorption of CO_2 on all five wet coals. The adsorption isotherm for each of the wet coals exhibits a maximum between 8-12 MPa. For each case, the adsorption maximum on the wet coal occurs at a higher pressure than that for the dry coal. Note that some of the error bars have been omitted in Figure 2.8 for the sake of clarity.

The error analysis indicates that the average uncertainties for the CO_2 adsorption measurements are approximately 7-13% for Illinois #6, Upper Freeport, and Pocahontas coals. The higher percentage uncertainties are usually obtained at the higher pressures, due mainly to the lower value of the Gibbs adsorption for CO_2 at the higher pressures and the higher uncertainties in the CO_2 compressibility factors (due to its proximity to its critical point). The average uncertainties for Beulah Zap and Wyodak coals were around 34%. However, these higher *percentage* uncertainties are a result of *lower* adsorption amounts for these two wet coals and amounted to only about 0.06 - 0.07 mmol/gm, on average.

In our data reduction technique, we accounted for the amount of gas dissolved in the water-rich adsorbed phase, which results in lower calculated adsorption amounts for higher moisture containing coals. The Beulah Zap and Wyodak coals contain 32.2% and 28% moisture, respectively. Chapter 5 presents an alternative approach wherein a different data reduction technique is used for estimating the amounts adsorbed.

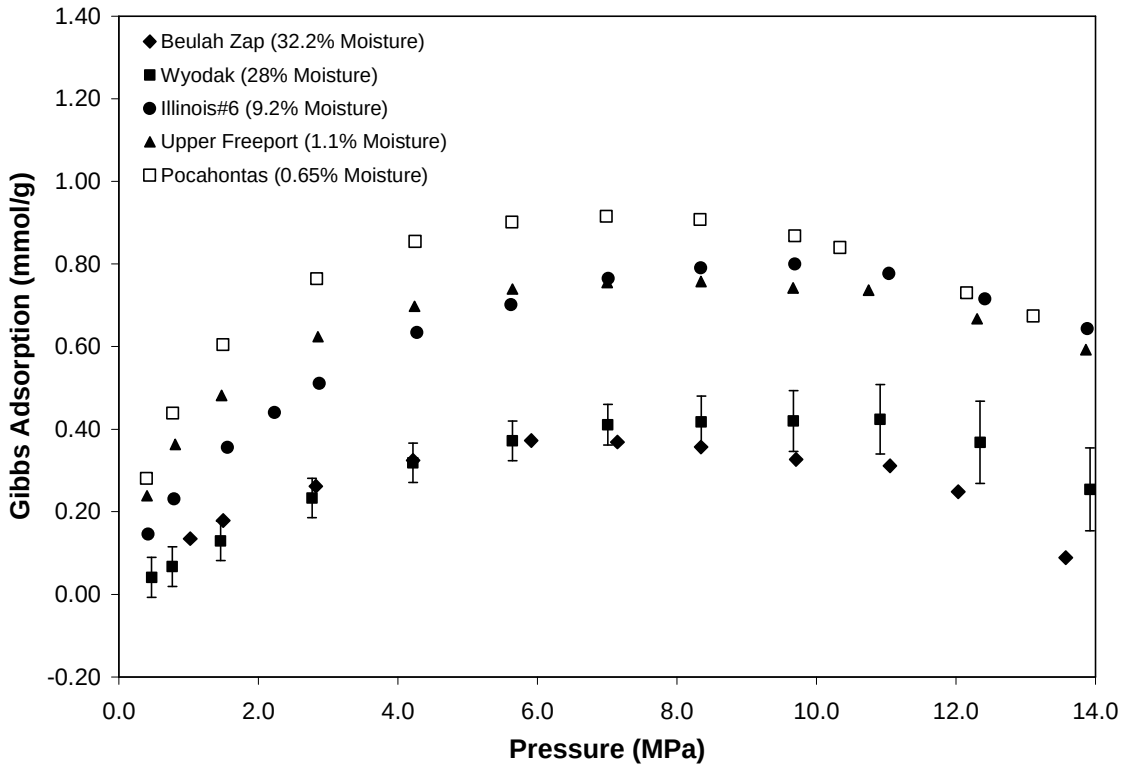

Figure 2.8 CO_2 Adsorption on Wet Argonne Coals at 328.2 K

B. Adsorption of Methane, Nitrogen and CO_2 on Dry and Wet Activated Carbon

The experimental data for the adsorption of pure nitrogen, methane and CO_2 on dry activated carbon are presented in Tables 2.9-2.11, respectively. These tables list the pressure (MPa), Gibbs adsorption (mmol/gm) and the expected experimental uncertainty "σ" (mmol/gm) for each datum. The adsorption data for these isotherms yielded expected uncertainties of 1-3%, on average. As expected, less gas adsorption is observed at 328.2 K than at 318.2 K (from our earlier experiments[7]); however, the new measurements agree with our previous data in regard to the relative amounts of nitrogen, methane and CO_2 adsorbed. In both cases, an approximate ratio of 1:1.6:2.4 was obtained at 7 MPa. Further, the desorption of CO_2 on dry activated carbon was also measured; and comparison of the adsorption and desorption isotherms indicated no hysteresis effect for this system.

The experimental data for the adsorption of pure nitrogen, methane and CO_2 on the *wet* activated carbon are presented in Tables 2.12-2.16, respectively. Figures 2.9-2.11 illustrate the adsorption isotherms for pure nitrogen, methane and CO_2 on wet activated carbon, respectively. The adsorption of these gases on dry activated carbon is also presented in these figures for comparison.

Table 2.9 Gibbs Adsorption of Pure Nitrogen on Dry Activated Carbon at 328.2 K

Pressure (MPa)	Gibbs Adsorption (mmol/g)	σ Gibbs (mmol/g)
0.81	1.015	0.041
1.46	1.473	0.040
2.93	2.075	0.039
4.19	2.407	0.039
5.53	2.651	0.039
6.98	2.834	0.039
8.36	2.945	0.039
9.69	3.018	0.040
11.08	3.068	0.039
12.54	3.100	0.040
13.70	3.108	0.040

Table 2.10 Gibbs Adsorption of Pure Methane on Dry Activated Carbon at 328.2 K

Pressure (MPa)	Gibbs Adsorption (mmol/g)	σ Gibbs (mmol/g)
1.50	2.845	0.047
2.78	3.555	0.046
4.11	3.936	0.045
5.59	4.167	0.045
7.07	4.277	0.045
8.38	4.310	0.045
9.18	4.306	0.045
9.77	4.306	0.045
11.11	4.273	0.046
12.43	4.221	0.046
13.74	4.145	0.047

Table 2.11 Gibbs Adsorption of Pure CO_2 on Dry Activated Carbon at 328.2 K

Pressure (MPa)	Gibbs Adsorption (mmol/g)	σ Gibbs (mmol/g)
0.33	2.432	0.117
0.74	3.684	0.115
1.49	4.887	0.113
2.85	5.885	0.110
4.22	6.321	0.108
5.62	6.462	0.107
7.07	6.396	0.106
8.31	6.134	0.105
9.62	5.616	0.106
11.11	4.524	0.132
12.49	3.522	0.137

Table 2.12 Gibbs Adsorption of Pure Nitrogen on Wet Activated Carbon at 328.2 K and 37% Moisture

Pressure (MPa)	Gibbs Adsorption (mmol/g)	σ Gibbs (mmol/g)
1.61	0.024	0.021
2.95	0.054	0.021
5.76	0.113	0.021
8.43	0.161	0.022
11.20	0.208	0.024
13.91	0.253	0.026

Table 2.13 Gibbs Adsorption of Pure Methane on Wet Activated Carbon at 328.2 K and 37% Moisture

Pressure (MPa)	Gibbs Adsorption (mmol/g)	σ Gibbs (mmol/g)
0.44	0.018	0.025
0.79	0.046	0.025
1.48	0.105	0.025
2.83	0.234	0.025
4.20	0.372	0.025
5.56	0.519	0.026
7.04	0.701	0.026

Table 2.14 Gibbs Adsorption of Pure CO_2 on Wet Activated Carbon at 328.2 K and 27% Moisture

Pressure (MPa)	Gibbs Adsorption (mmol/g)	σ Gibbs (mmol/g)
0.50	0.489	0.048
0.85	0.753	0.047
1.44	1.138	0.047
2.74	1.976	0.050
4.03	3.244	0.057
5.41	4.561	0.049
6.90	5.340	0.049
8.41	5.414	0.056
9.79	5.048	0.076
11.02	4.417	0.092
12.40	3.681	0.105
13.74	3.057	0.105

Table 2.15 Gibbs Adsorption of Pure CO_2 on Wet Activated Carbon at 328.2 K and 34% Moisture

Pressure (MPa)	Gibbs Adsorption (mmol/g)	σ Gibbs (mmol/g)
0.70	0.529	0.049
1.45	0.971	0.049
2.77	1.795	0.049
4.01	2.883	0.050
5.28	4.298	0.053
6.91	5.230	0.056
8.49	5.216	0.059
9.78	4.847	0.079
11.06	4.163	0.096
12.52	3.373	0.109
13.94	2.867	0.117

Table 2.16 Gibbs Adsorption of Pure CO_2 on Wet Activated Carbon at 328.2 K and 16% Moisture

Pressure (MPa)	Gibbs Adsorption (mmol/g)	σ Gibbs (mmol/g)
0.39	0.690	0.037
0.74	1.018	0.037
1.43	1.444	0.036
2.74	2.114	0.044
4.00	3.347	0.056
5.31	4.823	0.079
6.99	5.473	0.144
8.50	5.448	0.113
11.11	4.405	0.082
13.09	3.456	0.137

Using modified ASTM procedures, we estimated the equilibrium moisture content of activated carbon to be 27%. To study the effect of moisture on adsorption capacity, we conducted isotherm measurements at moisture contents of 16%, 27%, 34% and 37%. The adsorption isotherm measurements for nitrogen were conducted at a moisture content of 37%, which is above the equilibrium moisture content of about 27%. The nitrogen adsorption isotherm for the wet activated carbon indicated significant reduction in adsorption capacity below 7 MPa when compared to the adsorption on the dry activated carbon. For example, at 5.5 MPa, the amount adsorbed on the wet activated carbon (37% moisture content) is only 4% of the amount adsorbed on dry activated carbon. Further, the nitrogen adsorption capacity on wet activated carbon (Figure 2.9) was less than 10% of the adsorption on the dry activated carbon, indicating the large effect of water on the carbon surface. The data for this isotherm yielded expected uncertainties of 30%, on average. However, higher *percentage* uncertainties are a result of the extremely low adsorption levels of this isotherm and translate to only about 0.022 mmol/gm of

adsorption, on average. As such, the experimental uncertainty in terms of actual adsorption amounts is small and such behavior is expected.

The adsorption isotherm measurements for methane were also conducted at a moisture content of 37% and are shown in Figure 2.10. The data for this isotherm yielded expected experimental uncertainties of 28%, on average. As explained above, the large *percentage* uncertainties translate to small *amounts* of adsorption at these levels of moisture in the carbon.

The amount of methane adsorbed on the wet activated carbon is significantly less than the amount adsorbed on dry activated carbon at comparable conditions (Figure 2.10). For example, at 2.8 MPa, the wet activated carbon (37% moisture content) adsorbed 93% less methane than the dry activated carbon. Similarly, at 7 MPa, the adsorption of methane on the wet carbon is 84% lower than the adsorption on dry activated carbon. Thus, even at higher pressures, the presence of water significantly lowers the methane adsorption. There is some confirmation in the literature of a significant reduction of methane adsorption on an activated carbon in the presence of moisture.[53] Moreover, simulation results from the literature indicate that even small concentrations of water on the carbon surface can cause significant pore-blocking, thus significantly reducing adsorption sites available to methane gas. In their simulation study on adsorption of water-methane mixtures on activated carbon, Muller et al.[28] have shown that water can lead to 50% reduction in methane adsorption. Thus, the inter-connectivity of water molecules across the pore entrances may further restrict methane adsorption on a wet carbon.

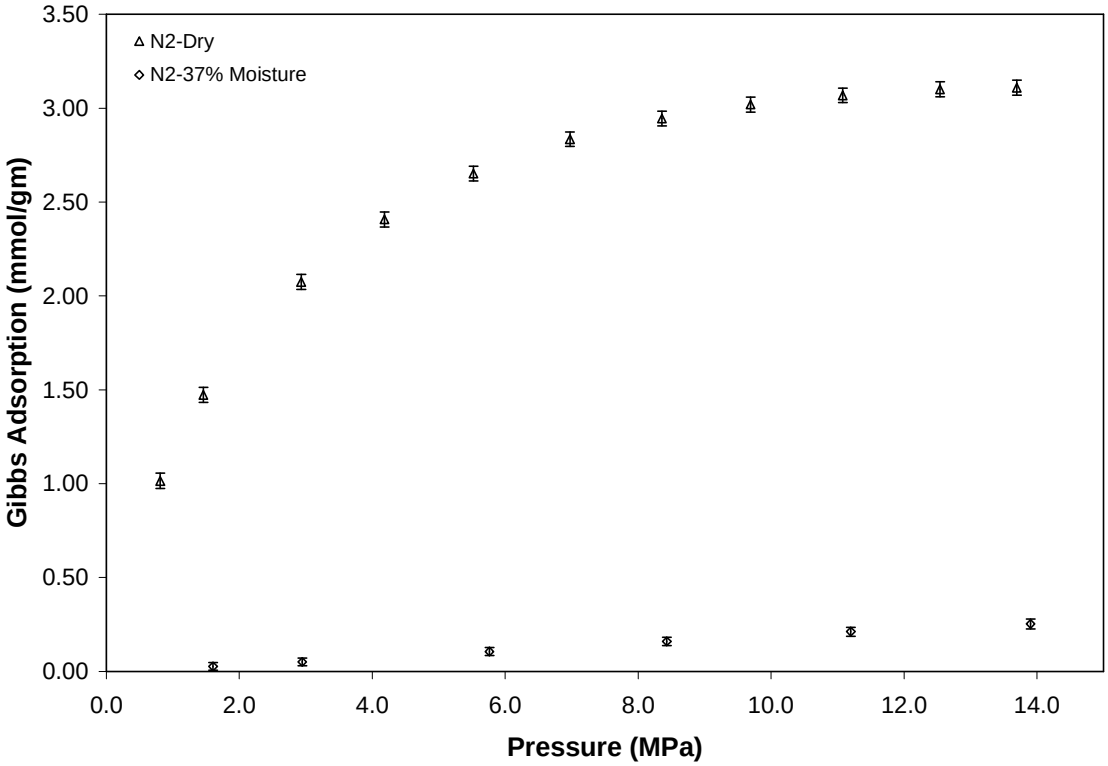

Figure 2.9 Nitrogen Adsorption on Wet Activated Carbon at 328.2 K and 37% Moisture

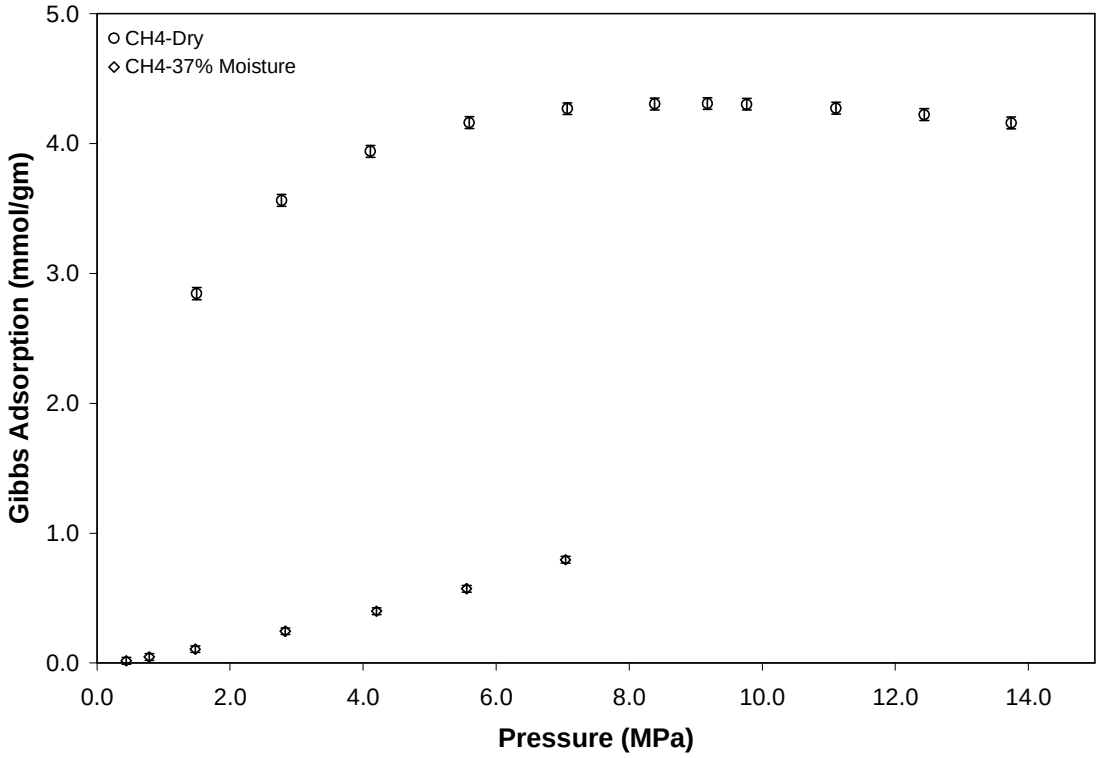

Figure 2.10 Methane Adsorption on Wet Activated Carbon at 328.2 K and 37% Moisture

The adsorption measurements for pure CO_2 on wet activated carbon were conducted at three levels of moisture, as shown in Figure 2.11. The activated carbon has an equilibrium moisture content of 27%; thus, the three moisture contents were selected to represent supersaturated, saturated and undersaturated conditions of the wet activated carbon with respect to moisture. First, CO_2 adsorption isotherm was measured at the equilibrium moisture content of 27%. Then, another isotherm was measured at moisture content of about 34%, which is 7% above the equilibrium moisture content. The third adsorption isotherm was measured at moisture content of about 16%, which is approximately one-half the equilibrium moisture content. The adsorption data for each of these three isotherms yielded expected experimental uncertainties of 3%, on average.

The adsorption of CO_2 on wet activated carbon at 34% moisture content exhibited, on average, an 8% decrease in the amount of gas adsorbed when compared to the adsorption on wet activated carbon at its equilibrium moisture content. The adsorption of CO_2 on wet activated carbon at 16% moisture content exhibited an increase of only 2% in the amount of gas adsorbed at 7 MPa when compared to the adsorption at a moisture content of 27%. For all three isotherms, the CO_2 adsorption data displayed an unexpected change in concavity at moderate pressures between 3 and 6 MPa (Figure 2.11). In general, lower moisture content shifted this concavity change to lower pressures.

Further, the wet activated carbon adsorption amount approaches that of the dry activated carbon at pressures above 8 MPa. This may be an artifact of our data reduction procedure, resulting from uncertainty in the gas density values we employed; this uncertainty could be caused by the presence of water vapor in the CO_2 gas phase. Some experimental evidence suggests that the presence of small concentrations of water in the

gas phase can increase the CO_2 gas density by as much as 10%.[54] A correction of this magnitude can lead to the adsorption on the wet activated carbon becoming lower than the adsorption on the dry activated carbon at pressures higher than 8 MPa. Currently, we know of no equation of state capable of accurately calculating the densities of CO_2–water mixtures at near-critical conditions. Since the methane and nitrogen are well removed from their critical points, and water solubility in the gas phase is much lower than for CO_2, the effect would be much smaller for the methane and nitrogen measurements.

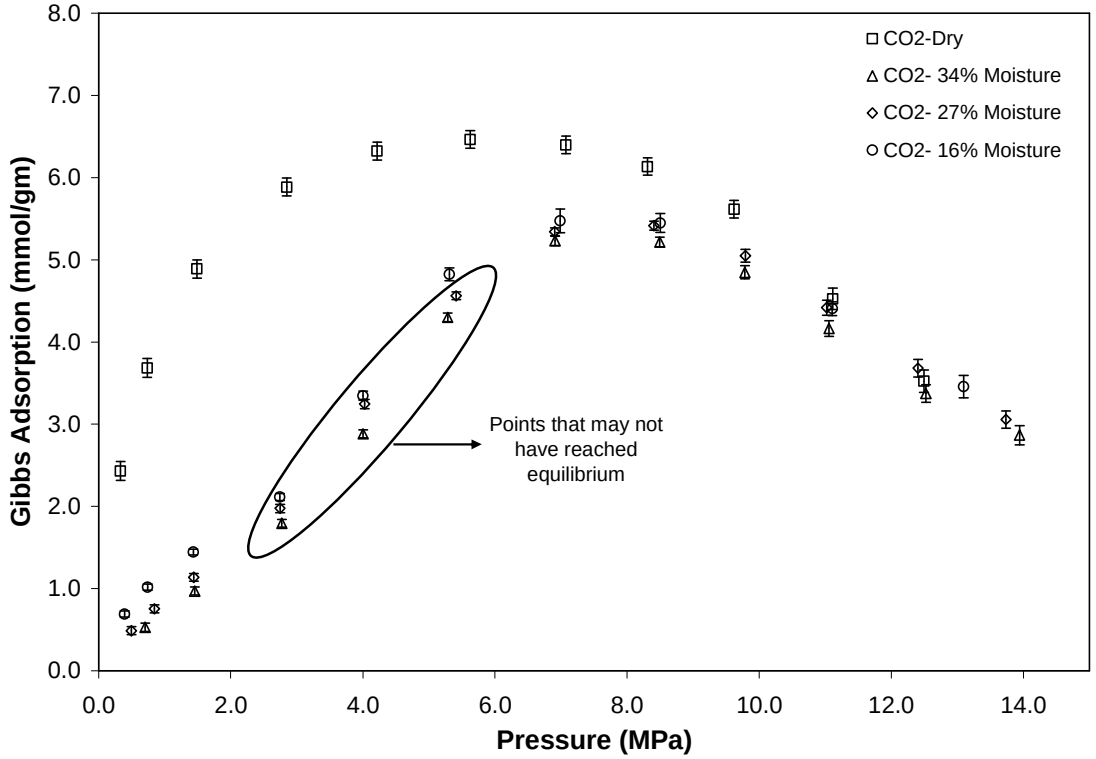

Figure 2.11 CO_2 Adsorption on Wet Activated Carbon at 328.2 K at Different Moisture Contents

As illustrated in Figure 2.11, our results indicate that even small amounts of moisture present in the adsorbent can lower significantly the gas adsorption, especially below 7 MPa, when compared with the adsorption on a completely dry adsorbent.

The kinetics of adsorption on wet activated carbon led to unusually long equilibration times (on the order of several days per datum) relative to our measurements on coals and on dry activated carbon, where the equilibration times are less than 24 hours. Lengthy equilibration time may be attributed to slow gas diffusion through the adsorbed water which covers some of the micropores of the carbon surface. Different mechanisms have been proposed for this adsorption behavior in the literature; however, most are centered on the fact that presence of moisture significantly blocks the pores of the carbon surface.

The longest equilibration times occur between 3 and 7 MPa, which coincides with the region where the changes in concavity of the adsorption isotherm were observed. This may indicate that the stripping of adsorbed water, coupled with the slow dispersion of the adsorbing gas, is partly responsible for the long equilibration times. Figure 2.12 presents the equilibration times for CO_2 adsorption isotherm on wet activated carbon at 34% moisture. The figure shows the total equilibration time for each data point of the isotherm. As evident from Figure 2.12, the equilibration times were much larger in the pressure range of 3 to 7 MPa.

Figure 2.13 presents the pressure drop rate for data points at 4 and 12 MPa of the same isotherm studied in Figure 2.12. There appears to be a continued drop in pressure at 4 MPa even after 200 hours of equilibration time. In comparison, the drop in pressure at 12 MPa had essentially ceased after 48 hours, as evident from Figure 2.13. This contrasting behavior for moderate and high pressure data points of the same isotherm highlights the unexplained behavior observed in the 3 to 6 MPa region of this isotherm.

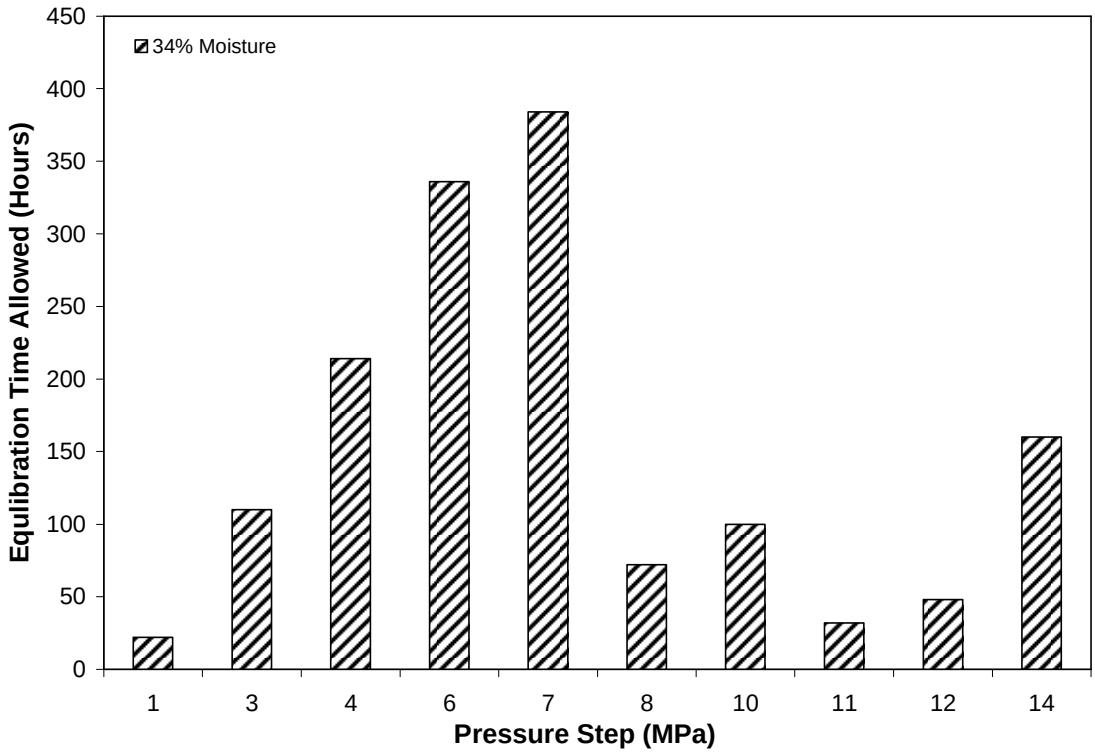

Figure 2.12 Equilibration Times for CO_2 Adsorption on Wet Activated Carbon at 328.2 K and 34% Moisture

We also observed that the equilibration time allowed for the data point at 7 MPa appeared to be sufficient for stabilization of pressure. In contrast, the isotherm points between 3 and 6 MPa may have needed substantially longer equilibration times. Therefore, based on our experience in measuring adsorption isotherms, a decision was made to progress to the next higher pressure data point in the isotherm after the equilibration times shown in Figure 2.12 (in the 3 to 6 MPa region). This was necessitated by practical time constraints for these isotherms. As such, the isotherm data points between 3 and 6 MPa *may* not have reached their final equilibrium state. This region is also indicated by an "envelope" in Figure 2.11.

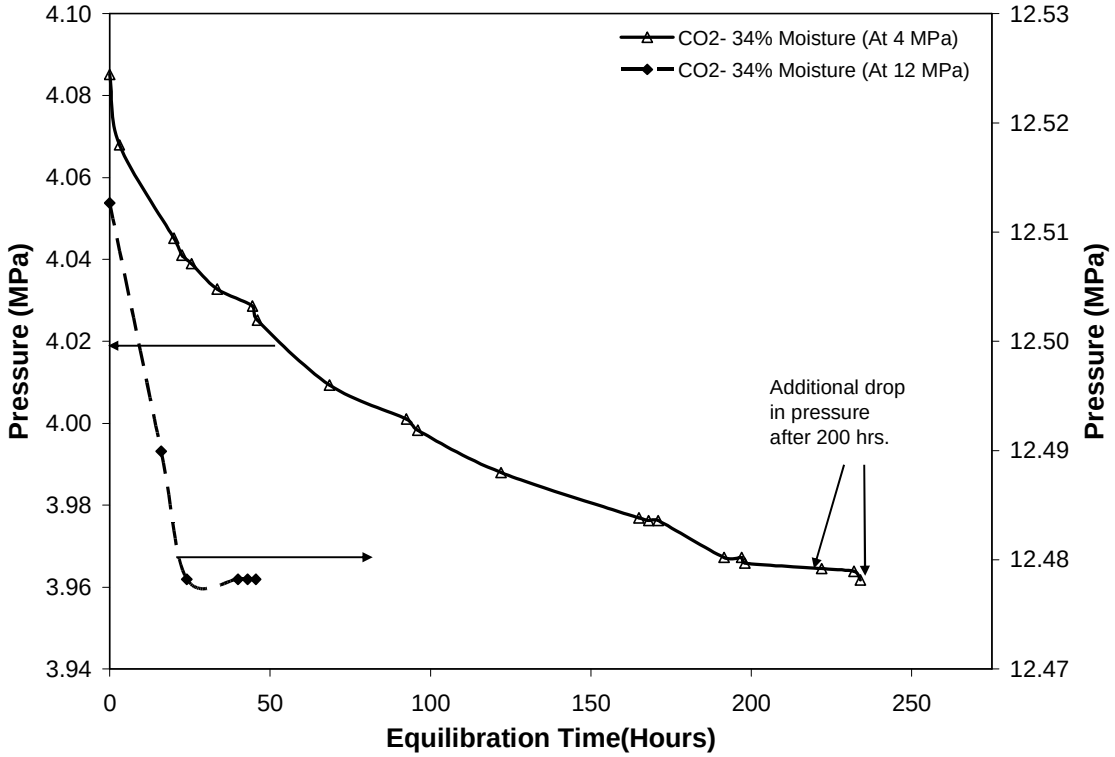

Figure 2.13 Pressure Drop Rate Data for CO_2 Adsorption on Wet Activated Carbon at 328.2 K and 34% Moisture: 4 and 12 MPa Pressure Steps

To our knowledge, there are no literature data for the adsorption of CO_2 under supercritical conditions on wet activated carbon at different levels of moisture. Since these appear to be the first measurements of their kind, additional work will be needed to delineate the cause of this unexpected behavior of CO_2 isotherms on wet activated carbon.

2.11 OSU CBM Adsorption Database

An adsorption database comprised of adsorption measurements for coalbed gases was assembled earlier.[8] The database contains the pure, binary, and ternary mixture adsorption measurements conducted at OSU. There are 35 systems in that OSU adsorption database. As part of the current study, eleven new systems comprising thirteen independently measured isotherms have been added to the extended database. Thus, each

"system" consists of at least one gas isotherm on a specific adsorbent. Our newly acquired adsorption measurements are presented in Table 2.17, which includes the adsorbates, the adsorbent, number of points and the corresponding temperature and pressure ranges for each system.

Table 2.17 Extended OSU Adsorption Database: New Systems in This Study

Adsorbent	Adsorbate	Temp. (K)	Pressure Range (MPa)	NPTS
Wet Illinois #6 Coal	CO_2	328	0.7 – 13.7	13
Wet Beulah Zap Coal	CO_2	328	0.7 – 13.7	11
Wet Wyodak Coal	CO_2	328	0.7 – 13.7	12
Wet Upper Freeport Coal	CO_2	328	0.7 – 13.7	12
Wet Pocahontas Coal	CO_2	328	0.7 – 13.7	12
Dry AC – F 400	N_2	328	0.7 – 13.7	11
Dry AC – F 400	CH_4	328	0.7 – 13.7	11
Dry AC – F 400	CO_2	328	0.7 – 13.7	11
Wet AC-F 400	CO_2	328	0.7 – 13.7	33
Wet AC-F 400	CH_4	328	0.7 – 13.7	9
Wet AC-F 400	N2	328	0.7 – 13.7	6

This extension of the database contains pure-gas adsorption measurements on six solid matrices: wet Illinois #6 coal, wet Beulah Zap coal, wet Wyodak coal, wet Upper Freeport coal, wet Pocahontas coal and wet/dry activated carbon. All isotherm measurements were conducted at 328.2 K and pressures to 13.8 MPa. Additional details of the OSU adsorption database can be found elsewhere.[8]

2.12 Monte Carlo Analysis of OSU Adsorption Error Analysis

The following material in Section 2.12 has been reproduced with permission from [Mohammad, S. A.; Fitzgerald, J. E.; Robinson, R. L., Jr.; Gasem, K. A. M., Experimental Uncertainties in Volumetric Methods for Measuring Equilibrium Adsorption. *Energy & Fuels* **2009,** DOI: 10.1021/ef8011257] Copyright [2009] American Chemical Society.

As mentioned above, a detailed error analysis was performed to estimate the uncertainty associated with each experimental datum by propagating the errors from the primary measurements of pressure, temperature and volume. The analytical error analysis was based on standard multivariate error propagation principles.[55] The detailed derivation of the analytical error analysis has been summarized elsewhere.[12, 20] In this study, a Monte Carlo analysis was conducted to confirm the validity of the analytical error analysis technique. In particular, a Monte Carlo analysis was performed for the CO_2 adsorption on dry Upper Freeport coal, and the results were compared with the analytical error estimates. To conduct this analysis, all independent variables of the experiment were perturbed with a normally-distributed random error. The experimental estimates for the uncertainties in the primary measured quantities of pressure, volume and temperature were used as the random error of the corresponding perturbed variable in the Monte Carlo analysis. The Monte Carlo analysis was conducted for approximately 1000 sets of these perturbed variables. Thus, for each set of perturbed variables, an amount adsorbed was evaluated. The average of these runs at each pressure was taken as the amount adsorbed at that pressure for a given set of perturbed variables. Further, the standard deviation of the amount adsorbed evaluated from these 1000 sets was taken as an estimate of the uncertainty in the acquired data for comparison with the experimental error derived analytically.

Figure 2.14 presents the comparison between analytical and Monte Carlo error estimates using the OSU adsorption apparatus for dry Upper Freeport coal. In this figure, sections marked as I, II and III represent three separate loadings of the pump that were required to complete the isotherm. The discontinuities at pressures around 10 and 12 MPa

are due to the reloading of pump, which was necessary for higher pressure injections. As evident from Figure 2.14, good agreement exists between the Monte Carlo and analytical error estimation methods. Thus, these results provide a reasonable confirmation of the analytical expressions that are used to estimate the uncertainties in the amount of gas adsorbed.

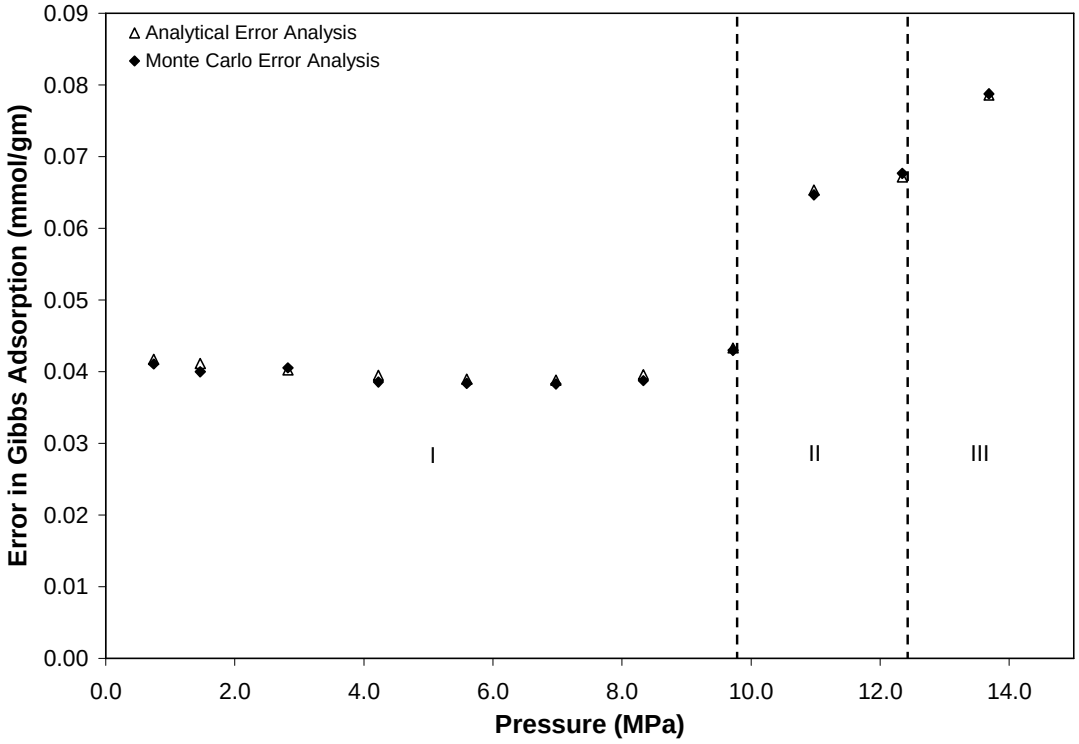

Figure 2.14 Comparison of Monte Carlo and Analytical Error Analyses for CO_2 Adsorption on Dry Upper Freeport Coal

To test for the normality of the distribution of errors from the Monte Carlo analysis, the histogram and cumulative distribution of these errors are shown in Figure 2.15. In this figure, "X", "Xbar" and "Sigma" represent the sample observation, mean and standard deviation of the distribution, respectively. As evident from the figure, the distribution displays essentially normal error distribution behavior.

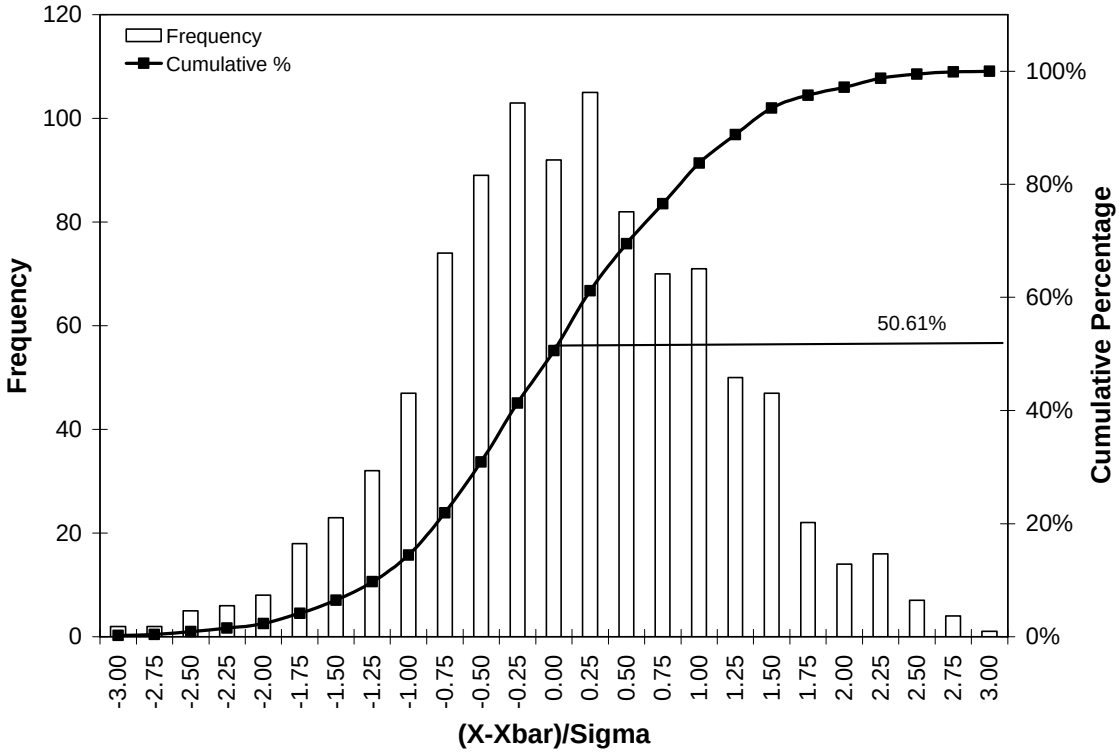

Figure 2.15 Histogram for the Distribution of Errors Evaluated from the Monte Carlo Error Analysis for CO_2 Adsorption on Upper Freeport Coal

CHAPTER 3

REVIEW OF ADSORPTION MODELS IN CBM-RELATED WORK

The material in this chapter has been reproduced with permission from [Gasem, Khaled; Mohammad, Sayeed; Robinson, R. L., Jr.; Modeling Coalbed Methane Adsorption and CO_2 Sequestration. *Encyclopedia of Chemical Processing* **2009,** DOI: 10.1081/E-ECHP-120043857] Copyright [2009] Taylor and Francis.

In this chapter, a number of adsorption models that have been used for CBM-related work are reviewed, and the potential weaknesses and strengths of some of these models are discussed. Among the adsorption models considered, this chapter concentrates on three theoretically-based models that have been developed for use in CBM and CO_2 sequestration modeling. The efficacy of these models in describing the adsorption behavior of coalbed gases is also discussed. Finally, the chapter outlines future work required to address some of the outstanding issues in adsorption modeling of CBM systems. The material presented herein is not intended to be all-inclusive; rather, it is an overview of some of the pertinent efforts in equilibrium adsorption modeling of CBM systems.

3.1 Adsorption Models in CBM-Related Work

Several frameworks can be used to describe the adsorption phenomenon and correlate pure- and mixed-gas adsorption isotherms in CBM systems. These include the Langmuir model[13], extended Langmuir model[56], the ideal adsorbed solution theory[15], real adsorbed solution theory[57], pore-filling theory[58] and its combination with the

vacancy solution model[59, 60], two-dimensional equation-of-state (2-D EOS) models[16, 17, 18], the simplified local-density (SLD) model[25], the Ono-Kondo (OK) model[20] and a variety of other models (see, e.g., Do[61]). These and some other models are briefly reviewed herein.

Langmuir/Extended Langmuir Models

The Langmuir model is the simplest adsorption model and is derived from kinetic considerations.[13] The model assumes that:

1. The solid surface is composed of localized adsorption sites, and each site can hold only one adsorbate molecule
2. The adsorption sites are energetically equivalent
3. There are no adsorbate-adsorbate interactions between neighboring adsorption sites
4. The molecules are adsorbed in a single layer only (monolayer coverage).

In principle, the Langmuir model can describe only monolayer adsorption on an ideal surface. An ideal surface has periodic energy fluctuations which are equal in magnitude and this magnitude is larger than the thermal energy, KT. This trough of energy acts as an adsorption site. When a molecule hits a surface, it can either be reflected or adsorbed depending on whether the site is vacant or is already occupied by a molecule. The dynamic equilibrium is attained when the rate of adsorption is equal to the rate of desorption/evaporation.

In terms of fractional loading, θ, the Langmuir model can be expressed as:

$$\theta = \frac{\omega}{L} = \frac{BP}{1 + BP} \tag{3.1}$$

where θ and ω are the fractional loading and the amount adsorbed at pressure P, respectively, B is an affinity parameter with units of inverse pressure, and L is the theoretical maximum amount adsorbed at infinite pressure. The parameter B is a measure of the partitioning of the adsorbate molecules between the adsorbed and the gas phases. It also introduces implicitly the temperature dependence of the adsorption isotherms in the model (i.e., B is temperature dependent).

The extended Langmuir model was first introduced by Markham and Benton[56] to describe mixture adsorption. It can be represented as:

$$\omega_i = \frac{L_i B_i P y_i}{1 + \sum_j B_j P y_j} \qquad j = 1, NC \tag{3.2}$$

where L_i and B_i are the temperature-dependent pure-component Langmuir model parameters and y_i is the gas-phase mole fraction of the adsorbing specie "i".

The selectivity factor, α, can be expressed in terms of the extended Langmuir model parameters, as follows:

$$\alpha_{ij} = \frac{\left(x/y\right)_i}{\left(x/y\right)_j} = \frac{L_i B_i}{L_j B_j} \tag{3.3}$$

where x and y are the adsorbed and gas-phase mole fractions of the two-components, respectively, and L and B are the corresponding pure-component model parameters.

Equation (3.3) reveals that the extended Langmuir model predicts a constant (pressure and composition independent) value for α, since the right side of equation (3.3) depends only on pure-component Langmuir model parameters. Thus, this model does not take into account mixed-gas equilibria and system pressure to evaluate mixed-gas

adsorption. As such, the extended Langmuir model is an entirely empirical model and is also thermodynamically inconsistent.[51]

Historically, the Langmuir and extended Langmuir models have been used extensively in the CBM field. Ease of application appears to be the main motivation for their use in CBM work. Arri and Yee[51] used the Langmuir/extended Langmuir models in their compositional coalbed methane simulator. They observed that the extended Langmuir model under-predicted the adsorption in gas mixtures at higher pressures. Similarly, Chaback et al.[62] applied the extended Langmuir model to model the adsorption/desorption of CO_2, methane and nitrogen binary mixtures. Levy et al.[31] correlated CO_2 and nitrogen Langmuir model parameters with the corresponding values for methane for a set of Bowen Basin coals. They found a linear correlation between them and observed that the CO_2 and nitrogen isotherms could be reliably predicted once the methane isotherm is known for such systems. However, this result is restricted to coals from a single basin.

Ideal Adsorbed Solution (IAS) Theory

Myers and Prausnitz[15] introduced the ideal adsorbed solution (IAS) theory. This theory is an adsorption analog to Raoult's law, which is used in vapor-liquid equilibria. The IAS theory assumes that the gas and adsorbed phases form ideal solutions, i.e. all activity coefficients are unity. The equilibrium relation for the adsorbed and the gas phase in the IAS theory is given as:

$$y_i P = P_{0,i}(\pi) x_i \qquad (3.4)$$

where P_0 is the equilibrium gas pressure corresponding to the temperature and spreading pressure, π, of the pure component, and x_i and y_i are the adsorbed and gas-phase mole

fractions, respectively. The spreading pressure is defined as the difference in surface tension between a clean surface and a surface covered with an (monolayer) adsorbate.[63]

The IAS theory is used to extend a pure-isotherm model to mixture adsorption. Any pure-component isotherm model can be used with the IAS theory; several authors have used IAS theory to describe mixture adsorption. Valenzuela et al.[64] used the Langmuir model with the IAS theory for different adsorption systems. Zhou et al.[17] and Hall et al.[6] utilized a 2-D EOS with the IAS theory to model mixture adsorption. Similarly, Manik[65] used the IAS theory with the Toth equation to model adsorption isotherms in their compositional coalbed methane simulator.

Real Adsorbed Solution (RAS) Theory

The real adsorbed solution theory takes into account the non-idealities in the adsorbed and the gas phases and, therefore, requires adsorbed-phase activity coefficients. These activity coefficients are assumed to be unity in the IAS model.

When the activity coefficients are considered, the real adsorbed solution (RAS) theory is obtained as follows[57]:

$$P y_i \phi_i = P_i^0 \phi_i^0 \gamma_i x_i \qquad (3.5)$$

where ϕ_i^0 is the gas-phase fugacity coefficient of the pure component 'i' at its reference pressure P_i^0, γ_i is the activity coefficient of the component 'i' in the adsorbed phase, and y_i and x_i are the mole fractions of the gas and adsorbed components, respectively. The adsorbed-phase reference pressure is defined as the pressure exerted by the pure component adsorbate at the same spreading pressure and temperature as the mixture, $P_i^0 = P_i^0(\pi, T)$, where π is the spreading pressure derived from surface work. The

adsorbed-phase activity coefficients are functions of temperature, pressure and composition.

Since the spreading pressure is an intensive thermodynamic variable, the spreading pressure group, ψ, is defined as[57]:

$$\psi = \frac{\pi A}{RT} \tag{3.6}$$

where A is the surface area of the adsorbent.

The spreading pressure of mixtures can be obtained from the Gibbs adsorption equation, which is related to the spreading pressure group as follows[57]:

$$d\psi = \sum_{i=1}^{NC} n_i d\ln(Py_i\varphi_i) - \frac{n_T}{\rho_a RT} dP \tag{3.7}$$

where ρ_a is the molar density of the adsorbed phase, n_i and n_T are the amount adsorbed of component 'i' and the total adsorbed amount, respectively.

Stevenson et al.[57] applied the IAS and RAS theories to model mixture adsorption. Interestingly, they observed that the IAS theory was superior to the RAS theory, especially at the higher pressures where the activity coefficients are close to unity. This was attributed to errors in the adsorbed-phase activity coefficients. In fact, no reported applications exist for estimating the adsorbed-phase activity coefficients at higher pressures; therefore, use of the RAS theory has been very limited.

Theory of Volume Filling of Micropores (TVFM)

Dubinin[66] extended Polanyi's potential theory[67] and developed the theory of volume filling of micropores (TVFM). This theory assumes that:

1. The adsorbate fills the adsorption surface through a pore-filling mechanism
2. A discrete monolayer is never formed in the pores

Dubinin had hypothesized that the adsorption mechanism on microporous adsorbents would be better described by pore-filling models (Dubinin-Polanyi approach) than surface coverage models (Langmuir model, etc.). The two most common forms of the Dubinin's pore-filling models are the Dubinin-Radushkevich (D-R) and Dubinin-Astakhov (D-A) equations.

The Dubinin-Astakhov (D-A) equation is given as[68]:

$$V = V_0 \exp\left\{-\left(\frac{RT}{\beta E_0}\ln\frac{P_0}{P}\right)^n\right\} \tag{3.8}$$

The Dubinin-Radushkevich (D-R) equation is obtained by setting n = 2 in Equation (3.8) above[63]:

$$V = V_0 \exp\left\{-\left(\frac{RT}{\beta E_0}\ln\frac{P_0}{P}\right)^2\right\} \tag{3.9}$$

where V is the adsorbed volume, V_0 is the micropore saturation volume corresponding to the saturated pressure P_0, n is a structural-heterogeneity parameter, β is an affinity coefficient and E_0 is the characteristic heat of adsorption of the adsorbed molecule. A range of 1-4 has been reported for 'n'[60], and the values of β have also been compiled for a number of adsorbates.[69]

The Dubinin's pore-filling models are pure-component isotherm models and, thus, require a mixture theory like the IAS theory to be extended to mixture adsorption. Several authors have used the pore-filling models and found them to be superior to the Langmuir model. Clarkson and Bustin[30] used the IAS theory and pore-filling models and compared them with the extended Langmuir model. They found the IAS/D-A model to perform better than the IAS/D-R, IAS/Langmuir and extended Langmuir models.

However, they found that none of these models was able to describe accurately the selectivity of the adsorbates and yielded either a constant selectivity (extended Langmuir) or an increasing selectivity with increasing feed composition of the larger adsorbing gas (IAS/D-R equation), both of which did not agree with their experimental data. Similarly, Harpalani et al.[70] modeled data for adsorption isotherms with the Langmuir, D-R and D-A equations and found the D-A equation to be superior to the other two models.

An important aspect of the D-A equation is the temperature-invariance of the characteristic plots ($RT\ln\frac{P_0}{P}$ vs. V). This feature can be used to predict adsorption at different temperatures based on data from a single isotherm. This capability notwithstanding, the pore-filling models are, however, developed for sub-critical adsorbates. Specifically, these models require the saturation pressure, P_0, of the respective isotherms. As such, an empirical modification is introduced when using a pore-filling model for CBM systems, which involve mostly near-critical and supercritical adsorbates. Although, a variety of modifications have been proposed[60, 71], there appears to be little theoretical justification behind them.

Coal Swelling

Another aspect of high-pressure gas adsorption behavior in coalbeds is the *potential* swelling of coal caused by adsorbates such as CO_2. Some investigators believe that adsorption of CO_2 can significantly alter the porous coal structure and these changes, if left unaccounted for, can result in large errors in the modeling of supercritical CO_2 adsorption on coals. In fact, several researchers have attempted to model the swelling of coal by incorporating volumetric corrections to the adsorption isotherm equations. Ozdemir et al.[46] used a variety of adsorption models, including the D-A model, to study

the volumetric effects of CO_2 adsorption on coals. Similarly, Dutta et al.[47] used the Langmuir and D-A models to account for the swelling of coal and dissolution of CO_2 in the coal matrix. Romanov et al.[48] have also attempted to interpret the volumetric changes in coals under CO_2 pressure. More recently, Pan and Connell[49], balancing the change in surface energy due to adsorption to the change in elastic energy of the coal matrix, developed a theoretical model to describe adsorption-induced coal swelling.

3.2 Theory-Based Equilibrium Adsorption Models

Beyond sound theoretical framing of the adsorption model, several desired attributes are sought when modeling CBM systems, including the model's ability to:

1. Correlate pure- and mixed-gas adsorption data within the experimental uncertainties at reservoir conditions
2. Facilitate *generalized* predictions of pure-gas isotherms based on accessible coal characterization and gas properties
3. Predict the individual component and the total adsorption of a multicomponent gas mixture based on pure-gas isotherms or pure-fluid model generalization
4. Account rigorously for the presence of moisture in the coal

Although, the traditional adsorption models described above have been used in CBM-related work, they lack some of these desired attributes. Moreover, they seem to lack the theoretical rigor of a multicomponent adsorption model that is needed in CBM work. In previous works at OSU[8, 12], researchers have tested three theory-based adsorption models for their CBM adsorption modeling capabilities. Although based on very different theoretical basis, the two-dimensional equation-of-state, the Ono-Kondo, and the simplified local-density models were found to be readily amenable to the modeling

demands of CBM systems.[8, 12] Following is a brief description of these three models that have been found useful in CBM-related work.

Two-Dimensional Equations of State

The two-dimensional (2-D) equations-of-state (EOS) models are essentially analogs of the 3-D EOS models used in vapor-liquid equilibria calculations. One of the main incentives in developing the 2-D EOS models is their potential for direct implementation in CBM simulations in a manner similar to 3-D EOS models used in conventional oil and gas reservoir simulations.

The 2-D EOS models offer several advantages. Specifically, they[17]:

1. Permit simultaneous calculation of equilibrium adsorption and volumetric properties
2. Are particularly suitable for extending pure-gas adsorption isotherms to multicomponent mixture predictions, using appropriate mixing rules
3. Are amenable to model-parameter generalization
4. Utilize a proven, familiar model format for use in reservoir simulations.

The assumptions used in developing the 2-D EOS models include[16]:

1. The adsorbent surface can be treated as a two-dimensional, imaginary mathematical surface; and this 2-D phase possesses its own thermodynamic properties
2. The adsorbent is thermodynamically inert.
3. The adsorbent provides a temperature-invariant surface area, which is accessible equally to all the adsorbate molecules.

4. The adsorbent surface is homotattic, i.e., it is made up of many homogeneous sub-regions.

As mentioned earlier, the 2-D EOS was developed by analogy to the 3-D cubic EOS. A generalized form of the cubic 3-D EOS used in vapor-liquid equilibrium calculations can be written as:

$$\left[p + \frac{a\rho^2}{1 + Ub\rho + W(b\rho)^2} \right]\left[1 - b\rho\right] = \rho RT \tag{3.10}$$

where a and b are the EOS parameters and values of U and W are specified to give various forms of 3-D EOS. The 2-D EOS is obtained simply by replacing two terms in the 3-D EOS - the bulk pressure, P, with the spreading pressure, π, and the bulk density, ρ, with the specific surface density, σ.

The generalized 2-D analog of the 3-D EOS, then, is given as:

$$\left[\pi + \frac{a_2\sigma^2}{1 + Ub_2\sigma + W(b_2\sigma)^2} \right]\left[1 - (b_2\sigma)^m\right] = \sigma RT \tag{3.11}$$

or $$\left[A\pi + \frac{\alpha\omega^2}{1 + U\beta\omega + W(\beta\omega)^2} \right]\left[1 - (\beta\omega)^m\right] = \omega RT \tag{3.12}$$

where A is the specific surface area of the adsorbent, π is the spreading pressure, σ is the surface density of the adsorbate, $\omega = \sigma A$ is the specific amount adsorbed, $\alpha = a_2/A$ and $\beta = b_2/A$ are the 2-D EOS model parameters and m is an additional parameter used to provide more flexibility to the model.[17] The model coefficients, U, W, and m are specified to obtain a particular form of the 2-D EOS. For example, a 2-D analog of the 3-D van der Waals (VDW) EOS is obtained by setting m = 1 and U = W = 0; similarly for the Soave-Redlich-Kwong (SRK) (m = U = 1 and W = 0); the Peng-Robinson (PR) (m =

1, U = 2, and W = -1); the Eyring (m = 1/2 and U = W = 0) EOS; and the Zhou-Gasem-Robinson (ZGR) (m = 1/3 and U = W = 0) EOS.[17]

Equilibrium Relations for Two-Dimensional EOS

The governing equations for adsorption equilibrium are entirely independent of the equation of state used in the model. At equilibrium, the chemical potential of specie *i* in the gas phase is equal to that in the adsorbed phase (see, e.g., Zhou et al.[17]):

$$\mu_i^a = \mu_i^g \text{ and } d\mu_i^a = d\mu_i^g \tag{3.13}$$

$$\int_{\pi^*}^{\pi} d\ln f_i^a = \int_{P^*}^{P} d\ln f_i^g \tag{3.14}$$

where μ_i is the component chemical potential, π^* is the spreading pressure at the standard conditions, f_i^a and f_i^g are the component fugacities in the adsorbed phase and the gas phase, respectively. Integrating Equation (3.14):

$$\ln f_i^a(\pi) - \ln f_i^a(\pi^*) = \ln f_i^g(P) - \ln f_i^g(P^*) \tag{3.15}$$

At very low pressure, P_i^*, $f_i^a(\pi^*) = \pi_i^*$ and $f_i^g(P^*) = P_i^*$.

Thus,

$$P_i^* f_i^a(\pi) = \pi_i^* f_i^g(P) \tag{3.16}$$

At very low pressure, the 2-D ideal gas law is obtained:

$$\pi_i^* A = \omega_i^* RT \tag{3.17}$$

where T is temperature, R is the universal gas constant, and ω_i^* is the amount adsorbed at low pressures. Further, the Henry's constant k_i can be defined as:

$$k_i = \frac{\omega_i^*}{P_i^*} \tag{3.18}$$

Therefore,

$$A\hat{f}_i^a = Ax_i\pi\hat{\phi}_i^a = k_i RT\hat{f}_i^g \tag{3.19}$$

For pure-gas adsorption, the equilibrium relation is given by:

$$\omega Z_a \varphi^a = k_i f^g \tag{3.20}$$

where ω is the amount adsorbed, Z_a is the 2-D compressibility factor, ϕ^a is the fugacity coefficient using the 2-D EOS, f^g is the fugacity for the gas phase.

The fugacity for the 2-D EOS is given by:

$$\ln\hat{\phi}_i^a = \int_0^{\omega}\left[\frac{1}{RT\omega}\frac{\partial(A\pi)}{\partial\omega_i}\bigg|_{T,M_s,n_j} - \frac{1}{\omega}\right]d\omega - \ln Z_a \tag{3.21}$$

where A is the specific surface area and M_s is the mass of the adsorbent. As evident from the above relations, the 2-D EOS enters the calculation through the fugacities and the 2-D compressibility factor. To perform adsorption equilibrium calculations using Equation (3.20) requires the values of $\alpha, \beta,$ and k. They are determined normally by direct regression of adsorption isotherm data. As such, the 2-D EOS is a three-parameter adsorption model.

Several researchers have utilized the 2-D EOS theory to model gas adsorption. Hill[72] and de Boer[73] used the van der Waals (VDW) EOS to correlate pure-gas adsorption. Hoory and Prausnitz[74] extended the 2-D VDW EOS to mixtures by introducing mixing rules. DeGance[16] applied the 2-D virial and Eyring EOS to correlate high-pressure pure gas adsorption isotherms. Zhou et al.[17] used the 2-D EOS model to describe pure- and mixed-gas adsorption on different adsorbents. Pan[18] introduced Gibbs-Free energy mixing rules into the 2-D EOS and developed temperature dependence relations for the 2-D model parameters.

Ono-Kondo Lattice Model

The Ono-Kondo (OK) adsorption model is based on lattice theory and was first proposed by Ono and Kondo.[19] Since then, Aranovich and Donohue[75-77] have generalized the model expressions for application to the adsorption of solutes in liquid solutions. Sudibandriyo[20] generalized the OK model parameters, extended the model to mixture adsorption of CBM systems and developed the temperature dependence relations for the model parameters.

Key features of the Ono-Kondo model include its ability to:

1. Provide a layering analogue to adsorption
2. Generate independent estimates for the adsorbed-phase densities
3. Incorporate accurate user-provided density estimates, which may reduce the correlative burden of the adsorption modeling.
4. Utilize the pure-gas adsorption isotherms to predict mixture adsorption without the use of binary interaction parameters

The assumptions used in developing the lattice Ono-Kondo model are (see, e.g., Sudibandriyo[20]):

1. The fluid system is composed of one or more layers of lattice cells containing fluid molecules and vacancies.
2. Molecular interactions exist only between the nearest neighboring molecules, i.e. in the adjacent lattice cells.
3. Adsorption equilibrium between the adsorbed layers and the bulk lattice gas is given by the equality of the chemical potential in each layer and the bulk gas.

For an adsorptive system, more fluid molecules would reside in the cells of the adsorbed-phase layers than in the cells of the bulk-phase layers due to the molecular interactions with the adsorbent surface. The OK model expression for the thermodynamic equilibrium between the gas-phase and a multi-layer adsorbed-phase is given as[75]:

$$\ln\left[x_t(1-x_b)/x_b(1-x_t)\right] + z_0(x_t - x_b)\varepsilon_{ii}/kT + (x_{t+1} - 2x_t + x_{t-1})\varepsilon_{ii}/kT = 0$$

$$\text{and } t = 1, 2, 3\ldots \tag{3.22}$$

where t represents the number of layers. For the first layer,

$$\ln\left[x_1(1-x_b)/x_b(1-x_1)\right] + (z_1x_1 + x_2 - z_0x_b)\varepsilon_{ii}/kT + \varepsilon_{is}/kT = 0 \tag{3.23}$$

where x_t is the reduced density or fraction of sites occupied by adsorbed molecules in layer t, and x_b is the fraction of sites occupied by fluid molecules in the bulk, z_0 and z_1 are the coordination numbers of the lattice cells, ε_{ii}/kT is the fluid-fluid interaction energy parameter, ε_{is}/kT is the fluid-solid interaction energy parameter, k is Boltzmann's constant and T is the absolute temperature. For a hexagonal lattice, the coordination numbers z_0 and z_1 are 6 and 4, respectively.

The Gibbs excess adsorption, Γ, in the OK model is given as:

$$\Gamma = C\sum_{t}^{m}(x_t - x_b) \tag{3.24}$$

where C is known as a "pre-factor," which is related to the capacity of the adsorbent for a specific adsorbate. The index m is the number of layers for the adsorption isotherm and is typically determined from the best description of the adsorption data. The reduced densities x_i and x_b can be expressed as $x_i = \rho_i/\rho_{mc}$ and $x_b = \rho_b/\rho_{mc}$, where ρ_i and ρ_b are the adsorbed and the bulk density of the adsorbate, respectively and ρ_{mc} is the maximum adsorbed-phase density. The maximum adsorbed-phase density, ρ_{mc}, can be estimated in

various ways. Two of the common ways of estimating the adsorbed-phase density are to use the saturated liquid density at atmospheric pressure[51] or the inverse of the VDW covolume.[8] Further, Hocker and Donohue[78] have used a theoretical value of the density of close-packed molecules.

Although the OK model allows for the formation of multiple layers, a monolayer has been shown to provide a satisfactory description of the adsorption data.[20] In the monolayer OK model, the adsorbed molecules are directly mapped onto parallel graphite planes, as shown in Figure 3.1. Further, when a 2D-hexagonal configuration is chosen, the thermodynamic equilibrium expression of Equation (3.22) simplifies as:

$$\ln\left[x_{ads}(1-x_b)/x_b(1-x_{ads})\right]+((z_1+1)x_{ads}-z_0x_b)\varepsilon_{ii}/kT+\varepsilon_{is}/kT=0 \qquad (3.25)$$

Therefore, the Gibbs excess adsorption expression for the monolayer OK model becomes:

$$\Gamma = 2C\ (x_{ads}-x_b) = 2C\left(\frac{\rho_{ads}}{\rho_{mc}}-\frac{\rho_b}{\rho_{mc}}\right) \qquad (3.26)$$

where ρ_{ads} is the adsorbed-phase density.

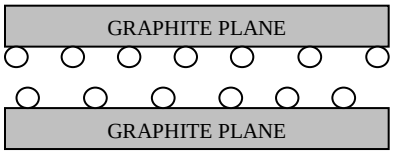

Figure 3.1 Ono-Kondo Model for Monolayer Adsorption on Graphite Slit (Slit Depiction Adopted from Sudibandriyo[20])

The OK model thus has four parameters: ρ_{mc}, ε_{ii}/k, ε_{is}/k and C. Two of these parameters can be estimated independently. Specifically, ρ_{mc} is estimated to be the inverse of the VDW covolume and ε_{ii}/k can be evaluated as[20]:

$$\varepsilon_{ii} = 0.432\varepsilon^* \qquad (3.27)$$

where ε^* is the well depth of the 12-6 Lennard-Jones potential. These assumptions yield the two-parameter (C and ε_{is}/k) OK model.

Simplified Local-Density/Peng-Robinson (SLD-PR) Model

The SLD model is a simplification of the more computationally-intensive local-density theory. According to this theory, the density profile is obtained by minimizing the total energy function, which depends on all point densities and their spatial derivatives.[79] The SLD model, thus, uses mean-field theory in calculating the chemical potential. In other words, the local fluctuations arising out of gradients in density are not considered in the micropores, where the majority of adsorption takes place. Further, the chemical potential of the fluid at each point is corrected for the proximity of the fluid molecule to the molecular wall of the adsorbent.[25]

The SLD model partitions the interactions of a gas molecule in the adsorbed phase into fluid-solid and fluid-fluid interactions. The fluid-solid interactions are modeled through a potential function such as the 10-4 Lee's potential[80] whereas the fluid-fluid interactions are modeled through a modified 3-D EOS.[81] Specifically, the attractive parameter in the EOS is modified to account for the presence of the adsorbent wall.

Several advantages distinguish the SLD framework. In particular, the model:

1. Provides a consistent framework that accounts for adsorbate-adsorbate (fluid-fluid) and adsorbate-adsorbent (fluid-solid) molecular interactions
2. Delineates the adsorbent structural properties based on well-described physical geometries of the adsorbent and
3. Predicts the adsorbed-phase density which facilitates prediction of absolute gas adsorption.

4. Offers the opportunity for model generalizations using molecular descriptors
5. Predicts the mixture-adsorption based solely on pure-gas isotherms or pure-fluid generalization

A number of assumptions have been used in developing the SLD model[22]:

1. The chemical potential at any point near the adsorbent surface is equal to the bulk phase chemical potential.
2. The chemical potential at any point above the surface is the sum of the fluid-fluid and fluid-solid interactions.
3. The attractive potential between fluid and solid at a point is independent of the number of molecules at and around that point.

Different geometries such as rectangular slits[8, 81], cylindrical pores[82], flat surfaces[8], etc. can be used to model the porous adsorbent structure. Using the slit geometry, the SLD model assumes the adsorbate molecules reside within a two-surface rectangular-shaped slit. The distance between the slit surfaces is L and the position of a molecule within the slit is z. The position, z, is orthogonal to the solid surface formed by the carbon atoms on the slit wall.

Therefore, the chemical potential of the fluid, μ, is expressed as the sum of the fluid-fluid and fluid-solid potentials at a position, z. At equilibrium:

$$\mu(z) = \mu_{ff}(z) + \mu_{fs}(z) = \mu_{bulk} \tag{3.28}$$

where subscripts "bulk", "ff" and "fs" refer to bulk fluid, fluid-fluid interactions, and fluid-solid interactions, respectively.

The chemical potential of the bulk fluid is expressed in terms of fugacity as:

$$\mu_{bulk} = \mu_0(T) + RT\ln\left(f_{bulk}/f_0\right) \tag{3.29}$$

where f is the fugacity, and μ_0 is the chemical potential at the reference state.

By analogy, the chemical potential from fluid-fluid interactions is written as:

$$\mu_{ff}(z) = \mu_0(T) + RT\ln\left(f_{ff}(z)/f_0\right) \tag{3.30}$$

where $f_{ff}(z)$ is the adsorbed fluid fugacity at a position z, and μ_0 is the chemical potential at the same reference state as in Equation (3.29). As mentioned above, the fluid-solid interactions are accounted for through a fluid-solid potential function. As such, the fluid-solid chemical potential, μ_{fs}, is given as:

$$\mu_{fs}(z) = N_A\left[\Psi^{fs}(z) + \Psi^{fs}(L - z)\right] \tag{3.31}$$

where $\Psi(z)$ and $\Psi(L-z)$ are the fluid-solid interactions from the two walls of a slit of length L, and N_A is the Avogadro's number.

Substituting Equations (3.29), (3.30) and (3.31) into Equation (3.28) yields the SLD equilibrium relationship for modeling adsorption within the slit:

$$f_{ff}(z) = f_{bulk}\exp\left(-\frac{\Psi^{fs}(z) + \Psi^{fs}(L-z)}{kT}\right) \tag{3.32}$$

where k is the Boltzmann's constant.

In Equation (3.32), Lee's partially-integrated 10-4 potential[80] is used to provide the fluid-solid interaction information, $\Psi^{fs}(z)$[22, 81]:

$$\Psi^{fs}(z) = 4\pi\rho_{atoms}\varepsilon_{fs}\sigma_{fs}^2\left(\frac{\sigma_{fs}^{10}}{5(z')^{10}} - \frac{1}{2}\sum_{i=1}^{4}\frac{\sigma_{fs}^4}{(z'+(i-1)\cdot\sigma_{ss})^4}\right) \tag{3.33}$$

$$\varepsilon_{fs} = \sqrt{\varepsilon_{ff}\times\varepsilon_{ss}} \tag{3.34}$$

where ε_{fs} is the fluid-solid interaction energy parameter, ρ_{atoms} = 0.382 atoms/Å^2 and z' is the center-center distance between fluid molecules and carbon atoms in the first plane.

The parameters σ_{ff} and σ_{ss} represent, respectively, the molecular diameter of the adsorbate and the carbon interplanar distances.

The excess adsorption (n^{Ex}), when applying the SLD model, is given as:

$$n^{Ex} = \frac{A}{2} \int_{\text{Left Side of Slit}}^{\text{Right Side of Slit}} (\rho(z) - \rho_{bulk}) dz \tag{3.35}$$

where n^{Ex} is the excess adsorption and A is the accessible surface area for the gas on a particular adsorbent. The left and right sides of the slit each comprise half of the total surface area, A/2. Thus, the excess adsorption can be calculated by numerical integration of Equation (3.35). Thus, the optimized parameters in the SLD model typically include the surface area A for each fluid, solid-solid interaction energy parameter ε_{ss}/K and the slit length L.[12]

The SLD model was developed by Rangarajan et al.[22] who used the van der Waals EOS to provide the fluid-fluid interaction information. Any EOS with appropriate modifications can be used within the SLD framework. In fact, over the years, researchers have used different EOSs such as the Peng-Robinson, Bender and Elliot-Suresh-Donohue (ESD) EOSs within the SLD framework to provide the fluid-fluid interaction information.[23, 24, 26, 81] Fitzgerald[25] used the SLD model with a modified Peng-Robinson (PR) EOS[83] to study the high-pressure adsorption of coalbed gases and their mixtures on dry and wet coals and activated carbons.

Further, the SLD model is capable of accounting for swelling of coal by varying the slit length with pressure. However, the modeling results obtained at OSU for high-pressure adsorption systems without the use of coal swelling were found to be satisfactory; therefore, to date, the inclusion of this effect could not be justified.

Gibbs and Absolute Adsorption

Adsorption data can be reported either in terms of Gibbs or absolute adsorption. Gibbs adsorption is calculated directly from experimentally-measured quantities and this accounts for the fact that there is additional material present near the adsorbent surface due to adsorption phenomenon. This additional material is *in excess* of that which would be present in the same (void) volume if there was no adsorption. This excess material is usually referred to as the Gibbs or excess adsorption. In contrast, the calculation of absolute adsorption requires knowledge of the adsorbed phase density, ρ_{ads}, which is not readily accessible by experimental measurement.

The exact mathematical expressions that highlight the physical interpretation of Gibbs adsorption and the approximate nature of calculated absolute adsorption have been presented elsewhere.[7] The relationship between the two quantities is given as

$$n_{ads}^{Abs} = n_{ads}^{Gibbs}\left(\frac{\rho_{ads}}{\rho_{ads} - \rho_{gas}}\right) \tag{3.39}$$

where n_{ads}^{Abs} and n_{ads}^{Gibbs} are the absolute and Gibbs adsorption, respectively, and ρ_{gas} and ρ_{ads} are the gas phase and the adsorbed phase densities, respectively. To calculate absolute adsorption from Equation (3.39), estimates of ρ_{ads} must be employed. A commonly used approximation for ρ_{ads} is the liquid density at the normal boiling point (as was done by Arri and Yee[51]) or the reciprocal of the VDW co-volume.[8]

3.3 Example Studies of Adsorption Modeling

In this section, the modeling capability of the 2-D EOS, OK and SLD-PR models as they apply to CBM systems is demonstrated. Specifically, the correlation capabilities of these models for pure-gas adsorption on dry and wet coals are illustrated. Several other

capabilities of these models that were demonstrated in earlier OSU studies have also been highlighted. Further, the generalization capabilities of these models are reviewed in Chapter 6. In particular, the coal structure-based generalization of SLD model is covered in Chapter 6, along with a review of other generalization efforts in the literature.

Statistical Quantities Used

In the results presented here, the sum of the squared weighted deviations, expressed in terms of the weighted root mean square, WRMS, was used for the objective function:

$$\mathrm{WRMS} = \sqrt{\frac{\sum_{i=1}^{\mathrm{NPTS}} \left(\frac{n_{\mathrm{calc}} - n_{\mathrm{exp}}}{\sigma_{\mathrm{exp}}} \right)_i^2}{\mathrm{NPTS}}} \tag{3.40}$$

where NPTS is the number of data points, n_{exp} is the experimental excess adsorption, n_{calc} is the calculated excess adsorption and σ_{exp} is the expected experimental uncertainty. In addition, the results were analyzed in terms of the average absolute percentage deviation (%AAD), the root mean square error (RMSE) and weighted average absolute deviation (WAAD):

$$\%\mathrm{AAD} = \frac{\sum_{i=1}^{\mathrm{NPTS}} \mathrm{abs}\left(\frac{n_{\mathrm{calc}} - n_{\mathrm{exp}}}{n_{\mathrm{exp}}} \right)_i}{\mathrm{NPTS}} \times 100\% \tag{3.41}$$

$$\mathrm{RMSE} = \sqrt{\frac{\sum_{i=1}^{\mathrm{NPTS}} \left(n_{\mathrm{calc}} - n_{\mathrm{exp}} \right)_i^2}{\mathrm{NPTS}}} \tag{3.42}$$

$$\mathrm{WAAD} = \frac{\sum_{i=1}^{\mathrm{NPTS}} \mathrm{abs}\left(\frac{n_{\mathrm{calc}} - n_{\mathrm{exp}}}{\sigma_{\mathrm{exp}}} \right)}{\mathrm{NPTS}} \tag{3.43}$$

Modeling Discussion

Correlation of Pure-Gas Adsorption on Dry and Wet Coals

The prediction of adsorption isotherms of pure methane, nitrogen and CO_2 on five dry coals and the adsorption isotherms of pure CO_2 on five wet coals are used to demonstrate the correlative abilities of the 2-D EOS, OK and SLD models. Each of these three models was used to represent the adsorption data on these coals. Table 3.1 lists the regressed parameters for the 2-D EOS, OK and SLD-PR models for each coal. Three parameters (α, β, and k) were regressed for the 2-D EOS model, two (ε_{fs}/k and C) for the OK model and three (surface area, ε_{ss}/k and L) for the SLD model. Further, the SLD parameter "L" was fixed at 1.15 nm. for the modeling on wet coals since there were data for only one gas on the wet coals.

Table 3.2 lists the summary statistics obtained for the three models on these coals. The overall WAAD for the five dry coals was 0.3, 0.4 and 0.5 for the 2-D EOS, OK and SLD models, respectively. In comparison, the overall WAAD for the five wet coals was 0.5, 0.3 and 0.5 for the 2-D EOS, OK and SLD models, respectively. Further, the overall %AAD for the five dry coals was 1.9%, 2.6% and 3.1% for the 2-D EOS, OK and SLD models, respectively. The corresponding statistics for the five wet coals were 7.9%, 6.5% and 5.4%, respectively. Thus, the three models were capable of correlating the pure-gas adsorption data on dry and wet coals within the experimental uncertainties.

Figures 3.2 to 3.6 present the model representation results obtained with the three models for the adsorption of methane, nitrogen and CO_2 on dry Illinois #6, dry Beulah Zap, dry Wyodak, dry Upper Freeport and dry Pocahontas coals, respectively. In general, the adsorption of CO_2 was correlated less precisely than adsorption of methane and

Table 3.1 Regressed Model Parameters for Representations of Pure-Gas Adsorption on Dry and Wet Coals

Coal	Gas	2-D PR EOS			Ono Kondo		SLD		
		α (bar cm^3 g/mmol / mol)	β $(mmol/g)^{-1}$	-ln k (mmol/g bar^{-1})	$\varepsilon_{fs/k}$ (K)	C (mmol/gm)	SA (m^2/gm)	L (nm)	ε_{ss}/k (K)
Dry Illinois -6	CH4	-18687.0	0.1268	3.1706	-920	0.81	60.50	1.34	30.32
	N2	-29997.0	0.2310	4.2612	-740	0.49	44.13		
	CO2	-8118.4	0.0545	2.1927	-1235	1.24	77.41		
Dry Beulah Zap	CH4	-34893.0	0.1794	2.6373	-1100	0.59	49.80	1.30	37.44
	N2	-45040.0	0.5448	4.0661	-880	0.34	34.76		
	CO2	-1599.6	0.6832	-2.5191	-1350	1.36	92.96		
Dry Wyodak	CH4	-26203.0	0.1561	2.8838	-990	0.71	56.95	1.32	31.52
	N2	-34602.0	0.2493	4.1342	-760	0.47	43.83		
	CO2	-4698.1	1.2698	-3.0130	-1250	1.49	96.27		
Dry Upper Freeport	CH4	-41306.0	0.2090	2.5948	-1140	0.52	47.10	1.18	37.20
	N2	-36845.0	0.4425	4.2939	-850	0.35	35.06		
	CO2	-26766.0	0.1281	1.7306	-1470	0.67	54.10		
Dry Pocahontas	CH4	-27464.0	0.2856	2.3489	-1210	0.65	63.05	1.15	36.83
	N2	-17684.0	0.5328	4.0695	-860	0.46	46.84		
	CO2	-23442.0	0.0997	1.3120	-1510	0.84	69.53		
Wet Illinois -6	CO2	-6615.9	0.0638	3.4702	-950	0.84	63.56	1.15	10.89
Wet Beulah Zap	CO2	16662.0	0.8225	4.1710	-1060	0.35	26.72	1.15	14.65
Wet Wyodak	CO2	24053.0	0.4943	4.7286	-670	0.63	41.78	1.15	6.48
Wet Upper Freeport	CO2	-24351.0	0.1426	2.3387	-1310	0.63	51.97	1.15	22.46
Wet Pocahontas	CO2	-20618.0	0.1008	2.1564	-1370	0.72	60.59	1.15	24.83

Table 3.2 Sample Results for Model Representations of Pure-Gas Adsorption on Dry and Wet Coals

Coal	Gas	2-D PR EOS			Ono Kondo			SLD		
		%AAD	RMSE (mmol/g)	WAAD	%AAD	RMSE (mmol/g)	WAAD	%AAD	RMSE (mmol/g)	WAAD
Dry Illinois -6	CH4	3.63	0.0233	0.51	3.56	0.0079	0.47	2.35	0.0133	0.38
	N2	1.43	0.0035	0.12	2.87	0.0053	0.21	4.35	0.0091	0.29
	CO2	3.86	0.0507	0.66	2.20	0.0310	0.32	6.37	0.0868	1.16
Dry Beulah Zap	CH4	1.85	0.0152	0.30	2.85	0.0129	0.37	1.99	0.0125	0.30
	N2	0.40	0.0020	0.04	1.95	0.0035	0.10	6.15	0.0133	0.42
	CO2	2.92	0.0808	0.50	3.40	0.0562	0.65	3.69	0.0604	0.88
Dry Wyodak	CH4	2.37	0.0201	0.42	3.09	0.0137	0.46	1.33	0.0080	0.24
	N2	1.29	0.0053	0.16	3.36	0.0080	0.26	3.45	0.0082	0.25
	CO2	0.77	0.0115	0.25	5.48	0.0993	1.43	5.24	0.0852	1.58
Dry Upper Freeport	CH4	0.43	0.0041	0.11	1.89	0.0062	0.36	1.18	0.0072	0.29
	N2	0.40	0.0012	0.06	1.63	0.0059	0.23	0.88	0.0018	0.09
	CO2	3.91	0.0370	0.49	2.30	0.0222	0.25	3.48	0.0287	0.65
Dry Pocahontas	CH4	0.50	0.0053	0.16	0.88	0.0084	0.24	1.11	0.0100	0.34
	N2	0.33	0.0014	0.06	1.39	0.0065	0.23	0.75	0.0021	0.09
	CO2	4.70	0.0606	0.60	2.75	0.0406	0.39	3.75	0.0430	0.77
Overall	-	**1.9**	**0.022**	**0.3**	**2.6**	**0.022**	**0.4**	**3.1**	**0.026**	**0.5**
Wet Illinois -6	CO2	9.70	0.0798	0.78	1.78	0.0098	0.15	8.84	0.0525	0.98
Wet Beulah Zap	CO2	14.08	0.0372	0.18	7.24	0.0570	0.44	3.60	0.0142	0.37
Wet Wyodak	CO2	3.80	0.0286	0.17	14.73	0.0221	0.34	6.56	0.0224	0.19
Wet Upper Freeport	CO2	7.51	0.0766	0.81	4.69	0.0344	0.37	5.02	0.0380	0.60
Wet Pocahontas	CO2	4.54	0.0524	0.58	3.44	0.0193	0.30	2.77	0.0214	0.59
Overall	-	**7.9**	**0.055**	**0.5**	**6.5**	**0.029**	**0.3**	**5.4**	**0.030**	**0.5**

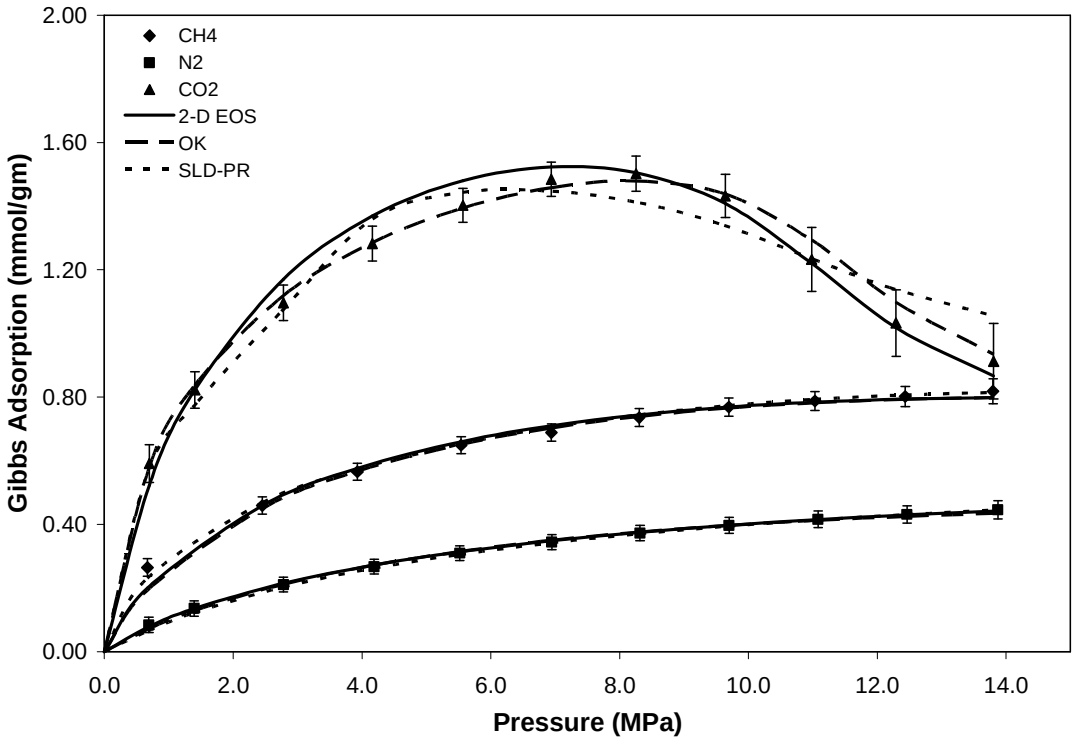

Figure 3.2 Model Representations for the Pure-Gas Adsorption on Dry Illinois-6 Coal at 328 K

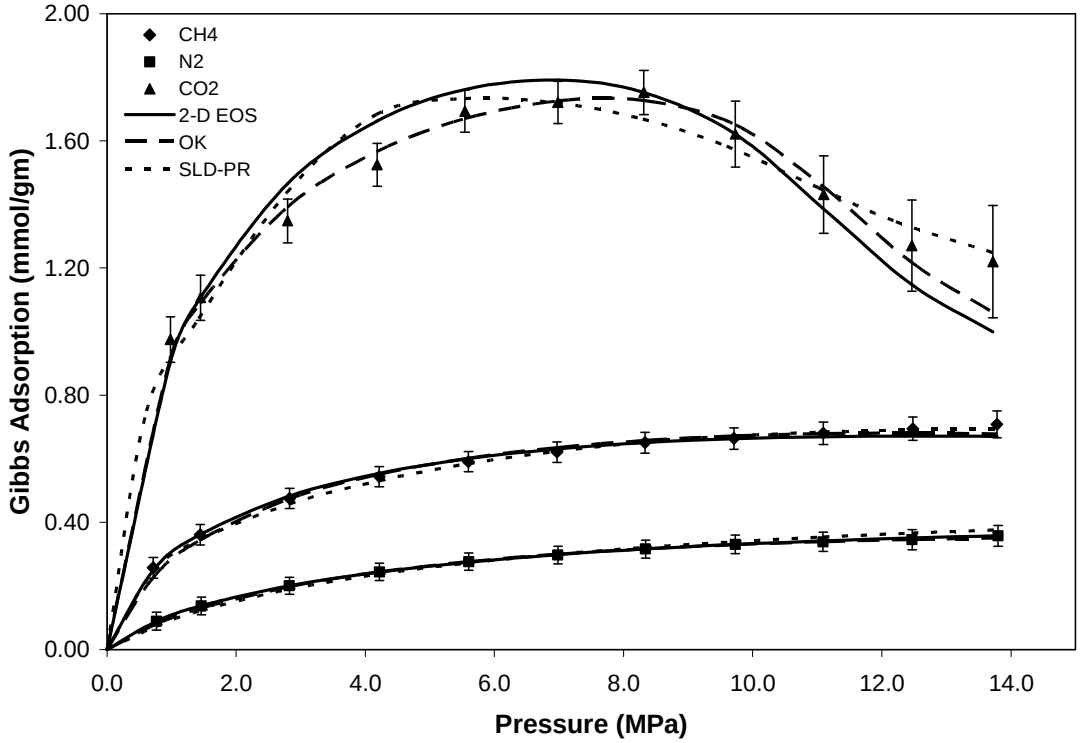

Figure 3.3 Model Representations for the Pure-Gas Adsorption on Dry Beulah Zap Coal at 328 K

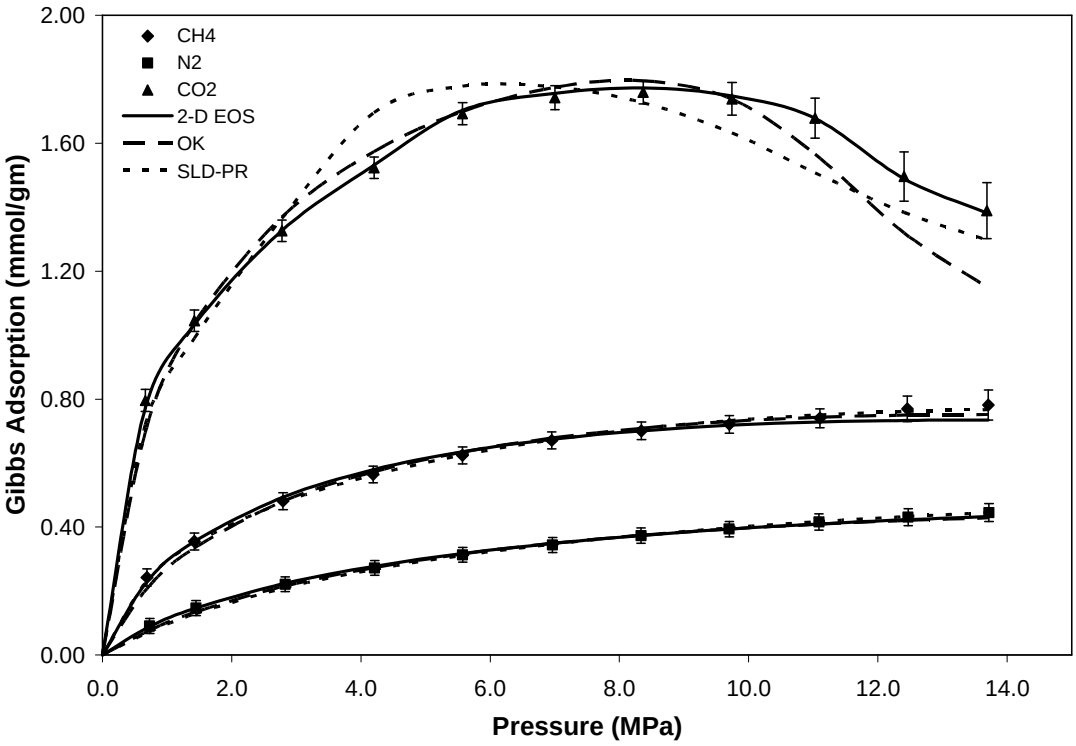

Figure 3.4 Model Representations for the Pure-Gas Adsorption on Dry Wyodak Coal at 328 K

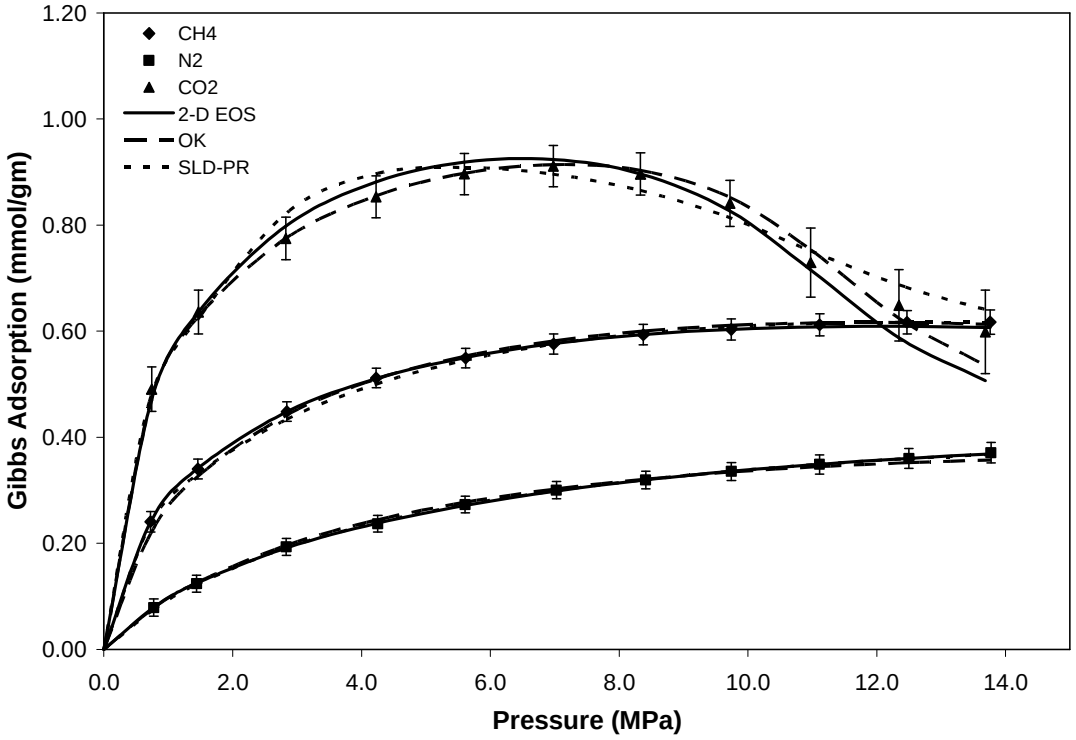

Figure 3.5 Model Representations for the Pure-Gas Adsorption on Dry Upper Freeport Coal at 328 K

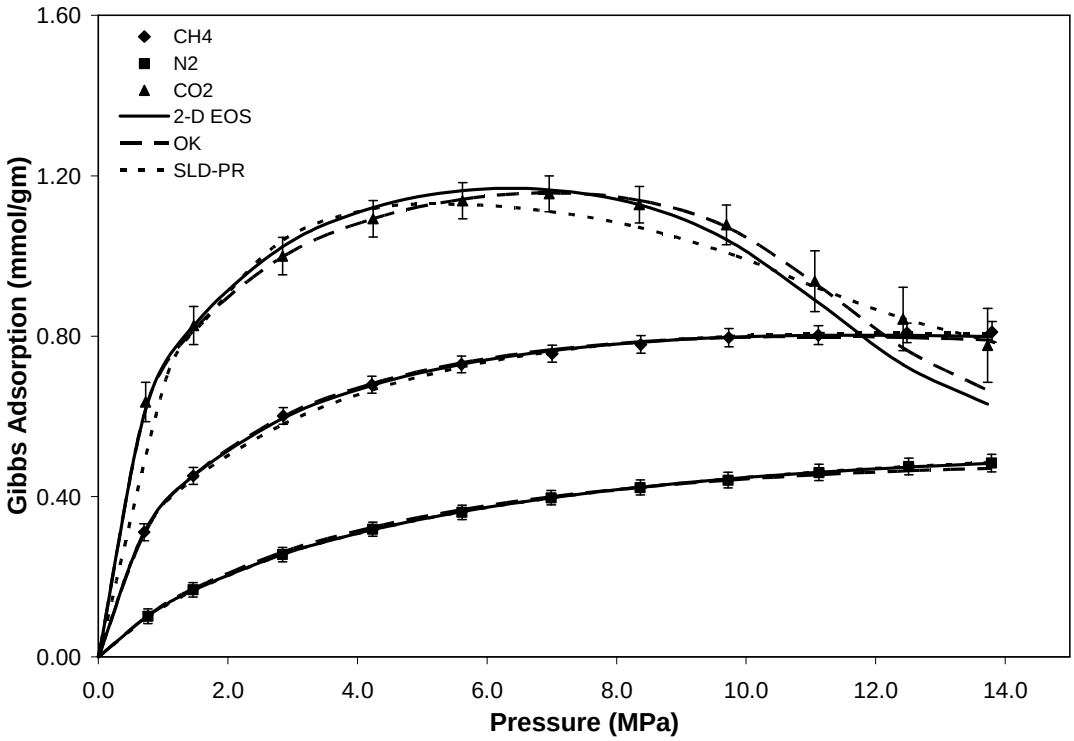

Figure 3.6 Model Representations for the Pure-Gas Adsorption on Dry Pocahontas Coal at 328 K

nitrogen by all three models, as evident from these figures. Similar results were obtained with the three models for CO_2 adsorption on wet coals and these are illustrated in Figures 3.7 to 3.11 for wet Illinois #6, wet Beulah Zap, wet Wyodak, wet Upper Freeport and wet Pocahontas coals, respectively. As evident from these figures, the 2-D EOS model has a tendency to under-predict the adsorption at higher pressures on some wet coals. In particular, the 2-D EOS under-predicts the CO_2 adsorption on wet Illinois #6, Upper Freeport and Pocahontas coals beyond 10 MPa. This could be related to the fact that the adsorbed phase density estimates used in the data reduction for wet coals may well be different from the density estimates on dry coals and activated carbons. Note that among the three models, only the 2-D EOS is expressed in absolute adsorption terms and thus, is prone to errors due to assumptions about the adsorbed phase densities on wet coals.

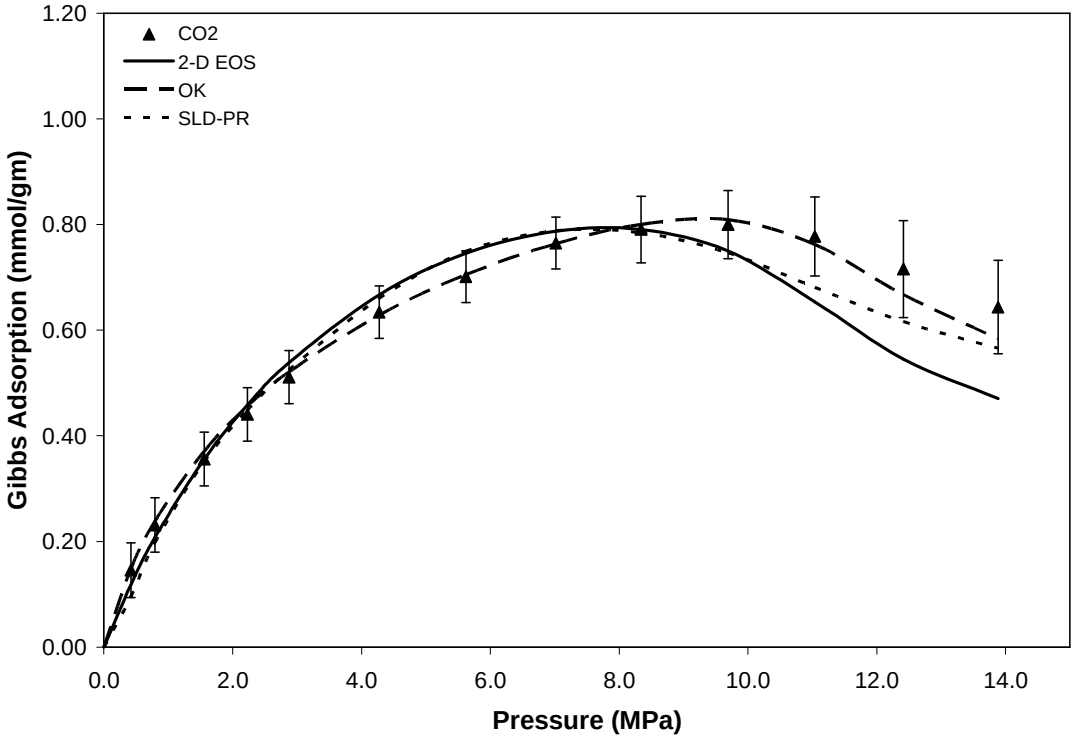

Figure 3.7 Model Representations for the CO_2 Adsorption on Wet Illinois #6 Coal at 328 K

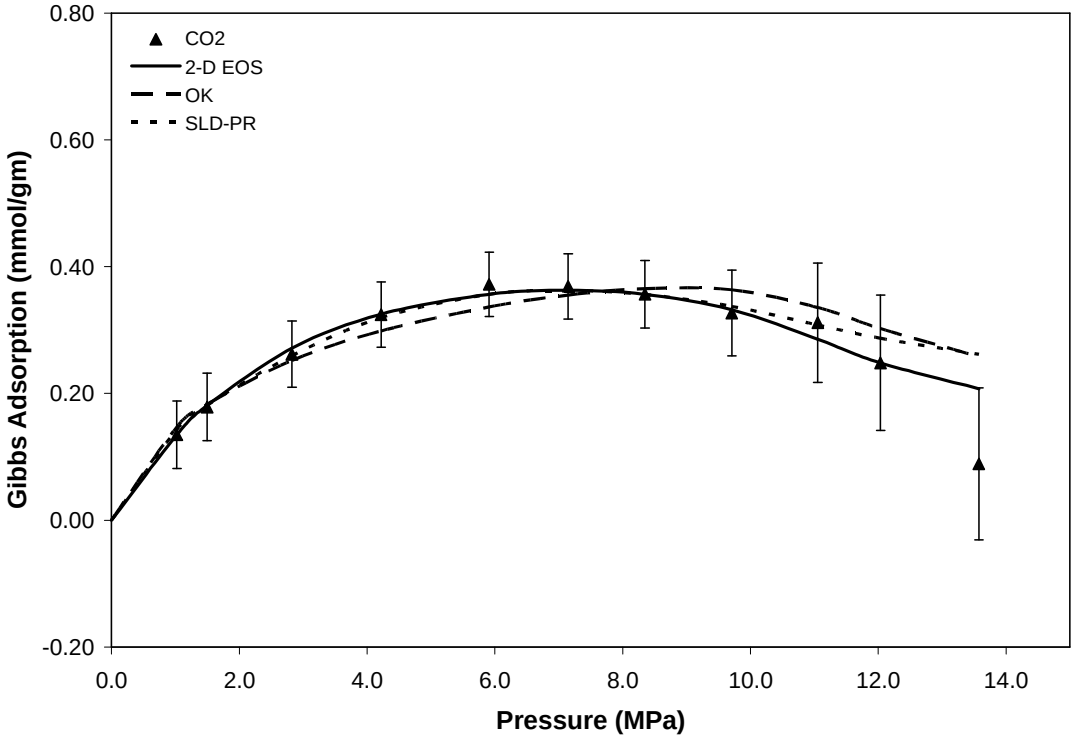

Figure 3.8 Model Representations for the CO_2 Adsorption on Wet Beulah Zap Coal at 328 K

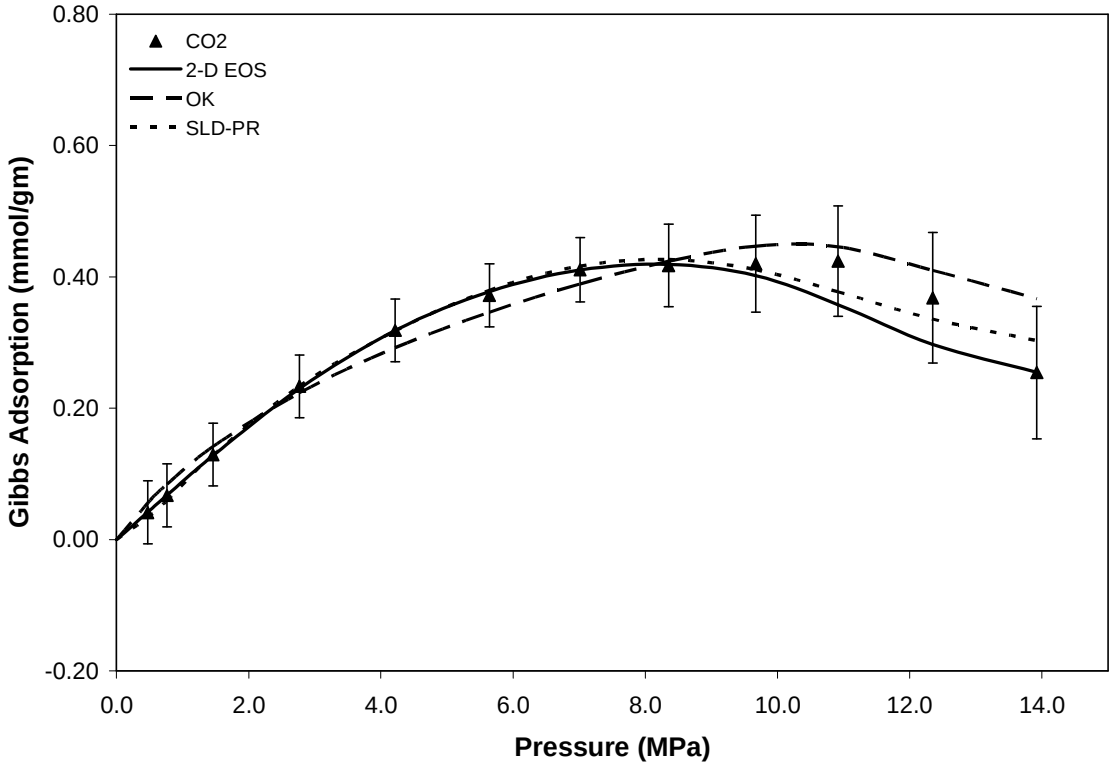

Figure 3.9 Model Representations for the CO_2 Adsorption on Wet Wyodak Coal at 328 K

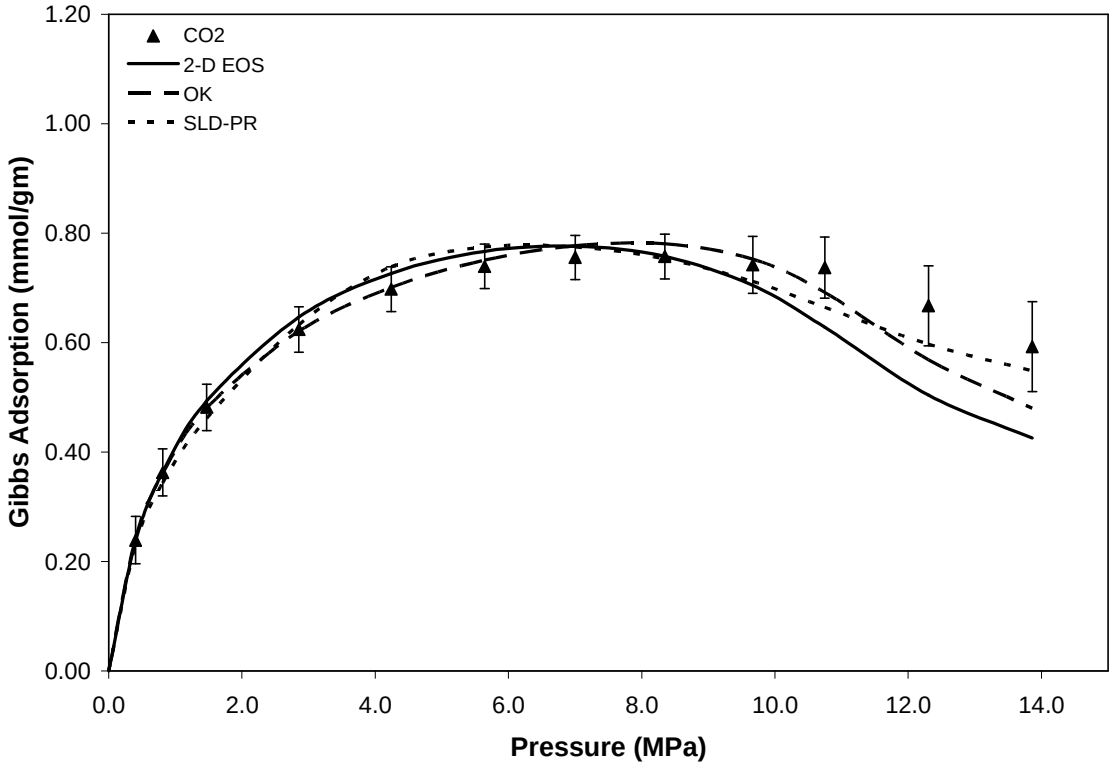

Figure 3.10 Model Representations for the CO_2 Adsorption on Wet Upper Freeport Coal at 328 K

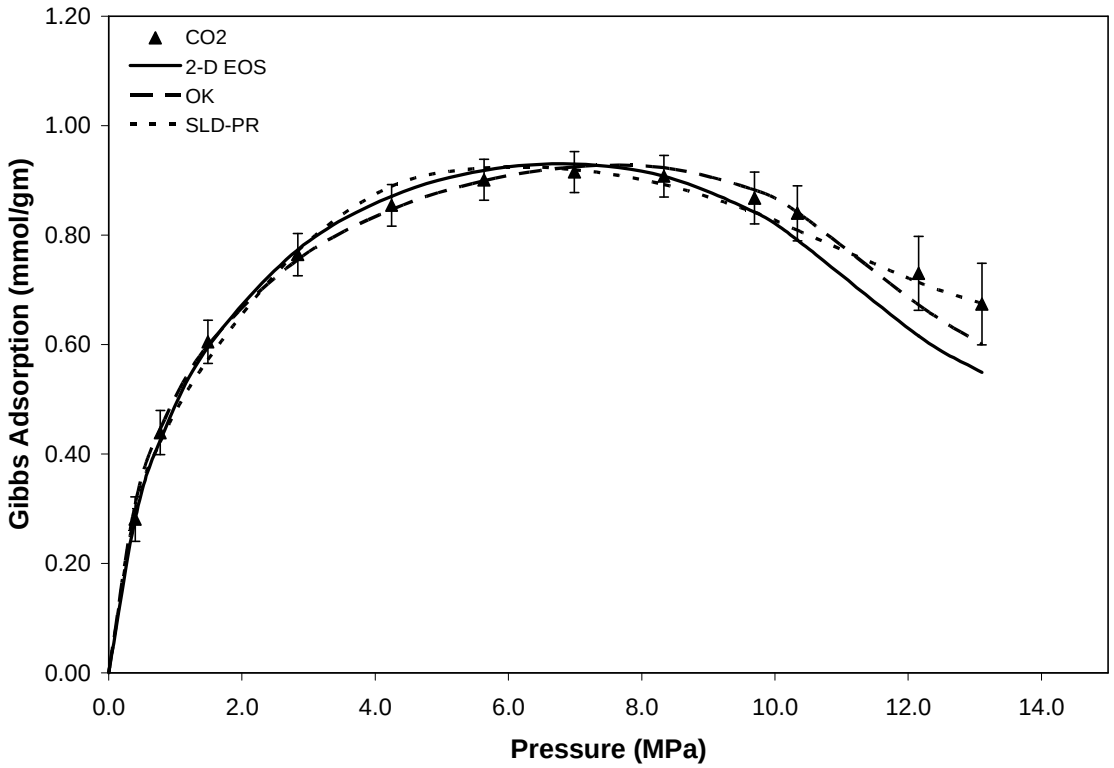

Figure 3.11 Model Representations for the CO_2 Adsorption on Wet Pocahontas Coal at 328 K

Earlier OSU Work with 2-D EOS, OK and SLD Models

Apart from the normal regressions, these models can also be used to predict adsorption at higher pressures from isotherm data at the lower pressures (at the same temperature). Further, these models are capable of using adsorption data from one gas to predict isotherms for other coalbed gases. These *matrix-calibrated* modeling capabilities have demonstrated the distinct advantage of these models over other rudimentary models.[8, 18, 20]

Another advantage of using a theory-based model is its capability to predict multicomponent or mixed-gas adsorption based solely on pure-gas isotherms. This is an important consideration in selecting a CBM adsorption model. Studies involving many coals have affirmed these capabilities in the 2-D EOS, OK and SLD-PR models.[8] In fact,

these models have been found capable of *a priori* predictions of mixed gas adsorption of coalbed gases within three times the experimental uncertainties.[8]

Since, a CBM reservoir is expected to have variable *in-situ* temperatures due to geothermal gradient, another desired attribute of a CBM adsorption model is its ability to model the temperature dependence of adsorption. To meet this requirement, temperature dependence relations for the 2-D EOS[18] and OK model[20] parameters have been developed which facilitate adsorption predictions at different temperatures without the need to regress the parameters for each isotherm. The above mentioned capabilities of these models have been demonstrated in an earlier work.[8]

3.4 Limitations and Future Work

Notwithstanding the modeling results and capabilities discussed above, some outstanding issues in adsorption modeling of CBM systems are highlighted below:

In current modeling of adsorption on wet coals, water is not treated as a *separate adsorbed component*. Presently, the adsorbed water is simply assumed to "pacify" the coal matrix, i.e., the adsorbed water is assumed to reduce the available surface area of the adsorbent, and this reduction is treated as being pressure independent. A more rigorous accounting for the adsorbed water should include the modeling of *competitive* adsorption for water and the other components in the coalbed gas *mixture*.

Further, the data reduction technique often employed in CBM adsorption experiments involving wet coals includes several key assumptions. These assumptions simplify how the presence of water in high-pressure adsorption systems is addressed. In particular, traditional data reduction techniques consider all the water present in the system to be in the adsorbed phase and the potential for a separate water-rich liquid phase

is not considered. Further, the composition of the gas phase is treated as being water-free. This also means that the density of the bulk gas is calculated as a *dry*-gas density. In addition, the data reduction includes accounting for the solubility of gas in the adsorbed water. The amount of gas solubility (if any) in the *adsorbed* water cannot be determined by ordinary experimental techniques. As a result, the gas solubility in adsorbed water is assumed to be identical to the solubility in liquid-phase water.

The above assumptions have been the accepted approach for the data reduction of such systems. The assumptions involved in this approach, however, can play a significant role in the material balance calculations. In fact, these assumptions may lead to significant errors in the calculated amount of gas adsorbed. Therefore, future work should be undertaken to assess the impact of these assumptions on adsorption data quality; and if necessary, develop improved experimental procedures and/or alternative data reduction techniques.

3.5 Conclusions

Recent developments in modeling equilibrium adsorption in CBM systems have yielded significant improvements in our abilities to describe the adsorption behavior of such systems within more physically-sound theoretical frameworks. Nevertheless, additional efforts are still needed to address rigorously the effects of moisture on adsorption capacity.

Following are some broad conclusions on the current state-of-the-art in CBM equilibrium adsorption modeling:

1. Although the Langmuir and similar traditional adsorption models lack the theoretical rigor required of a CBM adsorption model, these models are widely

used in the CBM work primarily because of their (semi-quantitative) usefulness in correlating existing data, simplicity and ease of use.

2. Recent studies have confirmed the correlative and the generalized predictive capabilities of theory-based models such as the 2-D EOS, OK and SLD-PR models, as they apply to CBM adsorption systems. On average, these models represent the experimental data of pure and mixed CBM gases within two times the experimental uncertainties and provide *a priori* predictions within three times these uncertainties.
3. The use of matrix-calibrated generalization of adsorption models using molecular descriptors offers an effective approach for minimizing the experimental effort required to obtain accurate adsorption predictions for CBM systems.
4. Additional work is needed in CBM adsorption modeling to account rigorously for the effects of moisture on adsorption behavior and remedy potential deficiencies in current data-reduction procedures when dealing with wet coals.

CHAPTER 4

REVIEW OF PURE WATER ADSORPTION

4.1 Introduction

As mentioned in Chapter 1, a necessary pre-requisite to the development of a generalized adsorption model is an accurate understanding of pure-water adsorption behavior on a variety of carbonaceous surfaces. Therefore, this chapter documents our investigation of the adsorption behavior of pure water on carbon surfaces such as activated carbons and coals.

A series of questions pertaining to water adsorption on carbons and coals motivated the review described in this chapter:

- What is the most probable mechanism of water adsorption on activated carbons and coals?
- What is the physical nature and other characteristics of water adsorbed on coals?
- What forms, types and bonds exist for water on coal and carbon surfaces?
- How different is the water adsorbed on coals than that in the bulk (liquid) water?
- Can water in the capillaries of coals be considered as "adsorbed"? Does it affect gas adsorption behavior?
- What can be inferred from what is commonly termed the "equilibrium moisture content" of a coal?

- What is the relationship between "equilibrium moisture content" and "inherent moisture" of a coal? Are they always equal? If not, which is a more reliable estimate of adsorbed water saturation capacity?
- What are the industry standards for estimating excess moisture in a coal sample, as well as the related definitions and terminologies used in the mining industry?
- Is it possible to predict, *a priori*, water saturation capacity on coals and activated carbons by utilizing the characterization information for the adsorbent?

This chapter on water adsorption attempts to provide answers to these questions by analyzing evidence from the literature, followed by suggestions for the modifications required in the SLD-PR model to accommodate the special nature of water adsorption.

Properly accounting for water adsorption behavior on activated carbons and coals presents an interesting and challenging problem. The adsorption behavior of water on carbons is fundamentally different from the adsorption of simple, non-polar fluids like nitrogen, methane and organic vapors. The difference arises mainly because the *fluid-fluid* interactions for water are much more strongly attractive than the *fluid-solid* interactions, and, because water forms hydrogen bonds with the oxygenated groups on the carbon surface.[32] This is in direct contrast to the adsorption behavior of non-polar molecules like methane and nitrogen. The adsorption of water on carbons is widely believed to occur first through the formation of hydrogen bonds at the primary adsorption sites composed of oxygen groups on the carbon surface (see, e.g., Brennan et al.[84]). The adsorbed water molecules then act as secondary adsorption sites allowing other water molecules to adsorb on them. At sufficiently high densities (or relative pressures), enough water molecules are present to form three-dimensional clusters[32], resulting in pore filling.

Thus, water adsorption does not occur by the formation of one or more layers, as hypothesized for non-polar molecules, but occurs primarily through hydrogen bonding.

For simple fluids and organic vapors, the heat of adsorption is considerably higher than the heat of condensation of their vapors. The heat released during adsorption of water is close to the heat of condensation of bulk water[85], confirming the major role played by the hydrogen bonds in such interactions.

Moreover, simulations[86] and experimental results[87] have shown that water adsorption depends more on the site density and the location of the active surface groups than on the extent of the carbon surface itself. This presents a unique challenge, since the traditional surface area, pore volume and other characterization information cannot be used to give reliable estimates of the water saturation capacity.

The discussion of water adsorption can be described in terms of the different shapes possible for the isotherms. For illustrative purposes, Figure 4.1 presents the different types of physisorption isotherms as classified by International Union of Pure and Applied Chemistry (IUPAC).[88] A Type I isotherm is characteristic of Langmuir-type monolayer coverage isotherm, Type II is a multilayer adsorption isotherm, Type III is characterized by heat of adsorption values near the heat of condensation, and Type IV and V can represent capillary condensation effects of an adsorptive system.[20] Water can exhibit Type III, IV or V isotherm behavior, whereas non-polar adsorbates would exhibit Type I isotherm behavior.

For an organic or non-polar adsorbate, the amount adsorbed is large even at low relative pressures, and isotherms are Type I in the IUPAC classification.[88] However, for water the coverage is low until high relative pressures, and the isotherm is Type V for

graphitic carbons. Further, for carbons having significant concentrations of functional groups on the surface, the isotherm shape for water can be either Type III or Type IV. This presents difficulties in developing an adsorption model that can account for water adsorption behavior observed on different carbonaceous surfaces.

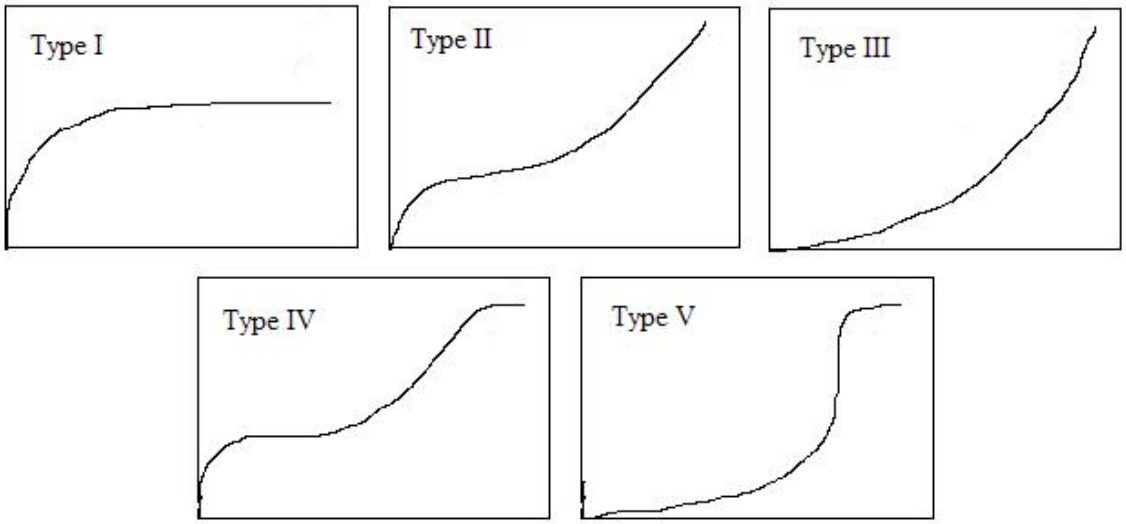

Figure 4.1 Types of Physisorption Isotherms (IUPAC[88])

The remainder of the chapter is organized in the following manner: Section A deals with the surface characterization of activated carbons and coals and its relation to water adsorption. Section B addresses the physical state of water naturally found on coals and how this affects the data reduction of an adsorption isotherm experiment. Section C discusses the water adsorption models available in the literature and proposes modifications to the SLD-PR model to account for the presence of water in a gas adsorption isotherm on a wet adsorbent. The modified SLD model is then used in Chapter 5 to study CO_2-water binary-mixture adsorption on wet Argonne coals.

Section A

4.2 Surface Characterization of Activated Carbons and Coals

Activated carbons, in general, are characterized by measuring the microporous surface area by the BET method[14], which is generally based on nitrogen adsorption at 77 K. In addition, the pore volume can be estimated from either nitrogen adsorption data at 77 K or CO_2 adsorption data at 273 or 298 K. For this purpose, the BET method or Dubinin's theory[66] is generally used. Further, the pore size distribution (PSD) can also be calculated from a density functional theory (DFT) approach.[89] These parameters can then be used to estimate the adsorption capacity of a carbon for a simple fluid. However, the reliability of estimated adsorbed water saturation capacity based on such surface characterization is uncertain. The purpose of the work described in this section is to investigate this aspect of water adsorption behavior.

Nitrogen at its boiling point (77 K) is commonly used as a probe molecule to estimate the characterization parameters mentioned above. In particular, nitrogen has been widely used to estimate the surface areas of porous and non-porous solids.[14] However, a part of the carbon pore system, which is inaccessible to nitrogen, is accessible to other molecules including water.[90] The diameter of water molecule (0.3150 nm.) is smaller than the nitrogen molecule (0.3798 nm.) and, hence, can penetrate pores which are inaccessible to nitrogen. Notwithstanding the different accessibilities, the pore volumes derived from water adsorption data are typically *lower* than volumes derived from nitrogen. A possible reason for this anomalous behavior could be the less-dense packing of water molecules in the adsorbed phase.[91]

The pore analysis method called the "t-method", resulting from the BET theory has been applied to water adsorption. Hagymassy et al.[90] were the first to apply the t-method of pore structure analysis to water vapor adsorption and they presented the t-curves for water vapor. A t-curve is defined as a plot of the statistical thickness of the film adsorbed on the surface of *non-porous* adsorbents vs. the relative pressure of the adsorbate. Hagymassy et al.[90] noted that the evaluation of t-curves for water vapor adsorption is complicated. Since water vapor adsorption is largely dependent on the type of surface, only a hydrophilic surface could be used for the t-curve analysis. Also, carbons with very small particles cannot be used for t-curve analysis due to possible capillary condensation in those pores. Further, the BET surface areas derived from water adsorption are often *lower* than the areas derived from nitrogen adsorption. These factors introduce uncertainties in the t-curves derived for water and consequently in the statistical thickness of layers of adsorbed water. These uncertainties aside, recent simulation results of water adsorption also suggest that water does *not* form layers like other molecules (and as envisioned by the BET method), but forms three-dimensional *clusters* through hydrogen bonding.[28, 32]

The adsorption of water on coals has also been reported in the literature. Mahajan and Walker[92] measured the adsorption of water on six coals and calculated the BET surface areas from CO_2 and water adsorption isotherms. The coals ranged from low-rank lignite to anthracite. Their results showed that the surface area of these coals derived from water adsorption data was considerably less than the area derived from CO_2 adsorption data at 25°C. They explained this difference by observing that the BET theory envisions non-polar adsorbates and the formation of layers; however, water adsorption

occurs through the formation of hydrogen bonds and typical layers are not formed. Therefore, Mahajan and Walker[92] concluded that the application of the BET theory to water vapor adsorption gives only a measure of the specific adsorption sites on the coal surface as provided by the oxygen functional groups, rather than the amount of water required for a 'monolayer' formation on the entire coal surface. Further, the coal surface areas estimated by Mahajan and Walker[92] by utilizing water adsorption data in conjunction with two methods (BET and t-method) agreed closely. They also found that there was no correlation between the surface areas derived from CO_2 and water adsorption data on a given coal. In fact, the fraction of the total surface area (as measured by CO_2 adsorption at 25°C) that was covered by a monolayer of water varied greatly from 12 to 60%. This demonstrates the difficulty in predicting the surface area accessed by water on a coal even if CO_2 adsorption data are available.

An inspection of the water saturation capacity of these coals and their surface area estimates from water adsorption data showed that for a coal containing about 32 wt.% moisture, the BET surface area (in this case, the area available due to the functional groups alone) could be as high as 250 m^2/gm. OSU's recent estimates have shown that a SLD-PR model-derived surface area of 800 m^2/gm is required to account for around 32% adsorbed water on a coal surface. Such unrealistically large areas for the coals can be explained as follows: The original SLD model has only one parameter to represent the surface area available for a given adsorbate. Since there is no aerial parameter that can be assigned to the adsorption due to the functional groups and the formation of clusters of water molecules, the entire water uptake is viewed as being due to a large 'surface area' of the coal. Thus, this area is to be viewed as the area representing the ultimate water

loading on the coal rather than the actual surface area of the coal. (Chapter 5 attempts to provide a hypothetical partitioning of the surface area for water adsorption from these two phenomena).

Youssef[93] has also measured moisture adsorption on coals. He concurred with the view that the adsorption of water depends more on the surface functional groups than on the extent of the surface (derived from BET and other methods). He compared the surface areas estimated from water adsorption isotherms by using the BET method to the areas calculated from CO_2 adsorption at 25°C by using the Dubinin's theory. The surface areas derived from water adsorption were significantly less than the areas derived from CO_2 adsorption, in agreement with other authors (Mahajan and Walker[92]). Further, Youssef also measured the infra red (I.R.) spectra of coal samples and found that water adsorption decreases when the number of oxygen groups on the surface decreases, quite independent of the actual surface area of the coal and its carbonized products. These results demonstrate the significant role played by the oxygenated surface sites in water adsorption behavior.

Similarities exist for the adsorption behavior of water on non-porous and porous carbons under similar conditions. Dubinin[85] investigated water vapor adsorption in non-porous carbon blacks and porous activated carbons. He observed that the shapes of water adsorption isotherm on a non-porous carbon black and activated carbons were similar. This indicates that water adsorption does not depend on the microporosity of the carbon. Further, hysteresis was observed only for the porous carbon. Non-porous carbons, in general, do not exhibit significant hysteresis. Dubinin[85] also observed that the differential

heats of adsorption of water on non-porous carbon black and activated carbon were similar and were close to the heat of condensation for all pressure ranges of the isotherm.

Dubinin[85] used theoretical estimates of the adsorption potentials of benzene and water on graphite and found that the dispersive interaction energy for water was six times lower than for benzene. The superposition of adsorption potentials of an organic vapor from opposite pore walls of carbon can greatly enhance the interaction energy of organic vapors. In contrast, water adsorption occurs largely due to the formation of hydrogen bonds with much lower adsorption energies. In fact, the dispersive forces for water adsorption were found to be weak and therefore could be neglected to a first approximation.[85]

Dubinin also compared surface areas estimated from the theory of volume filling of micropores (TVFM) with the BET and t-methods. The BET and t-method surface areas were significantly higher than the areas derived from TVFM. Therefore, he questioned the application of multilayer adsorption theories like the BET for estimating the specific surface areas of microporous adsorbents.

In another study, Barton et al.[94] investigated water adsorption on oxidized porous carbons and confirmed that bonds between the hydrogen and the surface oxides play a major role in water adsorption. They also observed that the enthalpy changes for water adsorption are governed by surface oxide concentration up to a threshold value. This threshold value represents the concentration of oxide sites which permits maximum hydrogen bonding with water. Additional water adsorption takes place through pore filling and is characterized by a relatively small enthalpy change. Further, the water adsorption at the threshold value amounted to only 40% of the nitrogen BET surface area

for these carbons. Thus, the total micropore volume does not markedly influence the surface interactions of water and the capacity of carbon for water uptake. Barton et al.[94] also estimated the monolayer coverage of water from the BET equation. For most carbons they studied, the monolayer coverage for water ranged from 8-22% of the water saturation capacity. These factors demonstrate the difficulty in predicting water adsorption from a typical structure characterization like the BET surface areas.

Stoeckli et al.[95] applied the Dubinin-Ashtakov (D-A) equation to adsorption of water on activated carbons. The characteristic energy in the D-A equation for normal inorganic and organic vapors is in the range of 15-30 KJ/mol. They noted that, when this characteristic energy in the D-A equation is lowered to around 2-3 KJ/mol, isotherm shape changes from Type I to Type V (*S-shaped*). They also observed that the isotherm parameters were temperature invariant, in accord with the Dubinin's theory. Interestingly, the pore volumes they estimated from benzene and water adsorption using the D-A equation were very similar. However, the average pore sizes estimated from the adsorption data of these two adsorbates were markedly different and were 2-4 times larger for water than for benzene.

Further, the pore volumes estimated from nitrogen adsorption are, in general, higher than the volumes estimated from water adsorption. Dimotakis et al.[96] investigated the adsorption of water on chemically modified activated carbon cloths. The activated carbon cloths were modified by treating them with HNO_3, NH_3 or Cl_2. They found that the pore volumes calculated from water adsorption at saturation were lower than the pore volumes estimated from nitrogen adsorption at 77 K by the BET method. This was true for all carbons they studied except the one which contained 32% oxygen, where the pore

volumes were similar. This illustrated the anomalous behavior of the parameters obtained from water adsorption data. They also noted that the carboxylic groups on the carbon surface were mainly responsible for enhanced adsorption of water at low relative pressures in these carbon cloths. The number of carboxylic groups on the carbon surface is increased by oxidation, resulting in increased water uptake at lower relative pressures/humidity.

Bandosz et al.[87] also investigated the effect of surface chemistry of activated carbons on water adsorption. The water uptake for one of the oxidized carbons they studied was slightly higher than the original carbon. This was in contrast to adsorption of non-polar molecules like nitrogen on the same carbons. They used the Dubinin-Serpinsky (D-S) equation[97] and the Darcy-Watt method[98], as applied by Evans[99], for the isotherm analysis. Both models were unable to characterize the water adsorption data for these carbons.

According to Rodrigues-Reinoso and co-workers[100], the region below the "plateau" of a water isotherm is governed by the chemical nature of the carbon surface; and the region at higher relative pressures is affected by the microporosity of the carbon sample. Although the models based on Dubinin-Serpinsky equation include such contributions, they have failed for even moderately oxidized carbons as noted elsewhere.[87]

Salame and Bandosz[101] measured water adsorption on a set of activated carbons with different degrees of oxidation. The oxidation of carbons resulted in decreasing the surface area and pore volumes; therefore, adsorption of non-polar adsorbates decreased accordingly. However, the highly oxidized carbons showed greater water uptake than less

oxidized carbons (at lower relative pressures). This was in reverse order to the adsorption of simple, non-polar fluids. The presence of functional groups, their number and strength is known to facilitate water adsorption by providing energetically favorable sites for water through hydrogen bonding. Salame and Bandosz[101] also observed an almost linear relationship between the amount of water adsorbed at lower relative pressures and the carboxylic group content of the carbon. They concurred with the view of Mahajan and Walker[92] and others[102, 103] that the water uptake is not a representation of the surface coverage as it is meant traditionally.

Further, even at low relative pressures, the isosteric heat of adsorption had the heat of condensation as its limiting value. This strongly suggests that the primary mechanism of water adsorption is hydrogen bonding to the surface groups on the carbon.

Slasli et al.[102, 103] modeled water adsorption with and without specific interactions with the surface sites. They found that the Dubinin-Astakhov equation, when used as a sum of Type I and Type V contributions, can model water adsorption for the carbons studied. The Type I contribution results from the specific interactions of water with the surface functional groups, whereas Type V results from the non-specific interactions. They also conducted Grand Canonical Monte Carlo (GCMC) simulations for water adsorption by utilizing the experimental pore size distribution and equivalent density of oxygen groups on the carbon surface. They achieved some success in modeling water adsorption by using such pore size distribution and oxygen + HCl equivalent content of the specific surface groups.

A Case Study of the SLD-PR Model Applied to Pure Water Adsorption

The above literature review led us to perform a case study of **pure** water adsorption on activated carbons using the simplified local-density/Peng-Robinson (SLD-PR) model to approximate the adsorption behavior. For this case study, ten well-characterized activated carbons from the literature were selected, and the SLD-PR model was used to represent the water saturation capacity of these carbons. The carbons ranged from as-received samples to highly oxidized activated carbon cloths. These activated carbons had been treated with oxidizing agents such as HNO_3, NH_3, Cl_2 or H_2O_2 by the original authors.

The SLD-PR model was utilized to represent the experimental water saturation capacity of these carbons. The SLD-PR has three model parameters; namely, surface area, slit length and ε_{ss}/k. The SLD model envisions a slit-like adsorbent surface; and the slit length is assumed to reflect an "effective pore size" of the carbon surface. The model also includes a solid-solid interaction energy parameter which is represented by ε_{ss}/k. For this case study, BET surface area estimates were used as the SLD surface areas and slit length was regressed for each carbon. Further, ε_{ss}/k was held constant at 40 K based on earlier work on gas adsorption.[20] This was also necessitated to maintain stability in calculations. Further, only the ultimate water loading or the adsorbed water capacity was used as a single datum for evaluating the slit length. In other words, the slit length was evaluated by utilizing the amount adsorbed at saturation as an indicator of ultimate water loading. For the purposes of this work, the representation of the water saturation capacity alone was required, and therefore no attempts were made to describe the complete water adsorption isotherm.

Table 4.1 summarizes the results of this case study. The table compares the SLD-PR model parameters to the corresponding values obtained by traditional experimental surface characterization measurements from the literature for these activated carbons. The SLD-PR model was able to provide good representation of water adsorption capacity, using estimated values of the slit length for each separate case. However, Table 4.1 reveals marked differences between pore volumes, where the experimental pore volumes derived from nitrogen measurements are generally *higher* than the model-derived pore volumes based on water adsorption data. Specifically, the average absolute error in pore volumes is around 20%. Such an error in pore volumes may result in larger errors in the estimated amounts of adsorbed water. The disagreement between the pore volumes derived from nitrogen and water adsorption data has also been noted elsewhere that involved water adsorption isotherm measurements.[96] Thus, this case study confirms such observations in the literature.

Moreover, the carbons with similar nitrogen BET surface areas have large differences in their water saturation capacity (V_{ads}). This indicates that the nitrogen BET surface areas alone cannot be used to estimate the saturation adsorption of water on a carbon sample. This further demonstrates the difficulty in utilizing the traditional surface characterization to predict, *a priori*, the water saturation capacity of activated carbons. For coals, such predictions would be more uncertain because reliable characterization information for coals is also generally unavailable.

For some of the carbons in Table 4.1, the experimental pore volume estimates from water adsorption data are also available. In comparison, they are *lower* than the SLD model estimates by around 20%. If the characterization information was a reliable

Table 4.1 SLD-PR Model Case Study for Pure-Water Adsorption on Activated Carbons from the Literature

Activated Carbon	Experimental Data				Calculated SLD-PR Model Parameters		Reference
	Water Saturation Capacity (mmol/gm)	N_2 BET Surface Area (m^2/gm)	Pore Volume (cc/gm)				
			Total (N_2)	Total (Water)	Slit Length (nm.)	V_{ads}* (cc/gm)	
BPL	25.6	900-1000	0.94	-	1.11	0.53	Barton et al.[104]
W	39.0	1500	0.80	-	1.08	0.81	Bandosz et al.[87]
W2	23.0	860	0.51	-	1.09	0.47	Bandosz et al.[87]
N	23.0	970	0.78	-	1.02	0.49	Bandosz et al.[87]
N1	15.0	625	0.43	-	1.02	0.32	Bandosz et al.[87]
N2	25.0	860	0.66	-	1.17	0.50	Bandosz et al.[87]
AC-4% N	37.5	1738	0.84	0.67	0.95	0.82	Dimotakis et al.[96]
AC-32% O	27.8	1105	0.47	0.49	1.07	0.59	Dimotakis et al.[96]
AC-7% Cl	28.3	1523	0.73	0.59	0.86	0.65	Dimotakis et al.[96]
AC-16% Cl	28.9	1374	0.66	0.53	0.94	0.64	Dimotakis et al.[96]

*V_{ads} is the product of model surface area and slit length.

way of predicting water saturation capacity, then one would expect a better agreement between the pore volume estimates from two different methods. Their lack of agreement and anomalous behavior suggests that even the traditional characterization information obtained directly from water adsorption data may not yield accurate estimates of the water saturation capacity. Hagymassy et al.[90] had also noted the limitations of such characterization information obtained from water adsorption data.

In conclusion, Table 4.1 and the discussion above demonstrate that the experimental characterization alone is not a reliable way of generating SLD model parameters for estimating the water saturation capacity.

A Note on the Validity of Characterization Methods

The validity of different approaches for characterizing porous adsorbents has also been reviewed. Sing[105] reviewed the use of nitrogen adsorption for the characterization of porous adsorbents. He highlighted the difficulties in the BET method and concluded that standard BET analysis based on nitrogen adsorption is strictly applicable when pores of molecular dimensions are absent and the BET plot is obtained over an appropriate pressure range of the isotherm. In another study, Stoeckli and Centeno[106] investigated the validity of the BET and immersion calorimetry methods. These two methods are frequently used for the determination of surface areas of activated carbons. They found that the BET analysis can yield physically reasonable surface areas only when average pore widths are between 0.8-1.1 nm. Further, immersion calorimetry can yield reliable surface area estimates only when the average pore size is less than 1 nm.

Notwithstanding these limitations, the above methods are still widely used for the characterization of porous materials. In particular, BET analysis applied to nitrogen

adsorption has been a 'standard' method of characterizing activated carbons of varying degrees of oxidation. These oxygenated groups strongly affect the adsorption behavior of water. One can expect that the non-polar nature of nitrogen does not fully capture the role of these active groups on the carbon surface. Therefore, the characterization information obtained from nitrogen measurements is not strictly applicable in describing water adsorption. This is also consistent with the case study discussed above.

The adsorption behavior of water on coals is even more complicated than that on activated carbons due to the heterogeneous nature of coals. The characterization of coal surfaces by nitrogen adsorption is not reliable due to well-known activated diffusion problems.[107] CO_2 has been suggested as a viable alternative. Walker and Kini[108] recommended the use of CO_2 adsorption at 25°C for determining the surface areas of coals. They had concluded that the surface areas estimated from CO_2 adsorption data at 25°C *essentially* represents the total surface area of coals. However, Mahajan[109] presented measurements which showed that coals with the same carbon content differ in their CO_2 areas by as much as 275 m^2/gm. Thus, the surface area of coals as determined by CO_2 adsorption data is not well correlated with coal rank. Mahajan[107, 110] also reviewed the determination of surface area of coals from CO_2 adsorption data and other aspects of physical characterization of coals. The measured surface areas of coals were found to be affected by parameters such as adsorption temperature, outgassing time and temperature prior to adsorption measurements, coal particle size and the molecular cross-sectional area of the adsorbate used. Mahajan believed that the true magnitude of the coal surface area and its pore-size distribution were largely unknown. He observed that coals

contain both open and closed porosity and that the macro-, meso-, and micropores in coals are interconnected.

In the BET method, the surface areas of carbons and coals are calculated by multiplying the monolayer volume and the cross-sectional area of an adsorbed molecule. Mahajan[107] noted that there are large uncertainties in the values of CO_2 monolayer volume and its cross-sectional area in the adsorbed state. Therefore, he concluded that the surface areas of the coals were *meaningless* and should not be reported.

Conclusions

The evidence cited above suggests that the surface characterization of carbons by non-polar molecules does not apply well to water adsorption behavior. The water saturation capacity can seldom be predicted with any certainty by using such characterization information. The estimation of these properties directly from water adsorption data is possible; however, due to the bimodal nature of water adsorption, it is often difficult to predict water saturation capacity from this information alone. On coals, there is added complexity due to the highly heterogeneous nature of its surface. Therefore, the estimation of water saturation capacity, *a priori*, from the surface characterization alone is not reliable.

Section B

4.3 The Physical State of Water Naturally Found on Coals

In-situ coals generally contain significant amounts of water. The behavior of water existing in coals is complex and unclear. Water on coals can exist in different states:

1. Free (liquid) water also known as bulk water or surface water

2. Capillary water existing in the capillary system of the coals
3. Bound water which exists in the complex porous system of the coal
4. Chemically bound or hydrogen-bonded water

This section addresses the characteristics of water naturally present on coals through a careful analysis of evidence in the literature. This evidence consists of adsorption/desorption isotherms, spectroscopic and calorimetric measurements, as well as a review of the standards defining the terms and definitions associated with water on coals. The spectroscopic measurements consisted of nuclear magnetic resonance techniques (NMR), calorimetric measurements from differential scanning calorimetry (DSC) and the standards included the ASTM standard D1412 and D3302 on coals and coke.[41, 111]

In particular, this section addresses the following questions:

- What is inferred by equilibrium moisture content and inherent moisture?
- What is the relationship between equilibrium moisture content and inherent moisture of a coal? Are they always equal? Which is a more reliable estimate of water saturation capacity on coals?
- Are the above the same as adsorbed water capacity, and are they always interchangeable?
- How different are the behaviors of adsorbed water and bulk (liquid) water?
- Would adsorbed water have gas solubilities similar to bulk water?

Different methods of moisture determination on coals have been attempted since the early 1900's (Mannheimer[112]). The determination of equilibrium moisture content of

coals is standardized by methods like the ASTM method D1412.[41] This method yields the equilibrium moisture in a coal.

Allardice and Evans[113] made a comprehensive study on the Brown coal/water system in Australia. These Victorian Brown coals typically contain large amounts of moisture. Allardice and Evans[113] measured water desorption isotherms on these coals and obtained sigmoidal isotherms with hysteresis extending to low relative pressures. They found that the BET monolayer coverage correlated well with the hydrophilic functional groups on the surface rather than the extent of the surface. This supported earlier findings by several workers[114-116] that BET monolayer coverage for water is proportional to the number of hydrophilic sites rather than the surface area itself.

The monolayer coverage (v_m) has been correlated with coal rank.[117] For higher rank coals, which would have less oxygen and consequently a smaller number of functional groups, v_m was lower. Allardice and Evans[113] classified water on Brown coals as monolayer, multi-layer, capillary and free water. As evident from their results, these coals contained free water; and no equilibrium moisture contents (at saturation) were provided, which makes further interpretation of their data difficult.

Schafer[118] investigated the factors affecting the equilibrium moisture contents of the acid-form and salt-form of low-rank coals. The acid-form of the coals was prepared by acid treatment and the salt-form of the coals was prepared by replacing the carboxylic acids cation with the corresponding metal acetate. The ‘equilibrium’ moisture content in this study was referred to as the moisture present at 52% relative humidity and 20°C. Schafer[118] found a linear correlation between the equilibrium moisture content and the carboxylic group content of the acid-form coals. The correlation between the equilibrium

moisture content and hydroxyl groups was much weaker. He also studied the salt-form of these coals where the carboxylic acids were replaced by the cation after treatment with the corresponding metal acetate. The equilibrium moisture content of the salt-form of the coals was found to be higher than the acid-form of these coals. Moreover, the moisture content increased linearly with increasing content of a given salt. The salt-form of coals also retains water more strongly than acid-form coals due to greater hydrogen bonding.

Matsyna[119] analyzed the forms and binding energies of moisture on coals. He classified various forms of water which can exist on coals as:

- Physicomechanical moisture - This is comprised of moisture in the macropores and the micropores.
- Physicochemical moisture - This is comprised of multi-layer and monolayer moisture.
- Chemical moisture - This referred to the hydrogen bonded water.

He studied the thermograms and drying curves of moisture on the coals. Interestingly, he considered only the monolayer and multilayer moisture as 'adsorbed water' and water in macropores and micropores was not considered as 'adsorbed.'

Kaji et al.[120] measured the water-holding capacities of several coals by immersing the coals in water. For some of the coals, they also measured the equilibrium moisture content at 100% RH. The water-holding capacity of the coals was only slightly higher than the equilibrium moisture content of the coals. Therefore, one can infer that these two quantities are nearly equivalent. In another work, Joubert et al.[29, 42] observed that adsorbed-water capacity was within the range of values of equilibrium moisture content of the coals.

Unsworth et al.[121] applied nuclear magnetic resonance (NMR) and microwave attenuation methods to differentiate between different forms of moisture on coals. NMR utilizes the fact that solid and liquid phases would have different mobility of molecules, and the microwave absorption technique utilizes the fact that the free water would absorb more microwave energy than bound water; thus, the two can be differentiated. Water in coals can exist within the internal pore structure of the coals, on exposed particle surfaces and in inter-particle voids. The maximum content of moisture held by the pores, measured at 96-97% RH and 30°C is referred to as "inherent moisture" (IM) by ASTM standard D1412. An inspection of the different standards, terms and definitions used by ASTM, International Organization for Standardization (ISO) and Bureau of Standards (BS) indicates that the terms inherent moisture, equilibrium moisture and water-holding capacity referred to the same quantity in these different standards. Further, surface moisture or free moisture appear to be equivalent terms; and referred to the *difference* between the inherent moisture and as-received moisture. Note here that the total moisture content of some bituminous coals can be larger than 30% by wt.

As mentioned earlier, water behavior on coals is expected to be complex and heterogeneous. A solid-to-liquid transition near 0°C is rarely achieved, and there was evidence of glass-like behavior at much lower temperatures.[122] Unsworth et al.[121] studied about 20 bituminous samples with NMR and found that approximately 20% of inherent moisture freezes at -20°C. Their microwave absorption tests also showed that the inherent moisture absorbs less energy than free moisture and is therefore considered ‘bound’ moisture. A comparison between these results showed that the inherent moisture is more

tightly bound to the coal. In fact, a large part of the inherent moisture is non-freezable and behaves quite differently than bulk or free water.

Suuberg et al.[123] investigated the shrinkage/swelling characteristics of bituminous coals when they are exposed to water and the consequences of such changes on the colloidal gel nature of the coals. Differential scanning calorimetry (DSC) results also suggest that water exists in freezable and non-freezable forms.[124, 125] Proton NMR results from Suuberg et al.[123] on brown coals also displayed similar trends. Their experiments with shrinkage/swelling discount the possibility of a capillary condensation-like mechanism for describing moisture retention on a large variety of bituminous coals, including Argonne coals. Their experiments also showed that water acts as a "plasticizing" agent for the coal.

Allardice et al.[126] characterized the different forms of water present in Brown coals. They measured the equilibrium uptake of water at four relative humidities at 30°C. They also applied DSC and proton NMR techniques to estimate the amount of non-freezable water (here, classified as water which remains liquid at -3°C). Their results showed that this amount was similar to the amount of water adsorbed on brown coals at 93% RH. The authors also observed that, for the brown coals, the total amount of non-freezing water is ten times greater than the amount of strongly adsorbed water or "monolayer" water estimated at 15-20% RH.

Unfortunately, the above studies were on coals which were not well-characterized and, therefore, detailed inferences about the exact nature of adsorbed water on these coals were more difficult. However, the studies discussed below were performed on well-characterized Argonne coal samples. Argonne coals have been widely studied, well-

characterized and present an opportunity to compare results obtained from different studies.

Norinaga et al.[127] classified water adsorbed on Argonne coals based on their congelation characteristics. They classified water into three types: free water that is identical with bulk water; bound water that freezes at a lower temperature than free water; and non-freezable water that does not freeze even at temperatures as low as 123 K. A liquid-to-solid transition is accompanied by the evolution of heat and decrease in molecular mobility. The evolution of heat can be detected by differential scanning calorimetry (DSC) and proton nuclear magnetic resonance (^{1}H NMR) can be used to record mobility of the phases. Norinaga et al.[127] used these principles in their study of water present on coals. Their study included four Argonne coals, namely, Beulah Zap, Wyodak, Illinois #6 and Blind Canyon. These samples were used as-received and thus they were at their reported inherent (equilibrium) moisture content values.[39] Their DSC results indicated that there was no free water present on the as-received samples of these Argonne coals. The DSC results also revealed that Beulah Zap, Wyodak and Illinois #6 coals had, respectively, 65, 62 and 50% water that was "non-freezable" even at 123 K. These results indicate that the amount of water referred to as equilibrium or inherent moisture content has markedly different thermodynamic properties than bulk water due to its interactions with the coal surface. Moreover, their proton NMR results validated the quantitative classification of freezable and non-freezable water observed in these coals. This was a significant result as it directly addressed the moisture present on as-received Argonne coals. In another study, Norinaga et al.[128] further observed that the differences in the freezing properties of bulk and bound water were related to the size of the cluster of

water molecules. A smaller size of such clusters in pores results in lowering the freezing point of water. Moreover, bound water was also found to have a lower heat of fusion than bulk water.

Similarly, Mraw and O'Rourke[124] measured the heat capacity of naturally-occurring moisture on a Wyodak coal and found that two-thirds of the water on the as-received coal was non-freezable and the remaining third was freezable. Further, they observed that even the freezable water only marginally resembled bulk water. Note here that the Wyodak coal used by Mraw and O'Rourke[124] was prior to the Argonne coal sample program and contained around 37% as-received moisture (compared to 28% for the Argonne premium sample). Their results demonstrated that the non-freezable water does not exhibit phase-transition and even the freezable water does not behave as bulk water since its fusion peak is rounded.

Lynch et al.[129] also investigated the nature of water adsorbed on a low-rank Australian coal. They also used proton nuclear magnetic resonance technique to characterize the interacting water on the coal. They observed a clear distinction between non-freezable and freezable portions of the interacting water, and these were independent of the amount of excess water present on the coals. They classified nearly all of the water termed as 'equilibrium water content' (EWC) as "interacting water". Interacting water also 'plasticized' part of the coal structure, providing evidence that coals are not inert substrates. This indicated that estimation of water uptake based on coal porosity alone would not be possible.

Further, the structure of adsorbed water on graphitic and activated carbons has also been studied. Iiyama et al.[130] used in-situ X-ray diffraction to study the structure of

adsorbed water in hydrophobic carbon nanopores. They found that adsorbed water is more ordered than bulk liquid water even at 303 K and has an ice-like structure. Further, they observed that there was no clear phase-transition point for adsorbed water from 143-303 K. In another study, Iiyama et al.[131] used in-situ small-angle X-ray scattering technique to study the molecular structure of adsorbed water in activated carbon fibers at 303 K. They found that water adsorption takes place by the formation of clusters in the hydrophobic micropores of carbon and does not form uniform layers. This observation is in agreement with earlier simulation results by McCallum et al.[32] and others.

Similarly, X-ray and neutron scattering techniques were also used by Bellissent-Funel et al.[132] to investigate the structure of water on activated carbon. They also performed differential thermal analysis of water adsorbed on activated carbon. Their analysis showed that a large proportion of adsorbed water (about 50%) does not crystallize when the temperature is lowered from room temperature to 77 K. Further, their X-ray and neutron scattering results showed that about half of the adsorbed water was non-freezable and more "structured" than bulk liquid water. Note here that their measurements were conducted at about 50% and 200% of the adsorbed water capacity.

Equilibrium Moisture, Inherent Moisture and Capillary Water in Coals

The ASTM method D1412 for determining the equilibrium moisture content of a coal requires the equilibration of the coal samples at 96-97% relative humidity and 30°C over a saturated solution of potassium sulfate. The amount of water present at the equilibrium conditions specified by this test is termed the equilibrium moisture content. The ASTM further defines inherent moisture as "*the moisture that exists as an integral part of the coal seam in its natural state, including water in the pores but not that present*

in macroscopically visible fractures. On removal of coal from a seam, the water originally present in fractures appears as surface moisture whereas coal containing only surface moisture appears dry".

Luppens[133] and Luppens and Hoeft[134] investigated the relationship between the equilibrium moisture and inherent moisture. Luppens and Hoeft[134] demonstrated that the equilibrium moisture from the ASTM method D1412 would underestimate the inherent moisture of many low-rank coals. They noted that the equilibrium moisture test by ASTM assumed that all the bed or inherent moisture is in small-sized capillary pores. The ASTM test further assumed that under the conditions of 96-97% relative humidity, only the surface or excess moisture is removed from the coal samples. However, for low-rank coals, the number of large-sized pores (macropores) which are larger than capillary-sized pores is significant.[135] Luppens believed that at least a portion of the moisture in these large-sized macropores is also removed, yielding equilibrium moisture values lower than the true inherent moisture.

Thus, the equilibrium moisture content can be equal to or lower than the inherent moisture depending on the rank of the coal. Luppens found that as the coal rank decreased, the difference between inherent and equilibrium moisture values became larger. The bituminous coals exhibited differences between the equilibrium moisture and inherent moisture of up to 0.5%. However, for lignites this difference was up to 10%. Therefore, he concluded that:

1. Equilibrium moisture test D1412 provides a reasonable approximation of inherent moisture for bituminous and some sub-bituminous coals

2. For sub-bituminous-C coals and lignites, equilibrium moisture results are significantly lower than inherent moisture.

Based on the above mentioned studies, the ASTM standard was revised and now it states that "*When samples are collected in conformity with ASTM Classification D388, the equilibrium moisture is considered to be equal to the bed moisture except for some low-rank coals that yield equilibrium moisture values below bed moisture"*.

As discussed above, there is a difference between the equilibrium moisture and inherent moisture for low-rank coals (sub-bituminous-C coals and lignites). Moreover, the excess moisture in a coal sample is defined as the moisture present in excess of the inherent moisture. Therefore, to account for this difference and for calculating excess moisture, a correction factor is generally applied by the Office of Surface Mining[136] to the equilibrium moisture results of low-rank coals to approximate the true inherent moisture for resource evaluation and tax purposes. The evaluation of this correction factor is also detailed in Appendix XI of the D1412 test method.[41]

From the ASTM definitions and the above mentioned studies, the inherent moisture is seen to be a more reliable estimate of total *pore-held* moisture.

Capillary Water and Adsorbed Water

The inherent moisture on coals can be broadly divided into two components: adsorbed water existing in the micropores and capillary water existing in the pores due to capillary action. Theoretically, capillary water may not be considered as "adsorbed". However, the ASTM standard D3302[111] states (in its appendix) that "*total moisture in principle represents a measurement of all of the water not chemically combined*". Brown [137] also termed all the inherent moisture as "physically bound". It becomes apparent, then,

that the total (or inherent) moisture is physically bound to the coal surface. Moreover, all of the inherent moisture affects gas adsorption behavior. This includes capillary water. Since the purpose of this work is to account for the effect of water on gas adsorption behavior, and the SLD model does not address capillary phenomenon separately, the capillary water, if any, would also be considered as "adsorbed" for modeling purposes. This assumption would be justified because the water saturation capacity of the coal is the quantity desired for further modeling of gas adsorption behavior on wet coals.

Conclusions

A careful analysis of the above cited studies and standard procedures (such as ASTM D1412) indicates that nearly all of the water classified as "equilibrium moisture" at 97% RH and 30°C can be considered to be in the "adsorbed" state for modeling purposes. The adsorbed water displays thermodynamic properties markedly different than bulk water.[124, 125, 127, 129, 130, 132, 138] The adsorbed water has much lower freezing point; and more than 50% of the adsorbed water (in case of some Argonne coals) is non-freezable even at 123 K. This suggests that adsorbed water on coals is strongly bound to the coal and has specific interactions with the surface of the coal.

Implications Regarding the Solubility of Gases in the Water on Coals

The above analysis may affect the manner in which adsorption data on wet coals are reduced and interpreted. Traditionally, the data reduction procedure used at OSU has specifically accounted for the solubility of gas in the water present on coals. This involves subtracting the amount of gas dissolved in adsorbed water from the amount of gas sorbed on a wet coal. Further, the adsorbed water is assumed to have the same gas solubility as bulk water. This procedure was necessitated because the gas solubility in

adsorbed water can not be determined experimentally. As a result, accounting for gas dissolved (if any) in the adsorbed water requires use of an educated assumption. One way to re-think the validity of the presently-used assumption is to compare the thermodynamic behavior of adsorbed water with bulk water. The above review indicates that adsorbed water has markedly different thermodynamic behavior than bulk water. Thus, there appears to be reasonable (but indirect) evidence that adsorbed water, due to its strong interactions with the coal, would not possess the type of gas solubility that bulk water does.

Therefore, the amount of water adsorbed might be more appropriately excluded from gas solubility calculations. The water present on the coal in excess of the equilibrium moisture, however, behaves like bulk water and, thus, can be expected to display similar solubility properties. Based on the above reasoning, only the excess moisture present on a coal should be included in gas solubility calculations in adsorption measurements on wet coals.

Section C

4.4 Water Adsorption Models

This section contains a discussion of water adsorption models present in the literature. This discussion includes semi-empirical models, which can describe the water adsorption data, as well as models based on intermolecular potentials used in molecular simulation studies. Based on the review presented below, a case is made for modification of the SLD-PR model to extend the model to water adsorption. Note that the list of water adsorption models highlighted here is by no means comprehensive; however, the models reviewed cover a variety of theories on describing water adsorption behavior.

The modeling of water adsorption demands special attention. This arises due to the fundamental differences in the mechanisms of adsorption of water and of non-polar molecules.[32] As mentioned previously, water adsorption can demonstrate Type III, IV or V behavior. Therefore, to model water adsorption, modifications are often required to account for such varied behavior. Different theories have been adapted for water adsorption, including:

1. Dubinin-Serpinsky method[97]
2. Darcy-Watt method[98] as applied by Evans[99]
3. Dubinin-Astakhov method[68]
4. Sircar's model[139]
5. Talu- Meunier method[140]
6. Virial-type model[101]
7. Do's model[91] and
8. Cooperative multimolecular sorption theory[141]

One of the earliest models for water adsorption was based on Dubinin's theory.[85] The Dubinin-Serpinsky (D-S) water adsorption model[97], derived from kinetic theory, postulates that water adsorption occurs first on the primary sites, which then act as secondary sites for additional water adsorption. The D-S model accounts for these primary sites and the isotherm data can be used to estimate the number of such primary sites. Several modifications to the original D-S equation have been proposed and applied to water adsorption. Barton et al.[104] analyzed water adsorption by three variants of the Dubinin-Serpinsky equation (DS-1, DS-2 and DS-3). Their results showed that none of the three equations could describe satisfactorily the water adsorption data on modified

carbons. The DS-1 and DS-2 models were unable to characterize the data at higher relative pressures. However, the results on BPL activated carbon were satisfactory for the DS-3 model.

Apart from the inability in characterizing data on modified carbons, the Dubinin-Serpinsky model has additional limitations. The model can represent Type I and III isotherms but cannot predict a correct saturation capacity for Type V isotherms.[141] The dependence of saturation capacity on kinetic parameters in the DS model is also found debatable.[91]

The Darcy-Watt method[98], as adapted by Evans[99], was an improvement over the D-S approach but has similar limitations. The method failed to represent the adsorption data even for medium densities of active sites on carbon surfaces.[101]

The Dubinin-Astakhov method[68] was applied by Slasli et al.[102, 103] to model Type V and Type IV adsorption. The Dubinin-Astakhov (D-A) equation, when used as a sum of Type I and Type V contributions, was able to model water adsorption for the carbons they studied. The Type I contribution results from the specific interactions of water with the surface functional groups, whereas Type V results from the non-specific interactions. The D-A approach also yields temperature invariant parameters; however, the model does not obey Henry's law at low concentrations.[141]

Sircar[139] developed an adsorption model incorporating capillary condensation for porous carbons. However, the model involves calculation of complex gamma functions and several parameters. The Talu-Meunier method also has limitations as shown by the simulation results.[32]

Salame and Bandosz[101] applied the Dubinin and Serpinsky equations and the modifications from the Darcy-Watt approach to water adsorption data. As mentioned previously, both methods failed to provide reasonable description of data, even for moderately oxidized carbons. Salame and Bandosz[101] also used a virial-type equation to describe water adsorption on these activated carbons. The virial model contains two sets of empirical parameters. However, due to the instability of higher order polynomials used in this formulation, this equation can be used only for certain isotherm shapes whose fit did not require higher order polynomials.

Do and Do[91] also presented a model for water adsorption based on the growth of clusters of water molecules around the functional groups on activated carbon. The model presupposes that five molecules or a pentamer has sufficient dispersion energy to penetrate the carbon pores and remain there. This four parameter model was tested against selected experimental data, and reasonable description of the data was obtained. Do and Do's model assumes that a minimum of five water molecules are required to exist in the micropores. However, Striolo et al.[142, 143] have shown in their recent simulation results that water can exist in the micropores without being a pentamer. This appears to be in direct contrast to the assumption used in Do and Do's water adsorption model.

Rutherford[141] extended the cooperative multimolecular sorption theory (CMMS) to water adsorption on molecular sieves. The model assumes a bimodal mechanism of water adsorption. This involves interactions with functional groups at low pressures and adsorption between the graphene layers at higher pressures. This five parameter model is a combination of Langmuir and Ising model contributions. The model was able to describe the data on these molecular sieves. Rutherford[141] extended the CMMS model to

account for Type IV isotherms, making it the only analytical model capable of representing all five types of isotherms. However, this bimodal isotherm model requires the fitting of five parameters to describe the data.

Some of the above-mentioned models can provide reasonable description of water adsorption data; however, the models may require up to five regressed parameters to represent the data satisfactorily.

Simulation Studies

Grand Canonical Monte Carlo simulations for water adsorption on carbons have been reported in the literature. These were conducted to investigate the effects of surface site density, location and strength on water adsorption. These factors cannot be studied separately by experiments; thus, molecular simulations provide an attractive avenue to study these effects.

Segarra and Glandt[144] presented a simulation study on water adsorption. They modeled the activated carbon as made up of graphitic platelets having dipoles on the surface to mimic the surface functional groups. However, the model was inadequate in predicting the correct trends in water adsorption.

Ulberg and Gubbins[145] reported a Grand Canonical Monte Carlo (GCMC) simulation study of water adsorption on graphitic carbons. They modeled water by the TIP4P potential for water-water interactions.[146] This potential accounts for the dispersive interactions by a Lennard-Jones potential and long-range electrostatic interactions were included as coulombic interactions between charged centers. The potential well-depth parameter in this model was 78 K and the collision diameter was 0.3150 nm. Further, the carbon atoms were modeled as slit-shaped pores. Their simulation results showed that

water molecules preferentially orient their dipole moments parallel to the wall surface. In the regions far removed from the wall, the orientation of the water molecules was more random. However, at higher water densities, the water molecules in this 'interlayer' also tend to have dipole moments parallel to the carbon wall. Ulberg and Gubbins[145] also observed that the hydrogen bonds close to the wall were weaker than in bulk water due to orientational restrictions. They also compared the fluid-fluid/fluid-solid ratio of the interaction energies for adsorbed methane and water and observed that for water, this ratio was about 14 as opposed to 1 for methane. Therefore, water-water interactions can exceed the water–carbon interaction by an order of magnitude for graphitic carbons. This is in direct contrast to non-polar adsorbing molecules like methane and nitrogen and other organic vapors. Thus, there is very little water uptake at lower relative pressures because of the hydrophobic nature of the carbon wall and the strong hydrogen-bonded network between bulk water molecules.

In another study, Maddox et al.[147] reported simulation results for water adsorption on graphitic and activated carbons. The water was modeled by the TIP4P potential for water-water interactions and the surface functional groups were modeled as being comprised of –COOH groups. The water-COOH interactions were represented by the OPLS potential.[148, 149] Like the TIP4P potential, the OPLS model also contains a Lennard-Jones term for dispersion interactions and a coulomb term for the hydrogen bonds. Their results showed a sharp change in water adsorption from hydrophobic to hydrophilic behavior as the number of acidic surface groups was increased. They varied the density and arrangement of active surface groups and found that water adsorption is strongly dependent on the arrangement of active surface groups.

The two studies mentioned above dealt with long range electrostatic forces when simulating water adsorption. Muller et al.[150] neglected such long range electrostatic interactions and simulated water adsorption on porous and non-porous activated carbons by using a square-well type hydrogen bond potential to account for the hydrogen bonds between water molecules and the active sites on the surface. The water molecules were modeled as Lennard-Jones spheres with four square well sites to account for hydrogen bonding. Two sites were hydrogen atoms and the remaining two represented the lone pair of electrons. The active sites on the carbon surface were also modeled as square-well sites. Their simulation results showed that water adsorption is characterized by the formation of three-dimensional clusters of water molecules involving a cooperative effect of fluid-fluid and fluid-solid interactions. Their square-well type model was given as:

$$\begin{aligned} \phi_{HB} &= -\varepsilon_{HB} \quad \text{if} \quad r_{AB} < \sigma_{HB} \\ \phi_{HB} &= 0 \qquad \text{otherwise} \end{aligned} \tag{4.1}$$

The parameter values were ε_{ff} = 90 K, σ_{ff} = 0.306 nm, ε_{HB} = 3600 K and $\sigma_{HB} = 0.2\sigma_{ff}$. The subscripts "ff" refers to the fluid-fluid potential and "HB" refers to the hydrogen bond interaction. Muller et al.[150] obtained these parameters from a best fit of vapor-liquid equilibrium properties of bulk water. In estimating these parameters, they also used the findings from neutron scattering results[151, 152] that a hydrogen bond is formed when two water molecules are about 0.94 molecular diameters apart. However, the ε_{HB} they used was twice the value obtained from spectroscopic measurements.[153] Muller et al.[150] used a higher value than the experimental estimate because electrostatic forces were neglected in their model and, therefore, the attractive forces were accounted for by an increase in ε_{HB}. Thus, the total water-wall potential function was given by:

$$\phi_{fs}(z) = \phi_{wall}(z) + \phi_{wall}(H - z) + \phi_{HB} \quad (4.2)$$

where "fs" refers to fluid-solid potential and "z" denotes the distance from the wall. Steele's 10-4-3 fluid-wall potential[154] was used for the first two terms above.

Muller et al.[150] simulation results showed that water molecules preferred to bond to previously adsorbed molecules rather than on inactivated portions of the carbon surface. The local density of the active sites and their relative locations were more important than their overall density. If two sites were close enough, cooperative bonding or bridging of water molecules also takes place.

This molecular model for water adsorption was compared with experimental results by McCallum et al.[32] This model accounts for the surface sites by treating carbonyl, carboxylic, phenolic, lactonic groups as –OH group. As a result, the model was called the "effective single group" model. Their results showed that the pore filling pressure was lowered at higher site densities. Also, at higher site densities the pore filling was continuous and no sharp transition (as in capillary condensation) was observed.

In a continuation of the McCallum et al.[32] study, Muller et al.[28] reported a GCMC study of adsorption of water vapor-methane mixtures on activated carbons. Their results showed that even for low site densities, water can significantly block the carbon pores thus limiting methane adsorption. Specifically, at a site density of 1.5 sites/nm^2, the adsorption of methane was reduced by more than 50%. This effect was even more profound for smaller pores.

Brennan et al.[86] improved upon the Muller et al.[28] model by considering long-range interactions and a more realistic carbon model. Their inter-connected carbon model was obtained by Reverse Monte Carlo techniques. The water potential model they used

was a fixed point charge model called the Buckingham exponential-6 potential. This potential contains an oxygen center and point charges around this center. The model is a three-parameter model. The surface sites were modeled as C=O groups and were modeled using OPLS format for the parameters. With the help of their inter-connected carbon model, Brennan et al.[86] were able to simulate the accessibility of pore space as water adsorption proceeds. They found that even low amounts of water adsorbed on the carbon can result in a significant section of the total pore volume being blocked. Moreover, some of the empty pores become inaccessible to other gas molecules due to the growth of three-dimensional water clusters around them. Further, the availability of empty pores shifts to smaller sizes as water adsorption proceeds.

Striolo et al.[142] simulated water adsorption in carbon nanopores. The water model used was the SPC/E model of Berendsen et al.[155] In this model, the long-range interactions are neglected with a spherical cut-off distance. The model represents water as a sphere with oxygen at its center. The center of the site also accounts for dispersion interactions represented by a Lennard-Jones potential. The hydrogen atoms are placed at 0.1 nm from the oxygen site and the H-O-H angle was 109.5. Partial charges are placed on these sites to account for electrostatic interactions. Specifically, the oxygen site has a charge of -0.8476 and two hydrogen sites have a charge of +0.4238 each for an overall neutral charge on the molecule. The Lennard-Jones parameters used were: σ_{ff} = 0.3166 nm and ε_{ff} = 78.2 K.

Striolo et al.[142] found that above a pore size of 1.6 nm, carbon-water interactions obtained from Steele's potential and from the summation of carbon–water pair interactions were similar. Therefore, Steele's potential was sufficient for calculating

carbon-water interactions for larger pores. Their results also confirmed earlier results[147] with TIP4 model that water molecules tend to orient their dipole moments parallel to the carbon surface. This orientation is favorable as it facilitates formation of hydrogen-bonded network of adsorbed water molecules. In another study, Striolo et al.[143] showed that pore filling pressure and the adsorption hysteresis loop decrease with decreasing pore size. They also calculated the radial distribution functions of confined water in carbon nanopores and found that before pore filling, confined water has structure typical of vapor and after pore filling the structure is typical of liquid. Therefore, the behavior was analogous to a vapor-liquid transition for water.

A comparison between the simulation studies and an analytical model on water adsorption has also been made. Kotdawala et al.[156] applied the mean field perturbation theory to model adsorption of polar molecules in nanopores. They considered electrostatic forces which included permanent dipole-dipole, dipole-induced dipole and induced dipole-induced dipole interactions. The relative contributions of these terms are about 80, 15 and 5%, respectively at 0°C. They also developed the Helmholtz free energy expression from statistical averages of such interactions. They compared their modeling results with the simulation results of Striolo et al.[143] and observed a reasonable agreement between the two studies.

4.5 Summary

A careful review of the literature evidence cited above and our case study on pure water adsorption led us to conclude the following regarding pure water adsorption behavior:

1. The formation of hydrogen bonds between the water and oxygenated functional groups on the carbon/coal surface is the primary mechanism of water adsorption on activated carbons and coals. Additional adsorption of water takes place by the formation of three-dimensional clusters of water molecules, which is a quite different phenomenon than the layering process expected for simple fluids like methane.
2. Inherent moisture is a more reliable estimate than equilibrium moisture for the water saturation capacity on low rank coals and lignites. Inherent moisture is also an industry standard in the method for estimating the excess moisture in a coal sample for reclamation and tax purposes.
3. Adsorbed water on coals has markedly different thermodynamic behavior than bulk water. The adsorbed water has a lower freezing point than bulk water; and up to 50% of adsorbed water is regarded as “non-freezable”. This finding suggests that the adsorbed water might properly be excluded from calculating gas solubility in water on coals during material balance calculations.
4. The use of traditional characterization information for the adsorbent (such as BET nitrogen surface area and pore volume) for performing *a priori* predictions of water saturation capacity on activated carbons and coals is not reliable.

4.6 Modeling Approaches

In the context of this work, there are two possible approaches to model water-gas adsorption behavior on wet coals. One method to account for the effect of water on gas adsorption behavior on wet coals is to evaluate water monolayer surface area and subtract this area from the measured or regressed pure gas surface area on a dry coal. This

approach was implemented by Mahajan and Walker[92] by utilizing the water adsorption isotherms on the coals. However, to our knowledge, none of the coals studied at OSU (including the Argonne coals) have such water adsorption isotherm data available. Moreover, recent simulation results have shown that water forms three-dimensional clusters and does not form layers as envisaged by the BET theory. Therefore, this approach would not be possible in our case.

A second approach is to obtain model parameters to represent water saturation capacity (inherent moisture) and then use those parameters as initial values for gas-water mixture adsorption calculations. In this approach, water will be modeled as an active mixture component with full accounting of its molecular interactions in the adsorbed phase. This method also provides for investigating the competitive nature of gas-water mixture adsorption on coals. Therefore, this second approach appears more realistic and will be used in Chapter 5 to model the CO_2-water mixture adsorption on wet Argonne coals.

Previous Study of Pure Water Adsorption with SLD Model

Pure water adsorption has been investigated previously using SLD theory[157] with the Elliot-Suresh-Donohue (ESD) EOS.[158] The study concluded that the model was incapable of describing accurately the adsorption of pure water on carbon surfaces, even with three adjustable parameters. The model failed in part due to the insufficient accounting for water-water interactions in the slit. Therefore, our approach, which is outlined below, would differ from this earlier study with the SLD model by accounting accurately for the water-water and carbon-water interactions in the slit.

4.7 Modifications to the SLD-PR Model

Based on the above studies, the following modifications to the SLD-PR model are recommended to model gas adsorption behavior in the presence of water.

The fluid-solid potential in the SLD model is estimated from the 10-4 Lee's potential.[80] This potential accounts for dispersive interactions alone. However, the contribution of the electrostatic interactions is significant in water adsorption. The large dipole moment of water must be accounted for in a successful water adsorption model. Hydrogen bonds play a major role in water adsorption. Therefore, accounting for the formation of hydrogen bonds would also be crucial in modeling water adsorption accurately. Thus, the 10-4 Lee's potential would be augmented with terms for the hydrogen bond energy[32] and dipole interactions[156] within water molecules as follows:

$$\Psi(z) = 4\pi\rho_{atoms}\varepsilon_{fs}\sigma_{fs}^{2}\left(\frac{\sigma_{fs}^{10}}{5(z')^{10}} - \frac{1}{2}\sum_{i=1}^{4}\frac{\sigma_{fs}^{4}}{\left(z'+(i-1)\cdot\sigma_{ss}\right)^{4}}\right) + \varepsilon_{HB} + DM \qquad (4.3)$$

where ε_{HB} is the hydrogen-bond potential between the functional groups on the carbon surface and water molecules and DM refers to the sum of three types of electrostatic contributions resulting from the dipole moment of water. Specifically, the term DM includes permanent dipole-dipole, dipole-induced dipole and induced dipole-induced dipole interactions of water molecule. (Chapter 5 contains additional details of these modifications.)

CHAPTER 5

SIMPLIFIED LOCAL-DENSITY/PENG-ROBINSON ADSORPTION MODEL

5.1 Introduction

In this chapter, the simplified local-density Peng-Robinson (SLD-PR) model for adsorption of pure and mixed gases is described. There have been two previous works at OSU dealing with SLD-PR adsorption model; therefore, some aspects of the following discussion of the SLD theoretical framework are similar to those previous works.[25, 27] However, the modifications introduced in the SLD model to account for the molecular interactions of water as an adsorbed fluid are unique to the current work.

5.2 SLD-PR Adsorption Model

The SLD model was developed by Rangarajan et al.[22] by applying the mean-field approximation to the more general density functional theory. Specifically, the model was developed by superimposing the fluid-solid potential on a fluid equation of state to predict the adsorption on flat walls[22] and in slit-shaped pores.[81] The fluid equation of state in SLD is further *simplified* with a local-density approximation in calculating the configurational energy of the inhomogeneous adsorbing fluid, thus giving the model its name.

The main assumptions used in developing the SLD model are[22]:

1. The chemical potential at any point near the adsorbent surface is equal to the bulk phase chemical potential.
2. The chemical potential at any point above the surface is the sum of the fluid-fluid and fluid-solid interactions.

Further, the fluid-solid attractive potential, at any point z, is assumed to be independent of the temperature and the number of molecules at or around that point. Thus, at equilibrium, the molar chemical potential can be given by the sum of the fluid-fluid and fluid-solid interactions as

$$\mu(z) = \mu_{bulk} = \mu_{ff}(z) + \mu_{fs}(z) \tag{5.1}$$

where subscripts "bulk", "ff" and "fs" refer to the bulk, fluid-fluid and fluid-solid chemical potentials, respectively, and "z" refers to the distance from the adsorbent surface.

The SLD model utilized in this work envisions the adsorbent (coal) as composed of rectangular slit-shaped pores. The adsorbate resides within the two-surface slit and, thus, has interactions with both the walls of the adsorbent. Using the slit geometry, Equation (5.1) can be written as

$$\mu(z) = \mu_{bulk} = \mu_{ff}(z) + \mu_{fs1}(z) + \mu_{fs2}(L - z) \tag{5.2}$$

where "L" is the slit-length and "z" or "L-z" refers to the position of the adsorbate molecule from either of the surfaces of the slit. Further, the position of the adsorbate, "z", is measured normal to the plane of the outermost carbon atoms.

The chemical potential for the bulk fluid can be written in terms of the fugacity as

$$\mu_{bulk} = \mu_0(T) + RT\ln\left(\frac{f_{bulk}}{f_0}\right) \tag{5.3}$$

where "f_{bulk}" is the bulk fugacity and "f_0" is the fugacity at an arbitrary reference state.

In a similar manner, the chemical potential of the adsorbed fluid due to fluid-fluid interactions can be written as

$$\mu_{ff}(z) = \mu_0(T) + RT\ln\left(\frac{f_{ff}(z)}{f_0}\right) \tag{5.4}$$

where "f_{ff} (z)" is the fluid fugacity at a position z and "f_0" is the fugacity at the same arbitrary reference state as in Equation (5.3).

For a parallel slit, the fluid-solid chemical potential can be given as:

$$\mu_{fs}(z) = N_A\left[\Psi^{fs}(z) + \Psi^{fs}(L - z)\right] \tag{5.5}$$

where "N_A" is Avogadro's number, "$\Psi(z)$" and "$\Psi(L-z)$" are the fluid-solid interactions from the two surfaces of a slit of length L.

Substituting Equations (5.3)-(5.5) into Equation (5.1) yields the equilibrium criterion for adsorption within a slit:

$$f_{ff}(z) = f_{bulk}\exp\left(-\frac{\Psi^{fs}(z) + \Psi^{fs}(L-z)}{kT}\right) \tag{5.6}$$

where k is the Boltzmann's constant and T is the absolute temperature.

The fluid-solid potential energy function, $\Psi^{fs}(z)$, is given by Lee's partially-integrated 10-4 potential model.[80] Following the work of Chen et al.[81]:

$$\Psi^{fs}(z) = 4\pi\rho_{atoms}\varepsilon_{fs}\sigma_{fs}^2\left(\frac{\sigma_{fs}^{10}}{5(z')^{10}} - \frac{1}{2}\sum_{i=1}^{4}\frac{\sigma_{fs}^4}{(z'+(i-1)\cdot\sigma_{ss})^4}\right) \tag{5.7}$$

$$\varepsilon_{fs} = \sqrt{\varepsilon_{ff}\times\varepsilon_{ss}} \tag{5.8}$$

where "ε_{fs}" is the fluid-solid interaction energy parameter, "ε_{ss}" is the solid-solid interaction energy, ρ_{atoms} = 0.382 atoms/Å^2 is the carbon atom density, "σ_{ff}" and "σ_{ss}" are

the molecular diameters of the adsorbate and the carbon interplanar distance, respectively. The carbon interplanar distance was taken to be that of graphite, 0.335 nm[82] and the values of σ_{ff} and ε_{ff} were taken from Reid et al.[159] The fluid-solid molecular diameter, σ_{fs}, and the distance coordinate, z', which is the perpendicular distance between the centers of the fluid molecule and the first plane of carbon atoms, are defined as

$$\sigma_{fs} = \frac{\sigma_{ff} + \sigma_{ss}}{2} \tag{5.9}$$

$$z' = z + \frac{\sigma_{ss}}{2} \tag{5.10}$$

Further, the fluid-solid interactions given by Equation (5.7) were truncated at the fourth plane of carbon atoms from the solid surface.[81]

The two major simplifications in SLD can be described as follows: In calculating the thermodynamic properties at a point z, a single value of density, $\rho(z)$, is used as a "local" average value, ignoring the gradients in density about the point z. This approximation is referred to as the local density approximation. Further, in calculating the chemical potential, the mean-field theory is applied that uses an averaged potential and ignores local fluctuations within the slit.[22]

The SLD model requires a fluid equation of state (EOS) to evaluate the densities and fugacities of the bulk and adsorbed phases, as seen in Equation (5.6). Several authors have used different EOS's with the SLD theory. These include the Van der Waals, Peng-Robinson, Elliot-Suresh-Donohue and Bender EOSs.[22-27, 81]

Following a previous work at OSU[25], the Peng-Robinson (PR) EOS is utilized in the current study. The PR EOS[83] can be expressed as:

$$\frac{P}{\rho RT} = \frac{1}{(1-\rho b)} - \frac{a(T)\rho}{RT\left[1+\left(1-\sqrt{2}\right)\rho b\right]\left[1+\left(1+\sqrt{2}\right)\rho b\right]} \tag{5.11}$$

where $$a(T) = \frac{0.457535\,\alpha(T)R^2T_C^2}{P_C} \tag{5.12}$$

$$b = \frac{0.077796\,RT_C}{P_C} \tag{5.13}$$

In Equation (5.12), the term $\alpha(T)$ was calculated with the following expression developed at OSU[160]:

$$\alpha(T) = \exp\left(\left(A + BT_r\right)\left(1 - T_r^{C+D\omega+E\omega^2}\right)\right) \tag{5.14}$$

where A, B, C, D and E are correlation parameters and their values, respectively, are 2.0, 0.8145, 0.134, 0.508 and -0.0467. The values used were based on accurate description of saturation pressures for the coalbed gases under conditions encountered in CBM operations.

The physical properties for methane, nitrogen, CO_2 and water used in the SLD model are listed in Table 5.1.

Table 5.1 Physical Properties of Fluids Used in SLD-PR Model

	Nitrogen	**Methane**	**CO_2**	**Water**
T_C (K)	126.19	190.56	304.13	647.09
P_C (MPa)	3.396	4.599	7.377	22.065
σ_{ff} (nm)	0.3798	0.3758	0.3941	0.2641
ε_{ff}/k (K)	71.4	148.6	195.2	809.1

The fugacity of a bulk fluid using the PR EOS is given as

$$\ln\frac{f_{bulk}}{P} = \frac{b\rho}{1-b\rho} - \frac{a(T)\rho}{RT\left(1+2b\rho - b^2\rho^2\right)}$$

$$-\ln\left[\frac{P}{RT\rho} - \frac{Pb}{RT}\right] - \frac{a(T)}{2\sqrt{2}bRT}\ln\left[\frac{1+(1+\sqrt{2})\rho b}{1+(1-\sqrt{2})\rho b}\right] \tag{5.15}$$

where "P" is the bulk fluid pressure, "ρ" is the density, "a" and "b" are the EOS constants given by Equations (5.12) and (5.13) above.

By analogy, the fugacity for fluid-fluid interactions of the adsorbed fluid can be written as

$$\ln\frac{f_{ff}(z)}{P} = \frac{b\rho(z)}{1-b\rho(z)} - \frac{a_{ads}(z)\rho(z)}{RT\left(1+2b\rho(z)-b^2\rho^2(z)\right)} - \ln\left[\frac{P}{RT\rho(z)} - \frac{Pb}{RT}\right] - \frac{a_{ads}(z)}{2\sqrt{2}bRT}\ln\left[\frac{1+(1+\sqrt{2})\rho(z)b}{1+(1-\sqrt{2})\rho(z)b}\right] \quad (5.16)$$

In Equation (5.16), the attractive term in the EOS, $a_{ads}(z)$, is a function of position in the slit, and therefore accounts for the fluid-fluid interactions in the slit. Chen et al.[81] developed the equations for $a_{ads}(z)$, which depends on the ratio of slit length L to the molecular diameter σ_{ff}.

Fitzgerald[25] adjusted the covolume b_{ads} in the PR EOS to improve the predictive capability for adsorption of pure gases on activated carbon and coals. The covolume has a significant effect on the local density of the adsorbed fluid near the surface. In addition, the covolume is important in determining the density profile at high pressures.

An empirical correction, Λ_b, was applied to the covolume to account more accurately for the repulsive interactions of adsorbed fluid at high pressures, given as

$$b_{ads} = b\left(1+\Lambda_b\right) \quad (5.17)$$

Typical values of Λ_b range from -0.4 to 0.0 for coalbed gases. The value is expected to be dependent to some extent on the amount of moisture on the coal. This is reasonable since the adsorbed-phase density of wet adsorbents can be expected to be higher than that of dry coals.

With this modification, Equation (5.16) can be written as

$$\ln\frac{f_{ff}(z)}{P} = \frac{b_{ads}\rho(z)}{1-b_{ads}\rho(z)} - \frac{a_{ads}(z)\,\rho(z)}{RT\left[1+2b_{ads}\rho(z)-b_{ads}^{2}\rho(z)^{2}\right]}$$

$$-\ln\left[\frac{1-b_{ads}\rho(z)}{RT\rho(z)}\right] - \frac{a_{ads}(z)}{2\sqrt{2}b_{ads}RT}\ln\left[\frac{1+(1+\sqrt{2})\rho(z)b_{ads}}{1+(1-\sqrt{2})\rho(z)b_{ads}}\right] \qquad (5.18)$$

Thus, Equation (5.15) and (5.18) are used to calculate the fugacities of the bulk and adsorbed phases which are necessary to solve the equilibrium criterion given by Equation (5.6).

The excess adsorption, n^{Ex}, in the SLD model is given as

$$n^{Ex} = \frac{A}{2}\int_{\text{Left Side of Slit}}^{\text{Right Side of Slit}}\left(\rho(z)-\rho_{bulk}\right)dz \qquad (5.19)$$

where n^{Ex} is the excess adsorption in number of moles per unit mass of adsorbent, and "A" is the surface area of the adsorbate on a particular adsorbent. The equation contains "A/2" because both walls contribute to the total surface area. The lower limit in the integration of Equation (5.19) is $3/8\sigma_{ff}$ or $3/8^{th}$ the diameter of an adsorbed molecule touching the left plane surface. The upper limit is L-$3/8\sigma_{ff}$, which is the location of an adsorbed molecule touching the right plane surface. Further, the local density is assumed to be zero for distances less than $3/8\sigma_{ff}$ from the wall. The value of $3/8\sigma_{ff}$ is chosen to account for most of the adsorbed gas; details are given elsewhere by Fitzgerald.[25]

In solving for the local density using the SLD equilibrium criterion, the slit is divided into two halves and each half is subdivided into 50 intervals. The local density is then determined for each interval. Once the local density is determined across the slit, the excess adsorption is calculated by integrating Equation (5.19) using Simpson's rule. Thus, the SLD model has three regressed parameters: A, ε_{ss} and L.

5.3 Modifications to SLD-PR Model for Pure Water Adsorption Modeling

As discussed in Chapter 4, two types of molecular interactions are important when considering water adsorption on activated carbons and coals. Specifically, these two interactions are:

(1) The hydrogen bonds between the adsorbed water molecules and the oxygenated groups on the adsorbent surface and

(2) The electrostatic interactions between adsorbed water molecules due to the large dipole moment of water.

The fluid-solid potential function, $\Psi(z)$, in the SLD model is typically estimated from the partially integrated 10-4 Lee's potential.[80] This potential accounts only for the dispersive interactions of the adsorbate molecules. Since the contributions of the electrostatic and polar interactions are significant in water adsorption, Lee's potential was augmented with terms for the hydrogen bond energy[32] and dipole interactions[156] within water molecules as follows:

$$\Psi(z) = 4\pi\rho_{atoms}\varepsilon_{fs}\sigma_{fs}^2\left(\frac{\sigma_{fs}^{10}}{5(z')^{10}} - \frac{1}{2}\sum_{i=1}^{4}\frac{\sigma_{fs}^4}{\left(z'+(i-1)\cdot\sigma_{ss}\right)^4}\right) + \varepsilon_{HB} + DM \qquad (5.20)$$

where ε_{HB} is the hydrogen-bond potential between the functional groups on the carbon surface and water molecules and DM refers to the sum of three types of electrostatic contributions resulting from the dipole moment of water. Specifically, the term DM includes permanent dipole-dipole, dipole-induced dipole and induced dipole-induced dipole interactions of water molecule.

Hydrogen Bond Potential

The hydrogen bond potential for water is adapted from the Grand Canonical Monte Carlo simulation work of Muller et al.[28] This potential models water as a Lennard-Jones sphere with four sites arranged in a tetrahedral geometry. In their simulations, two sites represented hydrogen atoms and two represented a lone pair of electrons capable of forming hydrogen bonds with the surface, and the oxygen atom was represented by the sphere. An off-center square-well potential was used to represent the interaction potential of the hydrogen bond. This potential has the following advantages[32] :

(1) The potential model is short-ranged

(2) It allows for highly localized attractive interactions, which more realistically model the hydrogen bonding

(3) Parameters can be obtained from the experimental adsorption data and/or gas-liquid co-existence properties of bulk water

Thus, the hydrogen bond potential of water with the adsorbent surface can be summarized as follows:

$$\begin{aligned} \varphi_{HB} &= -\varepsilon_{HB} \quad \text{if} \quad r_{AB} < \sigma_{HB} \\ \varphi_{HB} &= 0 \qquad \text{otherwise} \end{aligned} \tag{5.22}$$

There appears to be no literature study on water adsorption on carbons that includes *both* dipole moment and hydrogen bond contributions to the total potential. Further, the Lennard-Jones interaction energy, ε_{ff}/k, for the water molecule[159] used in this work was 809.1 K. This value of ε_{ff}/k was obtained from viscosity-based calculations[159] and appears to include polar contributions of the water molecule. Therefore, based on our analysis of new SLD parameterization, a value of 70 K was used for ε_{HB}/k to provide physically-reasonable *total* potential values for water calculated from Equation (5.20).

Dipole Interactions of Water

Kotdawala et al.[156] applied the mean-field perturbation theory to model the adsorption of polar molecules in nanopores. They considered the electrostatic interactions of water molecules which included the permanent dipole-dipole, dipole-induced dipole and induced dipole-induced dipole interactions. The relative contributions of these terms are about 80, 15 and 5%, respectively at 0ºC.[161, 162] In the work of Kotdawala et al.[156], these electrostatic interactions were also dependent on the bulk pressure and the density of water molecules in the slit. Following their approach, three dipole interaction terms[161] were added to the fluid-solid potential function in SLD to account for the polar nature of water molecules in the adsorbed phase:

$$\phi = -\left[\frac{2}{3}\frac{\mu^4}{(4\pi\varepsilon_0)^2 kTr^6} + \frac{2\mu^2\alpha'}{4\pi\varepsilon_0 r^6} + \frac{3}{4}\frac{(\alpha')^2 I}{r^6}\right] \tag{5.23}$$

where the three terms correspond to dipole-dipole, dipole-induced dipole and induced dipole-induced dipole attractive potentials, respectively. The physical constants used in Equation (5.23) are defined as[161]:

μ = Dipole moment of water, coulomb. m

$\alpha' = \frac{\alpha}{4\pi\varepsilon_0}$ = Polarizability volume of water, m^3

I = Ionization potential of water, J

ε_0 = Permittivity of free space, $Coulomb^2/J\ m$

k = Boltzmann's constant, J/K

The values of these physical constants were adopted from Tester et al.[161] and Prausnitz et al.[162] Based on Equation (5.23), the value of ϕ at 0°C is estimated to be about 250 x 10^-79 Jm^6 and was used in this work at the correct temperature since one of the terms is a

function of temperature. In particular, the dipole-dipole energy or the first term in Equation (5.23) is inversely proportional to the absolute temperature.

Excess Adsorption Isotherm Equation for Water Adsorption

In addition to the modifications discussed above, the excess adsorption isotherm equation in SLD given by Equation (5.19) was also modified to account for the bimodal nature of water adsorption.

The modified excess isotherm equation for water adsorption is given as

$$n_{\text{Water}}^{\text{Gibbs}} = \left(\frac{A_p}{2} + \frac{A_s}{2} \right) \int_{\text{Left Side of Slit}}^{\text{Right Side of Slit}} (\rho(z) - \rho_{bulk}) dz \qquad (5.24)$$

where "A_s" represents the surface area provided for adsorption of water by the clusters of water molecules. Specifically, "A_p" represents the primary adsorption of water molecules (at the surface sites) and "A_s" represents the secondary adsorption (water clusters). Additional details on these modifications to the SLD model are given in Section 5.6, which includes a discussion of the technique adopted in this work for modeling the CO_2-water *competitive* mixture adsorption on coals.

5.4 Representation of Adsorbed Water Capacity with SLD-PR Model

The new parameterization of the SLD-PR model was tested for its ability to represent the water adsorption capacity of several activated carbons and coals. Specifically, ten well-characterized activated carbons from the literature were selected, and the modified SLD-PR model was used to represent the adsorbed water capacity of these carbons. The carbons ranged from as-received samples to highly oxidized activated carbon cloths. The SLD-PR model includes two types of surface areas for water adsorption. The two parameters were estimated as follows:

The N_2 BET surface areas were available for all the ten activated carbons. Barton et al.[94] had observed for a set of activated carbons that the N_2 BET surface area of the carbons corresponded to about 40% of the surface coverage of water on those carbons. Further, this represented the upper limit of the traditional surface coverage for water adsorption on these carbons. In the absence of more accurate information on the exact partitioning of the two surface areas for water adsorption, the findings of Barton et al.[94] were adopted and the surface area "A_p" for primary adsorption of water was fixed at 40% of the N_2 BET surface area for each carbon. Further, the surface area "A_s" was *estimated* using the available experimental data on adsorbed water capacity. Although this is not an exact technique, the method has been used here solely to demonstrate the new parameterization of SLD model for modeling water adsorption.

Table 5.2 presents the results of this case study. The table lists the activated carbons, their experimental adsorbed water capacities reported in the literature, N_2 BET surface areas and the two surface areas for water adsorption in the SLD model. The surface area "A_s" was the only parameter *calculated* based on the water adsorption capacity. Similar to the findings in Chapter 4, the table shows that the N_2 BET surface *alone* may not provide complete information on water adsorbed capacity. This can be seen more clearly if the sum of two surface areas in SLD is compared with the experimental N_2 BET surface area. As evident from the table, large differences exist between the *total* surface area in SLD and BET surface area estimates.

Similarly, the new parameterization was used with coals for which BET surface area estimates were available. Mahajan and Walker[92] reported the water adsorption isotherms on a series of coals and provided the BET surface areas calculated directly

from water adsorption. Similar to the method described above, the SLD model was used to represent the adsorbed water capacity of these coals. Specifically, the surface area "A_p" for primary adsorption of water was fixed at the BET reported value for water and "A_s" was *estimated* with the experimental data. The results are shown in Table 5.3 and lead to similar conclusions as reached for the activated carbons above. Note here that surface areas "A_s" were evaluated based on the ultimate water uptake for the carbon or coal. This was done to facilitate subsequent modeling of mixed gas adsorption with water as one of the components. Therefore, no attempt was made to "fit" the complete, low-pressure water isotherms.

5.5 SLD-PR Model for Mixed-Gas Adsorption

In this section, the SLD-PR model for mixed gas adsorption is outlined. Specifically, the one-fluid mixing rules are used to extend the SLD-PR model for pure gas adsorption described in the previous section to mixtures.

When dealing with mixtures, the bulk fugacity of a component 'i' using the PR EOS is given as

$$\ln\left(\frac{\hat{f}_i^{bulk}}{y_i P}\right) = \frac{b_i}{b}(Z-1) - \ln\left(Z - \frac{pb}{RT}\right) + \frac{a}{2\sqrt{2}RTb}\left(\frac{b_i}{b} - \frac{2\sum_j y_j a_{ij}}{a}\right)\ln\left(\frac{\left(1+\rho b\left(1+\sqrt{2}\right)\right)}{\left(1+\rho b\left(1-\sqrt{2}\right)\right)}\right) \tag{5.25}$$

The familiar one-fluid mixing rules are used for the EOS constants "a" and "b" in the bulk phase and given as

$$a = \sum_i \sum_j y_i y_j (a_{bulk})_{ij} \tag{5.26}$$

Table 5.2 A Case Study with the New Parameterization of SLD-PR Model for Pure Water Adsorption on Activated Carbons

	Experimental Data		Estimated			
Activated Carbon	**Adsorbed Water Capacity (mmol/gm)**	**N_2 BET Surface Area (m^2/gm)**	**$A_{primary}$ (m^2/gm)**	**A_w (m^2/gm)**	**$A_{primary}+A_w$ (m^2/gm)**	**Reference**
BPL	25.6	900-1000	400	415	815	Barton et al.[104]
W	39.0	1500	600	644	1244	Bandosz et al.[87]
W2	23.0	860	344	389	733	Bandosz et al.[87]
N	23.0	970	388	345	733	Bandosz et al.[87]
N1	15.0	625	250	228	478	Bandosz et al.[87]
N2	25.0	860	344	453	797	Bandosz et al.[87]
AC-4% N	37.5	1738	695	501	1196	Dimotakis et al.[96]
AC-32% O	27. 8	1105	442	444	886	Dimotakis et al.[96]
AC-7% Cl	28.3	1523	609	294	903	Dimotakis et al.[96]
AC-16% Cl	28.9	1374	550	371	921	Dimotakis et al.[96]

Table 5.3 A Case Study with the New Parameterization of SLD-PR Model for Pure Water Adsorption on Coals

	Experimental Data		Estimated		
Coal	**Adsorbed Water Capacity (mmol/gm)**	**CO_2 BET Surface Area (m2/gm)**	**$A_{primary}$ (m2/gm)**	**A_w (m2/gm)**	**Reference**
912	1.2	17	17	21	Mahajan and Walker[92]
888	1.9	38	38	23	Mahajan and Walker[92]
885	1.8	42	42	15	Mahajan and Walker[92]

$$b = \sum_i y_i b_i \tag{5.27}$$

where the quadratic and linear combining rules were used for "$(a_{bulk})_{ij}$" and "b_i", respectively.

Similarly, the fugacity of a component "i" in the adsorbed phase using the PR EOS is given as

$$\ln\left(\frac{\hat{f}_i^{ads}(z)}{x_i(z)P}\right) = \frac{2\sum_j x_j(z)b_{ij} - b}{b}\left(\frac{P}{\rho_{ads}(z)RT} - 1\right) - \ln\left(\frac{P}{\rho_{ads}(z)RT} - \frac{Pb}{RT}\right) + \frac{a(z)}{2\sqrt{2}RTb}\left(\frac{2\sum_j x_j(z)b_{ij} - b}{b} - \frac{2\sum_j x_j(z)a_{ij}(z)}{a(z)}\right)\ln\left(\frac{\left(1+\rho_{ads}(z)b\left(1+\sqrt{2}\right)\right)}{\left(1+\rho_{ads}(z)b\left(1-\sqrt{2}\right)\right)}\right) \tag{5.28}$$

The mixing rules for the EOS constants in the adsorbed phase are given as

$$a = \sum_i \sum_j x_i x_j (a_{ads})_{ij} \tag{5.29}$$

$$b = \sum_i \sum_j x_i x_j (b_{ads})_{ij} \tag{5.30}$$

The cross coefficient $(a_{ads})_{ij}$ in Equation (5.29) is calculated with the geometric mean combining rule. For asymmetric mixtures, a binary interaction parameter (BIP), C_{ij}, is also used in the adsorbed phase as

$$(a_{ads})_{ij} = \sqrt{(a_{ads})_i (a_{ads})_j}\left(1 - C_{ij}\right) \tag{5.31}$$

Further, the attractive constant a_{ads} of each component "i" is calculated using the same method outlined for pure components. The constant a_{ads} is a function of position in the slit and fluid-fluid molecular distance and the equations relating these were given by Chen et al. [81]

The cross coefficient $(b_{ads})_{ij}$ is obtained from a linear combining rule with the empirical correction discussed in the previous section

$$\left(b_{ads}\right)_{ij} = \left(\frac{b_i\left(1+\Lambda_{b,i}\right)+b_j\left(1+\Lambda_{b,j}\right)}{2}\right) \tag{5.32}$$

where the Λ_b values for each component are from pure component adsorption data.

The equilibrium criterion in SLD for mixed gas adsorption, subject to the mass balance constraints, is given as

$$\ln\left(\frac{\hat{f}_i^{ads}[\rho(z),\rho_{ads}(z)]}{\hat{f}_i^{bulk}}\right) = -\left(\frac{\Psi_i^{fs}(z)+\Psi_i^{fs}(L-z)}{kT}\right) \qquad i = 1, NC \tag{5.33}$$

where the fugacity of the adsorbed phase is a function of pressure, temperature, local density and local composition at a given point z in the slit.

The fluid-solid potential function of each component for mixed gas adsorption is also calculated with the Lee's partially integrated 10-4 potential.[80] The potential function for mixed gas adsorption is given as[23, 25]

$$\Psi^{fs}{}_i(z) = 4\pi\rho_{atoms}\left(\varepsilon_{fs}\right)_i\left(\sigma_{fs}^2\right)_i\left(\frac{\left(\sigma_{fs}^{10}\right)_i}{5(z')^{10}}-\frac{1}{2}\sum_{i=1}^{4}\frac{\sigma_{fs,i}^4}{\left(z'+(i-1)\cdot\sigma_{ss}\right)^4}\right) \tag{5.34}$$

$$\left(\varepsilon_{fs}\right)_i = \sqrt{\varepsilon_{ff,i}\times\varepsilon_{ss}} \tag{5.35}$$

where $(\varepsilon_{fs})_i$ is the fluid-solid interaction energy parameter of component "i". The other physical quantities in these equations were similar to the case of pure gas adsorption.

The excess adsorption of a component "i" in a mixture is given as:

$$n_i^{Ex} = \frac{A}{2}\int_{\frac{3}{8}\sigma_{ff,8}}^{L-\frac{3}{8}\sigma_{ff,i}}\left(\rho_{ads}(z)\,x_i(z)-\rho_{bulk}\,y_i\right)dz \tag{5.36}$$

As shown in Equation (5.36), the excess amount adsorbed of each component is dependent on the composition in the bulk and adsorbed phases, as well as the densities in the bulk and adsorbed phases.

For mixture adsorption calculations, the pressure, temperature, feed mole fractions and void volume are necessary input information to calculate the experimental component excess adsorption for each component. Specifically, a mass balance equation is formulated and is given as

$$z_i = \frac{n_i^{Ex} + \rho_{bulk} V_{void} y_i}{n_{tot}^{Ex} + \rho_{bulk} V_{void}} \tag{5.37}$$

In the manner described for pure gas adsorption, half the slit is subdivided into 50 segments or intervals. The adsorbed phase mole fractions are initialized as the feed mole fractions. The system of non-linear algebraic equations given by Equation (5.33) is solved with the Newton's method that uses numerical derivatives for evaluating the elements of the Jacobian matrix.[163] Thus, the solution to the system of equilibrium criterion equations (Equation (5.33)) provides the local density and adsorbed-phase mole fractions in each interval of the slit, subject to the constraint on mole fractions, $\sum_i x_i = 1$. Using the calculated density and mole fractions, excess adsorption of each component is evaluated by Equation (5.36).

The excess adsorbed amounts calculated in the above step are then used to evaluate the bulk phase mole fractions using the mass balance given by Equation (5.37), subject to the constraint on mole fractions, $\sum_i y_i = 1$. The system of non-linear algebraic equations given by Equation (5.37) is also solved by the Newton's method.

If the calculated mole fractions do not satisfy the component mass balance equations, a new set of bulk mole fractions are used to calculate the next set of trial excess adsorbed amounts for each component. This procedure is continued until the component mass balances (Equation (5.37)), the equilibrium criterion (Equation (5.33)) and the constraints on the bulk and adsorbed mole fractions are all satisfied.

5.6 SLD-PR Modeling of CO_2-Water Mixture Adsorption on Wet Argonne Coals

As mentioned in Chapter 1, a more realistic modeling of gas adsorption on wet coals requires treating water as a *separate adsorbed component*. Therefore, in this section, the experimental data for CO_2 adsorption on wet Argonne coals is used to demonstrate this new approach of modeling these systems. Specifically, this effort comprised of the following steps:

(1) Implement a new data reduction method that attempts to account for the presence of water in as many as three phases (gas, adsorbed, liquid).

(2) Perform CO_2-water mixture adsorption calculations with the SLD model, wherein water is treated as an active component, using the newly reduced experimental data from Step 1.

(3) Conduct the Gibbs free energy or a phase-check analysis utilizing the converged calculations from Step 2 to analyze the possible presence of a third phase in these adsorptive systems.

The three steps outlined above were performed in sequence and are detailed below:

Step 1. New Data Reduction Method for CO_2-Water Mixture Adsorption

As mentioned above, the new data reduction method attempts to account for the presence of water in as many as three phases. Specifically, the method comprised of the following three corrections to the traditional data reduction technique for these systems.

(a) The adsorbed water was excluded from gas solubility calculations. In other words, the adsorbing gas (CO_2) was assumed to be soluble only in the *excess* (liquid-phase) water present on coals. The excess water was estimated to be the water present on coals that was in addition to their equilibrium moisture content.

(b) The mole fraction of water vapor in the bulk gas phase was assumed to be 1%, i.e. $y_{CO2} = 0.99$.

(c) The density of bulk gas phase containing water (wet gas) was increased by 1%.

The assumptions in (b) and (c) were based on our analysis of vapor-liquid equilibrium data for this system in the literature. These "typical values" are assumptions that were necessary due to the unavailability of vapor phase composition and density data for CO_2-water mixtures on wet adsorbents.

Using the above assumptions, the excess adsorption of CO_2 and water were calculated with the usual material balance calculations as outlined below:

The amount of CO_2 gas injected is given as

$$n_{inj}^{CO2} = \frac{P\Delta V}{ZRT} \tag{5.38}$$

where P is the bulk pressure, ΔV is the injected volume and Z is the compressibility factor of CO_2.

The amount of CO_2 in the unadsorbed phase is given as

$$n_{unads}^{CO2} = \frac{PV_{Void}\, y_{CO2}}{Z_{mix} RT} \tag{5.39}$$

where V_{void} is the void volume, y_{CO2} is the estimated bulk gas mole fraction of CO_2 and Z_{mix} is the corrected compressibility factor for the bulk phase CO_2-water mixture.

The amount of water in the unadsorbed phase is given with an equation analogous to Equation (5.39) as

$$n_{unads}^{water} = \frac{PV_{Void}\, y_{water}}{Z_{mix} RT} \tag{5.40}$$

Therefore, the excess adsorption of CO_2 is given as

$$n_{CO2}^{Ex} = n_{inj}^{CO2} - n_{unads}^{CO2} - n_{sol} \tag{5.41}$$

where n_{sol} is the amount of gas soluble in the excess water present (if any).

Similarly, the excess adsorption of water can be calculated by invoking the void volume definition and using the information available for the total amount of water present in the system.

$$n_{water}^{Ex} = n_{water}^{total} - n_{unads}^{water} - n_{water}^{liquid} \tag{5.42}$$

where n_{water}^{total} is the amount of water present in the system (known) and n_{water}^{liquid} is the amount of free water present (if any).

Using this new data reduction method, the raw CO_2 adsorption data on five wet Argonne coals were reprocessed. Figures 5.1-5.5 present the CO_2 adsorption isotherms on wet Pocahontas, Upper Freeport, Illinois #6, Wyodak and Beulah Zap coals, respectively. For comparative purposes, the CO_2 adsorption isotherms on both wet and dry Argonne coal, when using the traditional (original) data reduction method, are also illustrated in these figures. As evident from these figures, the new approach results in increasing the

calculated excess adsorption values on coals with large amounts of adsorbed water. Since the new data reduction technique excludes the adsorbed water from gas solubility calculations, this effect is expected.

Further, the calculated excess adsorption values using the new approach for two of the coals that contained less than 1% moisture (Pocahontas and Upper Freeport) are almost identical to the values calculated using the traditional (original) method. This is shown in Figures 5.1 and 5.2 for the two coals, respectively.

In summary, the exclusion of solubility of gas in adsorbed water results in increasing the calculated amount of gas adsorbed. Similarly, accounting for the solubility of water in the gas phase also increases the calculated values of adsorption. In contrast, accounting for the density of wet gas lowers the calculated values of adsorption.

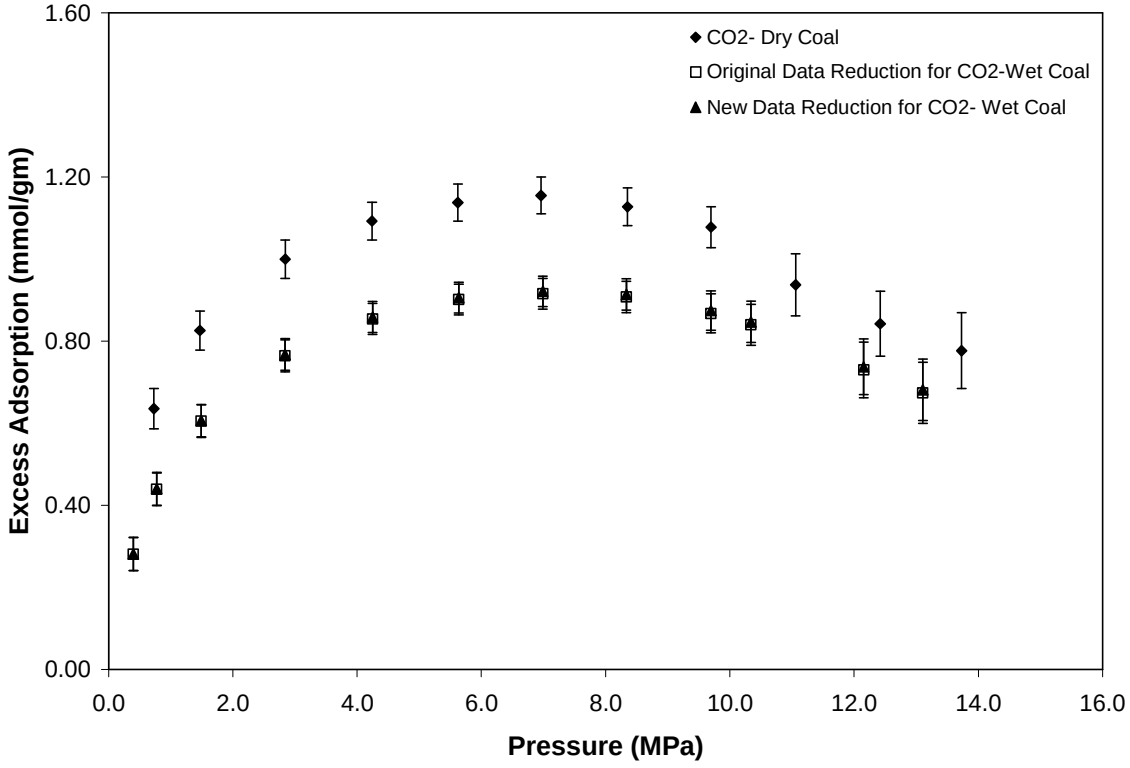

Figure 5.1 CO_2 Adsorption on Wet Pocahontas Coal with 0.65% Moisture at 328.2 K: New Data Reduction Method

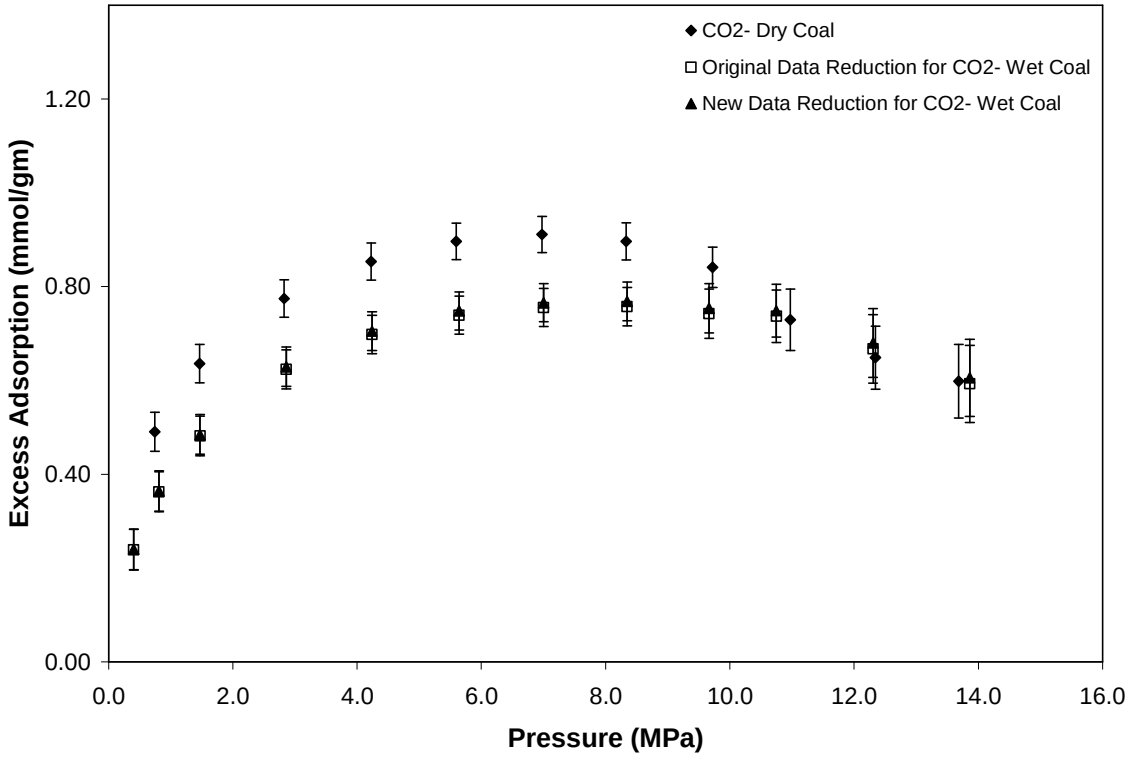

Figure 5.2 CO_2 Adsorption on Wet Upper Freeport Coal with 1.10% Moisture at 328.2 K: New Data Reduction Method

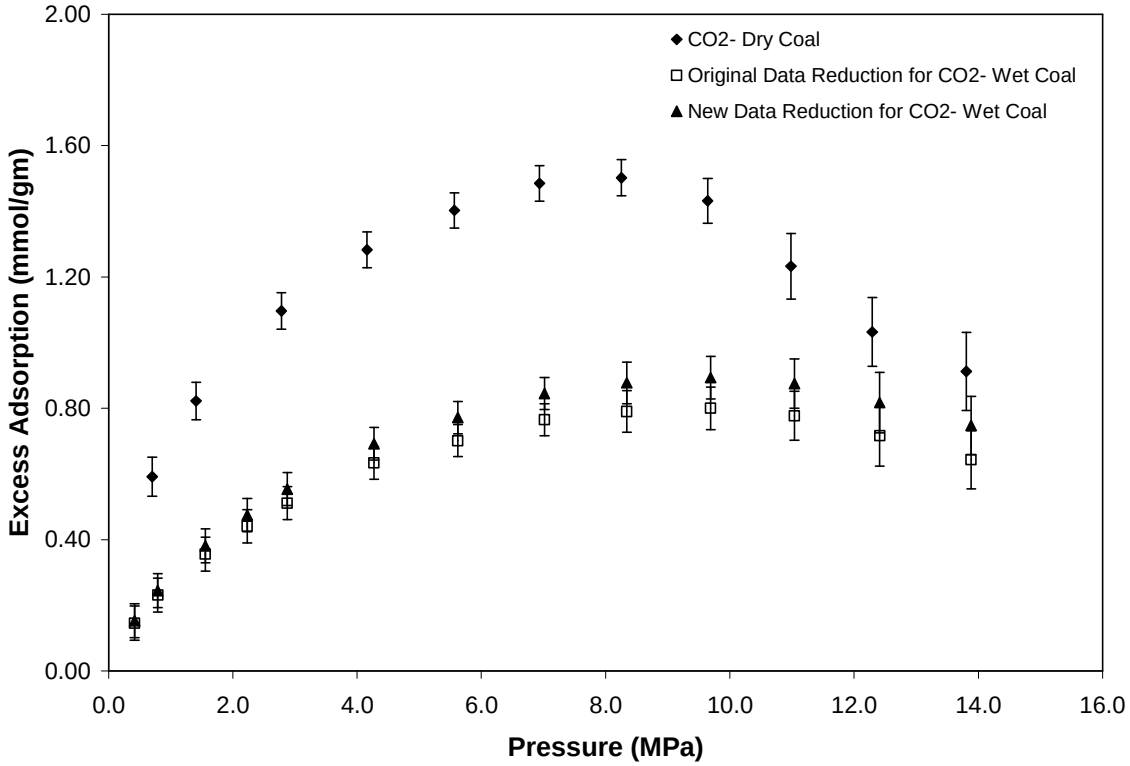

Figure 5.3 CO_2 Adsorption on Wet Illinois #6 Coal with 9.2% Moisture at 328.2 K: New Data Reduction Method

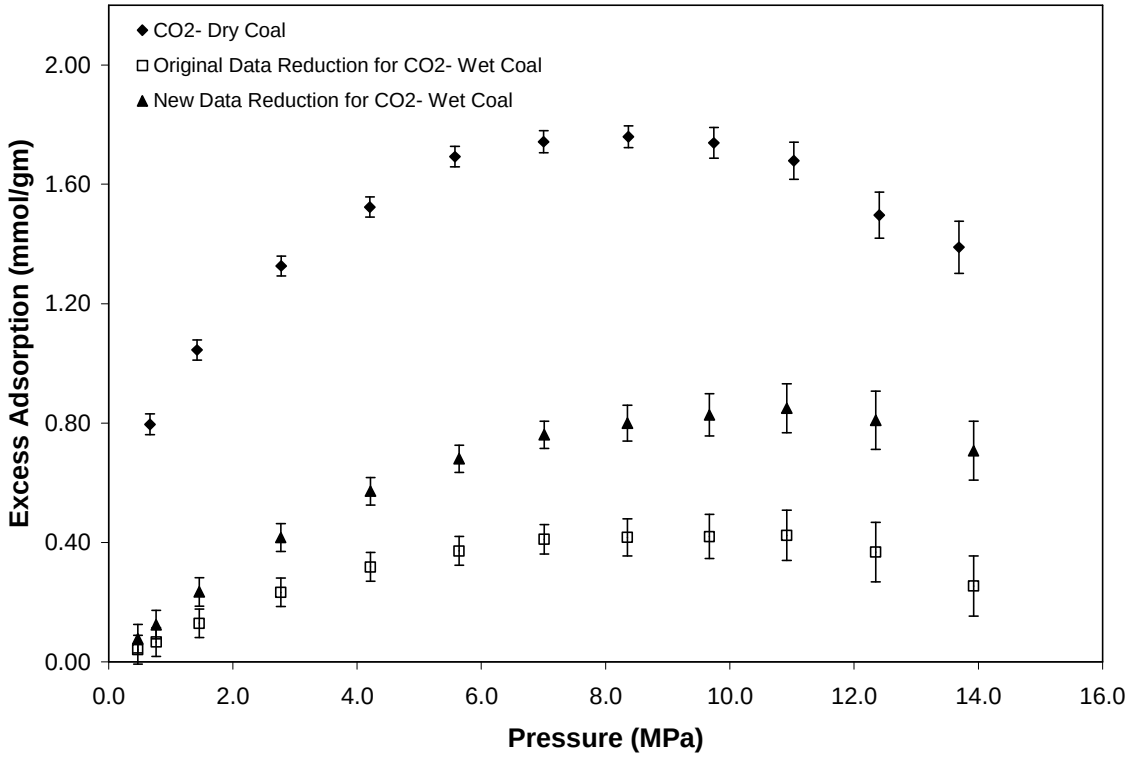

Figure 5.4 CO_2 Adsorption on Wet Wyodak Coal with 28.0% Moisture at 328.2 K: New Data Reduction Method

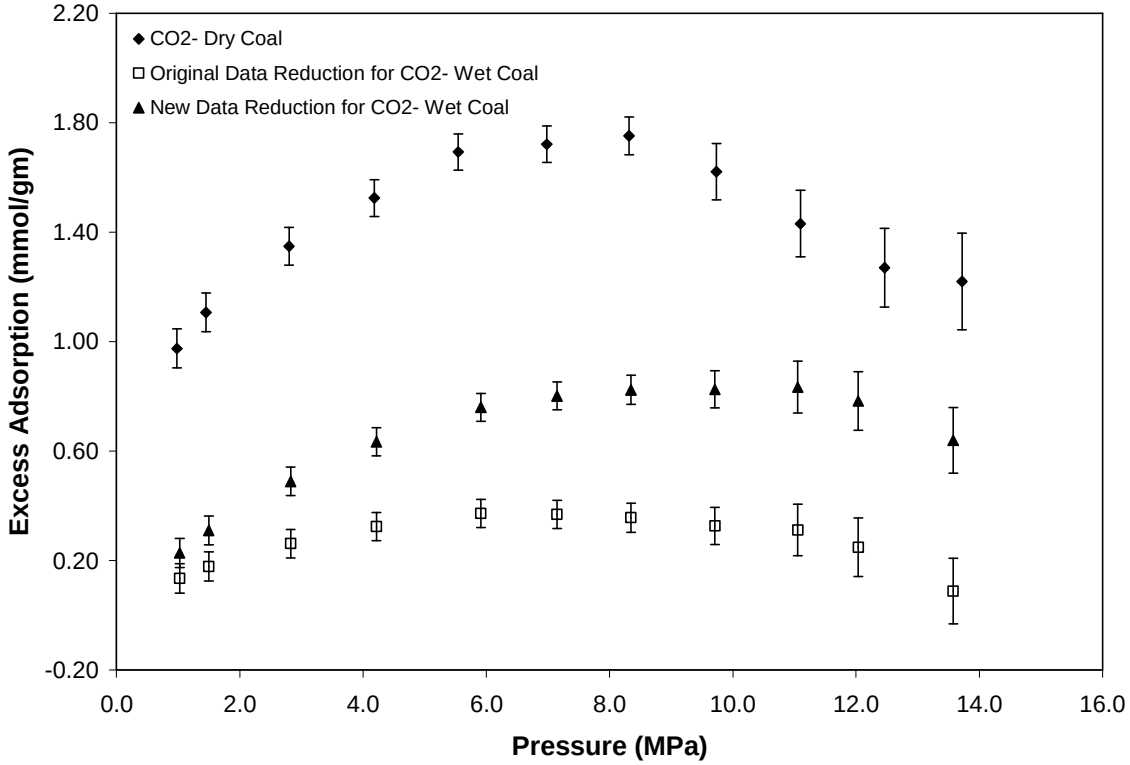

Figure 5.5 CO_2 Adsorption on Wet Beulah Zap Coal with 32.2% Moisture at 328.2 K: New Data Reduction Method

Step 2. CO_2-Water Mixture Adsorption Calculations

In this section, the SLD-PR modeling strategy for CO_2-water mixture adsorption on wet coals is described in detail. Specifically, the partitioning of the molecular interactions of water and CO_2 within a slit in the SLD model is discussed with a special emphasis on calculations involving this mixture.

The general SLD model partitions the molecular interactions of an adsorbing species in the slit into two contributions- *fluid-fluid* and *fluid-solid*. Specifically, for each component in a gas mixture, the molecular interactions in the bulk and adsorbed phases are accounted for in the following way:

$$\mu_i^{bulk} = \mu_i^{ff} + \mu_i^{fs} \tag{5.43}$$

For example, in a CO_2-CH_4 mixture, Equation (5.43) yields

$$\mu_{CO_2}^{bulk} = \mu_{CO_2}^{ff} + \mu_{CO_2}^{fs} \tag{5.44}$$

$$\mu_{CH_4}^{bulk} = \mu_{CH_4}^{ff} + \mu_{CH_4}^{fs} \tag{5.45}$$

These equations are solved simultaneously to model the competitive adsorption of a binary mixture of these components.

Equations (5.44) and (5.45) are intended for modeling the adsorption of largely non-polar molecules. When one of the components in a mixture is strongly polar (such as water), additional terms are needed to more effectively account for the unique molecular interactions of water in the adsorbed phase. These molecular interactions are a result of the large polarity of the water molecule. In fact, McCallum et al.[32] observed that the *fluid-fluid* interactions of water are stronger than the *fluid-solid* interactions in the adsorption of water on activated carbons. Muller et al.[28] have shown that water forms *three-dimensional clusters* in the slit and at the entrances to the pores resulting in a pore-

blocking effect. These clusters are formed because of strong fluid-fluid interactions or the dipole moment of water. Further, Kotdawala et al.[156] have developed a model based on perturbation theory that accounts for the dipole interactions of water confined in a slit as a homogenous fluid. When these polar and electrostatic interactions are included in the SLD model, the following equations are obtained for CO_2-water binary mixture:

$$\mu_{CO_2}^{bulk} = \mu_{CO_2}^{ff} + \mu_{CO_2}^{fs} \tag{5.46}$$

$$\mu_{Water}^{bulk} = \mu_{Water}^{ff} + \mu_{Water}^{fs} + \mu_{HB}^{fs} + \mu_{Dipole}^{ff} \tag{5.47}$$

Equation (5.47) for the chemical potential of water in the adsorbed phase contains four interaction terms that will be explained below:

The first term in Equation (5.47) represents the *fluid-fluid* interactions of water in the adsorbed phase that are obtained from the modified PR EOS in the SLD model. The second term in Equation (5.47) represents the *fluid-solid* dispersive interactions of water in the adsorbed phase with the solid adsorbent. These two terms account for the dispersive interactions of water adsorbed on the surface as well as the clusters of water molecules with the adsorbent surface. Further, these two terms are present for every adsorbing fluid, since these terms represent the non-polar, dispersive interactions which are considered to be dominant in the adsorption of most non-polar adsorbates.

The third term in Equation (5.47) accounts for the unique hydrogen-bond type interactions of water with the oxygenated surface sites on the adsorbent. Therefore, this term represents the *polar fluid-solid* interactions of water in the slit and accounts for the adsorption of water molecules on the adsorbent surface sites (primary adsorption).

The fourth term in Equation (5.47) is the sum of three types of electrostatic interactions of water that are considered to be dominant in a water molecule.[161, 162] The

term is a summation of dipole-dipole, dipole-induced dipole and induced dipole-induced dipole interaction energies of water molecule in the slit.[156] As such, this term represents the strongly *polar fluid-fluid* interactions of water in the adsorbed phase and, thus, accounts for the electrostatic interactions within the clusters of water molecules (secondary adsorption).

Figure 5.6 illustrates an idealized depiction of these molecular interactions within a two-surface slit. The figure depicts water and CO_2 molecules in the slit and shows the partitioning of molecular interactions that have been discussed above.

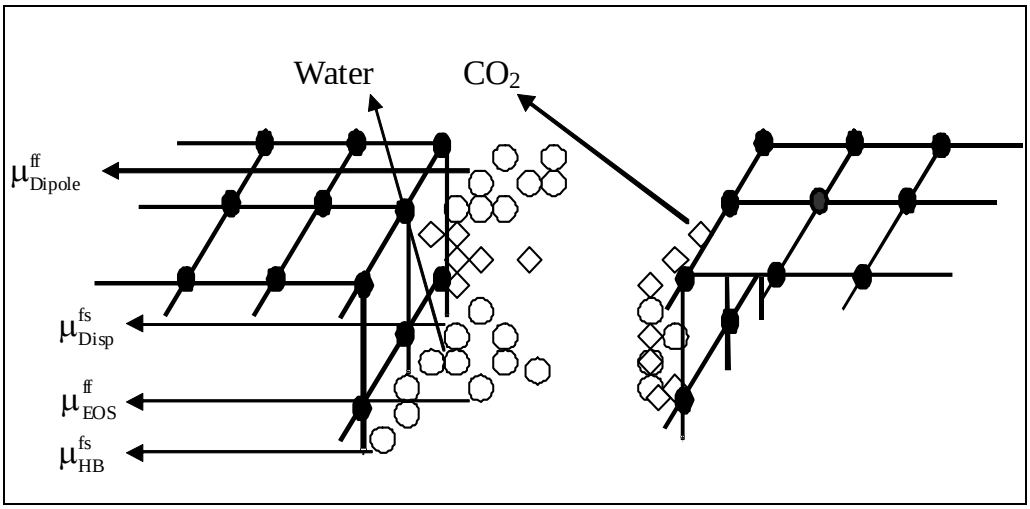

Figure 5.6. Idealized Depiction of Molecular Interactions of Water in the Slit (Slit Geometry Adapted from Fitzgerald[25])

Gibbs Isotherm Equation in SLD Model

The Gibbs or excess adsorption in the SLD model is given by Equation (5.19) which can be written as

$$n^{Gibbs} = \frac{A}{2}\int_{\text{Left Side of Slit}}^{\text{Right Side of Slit}} (\rho(z) - \rho_{bulk})dz \qquad (5.48)$$

Several authors[32, 92, 103, 141] have observed that the adsorption of water on activated carbons is bimodal. Equation (5.48) is intended for the modeling of unimodal adsorption.

Therefore, the excess adsorption isotherm equation needed a modification to account for the bimodal nature of water adsorption. The following equation accounts for the two modes of water adsorption:

$$n_{Water}^{Gibbs} = \left(\frac{A_p}{2} + \frac{A_s}{2} \right) \int_{Left\ Side\ of\ Slit}^{Right\ Side\ of\ Slit} (\rho(z) - \rho_{bulk}) dz \tag{5.49}$$

where A_p is the traditional surface area of water accessible on the solid adsorbent (primary adsorption) and A_s represents the "surface area" provided for water adsorption by the clusters of water molecules (secondary adsorption).

Further, the adsorption of CO_2 is given as

$$n_{CO2}^{Gibbs} = \frac{A_{CO2}}{2} \int_{Left\ Side\ of\ Slit}^{Right\ Side\ of\ Slit} (\rho(z) - \rho_{bulk}) dz \tag{5.50}$$

Therefore, the component material balances for CO_2 and water are given as

$$Z_{CO_2} = \frac{n_{CO_2}^{Ex} + V_{Void} \overline{\rho}_{gas} y_{CO_2}}{n_{Total}^{Ex} + V_{Void} \overline{\rho}_{gas}} \tag{5.51}$$

$$Z_{Water} = \frac{n_{Water}^{Ex} + V_{Void} \overline{\rho}_{gas} y_{water}}{n_{Total}^{Ex} + V_{Void} \overline{\rho}_{gas}} \tag{5.52}$$

where n_{Water}^{Ex} and $n_{CO_2}^{Ex}$ are given by Equations (5.49) and (5.50), respectively, and n_{Total}^{Ex} is the total excess adsorption.

Equations (5.51) and (5.52) are solved simultaneously to estimate the SLD model parameters for this system. As evident from the discussion above, the bimodal nature of water adsorption is accounted for by modifying the isotherm equation, which is then used in the material balance to model the *competitive* adsorption of this highly asymmetric mixture.

SLD Modeling Strategy

The CO_2-water mixture on wet coals with large amounts of adsorbed moisture represents a *highly asymmetric* mixture. Specifically, the amount of water adsorbed on some of these coals can be twenty-times larger than the amount of CO_2 adsorbed at a given pressure. This asymmetry, coupled with the polar/non-polar mixture characteristics, introduces computational difficulties in modeling adsorption behavior of this system.

Several modifications, as highlighted above, were necessary to successfully model this mixture. Specifically, these modifications comprised of incorporating polar and electrostatic interactions in the SLD model for water adsorption and including an additional term in the Gibbs isotherm equation for water adsorption to account for the "surface area" provided by the clusters of water molecules. With these modifications, the SLD model was able to more effectively model this mixture.

A case study on SLD modeling of CO_2-water binary mixed gas adsorption was conducted earlier at OSU.[164] The case study marked the first instance when this system was modeled as a binary mixture in the SLD model. The case study had shown some important aspects of this gas mixture. Chen and Gasem[164] showed a viable modeling method that can be implemented to obtain converged solutions and obtained useful results. However, at the time of that case study, the SLD model did not include the polar and electrostatic interactions of water as well as the modified Gibbs isotherm equation for water. These two modifications were the key aspects of current work at OSU.

The method adopted in modeling this mixture of sub-critical and super-critical components is detailed below:

The SLD-PR model with the new parameterization included many parameters that could be regressed to obtain model representations of this system. However, efforts were made to limit/reduce the number of regressed parameters to four-five that is typical for an ordinary binary gas mixture. Therefore, the regressed parameters comprised of the CO_2 and water surface areas, slit length (function of pressure) and a binary interaction parameter.

The surface area provided by the clusters of water molecules for the wet Argonne coals are unavailable at the time of this writing; therefore, this area was fixed at a nominal value based on the amount of adsorbed moisture on the coal and by obtaining the primary surface area necessary to obtain a physically reasonable pore volume of the coal. The SLD pore volume of the coal ranges from about 0.05 cc/gm to about 0.10 cc/gm.

The initial modeling results of this work and the earlier case study[164] showed that a single slit length was unable to represent adequately the adsorption behavior of this mixture. Therefore, the slit length was treated as a linear function of bulk pressure, as explained below.

The presence of water in the coal causes pore-blocking and restricts the accessibility of other adsorbing gases such as CO_2. Further, the pore-blocking is more dominant for the smaller sized pores than the larger sized pores.[28] Therefore, as pressure increases, CO_2 would be only able to access relatively larger pores on the coal surface. As a result, the slit length can be expected to increase with bulk pressure.

In addition to the parameters mentioned above, a binary interaction parameter in the adsorbed phase was also regressed due to the large asymmetric nature of this mixture. In summary, the regressed parameters for these coals were: CO_2 surface area, water

surface area (primary), binary interaction parameter (C_{ij}) and the constants for the linear pressure dependence of slit length.

SLD-PR Results for CO_2-Water Mixture Adsorption on Wet Coals

Table 5.4 presents the SLD-PR modeling results for the adsorption of CO_2-water mixtures on five wet Argonne coals. The table lists the model parameters and the weighted average absolute deviation (WAAD) for CO_2 and water adsorption on the five coals. As evident from the table, the new parameterization of the SLD model coupled with the modeling strategy described in the previous section was able to represent precisely the adsorption of this asymmetric mixture on these coals. Specifically, the overall WAAD for CO_2 and water adsorption of these coals were 0.50 and 1.01, respectively.

Figures 5.7-5.11 present these results on wet Pocahontas, Upper Freeport, Illinois #6, Wyodak and Beulah Zap coals, respectively. For two of the coals that contained large amounts of adsorbed moisture (Wyodak and Beulah Zap), two different linear functions of slit length were required to represent precisely the adsorption data at pressures beyond 1500 psia. This artifact could also be attributed to some of the assumptions used in the new data reduction method that were approximate in nature due to the limited available information.

Surface areas of coals

The surface areas obtained in the current work should be viewed with some caution. There appears to be no reliable method to estimate/validate experimentally the actual surface areas of coals. After a comprehensive review of this topic, Mahajan[107] concluded that "*surface areas of coals have no physical meaning and should not be*

Table 5.4 SLD-PR Model Representations of CO_2-Water Binary Mixture Adsorption on Wet Argonne Coals

					Slit Length Function		WAAD	
Coal	**CO_2 Surface Area (m^2/gm)**	**Water Surface Area (primary) (m^2/gm)**	**Water Surface Area A_s (Secondary) (m^2/gm)**	**C_{ij}**	**Slope (nm/psia)**	**Intercept (nm)**	**CO_2**	**Water**
Pocahontas	91.9	69.5	-	-0.1600	9.01E-05	0.92	0.57	1.36
Upper Freeport	92.6	94.5	-	-0.1800	1.65E-04	0.81	0.53	1.10
Illinois #6	98.0	129.4	80	-0.0153	2.76E-04	1.41	0.91	1.25
Wyodak	115.0	166.8	650	-0.2662	3.11E-04	1.00	0.28	0.74
Beulah Zap	95.0	194.8	950	-0.1224	2.64E-04	0.92	0.23	0.62
Overall							**0.50**	**1.01**

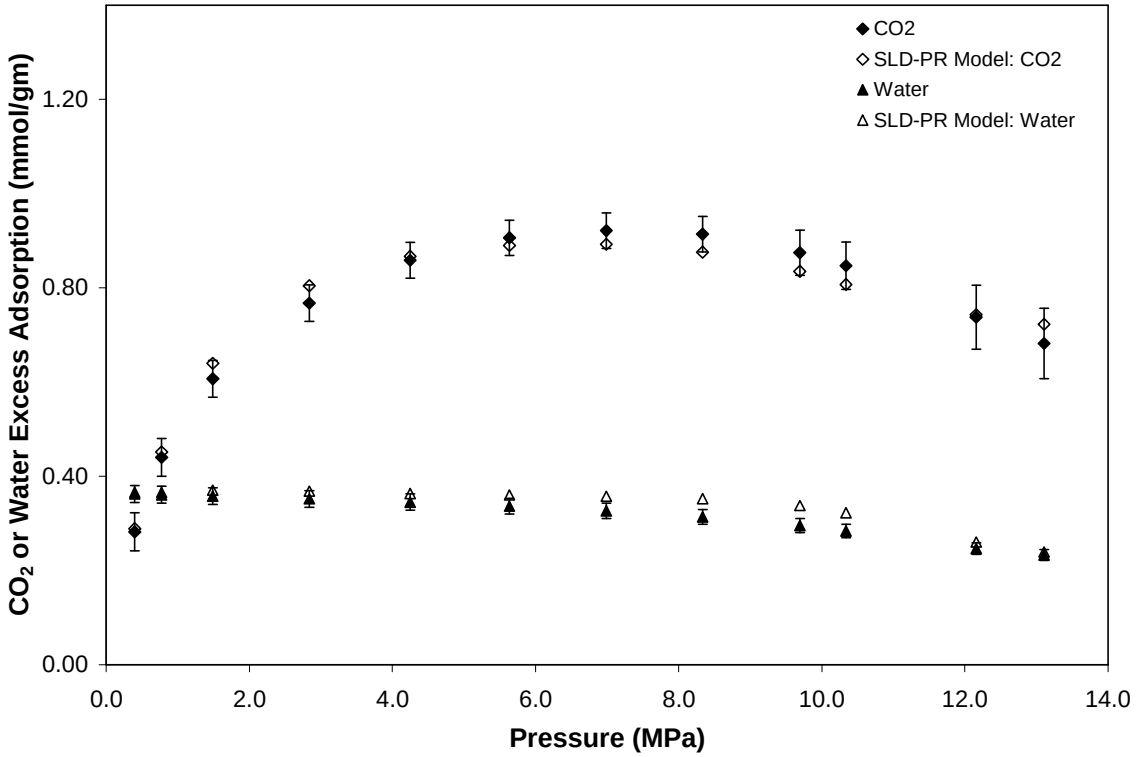

Figure 5.7 SLD-PR Model Representations for CO_2-Water Mixture Adsorption on Wet Pocahontas Coal

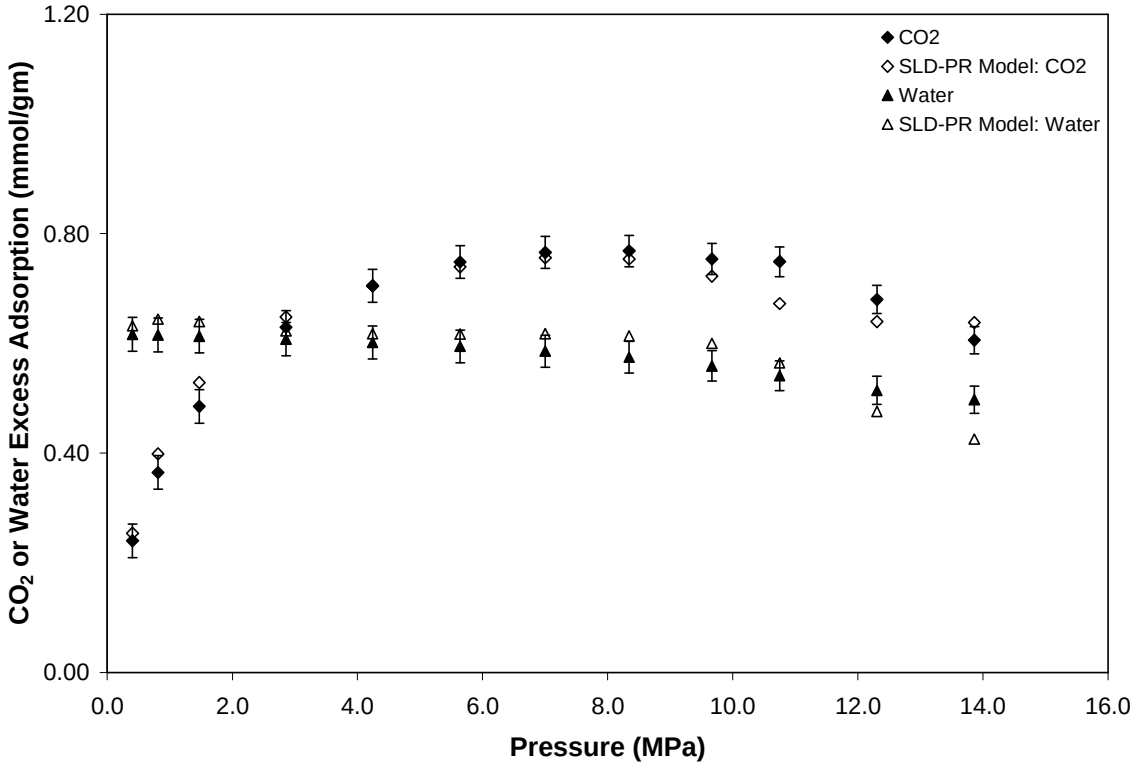

Figure 5.8 SLD-PR Model Representations for CO_2-Water Mixture Adsorption on Wet Upper Freeport Coal

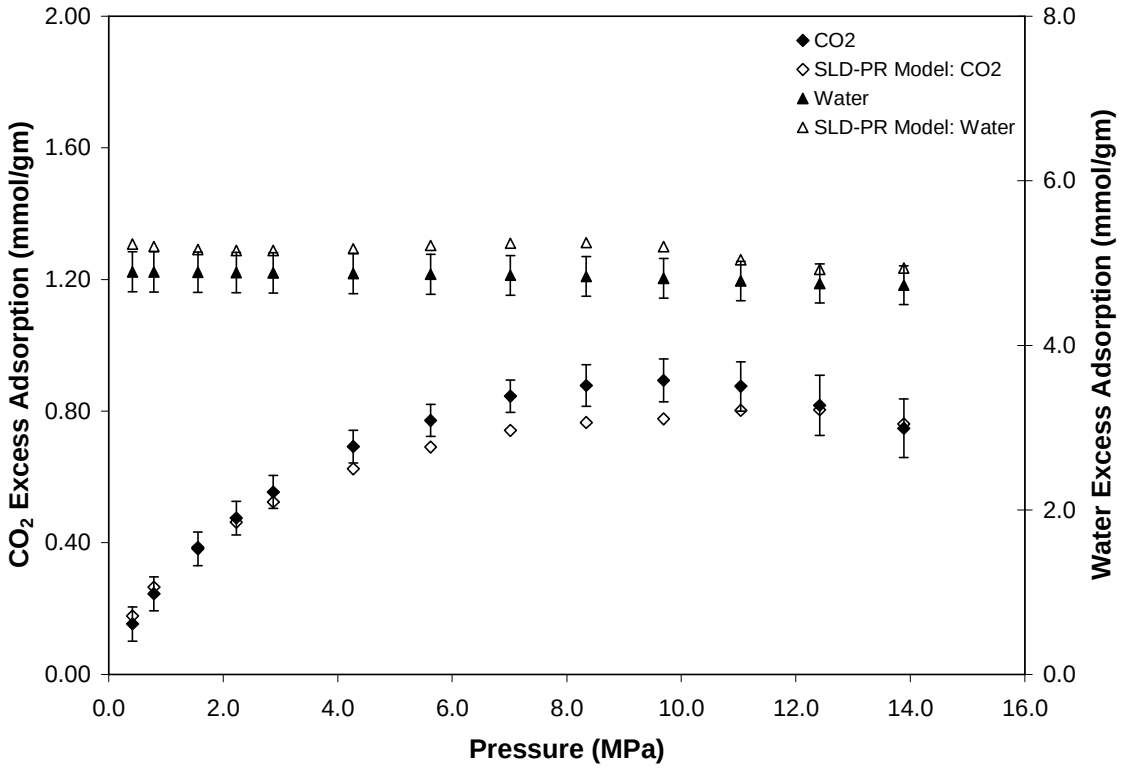

Figure 5.9 SLD-PR Model Representations for CO_2-Water Mixture Adsorption on Wet Illinois #6 Coal

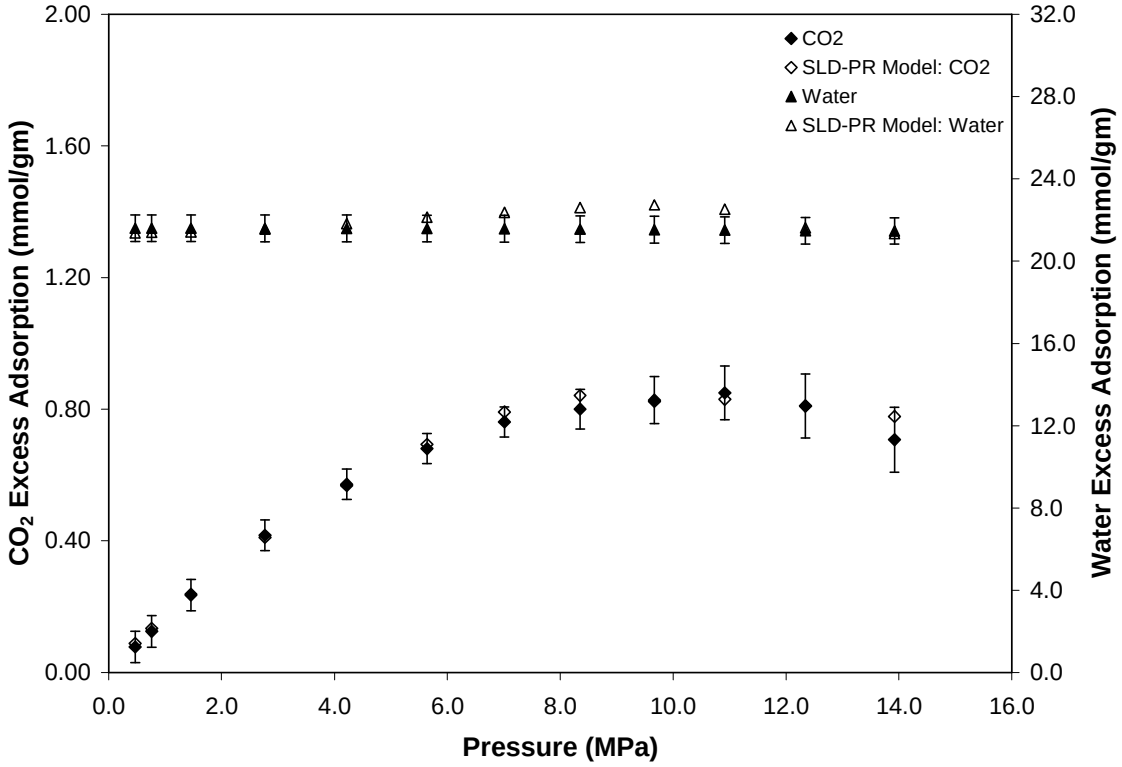

Figure 5.10 SLD-PR Model Representations for CO_2-Water Mixture Adsorption on Wet Wyodak Coal

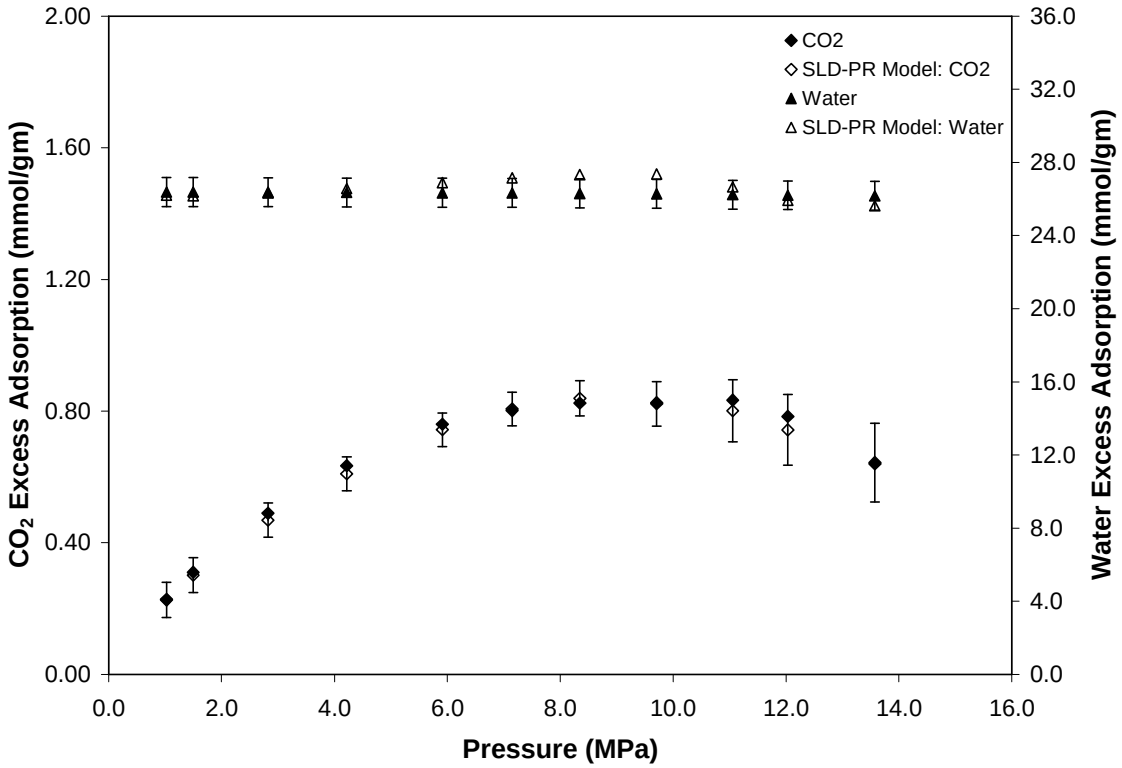

Figure 5.11 SLD-PR Model Representations for CO_2-Water Mixture Adsorption on Wet Beulah Zap Coal

reported". This highlights the fact that the model-regressed surface areas for coals represent a largely abstract quantity.

Further, from a model perspective, the coal surface areas are not to be considered "additive". In other words, the surface areas of pure CO_2 and water adsorption on a given coal would not approximate the corresponding areas obtained in a CO_2-water mixture, since the pure components and their mixtures may exist at different adsorbed-phase densities on the *same* coal. Therefore, such a comparison of surface areas of coals is not feasible.

In conclusion, the surface areas of coals obtained here should be seen as model-regressed parameters that approximate (perhaps only roughly) the accessible surface area of the adsorbent for each component.

The results discussed above have highlighted two important aspects of CO_2 adsorption on wet coals. They are:

(1) The new data reduction method when applied to CO_2 adsorption isotherms on coals containing large amounts of moisture can result in significant differences in the calculated amounts of excess adsorption of CO_2 relative to the amounts calculated based on the traditional data reduction method. These differences arise *mainly* due to the assumptions regarding the solubility of gas in adsorbed water and the corrections to the wet gas density relative to the dry gas density. In fact, the new method will invariably lead to larger amounts of gas adsorbed when compared with the traditional method for coals with more moisture. These differences in data reduction procedures can be significant and affect the calculated gas adsorption capacities of these coals.

(2) The current study also indicates that for coals with large amounts of moisture, the conventional treatment of water as an inactive "pacifier" of the coal matrix independent of pressure could be an oversimplification. In fact, if the conventional modeling approach for water was used (hypothetically) with the new data reduction method, the model parameters obtained would greatly differ for some of the coals. In contrast, these differences appear to be minor for coals that contain low levels of moisture.

Step 3. Gibbs Energy Change or Phase-Check Analysis for CO_2-Water Mixture Adsorption on Wet Argonne Coals

In this section, a phase-check analysis is performed for CO_2-water mixture adsorption on wet Argonne coals. In particular, the converged calculations from Step 2

are used to investigate the possibility of formation of a third (liquid water) phase in these systems. This was conducted as follows:

The SLD-PR model parameters obtained for each coal in Step 2 were used to evaluate the partial fugacity of water in the gas (or adsorbed) phase. Since these values were from converged equilibrium calculations, they can be used to estimate reliably the phase-distribution of water in these systems. Further, the partial fugacity of water in the liquid state at the given temperature, pressure and composition was estimated for each coal. For this purpose, the liquid phase composition was estimated from the CO_2-water solubility correlation discussed in Chapter 2. A direct comparison of the partial fugacity of water in the gas and liquid phases was made for each coal. If the partial fugacity of water in liquid state is *lower* than in the gas phases, this would indicate possible formation of a liquid phase for that coal. While this approach does not involve the simultaneous application of the material balance and the equilibrium relations for three coexisting phases (i.e., a complete Gibbs energy minimization to establish the equilibrium condition), it provides some insight on the potential formation of a standing aqueous phase. The more rigorous Gibbs analysis approach is discussed in Section 5.7.

Tables 5.5-5.9 present the results obtained for wet Pocahontas, Upper Freeport, Illinois #6, Wyodak and Beulah Zap coals, respectively. These tables include the pressure, temperature, the molar compositions and partial fugacities of water in the gas and liquid phases for the complete isotherms. For convenience, the pressure values are presented in "psia" in these tables. As evident from Table 5.5 and 5.6, the calculated partial fugacities of water for the wet Pocahontas and Upper Freeport coals in the liquid phase are *higher* than the corresponding values in the gas phase. Therefore, the formation

of a liquid phase for these coals is not supported from these results. This appears reasonable since these low-moisture coals contain only about 1% moisture.

In contrast, the results indicate that there may be formation of a liquid phase for wet Illinois #6 and Wyodak coals. In fact, the CO_2 adsorption isotherm on Illinois #6 coal was measured at moisture content slightly above the equilibrium level of about 8%. Therefore, there was a greater possibility of the presence of a liquid phase (experimentally at least) for this coal, since there was *excess* moisture present in the system. This is supported by the results obtained for this coal and listed in Table 5.7. The possible formation of a liquid phase is also indicated for wet Wyodak coal (Table 5.8) which contains about 28% moisture. In contrast, the results for Beulah Zap coal (Table 5.9) do not indicate the presence of a third phase, although this coal contains 32% moisture. A plausible explanation of this result is as follows.

Beulah Zap coal is a low-rank, lignitic coal. The low-rank coals and lignites are known to contain large amounts of moisture (for e.g. the Victorian brown coals studied by Allardice and Evans[113] contain large amounts of moisture). Further, as mentioned in Chapter 4, the number of large-sized pores (macropores) for low-rank coals is larger than capillary-sized pores.[135] It is possible that a portion of the moisture in these large-sized macropores is also removed; yielding equilibrium moisture values lower than the true inherent moisture for these coals.[133, 134] As such, Beulah Zap coal *may* have the adsorptive capacity for more moisture than the reported as-received value of 32%. This would explain the results obtained for this coal that indicate the lack of formation of a third (water-rich) phase for this coal at 32% moisture.

Table 5.5 Phase-Check Analysis for CO_2-water Mixture Adsorption on Wet Pocahontas Coal

P (psia)	T (K)	Mole Fraction of Water in Gas Phase y_{water}	Mole Fraction of Water in Liquid Phase x_{water}	PF_{water} (Gas phase) (psia)	PF_{water} (Liq. phase) (psia)
57.6	328.2	0.0137	0.9986	0.75	2.04
112.2	328.2	0.0089	0.9973	0.89	2.04
216.0	328.2	0.0061	0.9950	1.07	2.05
411.6	328.2	0.0040	0.9913	1.07	2.06
616.1	328.2	0.0033	0.9882	1.01	2.08
817.1	328.2	0.0031	0.9857	0.98	2.10
1013.6	328.2	0.0034	0.9838	0.95	2.12
1208.7	328.2	0.0040	0.9823	0.91	2.14
1405.9	328.2	0.0053	0.9811	0.85	2.16
1499.4	328.2	0.0063	0.9807	0.80	2.17
1763.1	328.2	0.0087	0.9797	0.59	2.20
1901.0	328.2	0.0093	0.9793	0.51	2.21

Table 5.6 Phase-Check Analysis for CO_2-water Mixture Adsorption on Wet Upper Freeport Coal

P (psia)	T (K)	Mole Fraction of Water in Gas Phase y_{water}	Mole Fraction of Water in Liquid Phase x_{water}	PF_{water} (Gas phase) (psia)	PF_{water} (Liq. phase) (psia)
58.6	328.2	0.0279	0.9986	1.55	2.04
117.5	328.2	0.0167	0.9972	1.74	2.04
213.5	328.2	0.0106	0.9951	1.82	2.05
414.3	328.2	0.0059	0.9913	1.58	2.06
615.0	328.2	0.0048	0.9882	1.50	2.08
818.4	328.2	0.0046	0.9857	1.42	2.10
1015.6	328.2	0.0048	0.9838	1.34	2.12
1210.4	328.2	0.0056	0.9823	1.26	2.14
1402.0	328.2	0.0076	0.9811	1.18	2.16
1559.0	328.2	0.0108	0.9804	1.08	2.17
1784.7	328.2	0.0150	0.9796	0.87	2.20
2010.6	328.2	0.0164	0.9790	0.72	2.23

Table 5.7 Phase-Check Analysis for CO_2-water Mixture Adsorption on Wet Illinois #6 Coal

P (psia)	T (K)	Mole Fraction of Water in Gas Phase y_{water}	Mole Fraction of Water in Liquid Phase x_{water}	PF_{water} (Gas phase) (psia)	PF_{water} (Liq. phase) (psia)
60.5	328.2	0.2449	0.9985	14.42	2.04
114.9	328.2	0.1675	0.9973	18.45	2.04
225.7	328.2	0.1115	0.9949	23.51	2.05
323.2	328.2	0.0892	0.9930	26.36	2.06
416.7	328.2	0.0755	0.9913	28.22	2.07
619.6	328.2	0.0575	0.9882	30.75	2.08
815.4	328.2	0.0470	0.9858	31.90	2.10
1017.7	328.2	0.0386	0.9839	31.63	2.12
1209.6	328.2	0.0321	0.9824	30.39	2.15
1405.6	328.2	0.0257	0.9812	27.61	2.17
1601.1	328.2	0.0193	0.9803	23.29	2.19
1800.5	328.2	0.0154	0.9796	20.33	2.21
2013.6	328.2	0.0137	0.9791	19.36	2.24

Table 5.8 Phase-Check Analysis for CO_2-water Mixture Adsorption on Wet Wyodak Coal

P (psia)	T (K)	Mole Fraction of Water in Gas Phase y_{water}	Mole Fraction of Water in Liquid Phase x_{water}	PF_{water} (Gas phase) (psia)	PF_{water} (Liq. phase) (psia)
68.2	328.2	0.0801	0.9983	5.11	2.04
110.9	328.2	0.0518	0.9973	5.15	2.04
211.7	328.2	0.0270	0.9951	4.61	2.05
401.7	328.2	0.0136	0.9915	3.57	2.06
611.6	328.2	0.0090	0.9883	2.79	2.08
818.1	328.2	0.0072	0.9857	2.25	2.10
1016.9	328.2	0.0066	0.9838	1.83	2.12
1211.2	328.2	0.0068	0.9823	1.52	2.14
1402.6	328.2	0.0080	0.9811	1.25	2.16
1583.1	328.2	0.0094	0.9803	0.90	2.18
1790.7	328.2	0.0109	0.9796	0.68	2.20
2019.3	328.2	0.0125	0.9790	0.58	2.23

Table 5.9 Phase-Check Analysis for CO_2-water Mixture Adsorption on Wet Beulah Zap Coal

P (psia)	T (K)	Mole Fraction of Water in Gas Phase y_{water}	Mole Fraction of Water in Liquid Phase x_{water}	PF_{water} (Gas phase) (psia)	PF_{water} (Liq. phase) (psia)
148.4	328.2	0.0113	0.9965	1.44	2.04
217.0	328.2	0.0088	0.9950	1.53	2.05
409.7	328.2	0.0061	0.9914	1.62	2.06
611.7	328.2	0.0051	0.9883	1.56	2.08
857.4	328.2	0.0044	0.9853	1.36	2.10
1036.4	328.2	0.0044	0.9836	1.20	2.12
1210.7	328.2	0.0045	0.9823	1.02	2.14
1408.1	328.2	0.0052	0.9811	0.82	2.16
1603.4	328.2	0.0062	0.9802	0.61	2.18
1745.5	328.2	0.0074	0.9797	0.53	2.20
1968.7	328.2	0.0094	0.9791	0.48	2.22
148.4	328.2	0.0113	0.9965	1.44	2.04

For illustrative purposes, Figure 5.12 presents the partial fugacity of water in liquid and gas phases as a function of bulk pressure for wet Pocahontas coal. The figure shows that the gas phase fugacities of water are lower than the values in the liquid phase through out the pressure range of the isotherm. Results for other coals can also be similarly inferred from Tables 5.6-5.9.

Gibbs Minimization Approach for Phase-Stability Analysis

A more rigorous approach to investigate the phase-stability of CO_2-water-adsorbent systems would be to minimize the overall Gibbs free energy of this system, subject to the mass balance constraints. In fact, the number of stable phases which can coexist at equilibrium can be obtained from the change in Gibbs energy (ΔG). In particular, minimizing the Gibbs energy will yield the number of phases that are stable at equilibrium.

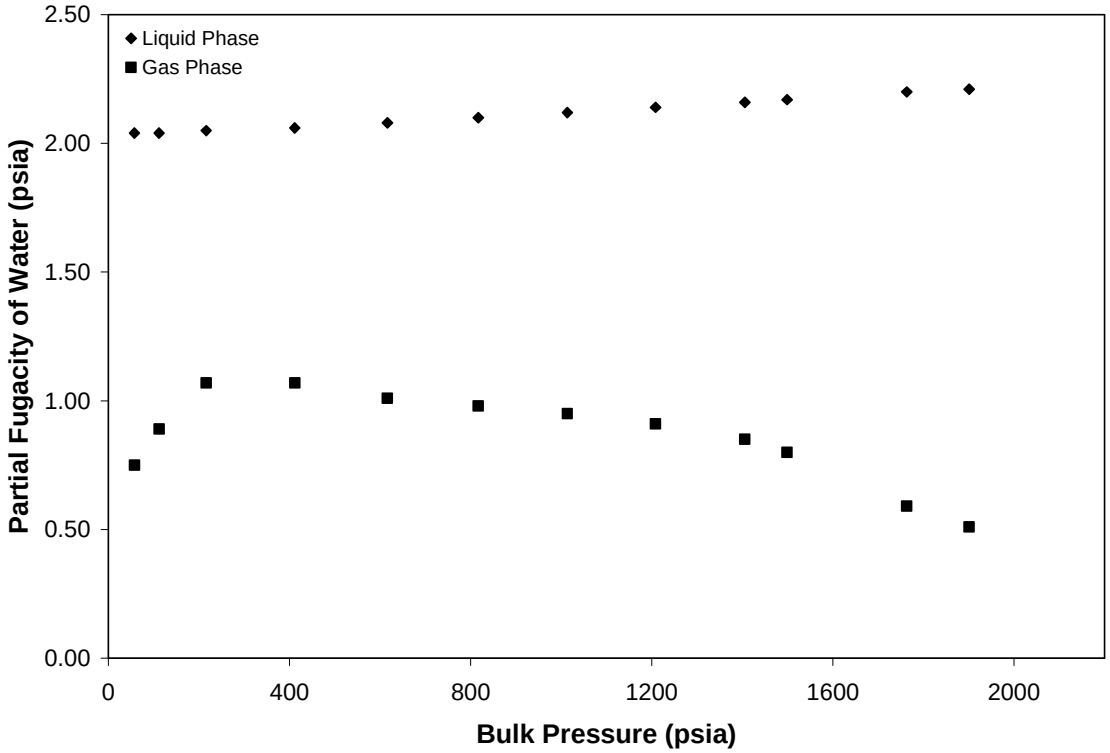

Figure 5.12 Partial Fugacities of Water in Liquid and Gas Phases for CO_2-water Mixture Adsorption on Wet Pocahontas Coal

To ascertain the number of stable phases at a given pressure and temperature, the following function, ΔG, is minimized:

$$\Delta G = RT\sum_{i}^{m}\sum_{j}^{n} N_{ij} \ln \hat{f}_{ij} \tag{5.53}$$

where N_{ij} is the number of moles of j^{th} component in i^{th} phase and $\hat{f}_{ij}$ is the partial fugacity of the component in that phase.

Equation (5.53) is solved subject to the following mass balance constraints:

$$\sum_{i}^{m} N_i x_{ij} - F z_{ij} = 0 \qquad \text{for } j = 1, n \tag{5.54}$$

$$\sum_{j}^{n} x_j = \sum_{j}^{n} z_j = 1.0 \tag{5.55}$$

where F is the total number of moles in the feed, and i and j represent the number of phases and the number of components, respectively.

For an adsorption calculation involving water, three phases may coexist at equilibrium. Therefore, expanding Equation (5.53) for the three phases gives

$$\frac{\Delta G}{RT} = \sum_j V_{ads}\rho_{ads} x_j^{ads} \ln \hat{f}_j^{ads} + V_{gas}\rho_{gas} y_j^{gas} \ln \hat{f}_j^{gas} + V_{wat}\rho_{wat} x_j^{wat} \ln \hat{f}_j^{wat} \qquad (5.56)$$

where V and ρ represent the volume and density of the phases denoted by the subscripts, x_j^{ads}, y_j^{gas} and x_j^{wat} are the phase compositions of j^{th} component in the adsorbed, gas and water-rich phases, respectively.

The above approach is based on the *extensive* thermodynamic state of the system. The application of this method requires the development of a multi-phase algorithm (three or more phases). This development is currently not feasible due to limitations imposed by the lack of availability of (a) vapor-liquid equilibrium data and (b) density and gas solubility data for the systems of interest. As a result, this task was beyond the scope of the current work.

5.7 Case Study Conclusions

The above analysis has shown that the formation of a liquid phase is possible for coals with higher moisture content (with the exception of Beulah Zap lignite). The scope of this work was limited to an analysis of presence of a third phase in these adsorptive systems. Further advancement of this approach will require several key developments. These include:

(1) The relative areas occupied by water at the primary and secondary adsorption sites will need to be inferred more reliably. The clustering behavior of water can

be investigated with techniques such as X-ray diffraction and small-angle X –ray and neutron scattering *in-situ* experiments for water adsorption on carbons and coals. These techniques have been used in the literature to study clustering behavior during water adsorption on carbons.[131, 132]

(2) The phase-check analysis has demonstrated the need for an equation-of-state that can more accurately describe the vapor-liquid equilibria of water and coalbed gases at the conditions encountered in CBM systems.

(3) The new data reduction procedure has highlighted the need for accurate measurements of the density of the gas phase in adsorptive systems that contain water (wet gases). The density for wet gases, if found considerably different from dry gas densities, can lead to significant corrections to the adsorption isotherms on wet coals that use the traditional data reduction method. The density measurements would also be necessary in the development of EOS for CBM systems.

CHAPTER 6

GENERALIZATION OF SLD-PR MODEL

As stated in Chapter 3, one of the desired attributes of a successful CBM adsorption model is its ability to facilitate generalized predictions of CBM gas adsorption based solely on accessible adsorbate properties and adsorbent characterization. This capability is essential for reliable *a priori* predictions of gas adsorption behavior at conditions encountered in CBM production and CO_2 sequestration. The SLD-PR model discussed in Chapter 5 provides a theoretically-rigorous framework that can be used to achieve this objective. In this chapter, the SLD-PR model has been generalized; specifically, it is generalized by expressing the model parameters in terms of readily-available coal characterization, i.e., the ultimate and proximate analyses of the coals. Further, the generalized model was used to predict *a priori* binary and ternary gas adsorption based solely on the pure-gas adsorption generalization. Finally, the newly developed generalized model was validated by testing its predictive capability for a set of external data for CO_2 adsorption on coals of varying ranks.

6.1 Generalization Approach

In order to develop the generalized SLD-PR adsorption model, the following approach was adopted:

1. The SLD-PR model parameters, namely, surface areas, solid-solid interaction energy and slit length, were regressed for each coal to obtain precise representations of pure-gas adsorption data.
2. The regressed model parameters were then expressed as functions of coal-structure characterization, i.e., the ultimate and proximate analyses of the coals.
3. The coefficients of the generalized correlations were then re-regressed by utilizing adsorption data on all coals simultaneously and minimizing the weighted sum-of-squares objective function, WRMS.

The details of each step are discussed in this chapter. In the above approach, trial-and-error methods were avoided by employing rigorous regression techniques, as highlighted in the following sections.

6.2 Database Employed in this Study

Experimental isotherm measurements have been conducted at OSU for many years.[6, 8, 12] Table 6.1 documents the details of the adsorption database used in developing the generalized model. The table lists the coal adsorbent, adsorbate, number of points, temperature and pressure ranges of each system. Specifically, the adsorption database shown in Table 6.1 is comprised of experimental measurements on nine coals and contains more than one-hundred independently measured isotherms involving approximately one-thousand data points. Further, the database includes both pure- and mixed-gas adsorption data on dry and wet coals. The database contains methane, nitrogen and CO_2 adsorption data on wet Illinois #6, wet Fruitland, wet Lower Basin Fruitland and wet Tiffany coals. The adsorption isotherms on these wet coals were measured at 319.3 K

and pressures to 12.4 MPa, with the exception of wet Tiffany coal, on which the measurements were conducted at 327.6 K and pressures to 13.7 MPa. The adsorption data on the above wet coals were measured in a series of previous works at OSU.[6, 8]

Table 6.1 Adsorption Database Used For SLD-PR Model Generalization

Coal	Adsorbate	Temp. (K)	Pressure Range (MPa)	NPTS*
Wet Fruitland	N_2: CH_4: CO_2	319	0.7 – 12.4	57: 40: 52
Wet Fruitland	N_2 +CH_4	319	0.7 – 12.4	41
Wet Fruitland	CH_4 + CO_2	319	0.7 – 12.4	40
Wet Fruitland	N_2 + CO_2	319	0.7 – 12.4	40
Wet Illinois #6	N_2: CH_4: CO_2	319	0.7 – 12.4	20:20:30
Wet Illinois #6	N_2 +CH_4	319	0.7 – 12.4	40
Wet Illinois #6	CH_4 + CO_2	319	0.7 – 12.4	40
Wet Illinois #6	N_2 + CO_2	319	0.7 – 12.4	40
Wet Tiffany	N_2: CH_4: CO_2	328	0.7 – 13.7	21:22:16
Wet Tiffany	N_2 +CH_4	328	0.7 – 13.7	11
Wet Tiffany	CH_4 + CO_2	328	0.7 – 13.7	11
Wet Tiffany	N_2 + CO_2	328	0.7 – 13.7	11
Wet Tiffany	N_2 +CH_4+ CO_2	328	0.7 – 13.7	11
Wet LB Fruitland	N_2: CH_4: CO_2	319	0.7 – 12.4	17:16:48
Dry Illinois #6	N_2: CH_4: CO_2	328	0.7 – 13.7	16:15:22
Dry Beulah Zap	N_2: CH_4: CO_2	328	0.7 – 13.7	15:14:33
Dry Wyodak	N_2: CH_4: CO_2	328	0.7 – 13.7	14:14:22
Dry Upper Freeport	N_2: CH_4: CO_2	328	0.7 – 13.7	14:14:22
Dry Pocahontas	N_2: CH_4: CO_2	328	0.7 – 13.7	14:14:22

*NPTS = Number of points

The database also contains pure methane, nitrogen and CO_2 adsorption data on dry Illinois #6, dry Beulah Zap, dry Wyodak, dry Upper Freeport and dry Pocahontas coals from the Argonne coal sample program.[39] These isotherms were measured at 328.2 K and pressures to 13.8 MPa.[21]

Tables 6.2 and 6.3 present the ultimate and proximate analyses of the coals used in this study. Table 6.2 documents this information for OSU coals. The coals in Table 6.2 are labeled as OSU coals to distinguish them from coals that were prepared by the

Argonne National Laboratory. Table 6.3 presents the analyses of Argonne premium coals that were acquired from the Argonne National Laboratory. Among the OSU coals in Table 6.2, the wet Fruitland, wet Lower Basin Fruitland and wet Tiffany coals each had two different samples. The two Tiffany samples had quite similar adsorption capacities[8] and, therefore, a simple average of their characterization was used in the generalization. The Fruitland coal is a medium volatile bituminous coal from the San Juan coal basin. The Lower Basin Fruitland coal is also from the same coal basin as the Fruitland coal; however, the Lower Basin sample was collected from a different coal seam. The Tiffany coal samples are also from San Juan basin and belong to the BP Amoco injection wells #1 and 10.[8] The Illinois #6 coal is a high volatile bituminous coal. The percent carbon of these coals ranged from about 40% for the Lower Basin Fruitland coal to 71% for the Illinois #6 coal.

Some of the percentages shown in Table 6.2 do not add to 100% due to poor replication of the carbon analysis. As explained in an earlier work[25], the carbonates in the ash contributed both to the analysis of carbon and ash contents of these coals.

Further, the Lower Basin Fruitland coal has the highest ash percentage of about 52%. The volatile matter of these coals ranged from about 15% to 30%, while the equilibrium moisture content ranged from 2% to 4%. These coal samples were moistened and their moisture content was maintained well above their equilibrium moisture contents during the isotherm measurements on these coals. Additional details on these coals can be found elsewhere.[8]

Table 6.2 Compositional Analyses of OSU Coals Used in this Study

Analysis*	Fruitland OSU #1	Fruitland OSU #2	Illinois #6	LB Fruitland OSU #3a	LB Fruitland OSU #3b	Tiffany Well #1	Tiffany Well #10
Ultimate							
Carbon %	68.63	66.58	71.47	38.92	40.20	47.78	56.75
Hydrogen %	4.27	4.23	5.13	3.08	3.10	2.62	2.77
Oxygen %	0.89	5.08	9.85	3.75	2.87	6.19	5.16
Nitrogen %	1.57	1.47	1.46	0.87	0.89	0.92	1.02
Sulfur %	4.19	0.72	1.27	1.73	2.14	0.57	0.52
Ash %	20.45	21.92	10.81	51.66	50.81	49.71	47.74
Proximate							
Vol. Matter %	20.20	20.33	30.61	20.01	14.00	15.48	15.35
Fixed Carbon %	59.35	57.75	55.90	28.33	35.19	34.82	36.91
Moisture %	2.20	2.20	3.90	4.00	4.00	3.80	3.70

* Huffman Laboratories, Inc., Golden, Colorado.

Table 6.3 Compositional Analyses of Argonne Premium Coals Used in this Study

Analysis*	Beulah Zap	Wyodak	Illinois #6	Upper Freeport	Pocahontas
Ultimate					
Carbon %	72.9	75.00	77.70	85.50	91.10
Hydrogen %	4.83	5.35	5.00	4.70	4.44
Oxygen %	20.30	18.00	13.50	7.50	2.50
Sulfur %	0.80	0.63	4.83	2.32	0.66
Ash %	9.70	8.80	15.50	13.20	4.80
Proximate					
Vol. Matter %	30.50	32.20	36.90	27.10	18.50
Fixed Carbon %	30.70	33.00	40.90	58.70	76.10
Moisture %	32.20	28.10	8.00	1.10	0.70
Ash %	6.60	6.30	14.30	13.00	4.70

* Argonne National Laboratory

Among the Argonne premium coal samples, the Illinois #6 coal is a high-volatile bituminous coal from the Illinois #6 or Herrin seam. The Wyodak coal is a sub-bituminous coal from the Wyodak-Anderson seam. The Upper Freeport coal is a medium-volatile bituminous coal, Pocahontas coal is a low-volatile bituminous coal and Beulah Zap coal is lignite.[39] These coal samples were obtained from the Argonne National Laboratory, Argonne, Illinois in ampoules containing 5 grams of -100 mesh material of each coal. The percent carbon of these Argonne coals ranged from about 73% for Beulah Zap coal to about 91% for Pocahontas coal. The moisture content of these coals also varied from 0.7% to 32%. Further, the Argonne coals appear to contain less ash and more oxygen than the OSU coals. Typically, the coal moisture and oxygen content decrease with coal maturity/rank and, therefore, coals with higher percent carbon have lower levels of moisture and oxygen.

The coals in the adsorption database presented in Table 6.1 covered a wide range of coal ranks. Specifically, the percent carbon, which is an indicator of coal rank, ranged from about 40% to 91% on a dry-ash-free basis. The presence of such a wide range of coals in the database provided a valuable basis for developing a generalized adsorption model with reliable predictive capabilities over the range of coal ranks encountered in CBM applications. Thus, the adsorption database discussed above was used to first assess the correlative abilities of the SLD-PR model and then generalized correlations for the model parameters were developed by utilizing the above coal characterizations.

6.3 SLD-PR Model Representation of Pure-Gas Adsorption Data

The first step in developing the generalized model was to obtain precise representations of available pure-gas adsorption data for methane, nitrogen and CO_2

gases on dry and wet coals. For this purpose, the experimental measurements on coals in the OSU adsorption database were used. The SLD-PR model parameters, namely, surface area "A", solid-solid interaction energy "ε_{ss}/k", and slit length "L", were regressed for each coal to obtain precise representations on pure-gas adsorption on these coals. Table 6.4 presents the model representation results for the adsorption of pure methane, nitrogen and CO_2 on dry and wet coals. The table lists the model parameters and statistics for each coal and each gas. Specifically, the WAAD, %AAD and RMSE of each coal has been included in Table 6.4. The highest WAAD was observed for CO_2 adsorption on dry Wyodak coal, whereas the highest %AAD was observed for nitrogen adsorption on wet Fruitland coal. Overall, the SLD-PR model was capable of representing the pure-gas adsorption data on dry and wet coals with a WAAD of 0.53, which is well within the expected experimental uncertainties. Further, the overall %AAD and RMSE were 4.1% and 0.0262 mmol/gm, respectively. Figure 6.1 presents the deviation plot of the SLD-PR pure-gas adsorption representations for methane, nitrogen and CO_2. Overall, about 80% of the data was predicted within the experimental uncertainties and 96% of the data were predicted within two times the experimental uncertainties.

The amount of CO_2 adsorbed is higher than the amount of methane and nitrogen adsorbed on a given coal. Accordingly, the regressed surface areas for CO_2 are greater than the areas for methane and nitrogen. Further, the ratio of methane and nitrogen surface areas is about 1:0.7, whereas the ratio of methane and CO_2 areas ranges from 1: 1.1 to 1:1.9. The larger variation in the ratio of methane and CO_2 areas can be attributed to the greater affinity of CO_2 for the coal surface. As a result, in some cases, CO_2 can access a disproportionately greater surface area than methane and nitrogen.

Table 6.4 SLD-PR Model Representations of Pure-Gas Adsorption on Coals

Coal	Adsorbate	Parameters			WAAD	%AAD	RMSE (mmol/gm)
		Surface Area (m^2/gm)	ε_{ss}/k (K)	L (nm)			
Wet Fruitland Coal	CH_4	61.29	22.63	1.13	0.36	1.4	0.0081
	N_2	41.46			1.17	9.3	0.0286
	CO_2	66.56			0.84	8.5	0.1003
Wet Illinois# 6 Coal	CH_4	33.62	19.41	1.27	0.29	2.2	0.0066
	N_2	19.92			0.12	3.0	0.0039
	CO_2	47.76			0.39	6.8	0.0620
Wet Tiffany Coal	CH_4	34.34	19.75	1.03	0.61	4.3	0.0113
	N_2	22.03			0.60	6.6	0.0071
	CO_2	43.12			0.76	6.9	0.0410
Wet LB Fruitland Coal	CH_4	26.20	19.48	1.09	0.67	3.7	0.0129
	N_2	16.07			0.39	4.7	0.0051
	CO_2	31.61			0.41	6.8	0.0294
Dry Illinois#6 Coal	CH_4	60.50	30.32	1.34	0.38	2.3	0.0133
	N_2	44.13			0.29	4.4	0.0091
	CO_2	77.41			1.16	6.4	0.0868
Dry Beulah Zap Coal	CH_4	49.80	37.44	1.30	0.30	2.0	0.0125
	N_2	34.76			0.42	6.1	0.0176
	CO_2	92.96			0.88	3.7	0.0604

Table 6.4 SLD-PR Model Representations of Pure-Gas Adsorption on Coals (Cont'd.)

Coal	Adsorbate	Parameters			WAAD	%AAD	RMSE (mmol/gm)
		Surface Area (m^2/gm)	ε_{ss}/k (K)	L (nm)			
Dry Wyodak Coal	CH_4	56.95	31.52	1.32	0.24	1.3	0.0080
	N_2	43.83			0.25	3.4	0.0068
	CO_2	96.27			1.58	5.2	0.0852
Dry Upper Freeport Coal	CH_4	47.10	37.20	1.18	0.29	1.2	0.0072
	N_2	35.06			0.09	0.9	0.0018
	CO_2	54.10			0.65	3.5	0.0287
Dry Pocahontas Coal	CH_4	63.05	36.83	1.15	0.34	1.1	0.0100
	N_2	46.84			0.09	0.8	0.0021
	CO_2	69.53			0.77	3.8	0.0430
Overall					**0.53**	**4.1**	**0.0262**

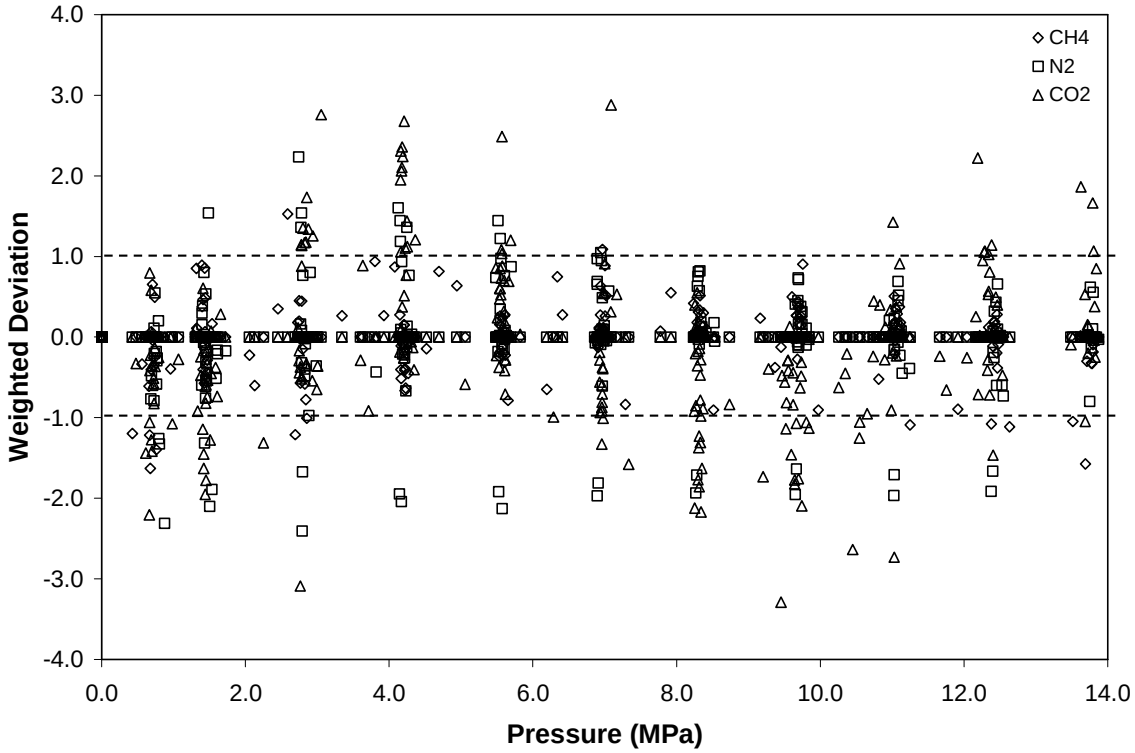

Figure 6.1 Deviation Plot of SLD-PR Model Representations of Pure-Gas Adsorption on Coals

Nevertheless, the surface areas for the three gases are well correlated. Figure 6.2 illustrates the degree of correlation between the surface areas of methane, nitrogen and CO_2 observed on the nine coals. As evident from the figure, the methane and nitrogen areas are correlated with a R^2 of 0.98, whereas the methane and CO_2 areas are correlated with a R^2 of 0.58. This indicates that the surface area of one gas can be used to predict reliably the areas for other two gases. Since, the CO_2 surface areas are less precisely correlated with the areas for methane (and nitrogen), this also indicates that a correction may be required to predict reliably the CO_2 areas from either methane or nitrogen.

The three model parameters, namely, surface area "A", solid-solid interaction energy "ε_{ss}/k" and slit length "L," appear to be slightly correlated. Table 6.5 presents the correlation matrix for methane surface area, ε_{ss}/k and L for the nine coals.

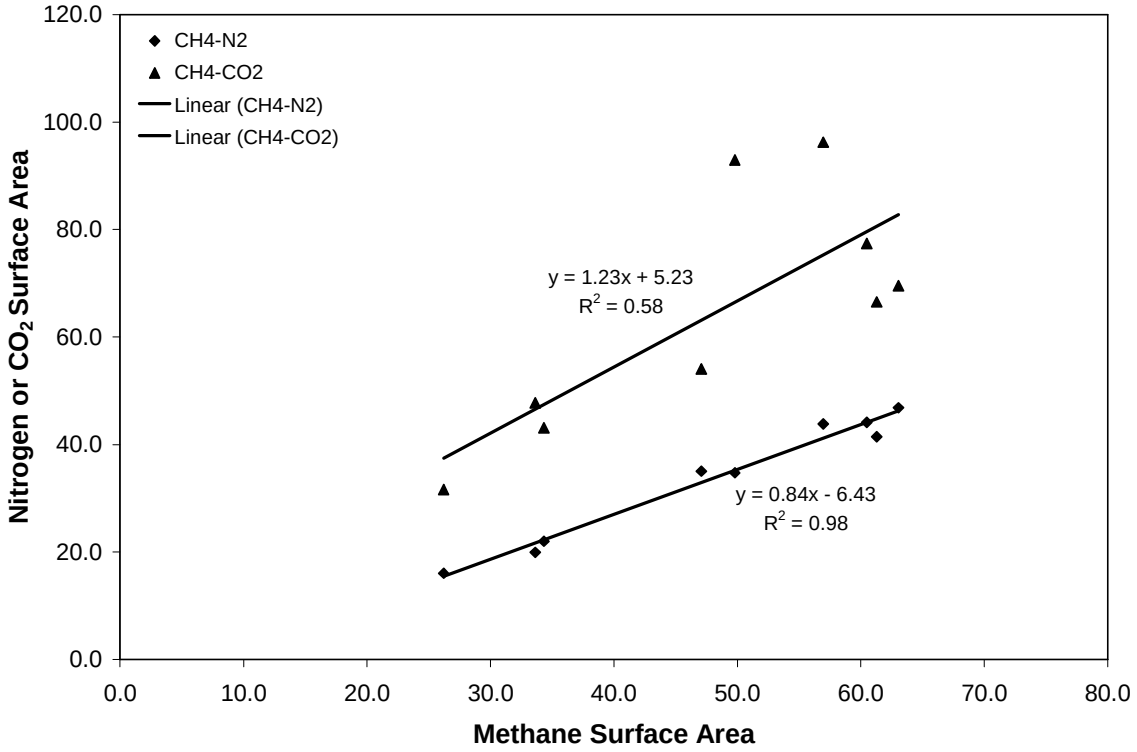

Figure 6.2 Degree of Correlation between the Regressed Surface Areas for Methane, Nitrogen and CO_2 on Coals

The correlations of nitrogen and CO_2 surface areas with ε_{ss}/k and L were very similar to the correlations for methane surface areas in Table 6.5 and, therefore, they are not included here. The methane area correlates with ε_{ss}/k and L with a correlation coefficient "r" of 0.63 and 0.41, respectively. Further, the solid-solid interaction energy "ε_{ss}/k" and slit length "L" correlate with a correlation coefficient of 0.44. In fact, the surface area and slit length together yield the accessible pore volume for the adsorbate and a slight degree of correlation between the two parameters can thus be expected.

Table 6.5 Correlation Matrix of SLD-PR Model Regressed Parameters for Coals

	Methane Area	**ε_{ss}/k**	**L**
Methane Area	1.00	-	-
ε_{ss}/k	0.63	1.00	-
L	0.41	0.44	1.00

Further, the ε_{ss}/k was found to increase with an increase in surface areas; however, this trend displayed reasonably large scatter. Although the model parameters displayed a slight degree of correlation, this is not significant enough to limit the model's predictive capabilities.

6.4 Generalized Correlations

The second step in developing the generalized model was to develop generalized correlations for the regressed model parameters. Specifically, the model parameters were expressed as functions of coal characterization parameters from the ultimate and proximate analyses of the coals. Prior to undertaking this task, the coal properties were analyzed for their inter-correlation. Table 6.6 presents the correlation matrix for the coal properties available from the ultimate and proximate analyses of coal samples. There was a good correlation between ash% with carbon% and hydrogen%. Further, oxygen% and moisture% were also well correlated. These significant correlations have been highlighted in Table 6.6. However, none of the other correlation coefficients in Table 6.6 was considered significant statistically.

Therefore, the eight properties listed in Table 6.6 were used for developing the generalized correlations for the five model parameters- three surface areas (one for each adsorbent), ε_{ss}/k and L. Here, instead of relying on graphical trends and trial-and-error procedures, emphasis was laid on developing generalized correlations utilizing rigorous regression techniques. In particular, a multilinear regression program developed recently at OSU was utilized.[165] In implementing this regression program, predictors are added to the model until there is no further significant improvement to the correlation coefficient. More importantly, the program is capable of including five different types of non-linear

Table 6.6 Correlation Matrix of Coal Properties (Linear Correlations)

Coal Property	Carbon %	Hydrogen %	Oxygen %	Sulfur %	Ash %	Vol. Matter %	FC %	EMC%
Carbon %	1.00	-	-	-	-	-	-	-
Hydrogen %	0.75	1.00	-	-	-	-	-	-
Oxygen %	0.21	0.59	1.00	-	-	-	-	-
Sulfur %	-0.17	-0.03	-0.39	1.00		-	-	-
Ash %	-0.92	-0.92	-0.42	0.11	1.00	-	-	-
Vol. Matter %	0.40	0.82	0.79	-0.03	-0.58	1.00	-	-
FC* %	0.66	0.24	-0.55	0.13	-0.50	-0.24	1.00	
EMC%**	0.07	0.43	0.89	-0.32	-0.32	0.52	-0.60	1.00

*FC = Fixed Carbon

**EMC = Equilibrium Moisture Content

transformations of each predictor variable. Since there were eight possible predictor variables, this resulted in a total of forty *possible* predictors. The use of non-linear transforms such as square root, square, logarithm, etc. ensure that any significant non-linear relationships between the predictor variables and the regressands are not ignored. In fact, the model parameters (regressands) were found to be correlated with the coal properties in a non-linear manner. Further, the model parameters ε_{ss}/k and L were easily correlated with the coal characterization. However, none of the coal properties could predict reliably the surface area of the adsorbates. Our analysis indicated that the surface areas could be predicted accurately by utilizing a single experimental adsorption datum - the amount of methane adsorbed at 1.4 MPa.[12] Since this experimental isotherm datum was required as input to the model, this rendered the model a "calibrated generalized model". The requirement of this experimental point was considered a serious limitation in developing a completely generalized model. Therefore, in this study, efforts were undertaken to predict the amount of methane adsorbed at 1.4 MPa from coal properties. Using the sequential regression technique mentioned above, the amount of methane adsorbed at 1.4 MPa (calibration point) was predicted with a %AAD of 3%, using only three coal properties. This marked a significant step in developing a completely generalized model that is not dependent on experimental isotherm information as input.

One correlation was developed for each of the five model parameters. Thus, the generalized correlations can be expressed in the following mathematical format:

$$\{SA, \varepsilon_{ss}/k, L\} = f\{\text{Coal Characterization}\} \quad (6.1)$$

6.5 SLD-PR Generalized Model for Pure-Gas Adsorption on Coals

The third step in developing the generalized model was to optimize simultaneously the coefficients of the generalized correlations. This was achieved by regressing the generalized correlation parameters using the adsorption data on all coals simultaneously. The objective function used was the weighted root-mean square (WRMS), where the weights were the expected experimental uncertainties in adsorption data.

The results thus obtained with the newly developed generalized model are presented in Table 6.7. The table lists the statistics obtained for the pure-gas adsorption of methane, nitrogen and CO_2 on nine coals. Specifically, the table lists the WAAD, %AAD and RMSE of each coal and each gas. The highest WAAD of 2.29 was observed for methane adsorption on dry upper Freeport coal. Further, the CO_2 adsorption on dry Upper Freeport coal yielded a WAAD of 2.06. All other predictions were within two times the experimental uncertainties. The largest %AAD of about 24% was observed for the nitrogen adsorption on wet Illinois #6 coal; however, the relatively large experimental uncertainties for this system led to a WAAD of 0.98 and, thus, the prediction errors are within the experimental uncertainties.

The largest overall WAAD was observed for the adsorption on dry Upper Freeport coal. This can be attributed to the larger deviations observed in the generalized parameters of this coal when compared to the corresponding regressed parameters. During the generalization, our analysis indicated that an attempt to better predict the adsorption on dry/wet Illinois #6 coal worsened the predictions for adsorption on dry Upper Freeport and Pocahontas coal. Since the generalized model achieves the overall

minima, such large deviations for some of the coals may well be unavoidable. Further, the current generalized model may not reflect **all** the effects of coal properties on gas adsorption behavior.

As evident from Table 6.7, most of the predictions are well within two times the experimental uncertainties. Overall, the WAAD for adsorption of methane, nitrogen and CO_2 on nine coals was 1.05, whereas the %AAD and RMSE were 8.0% and 0.0430 mmol/gm, respectively. Further, all the methane adsorption data on nine coals can be predicted with a WAAD of 1.03. The corresponding statistics for nitrogen and CO_2 adsorption data were 0.90 and 1.23, respectively. These results demonstrate that the generalized model was able to predict the adsorption of all three gases with similar levels of accuracy.

Table 6.8 presents the %AAD observed between the regressed and generalized model parameters. The methane and nitrogen surface areas were within 10% of their regressed values, with the exception of wet Tiffany, dry Beulah Zap and Upper Freeport coals. Further, the CO_2 surface areas displayed slightly larger deviation from their regressed values. In particular, the generalized surface area for CO_2 adsorption on dry Illinois #6 coal was about 40% larger than the regressed value. Notwithstanding this large deviation, the generalized model was able to predict CO_2 adsorption on dry Illinois #6 coal with a WAAD of 1.57. In contrast, the WAAD for direct regression of this data was 1.16 (Table 6.4). This modeling artifact can be attributed to the correlation observed between the regressed model parameters as shown in Table 6.5. As a result, different values of the surface areas were able to predict the adsorption of CO_2 on dry Illinois #6 coal with comparable accuracy in this case.

Table 6.7 Summary Results of SLD-PR Pure-Gas Model Generalization for Coals

	WAAD				%AAD				RMSE (mmol/gm)			
Coal	**CH_4**	**N_2**	**CO_2**	**Overall**	**CH_4**	**N_2**	**CO_2**	**Overall**	**CH_4**	**N_2**	**CO_2**	**Overall**
Wet Fruitland Coal	0.65	1.38	0.87	0.97	2.5	11.1	8.6	7.4	0.0157	0.0290	0.1031	0.0493
Wet Illinois# 6 Coal	1.17	0.98	1.03	1.06	8.1	23.6	16.4	16.1	0.0187	0.0204	0.1395	0.0595
Wet Tiffany Coal	1.17	0.81	1.10	1.02	6.7	8.4	8.5	7.9	0.0227	0.0110	0.0424	0.0253
Wet LB Fruitland Coal	0.66	0.39	0.69	0.58	3.7	4.7	10.3	6.2	0.0132	0.0056	0.0425	0.0204
Dry Illinois#6 Coal	0.61	0.51	1.57	0.90	3.8	6.8	6.4	5.7	0.0229	0.0137	0.0972	0.0446
Dry Beulah Zap Coal	1.18	0.85	1.09	1.04	6.9	11.1	4.8	7.6	0.0452	0.0301	0.0789	0.0514
Dry Wyodak Coal	0.32	1.11	1.80	1.08	2.2	10.8	6.4	6.5	0.0138	0.0266	0.1100	0.0501
Dry Upper Freeport Coal	2.29	0.58	2.06	1.64	8.1	5.2	11.1	8.1	0.0517	0.0109	0.0930	0.0519
Dry Pocahontas Coal	1.22	1.52	0.85	1.19	4.9	10.0	4.2	6.4	0.0306	0.0282	0.0448	0.0345
Overall	**1.03**	**0.90**	**1.23**	**1.05**	**5.2**	**10.2**	**8.5**	**8.0**	**0.0260**	**0.0195**	**0.0835**	**0.0430**

Table 6.8 Comparison of Generalized and Regressed Model Parameters

Coal	Parameter (%AAD)				
	Methane Area	**Nitrogen Area**	**CO_2 Area**	**ε_{ss}/k**	**L**
Wet Fruitland Coal	4.6	1.7	0.0	4.6	1.0
Wet Illinois# 6 Coal	4.3	5.0	15.7	27.4	4.7
Wet Tiffany Coal	12.9	13.3	12.8	13.1	4.3
Wet LB Fruitland Coal	3.9	5.0	3.7	6.9	2.6
Dry Illinois#6 Coal	0.3	0.5	41.5	9.0	9.7
Dry Beulah Zap Coal	20.9	25.3	11.3	25.4	5.8
Dry Wyodak Coal	9.1	2.9	18.6	11.4	4.5
Dry Upper Freeport Coal	20.0	15.7	16.3	23.3	0.0
Dry Pocahontas Coal	7.7	6.3	7.4	22.3	4.0
Overall (%AAD)	**9.3**	**8.4**	**14.2**	**15.9**	**4.1**

The generalized and regressed values of ε_{ss}/k are also presented in Table 6.8. There were large deviations observed between the generalized and regressed values for ε_{ss}/k for four coals- wet Illinois #6, dry Beulah Zap, dry Upper Freeport and dry Pocahontas coals. Specifically, the deviations in parameter values for these coals were about 25%. Overall, the %AAD between the generalized and regressed values of ε_{ss}/k was 16%. However, these larger deviations had a relatively marginal effect on the generalized gas adsorption predictions, as evident from the statistics in Table 6.7.

The generalized and regressed values of slit length for the nine coals were within 5%, on average. The largest deviation was observed for dry Illinois #6 coal. Although there were deviations between the generalized and regressed model parameters ranging from 5% to 15%, the predictions obtained from the generalized model were well within three times the experimental uncertainties for all the nine coals.

Figure 6.3 presents the comparison between the generalized and regressed parameters. The generalized surface areas for CO_2 adsorption on dry Illinois #6, dry Beulah Zap and dry Wyodak coals showed the larger deviations from their respective

regressed values. This also affected the CO_2 adsorption predictions on these coals, as evident from Table 6.7. Further, the non-absolute percent deviations of the generalized parameters were well distributed about their regressed values, as evident from Figure 6.3.

To illustrate the quality of generalized predictions, Figure 6.4 -6.12 present the pure-gas adsorption predictions on the nine coals. In these figures, the solid lines represent the generalized model predictions obtained for each system. Figure 6.4 presents the results obtained for wet Fruitland coal. The nitrogen and CO_2 adsorptions on this coal were slightly over-predicted at low to moderate pressures, as evident from the figure. Similarly, Figure 6.5 illustrates the predictions on wet Illinois #6 coal. The CO_2 adsorption appears to be under-predicted for this coal at higher pressures; however, the relatively large experimental uncertainties for this coal at the higher pressures are also clearly noticeable.

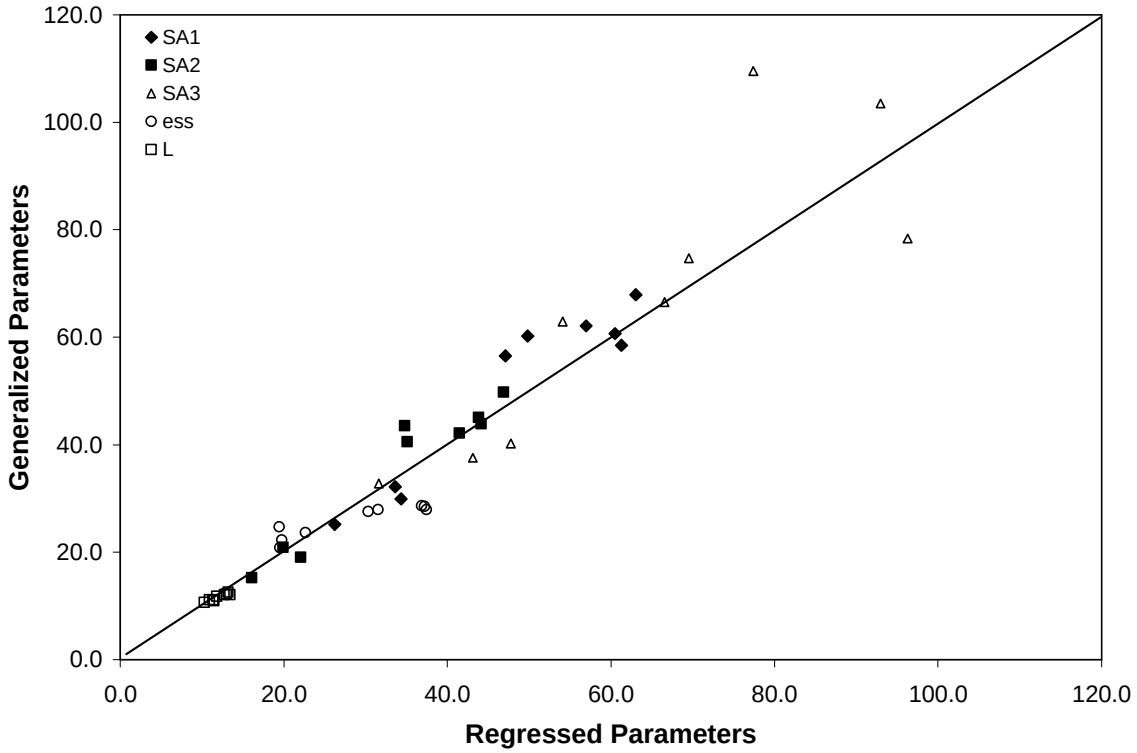

Figure 6.3 Comparison of Generalized and Regressed Model Parameters

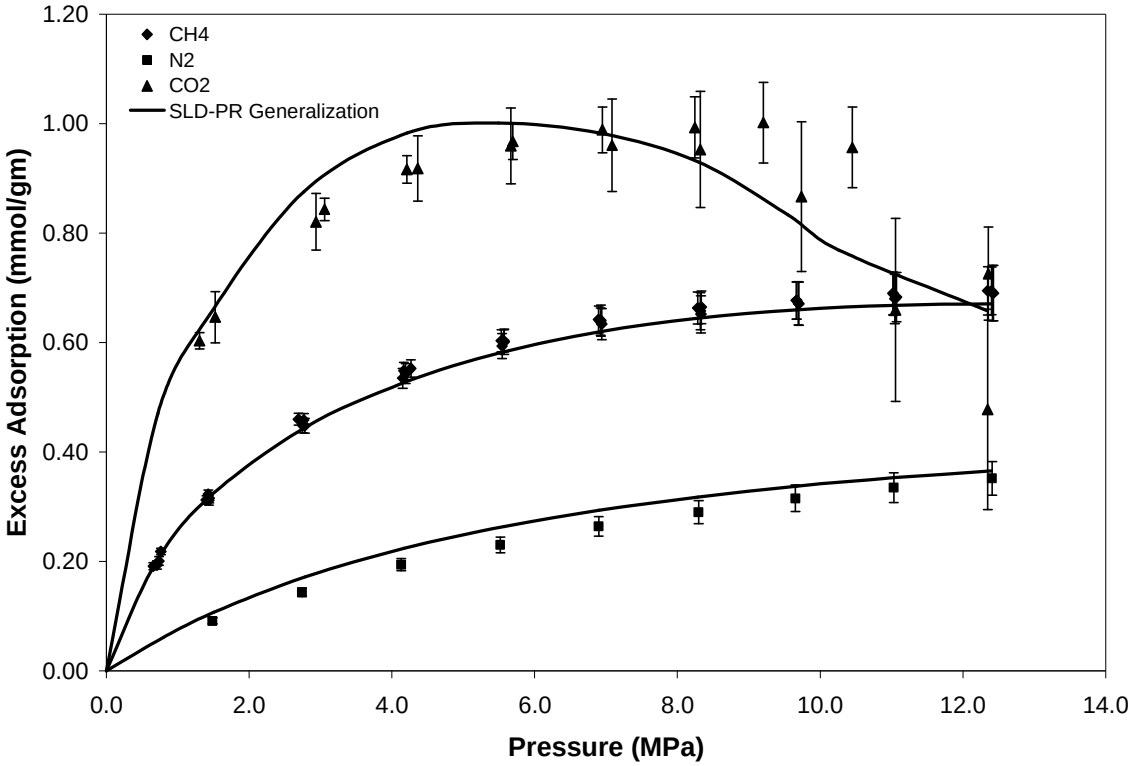

Figure 6.4 Generalized SLD-PR Model Predictions for Pure-Gas Adsorption on Wet Fruitland Coal at 319.3 K

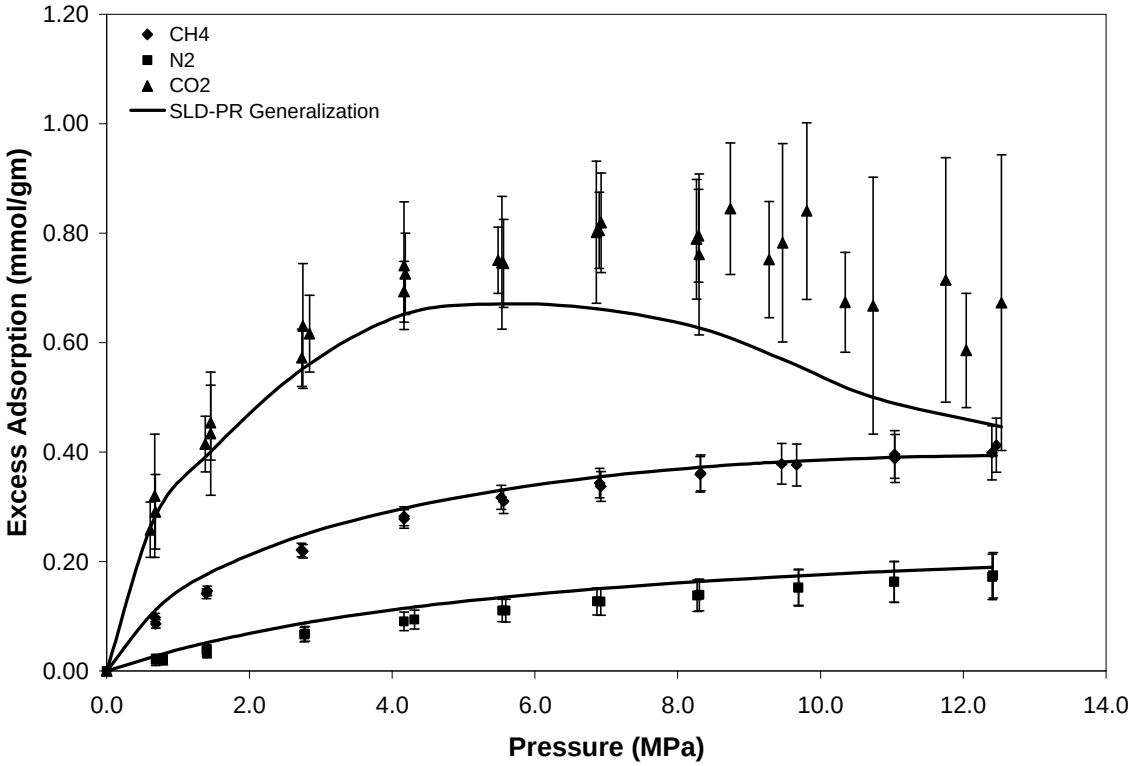

Figure 6.5 Generalized SLD-PR Model Predictions for Pure-Gas Adsorption on Wet Illinois #6 Coal at 319.3 K

Figures 6.6 and 6.7 present the pure-gas adsorption generalized predictions on wet Tiffany and wet Lower Basin Fruitland coals, respectively. Figures 6.8-6.12 present the predictions on the five Argonne coals in this study- dry Illinois #6, dry Beulah Zap, dry Wyodak, dry Upper Freeport and dry Pocahontas coals, respectively. The methane and nitrogen adsorption on dry Illinois #6 coal were predicted within the experimental uncertainties. However, the CO_2 adsorption was under-predicted at moderate pressures. In contrast, the CO_2 adsorption on dry Beulah Zap coal was slightly over-predicted, as evident from Figure 6.9.

Further, the generalized model over-predicted the methane and CO_2 adsorption on dry Upper Freeport coal beyond 4 MPa. The predictions on these two isotherms also had a WAAD of greater than 2.0, as evident from Table 6.7. In comparison, the predictions on dry Pocahontas coal were relatively more accurate. Figure 6.11 and 6.12 present these results for dry Upper Freeport and Pocahontas coals, respectively.

Figure 6.13 presents the deviation plot for the pure-gas adsorption generalized predictions. Overall, about 89% of the adsorption data for the three gases were predicted within two times the experimental uncertainties. Further, about 96% of the adsorption data were within three times the experimental uncertainties. These results demonstrate that the generalized SLD-PR model appears effective in predicting pure-gas adsorption on coals of varying ranks within three times the experimental uncertainties based solely on the coal characterization information.

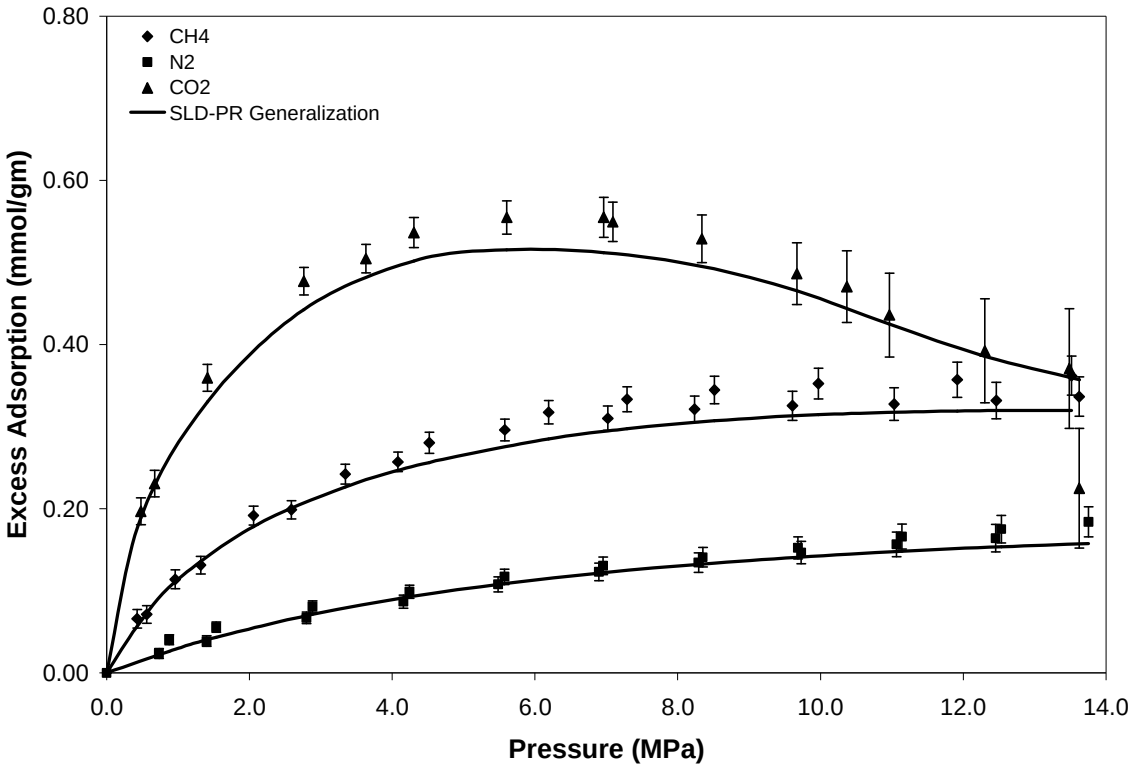

Figure 6.6 Generalized SLD-PR Model Predictions for Pure-Gas Adsorption on Wet Tiffany Coal at 327.6 K

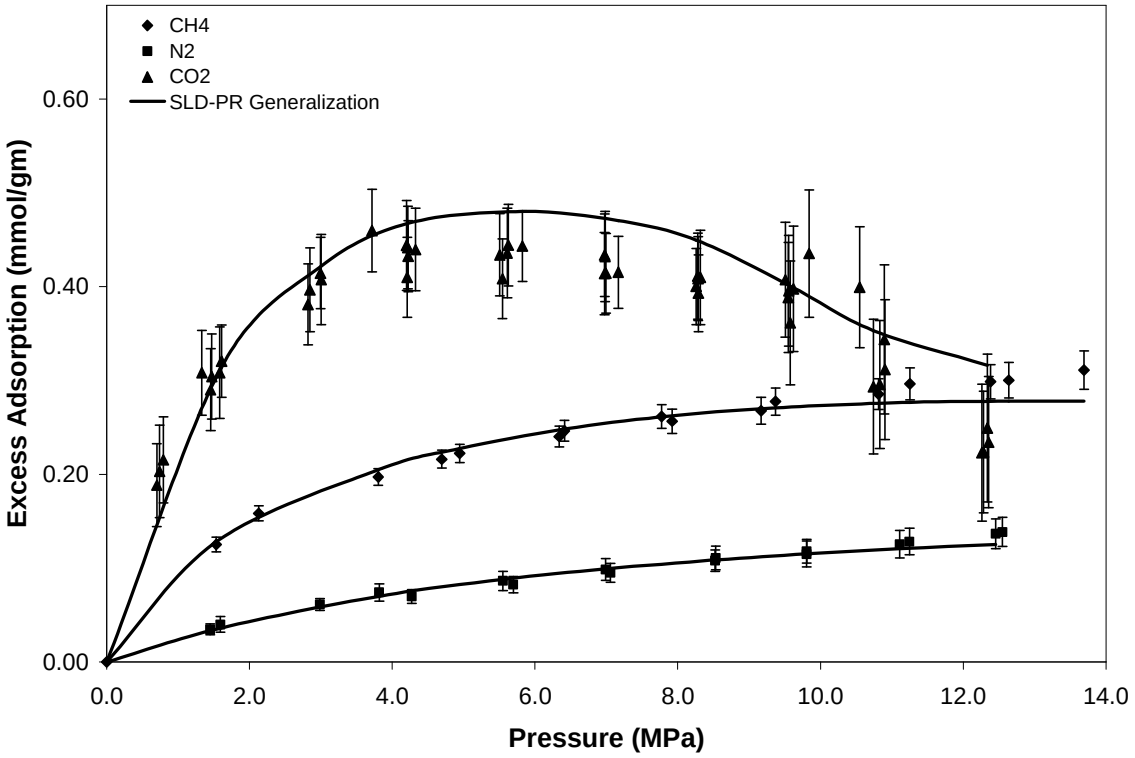

Figure 6.7 Generalized SLD-PR Model Predictions for Pure-Gas Adsorption on Wet Lower Basin Fruitland Coal at 319.3 K

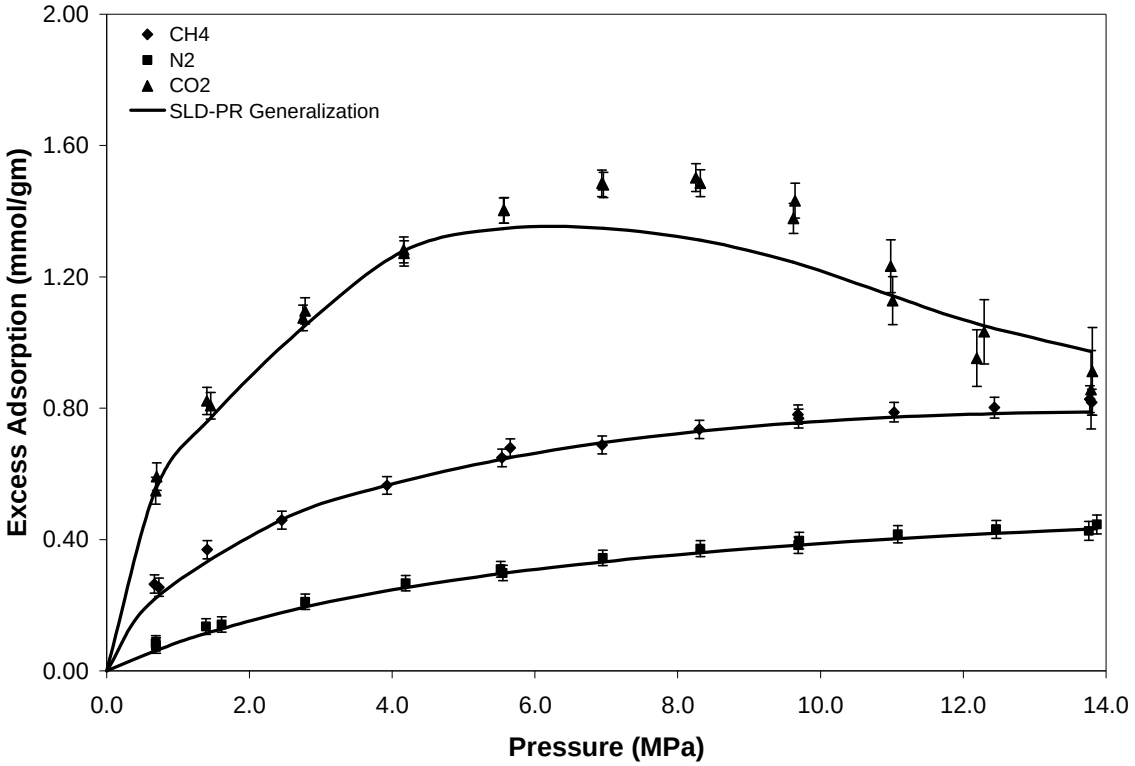

Figure 6.8 Generalized SLD-PR Model Predictions for Pure-Gas Adsorption on Dry Illinois #6 Coal at 328.2 K

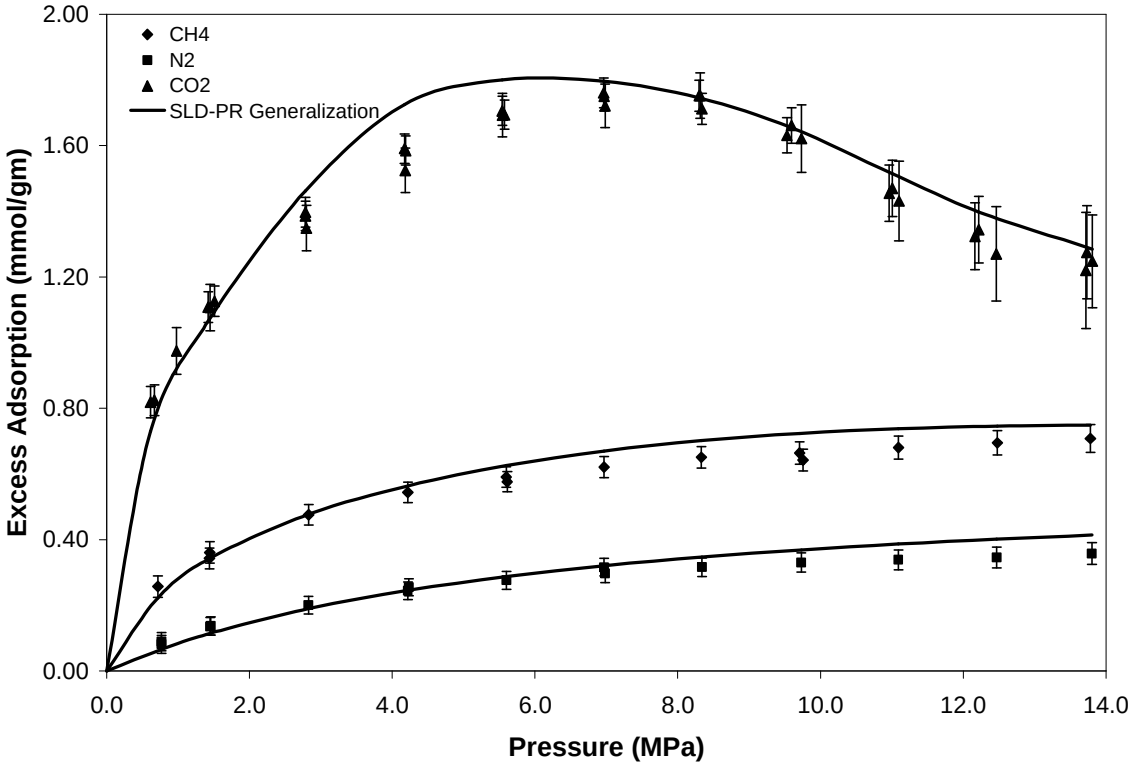

Figure 6.9 Generalized SLD-PR Model Predictions for Pure-Gas Adsorption on Dry Beulah Zap Coal at 328.2 K

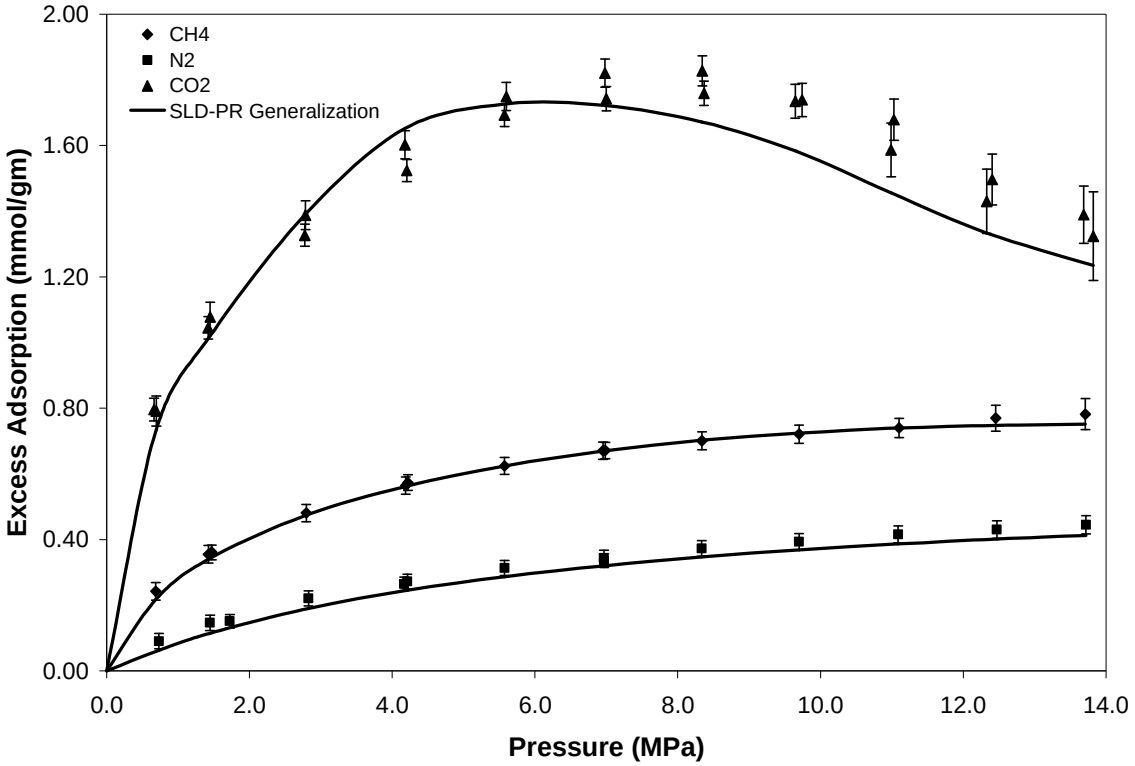

Figure 6.10 Generalized SLD-PR Model Predictions for Pure-Gas Adsorption on Dry Wyodak Coal at 328.2 K

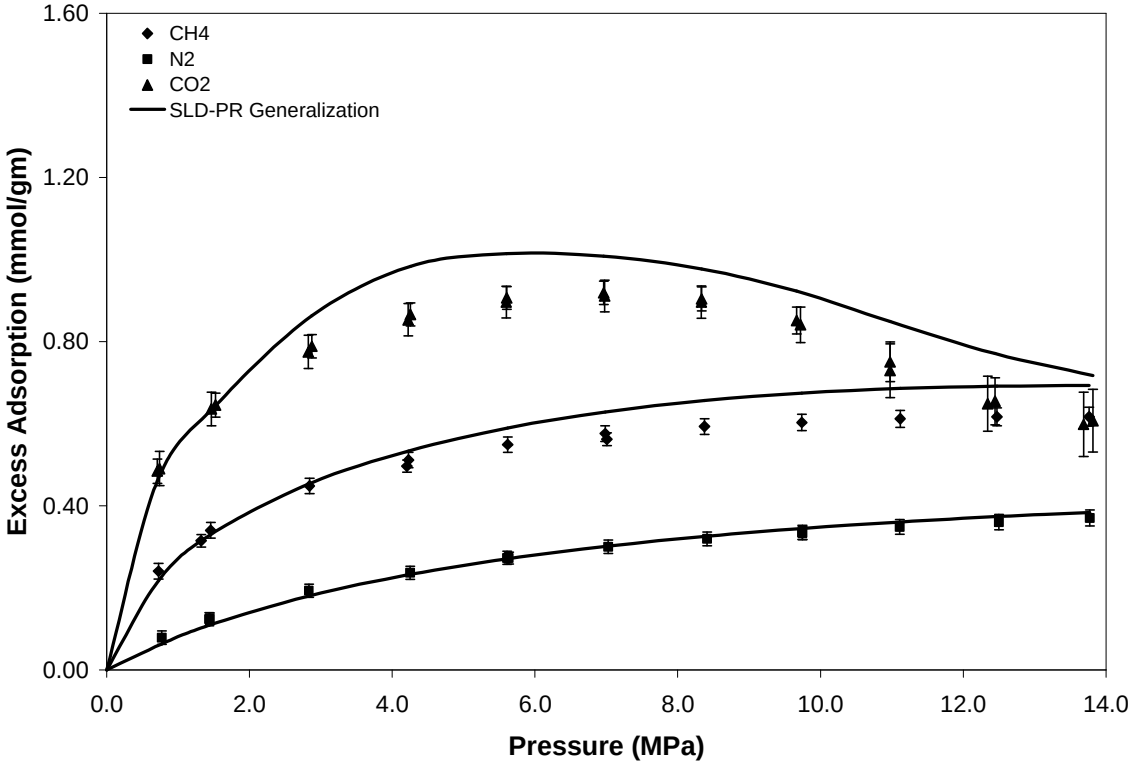

Figure 6.11 Generalized SLD-PR Model Predictions for Pure-Gas Adsorption on Dry Upper Freeport Coal at 328.2 K

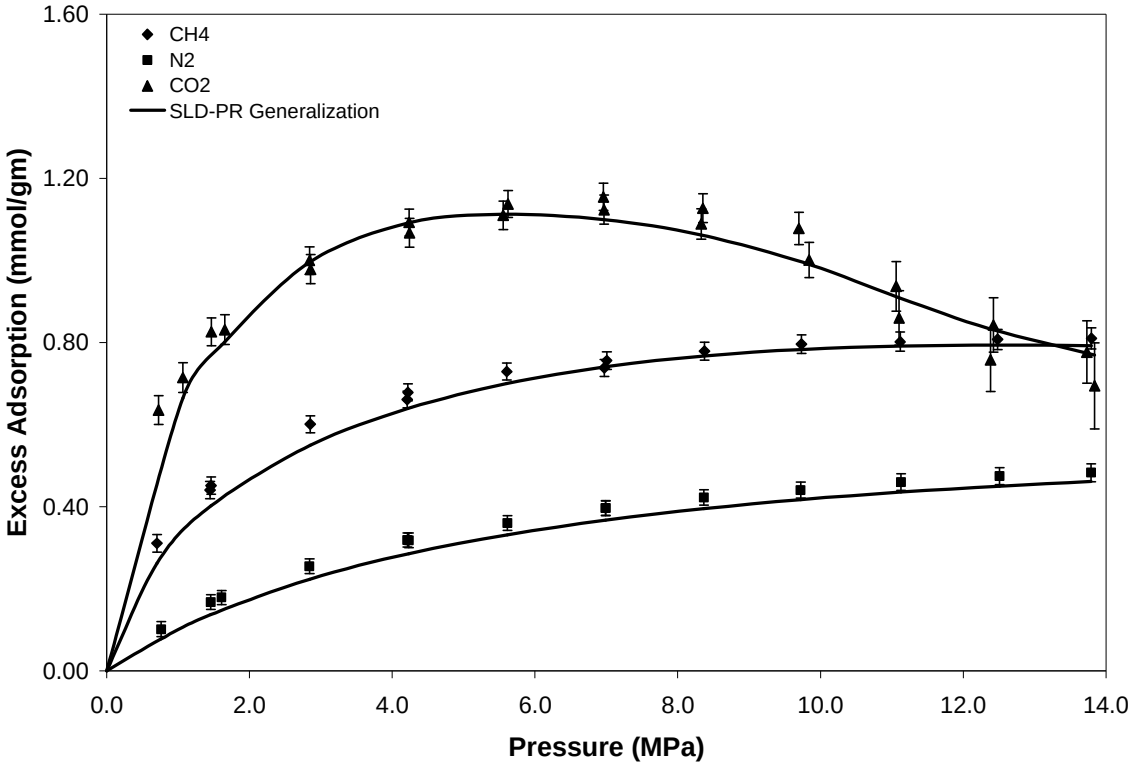

Figure 6.12 Generalized SLD-PR Model Predictions for Pure-Gas Adsorption on Dry Pocahontas Coal at 328.2 K

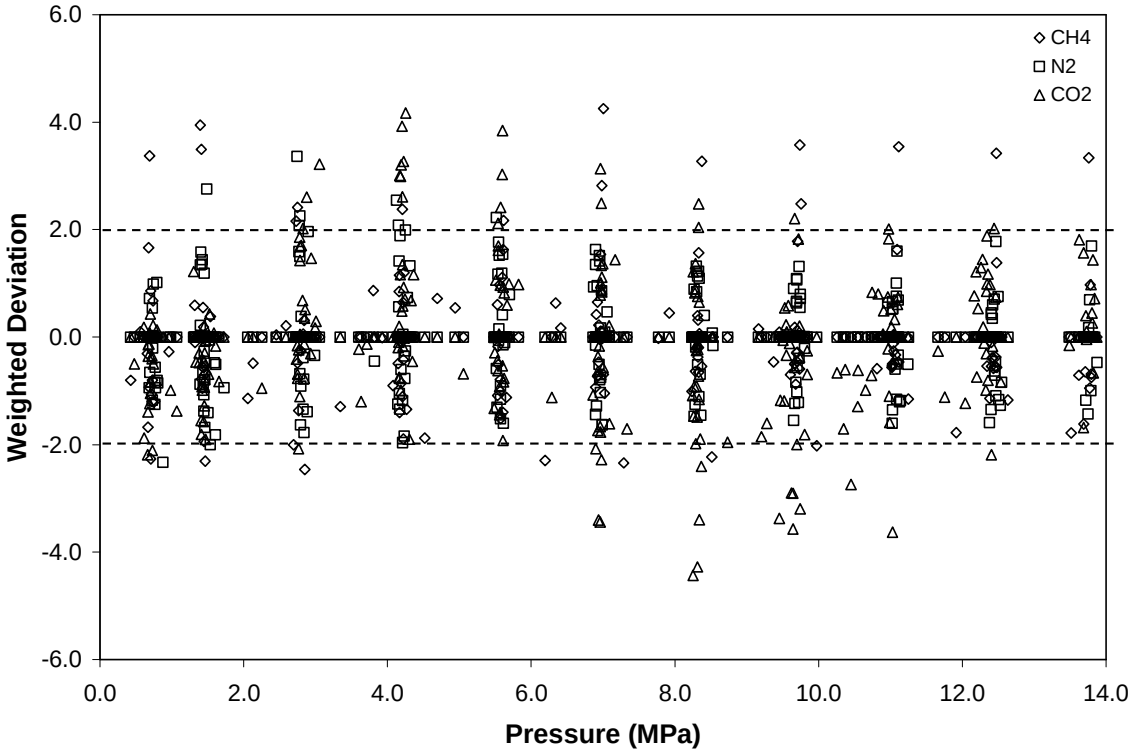

Figure 6.13 Deviation Plot for the Generalized SLD-PR Model Predictions for Pure-Gas Adsorption on Coals

6.6 Previous Generalization Studies

Model generalizations based on coal characterization have been investigated in the literature. For example, Reeves et al.[166] generalized the Langmuir model parameters of methane, nitrogen and CO_2 in terms of vitrinite reflectance (coal rank). Their uni-variate analysis indicated a reasonable trend of methane and nitrogen sorption capacity (Langmuir volume) with vitrinite reflectance. However, Reeves et al. observed that CO_2 sorption capacity did not display a linear trend with coal rank. Further, they concluded that no uni-variate trends were able to predict Langmuir pressure for any of the three gases. They also employed multiple-regression analysis to predict the two Langmuir parameters from the coal characterization alone. Specifically, their model required seven input variables for each of the six Langmuir constants (two for each gas). Although this analysis yielded a reasonable model, the large number of parameters required in the multiple-regression model limits the robustness of their generalized model. Moreover, when the extended Langmuir model was applied to mixed-gas adsorption, errors greater than 100% have been found for N_2/CO_2 mixtures.[34] Therefore, the generalization of Langmuir-type models would have limited capability to predict *a priori* mixed-gas adsorption. As such, a theory-based multi-component adsorption model capable of predicting mixed-gas adsorption from pure component data is required.

Further, phenomenological models like the SLD, 2-D EOS and Ono-Kondo lattice model, through their generalization, are better suited for accurate predictions of gas adsorption over wide ranges of pressures, temperatures and compositions. Specifically, model generalization through the use of coal characterization and molecular properties of the adsorbates can facilitate reliable and accurate *a priori* predictions for simulations of

enhanced coalbed methane recovery. In some of the previous works at OSU[18, 20, 21], efforts were made to develop such generalized models. Sudibandriyo[20] generalized the Ono-Kondo model parameters in terms of the adsorbent characteristics and molecular properties of the adsorbates. Specifically, the model parameters were generalized in terms of the maximum surface adsorbed-phase density, thermal expansion coefficient and molecular properties of the adsorbates. The model generalization appeared to be effective in predicting gas adsorption on dry and wet coals. However, the adsorbent surface area had to be regressed and the fluid-solid energy required a correction factor to account for the chemical structure of the coal. Arumugam[21] improved upon the Ono-Kondo model generalization by generalizing the fluid-solid energy in terms of the fixed carbon content of the coal and critical temperature of the adsorbates. The model was capable of describing the adsorption behavior of pure methane, nitrogen, CO_2 and C_2H_6 on dry Argonne coals within the expected experimental uncertainties. However, the maximum adsorption capacity, C, had to be regressed since this parameter could not be generalized in terms of adsorbent characteristics. This represents the extent of the Ono-Kondo model generalization, currently.

Pan[18] generalized the 2-D EOS model parameters in terms of the molecular properties of the adsorbates and accessible surface area of the adsorbent. The 2-D EOS generalized model predictions on activated carbon were within three times the expected experimental uncertainties. However, the generalized model has not yet been extended to gas adsorption on coals.

Recently, efforts were also made to generalize the SLD-PR model.[12, 27] These authors improved upon the previous generalizations by generalizing simultaneously the

gas adsorption on dry and wet coals. Further, the previous generalizations by Pan[18] and Sudibandriyo[20] were developed for activated carbons and then extended for coals. In contrast, the SLD-PR generalization developed recently[12, 27] was developed and implemented specifically for coals. However, this generalization also had one important limitation. Specifically, the model required the knowledge of the amount of methane adsorbed at 1.4 MPa (400 psia) on the coal sample. This was essential to estimate reliably the accessible surface area of the adsorbates on a given adsorbent. This limitation renders the model a *matrix-calibrated* model rather than a completely generalized one.

In this study, efforts were made to generalize the amount of methane adsorbed at 1.4 MPa such that the surface areas can be predicted without the need for experimental isotherm measurements. In fact, as discussed above in Section 6.5, the amount of methane adsorbed at 1.4 MPa (calibration point) was predicted with a %AAD of 3%, using only three coal properties. Thus, the newly developed generalized model is capable of predicting gas adsorption on coals based solely on the coal characterization and does not require any isotherm experimental information as input.

In fact, the surface area of coals has been a subject of debate for many years. After an extensive review, Mahajan[107] had concluded that the surface areas of coals have no physical meaning. The previous model generalizations mentioned above have consistently required regression of the accessible surface area of coals. The current study marks the first instance when the surface areas were not regressed directly, but were predicted from the coal characterization alone.

The generalized SLD-PR model developed in this study also has certain limitations. A simplification of the model generalization resulted from two key

assumptions used in the data reduction techniques. Specifically, the total amount of water present on a wet coal was assumed to be adsorbed water; and no separate water-rich phase was assumed to exist. Further, the gas-phase was considered to be free from water. This means that the density of the bulk gas was calculated as dry gas density. In addition, the solubility of the gas in the adsorbed water was subtracted from the calculated values of Gibbs adsorption. The amount of gas soluble in adsorbed water, if any, cannot be determined by ordinary experimental techniques. As a result, the adsorbing gas was considered to have the same solubility in the adsorbed water as it does in liquid water.

The above simplifying assumptions were invoked in our data reduction procedures. However, the recent review on the characteristics of adsorbed water highlighted in Chapter 4 indicates that the thermodynamic behavior of the adsorbed water is markedly different from that of bulk (liquid) water. Therefore, the adsorbed water may not possess the same gas solubility as bulk water does. The water present on the coal in excess of the adsorbed water, however, behaves like bulk water and thus can be expected to display similar solubility properties. The above reasoning suggests that only the "excess" moisture present on a coal should be included in gas solubility calculations. However, to date, we have not reprocessed our data to neglect gas solubility in adsorbed water.

Further, in our modeling, water was not treated as a *separate adsorbed component*. Specifically, the water present with the coals was treated as a "pacifier" of the coal matrix, i.e., it was considered to occupy part of the porous coal surface, thus limiting the accessible area for the adsorbing gases. In effect, this reduction of surface available for adsorption of gases like methane, nitrogen and CO_2 (caused by the adsorbed

water) is treated as being constant over the pressure range of the measurements. Thus, in our current modeling technique, the effect of water is reflected implicitly in the model parameters.

6.7 Sensitivity Analysis of SLD-PR Model Generalization

A sensitivity analysis was conducted for the SLD-PR model generalized parameters. The modeling results had shown that the generalized parameters are capable of predicting excess adsorption of gases within three times the experimental uncertainties, on average (Table 6.7). However, a more realistic estimate of the level of accuracy in these predictions is obtained when the parameter values are perturbed to their maximum expected levels of deviations. Table 6.8 documents the deviations observed between the generalized and regressed parameter values. These results show that the generalized parameters can deviate from 5% to 15% from their regressed values. Therefore, the SLD-PR model parameters were perturbed by up to 15% in the sensitivity analysis. Specifically, a wet coal (Fruitland coal) was selected and the three surface areas and ε_{ss}/k were perturbed by 15% each from their regressed values. Further, the slit length was perturbed by 5% based on the results shown in Table 6.8.

The excess adsorption predictions on Fruitland coal were evaluated for each of these perturbations of model parameters. In this manner, twenty-seven scenarios were obtained including the original regressed parameters. These correspond to all the possible positive and negative deviations in the five SLD-PR parameters, namely, the three surface areas, ε_{ss}/k and L.

Table 6.9 summarizes the results obtained for the sensitivity analysis. The table lists the percentage deviations of model parameters for each case and the corresponding

weighted average absolute deviation (WAAD) of the calculated Gibbs adsorption obtained in each case. As shown in Table 6.9, when all the parameter deviations are in the same direction (positive or negative), they yield the largest error in predictions. Specifically, the largest overall WAADs were 4.2 and 4.1 for scenarios 2 and 15, respectively. These two scenarios have been highlighted in Table 6.9. The statistics for the original regressed and generalized parameters are also listed in the table for completeness.

Although, large deviations were noticed for scenarios 2 and 15, the overall WAADs for most of the twenty-seven scenarios were within four times the experimental uncertainties. In reality, there is more likelihood of opposite errors in the parameter estimation "canceling out" and yielding reasonably accurate predictions. In fact, about 16 of the twenty-seven scenarios in Table 6.9 yield WAADs less than 3.0 owing to the cancelation of opposite errors in parameters' estimation.

Further, the deviations in surface area have the largest effect (for e.g., a 10% change would yield 10% different predictions of amount adsorbed). The effects of slit length and ε_{ss} are much smaller. This is indicated by scenarios 20 to 27 in Table 6.9, wherein single parameter perturbations are available. These scenarios show that individual perturbations of slit length and ε_{ss} have smaller effects than perturbations of surface area.

Figures 6.14-6.16 present the sensitivity analysis results for the pure gas adsorption of methane, nitrogen and CO_2 on wet Fruitland coal, respectively. As shown in these figures, positive deviations in parameters result in over-predicting the Gibbs

adsorption and negative deviations in parameters result in under-predicting the Gibbs adsorption isotherms.

Table 6.9 Sensitivity Analysis of SLD-PR Model Parameters for Pure-Gas Adsorption on Wet Fruitland Coal at 319.3 K

		WAAD			
Case No.	**Parameter Deviations**	**CH_4**	**N_2**	**CO_2**	**Overall**
1	Surface Areas: 0%, ε_{ss}/k : 0%, L: 0% (Original Regressed)	0.4	1.2	0.8	0.8
2	Surface Areas:+15%, ε_{ss}/k :+15%, L:+5%	6.6	3.2	2.8	4.2
3	Surface Areas:+15%, ε_{ss}/k :+15%, L:- 5%	6.1	3.1	1.8	3.7
4	Surface Areas:+15%, ε_{ss}/k :+15%, L: 0%	6.4	3.2	2.2	3.9
5	Surface Areas:+15%, ε_{ss}/k :-15%, L:+5%	1.9	1.4	1.6	1.6
6	Surface Areas:+15%, ε_{ss}/k :-15%, L:-5%	1.4	1.3	0.9	1.2
7	Surface Areas:+15%, ε_{ss}/k :-15%, L: 0%	1.6	1.3	1.2	1.4
8	Surface Areas:+15%, ε_{ss}/k : 0%, L:+5%	4.2	1.9	2.2	2.8
9	Surface Areas:+15%, ε_{ss}/k : 0%, L:-5%	3.8	1.9	1.3	2.3
10	Surface Areas:+15%, ε_{ss}/k : 0%, L: 0%	4.0	1.9	1.7	2.5
11	Surface Areas:-15%, ε_{ss}/k : +15%, L: +5%	1.9	1.2	1.4	1.5
12	Surface Areas:-15%, ε_{ss}/k : +15%, L: -5%	2.3	1.3	2.3	2.0
13	Surface Areas:-15%, ε_{ss}/k : +15%, L: 0%	2.1	1.2	1.9	1.7
14	Surface Areas:-15%, ε_{ss}/k : -15%, L: +5%	5.7	3.0	2.4	3.7
15	Surface Areas:-15%, ε_{ss}/k : -15%, L: -5%	6.0	3.1	3.2	4.1
16	Surface Areas:-15%, ε_{ss}/k : -15%, L: 0%	5.9	3.1	2.8	3.9
17	Surface Areas:-15%, ε_{ss}/k : 0%, L: +5%	3.7	1.9	1.8	2.5
18	Surface Areas:-15%, ε_{ss}/k : 0%, L: -5%	4.0	2.0	2.7	2.9
19	Surface Areas:-15%, ε_{ss}/k : 0%, L: 0%	3.9	2.0	2.3	2.7
20	Surface Areas: 0%, ε_{ss}/k :+15%, L:+5%	2.4	1.6	1.1	1.7
21	Surface Areas: 0%, ε_{ss}/k :+15%, L:-5%	1.9	1.6	1.0	1.5
22	Surface Areas: 0%, ε_{ss}/k :+15%, L: 0%	2.2	1.6	0.9	1.5
23	Surface Areas: 0%, ε_{ss}/k :-15%, L:+5%	2.1	1.3	1.0	1.5
24	Surface Areas: 0%, ε_{ss}/k :-15%, L:-5%	2.5	1.4	1.5	1.8
25	Surface Areas: 0%, ε_{ss}/k :-15%, L: 0%	2.3	1.4	1.1	1.6
26	Surface Areas: 0%, ε_{ss}/k : 0%, L:+5%	0.6	1.2	0.9	0.9
27	Surface Areas: 0%, ε_{ss}/k : 0%, L:-5%	0.4	1.2	1.1	0.9
-	Original Generalized	0.7	1.4	0.9	1.0

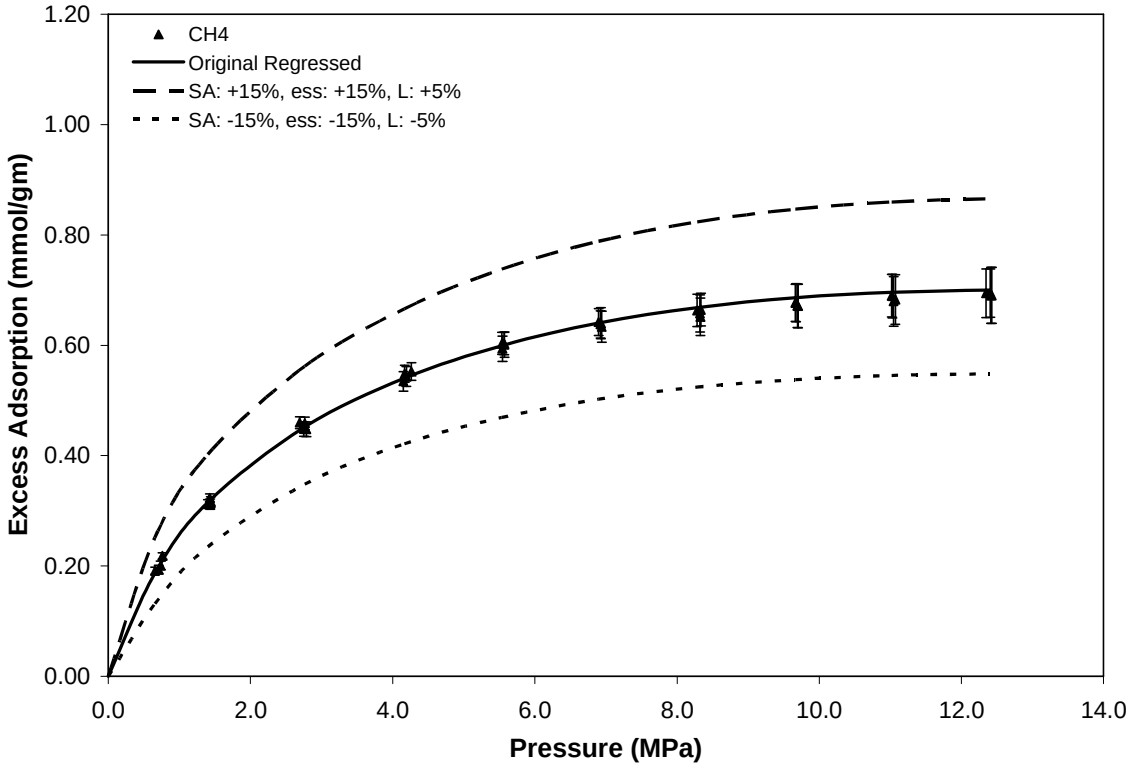

Figure 6.14 Sensitivity Analysis of SLD-PR Generalized Model for Methane Adsorption on Wet Fruitland Coal at 319.3 K

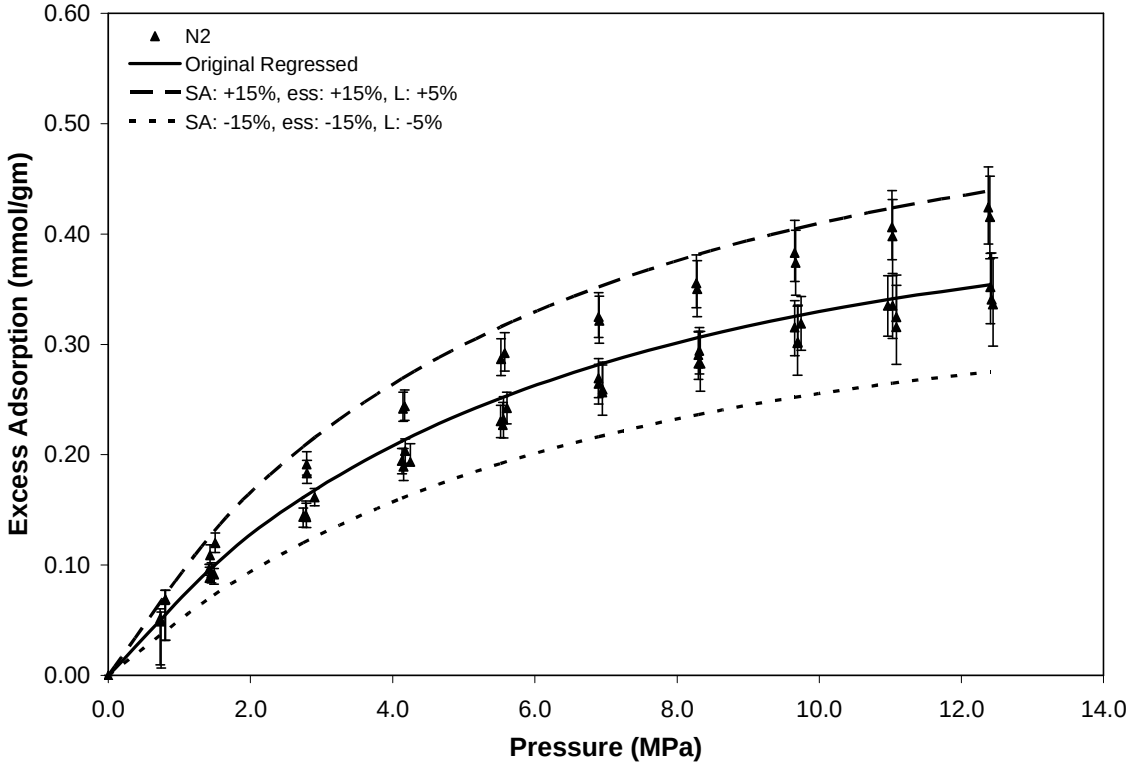

Figure 6.15 Sensitivity Analysis of SLD-PR Generalized Model for Nitrogen Adsorption on Wet Fruitland Coal at 319.3 K

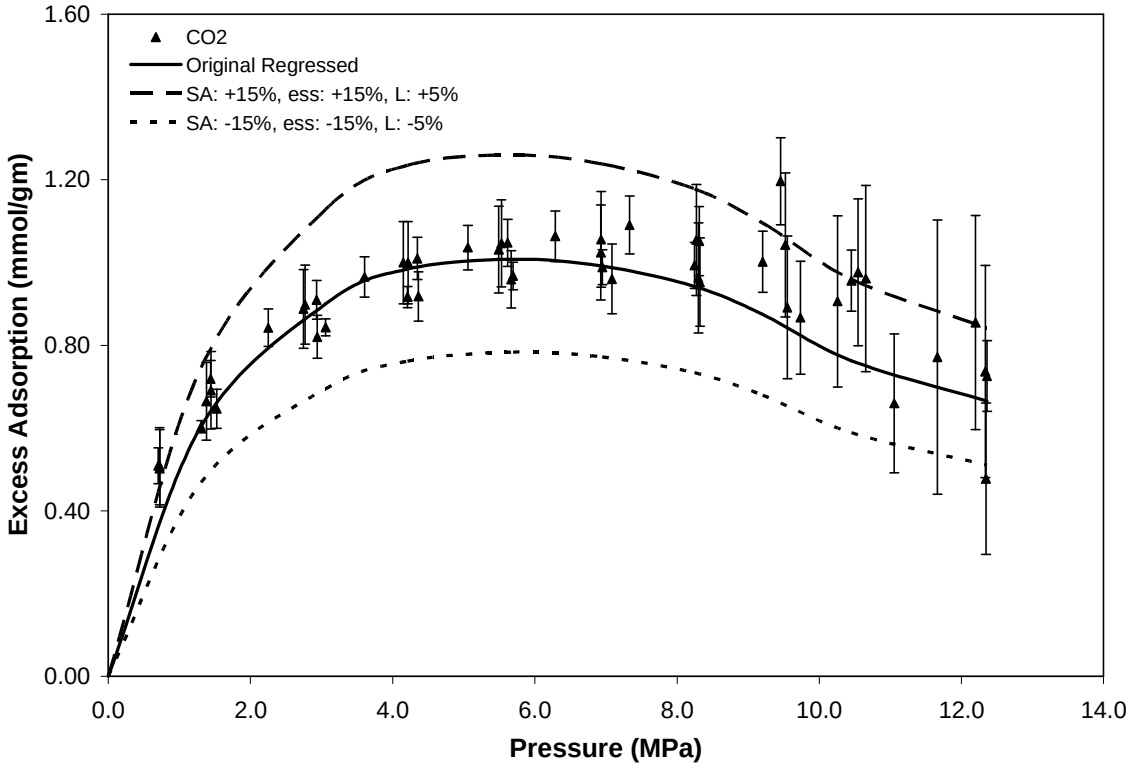

Figure 6.16 Sensitivity Analysis of SLD-PR Generalized Model for CO_2 Adsorption on Wet Fruitland Coal at 319.3 K

6.8 SLD-PR Generalized Model Predictions for Mixed-Gas Adsorption

The generalized SLD-PR model discussed above was also used to predict *a priori* mixed-gas adsorption on coals. Specifically, one-fluid mixing rules were used within the SLD framework to predict binary and ternary gas adsorption on wet coals. In these model evaluations, all binary interaction parameters were set to zero and no parameter regressions were undertaken. In fact, the pure-gas generalized model was applied directly to model multi-component gas adsorption with the selected mixing rules.

Table 6.10 presents the summary results obtained for generalized predictions of mixed-gas adsorption on wet coals. The table lists the three binary pairs formed by mixtures of methane, nitrogen and CO_2. For example, CH_4/N_2 in Table 6.10 refers to the mixed-gas adsorption of methane and nitrogen, and so on. The table lists the WAADs of

the component adsorption for the binary gas adsorption on wet Fruitland, wet Illinois #6 and wet Tiffany coals. Further, the statistics for ternary gas adsorption on wet Tiffany coal are also included in Table 6.10. The binary gas adsorption isotherms on wet Illinois #6 and wet Fruitland coals were measured at four nominal feed molar compositions that were 20/80, 40/60, 60/40 and 80/20 for a given binary pair. In contrast, the binary gas adsorption isotherms on wet Tiffany coal were measured for a single feed composition for each of the three binary pairs. Further, the ternary gas feed composition was 10/40/50 for $CH_4/N_2/CO_2$ mixture. More details about the feed compositions of these mixtures can be found in the OSU adsorption database.[12] For simplicity, the statistics presented in Table 6.10 are the overall averages for all feed compositions of a given mixture.

Table 6.10 Summary Results of Generalized SLD-PR Predictions for Mixed-Gas Adsorption on Coals

Coal	WAAD					
	CH_4/N_2		CH_4/CO_2		N_2/CO_2	
	CH_4	N_2	CH_4	CO_2	N_2	CO_2
Wet Fruitland Coal	0.52	0.80	0.77	0.48	0.46	0.29
Wet Illinois# 6 Coal	0.66	0.92	0.86	0.47	0.97	0.53
Wet Tiffany Coal	2.87	1.90	3.92	0.49	1.48	1.11
	$CH_4/N_2/CO_2$ (Ternary)					
	CH_4		N_2		CO_2	
	0.62		2.31		0.58	

The predictions were least accurate for methane component adsorption on wet Tiffany coal. Specifically, the WAADs for methane component adsorption in CH_4/N_2 and CH_4/CO_2 mixtures were 2.87 and 3.92, respectively. Fitzgerald[25] had also observed large deviations in non-generalized predictions of methane component adsorption in the above mixtures.

The predictions on wet Fruitland and wet Illinois #6 coals were more accurate than those on wet Tiffany coal. Interestingly, the ternary gas adsorption predictions on

wet Tiffany coal were more accurate than the binary predictions on the same coal and yielded WAADs of 0.62, 2.31 and 0.58 for the component adsorption of methane, nitrogen and CO_2, respectively. Overall, the generalized model predictions for all the coals were within three times the experimental uncertainties, on average.

Figures 6.17-6.22 present the generalized prediction results for binary gas adsorption on wet Fruitland coal. In these figures, the percentages refer to the different feed compositions of the gas mixture in mole percent (e.g., 80% CH_4 in a CH_4/N_2 mixture refers to 80 mole percent methane and 20 mole percent nitrogen in the feed). The dashed lines in these figures are the generalized predictions of the SLD-PR model.

As illustrated in Figure 6.18, the nitrogen component adsorption on wet Fruitland coal is over-predicted for the 80% and 60% nitrogen feed compositions. In contrast, the methane/CO_2 and nitrogen/CO_2 mixtures on the same coal are predicted within the experimental uncertainties, on average. The results for these mixtures are illustrated in Figures 6.19-6.22, respectively.

The competitive adsorption behavior is clearly evident from the binary adsorption isotherms of these gases. In particular, for some of the nitrogen/CO_2 mixtures as shown in Figure 6.21, the component excess adsorption of nitrogen at the higher pressures becomes negative owing to the competitive adsorption between nitrogen and CO_2. Further, the generalized model is able to predict accurately the observed competitive adsorption between these two gases, as evident from Figure 6.21.

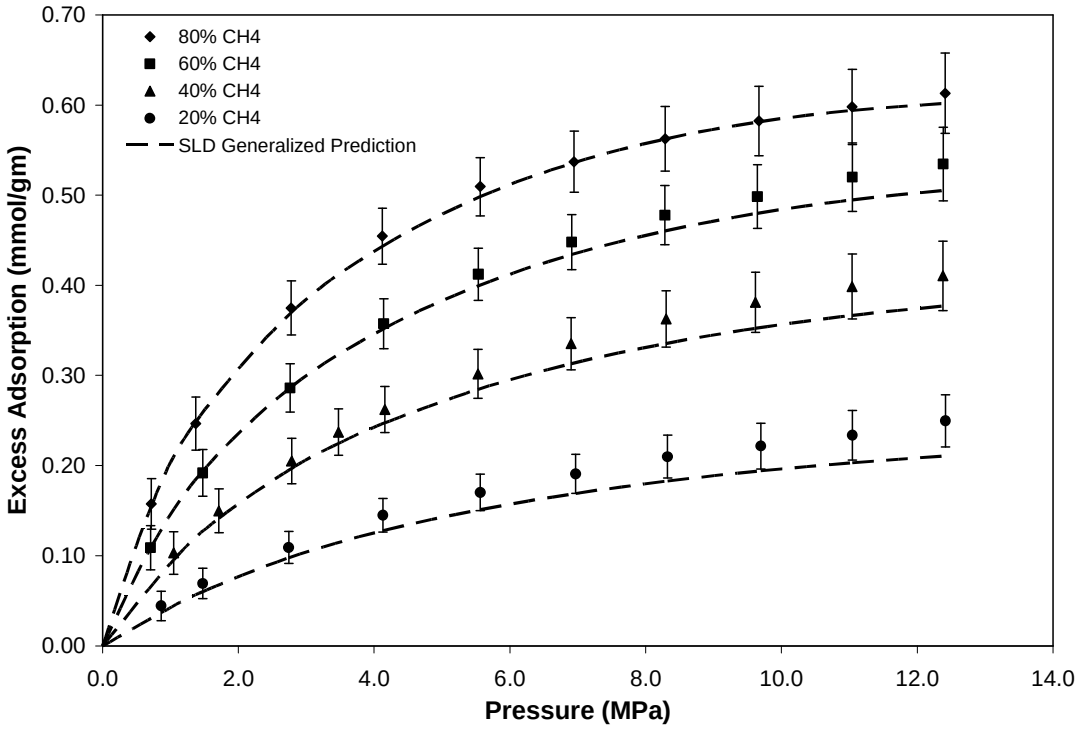

Figure 6.17 Generalized SLD-PR Model Predictions for Methane Component Adsorption in Methane/Nitrogen Mixtures on Wet Fruitland Coal at 319.3 K

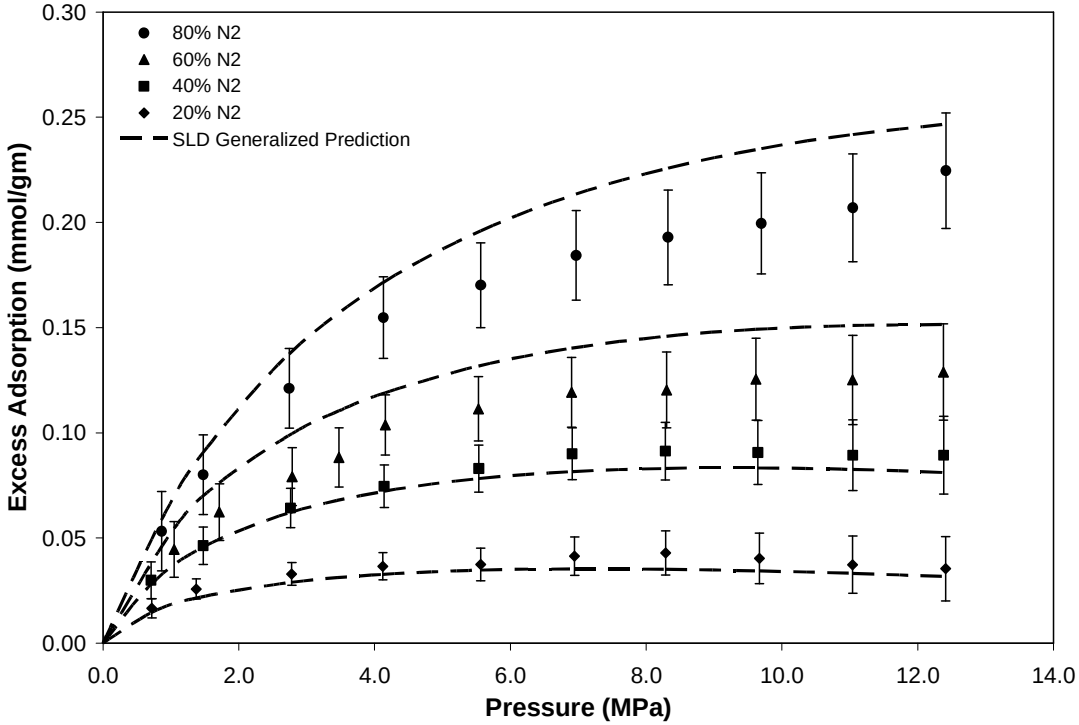

Figure 6.18 Generalized SLD-PR Model Predictions for Nitrogen Component Adsorption in Methane/Nitrogen Mixtures on Wet Fruitland Coal at 319.3 K

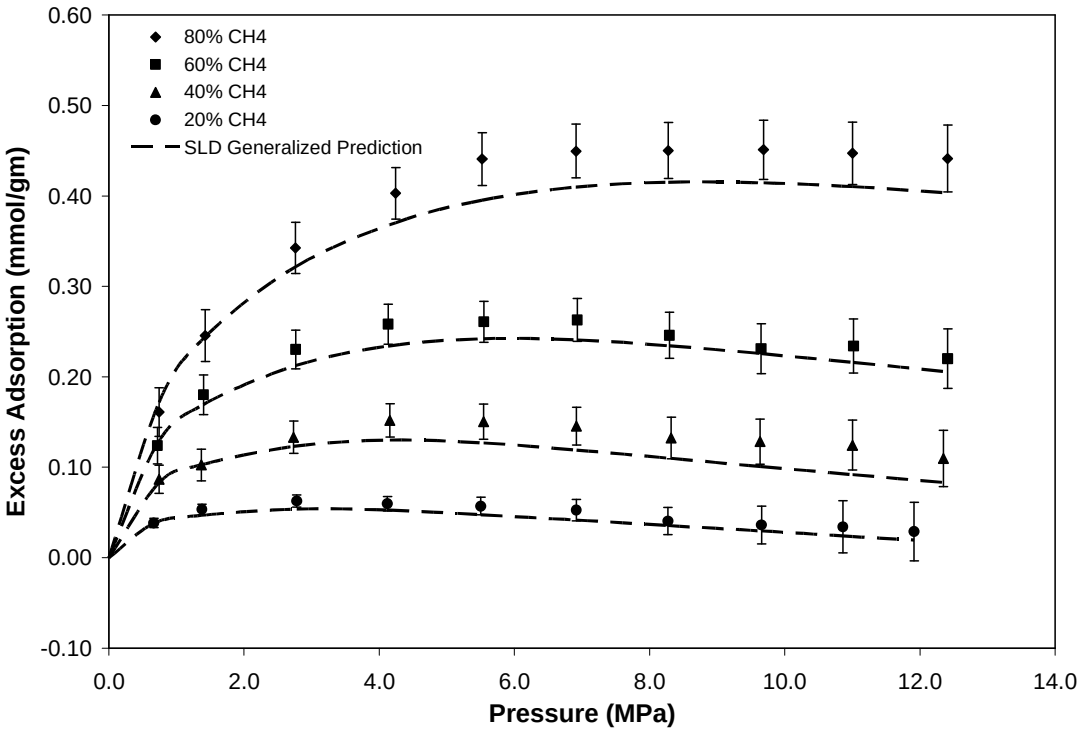

Figure 6.19 Generalized SLD-PR Model Predictions for Methane Component Adsorption in Methane/CO_2 Mixtures on Wet Fruitland Coal at 319.3 K

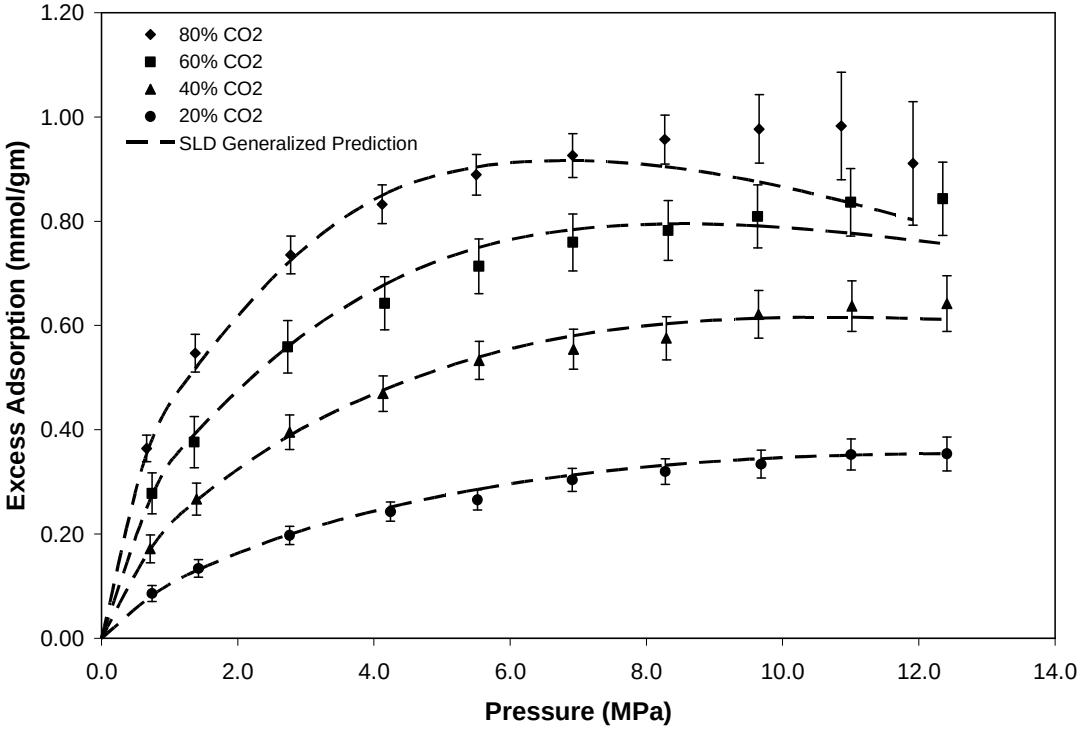

Figure 6.20 Generalized SLD-PR Model Predictions for CO_2 Component Adsorption in Methane/CO_2 Mixtures on Wet Fruitland Coal at 319.3 K

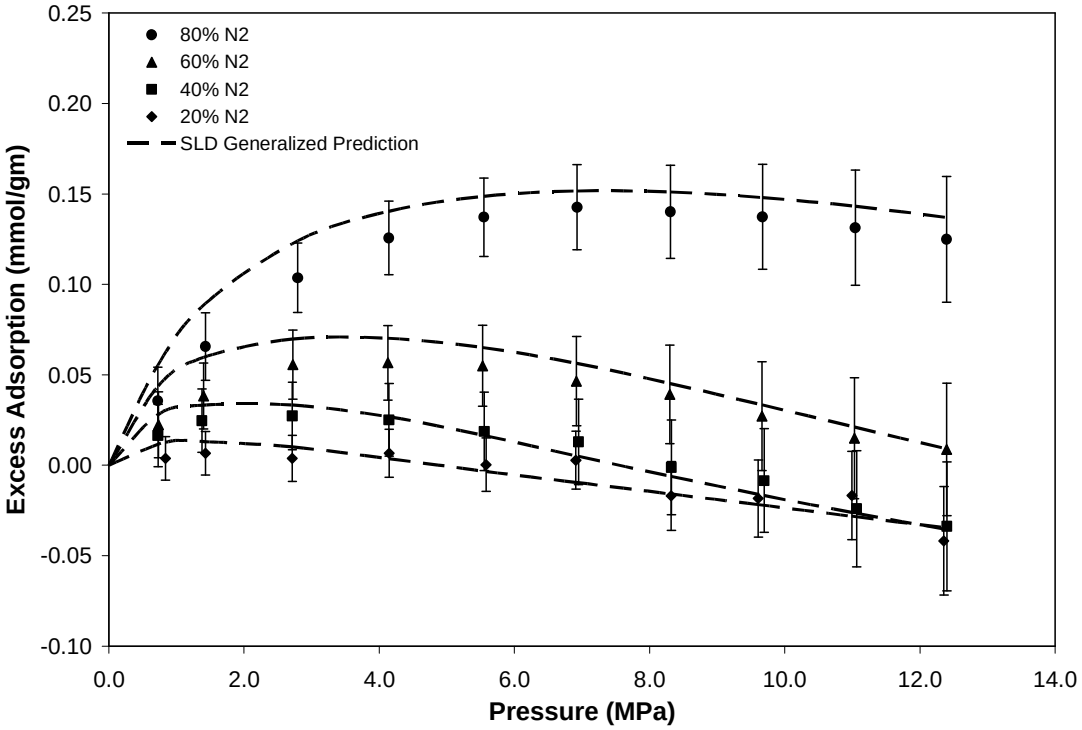

Figure 6.21 Generalized SLD-PR Model Predictions for Nitrogen Component Adsorption in Nitrogen/CO_2 Mixtures on Wet Fruitland Coal at 319.3 K

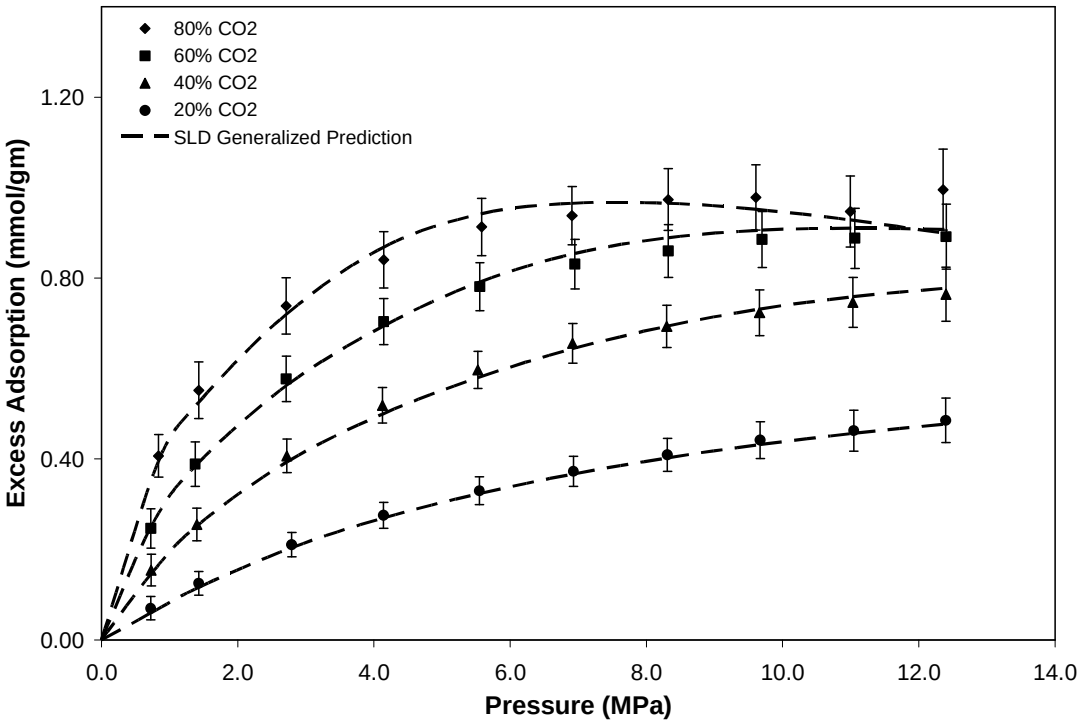

Figure 6.22 Generalized SLD-PR Model Predictions for CO_2 Component Adsorption in Nitrogen/CO_2 Mixtures on Wet Fruitland Coal at 319.3 K

Figures 6.23-6.28 present the generalized prediction results obtained for the mixed-gas adsorption on wet Illinois #6 coal. As shown in Figure 6.24, the nitrogen component adsorption was over-predicted for the methane/nitrogen mixture. Similarly, the methane component adsorption was over-predicted for 80% and 60% methane feed compositions of the methane/CO_2 mixture (Figure 6.25). However, the overall WAAD of all the feed compositions for the three binary mixtures on wet Illinois #6 coal were within the experimental uncertainties.

Figures 6.27 and 6.28 present the generalized prediction results for nitrogen/CO_2 adsorption on wet Illinois #6 coal. The overall WAAD for both nitrogen and CO_2 component adsorption were found to be within the experimental uncertainties.

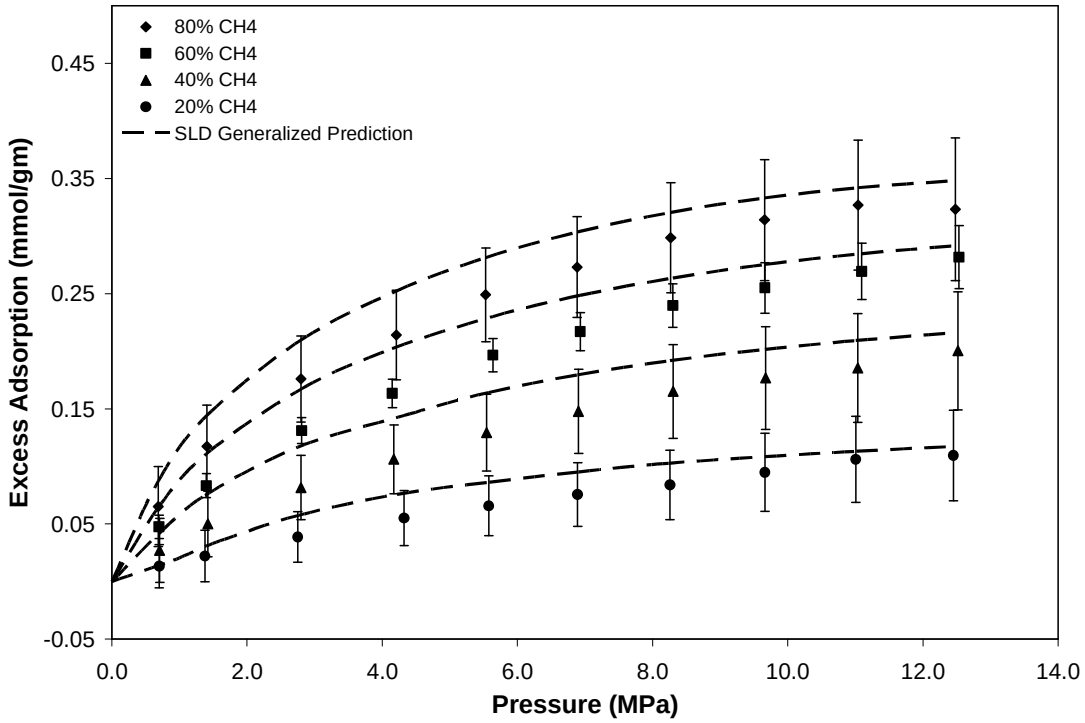

Figure 6.23 Generalized SLD-PR Model Predictions for Methane Component Adsorption in Methane/ Nitrogen Mixtures on Wet Illinois #6 Coal at 319.3 K

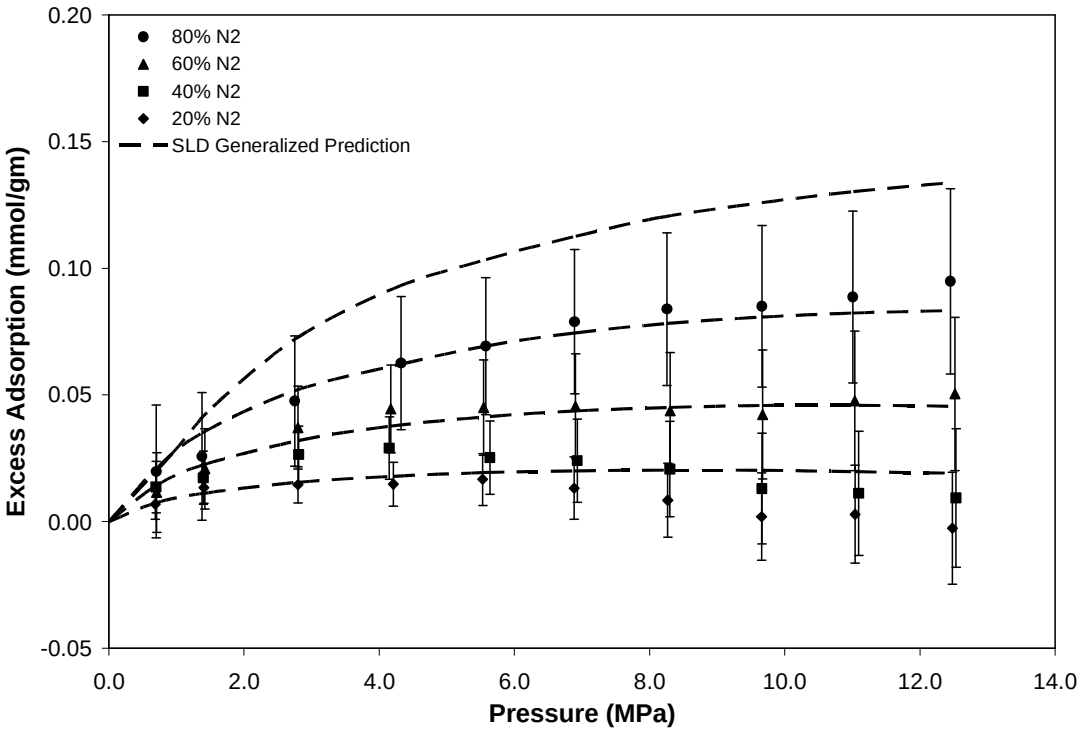

Figure 6.24 Generalized SLD-PR Model Predictions for Nitrogen Component Adsorption in Methane/ Nitrogen Mixtures on Wet Illinois #6 Coal at 319.3 K

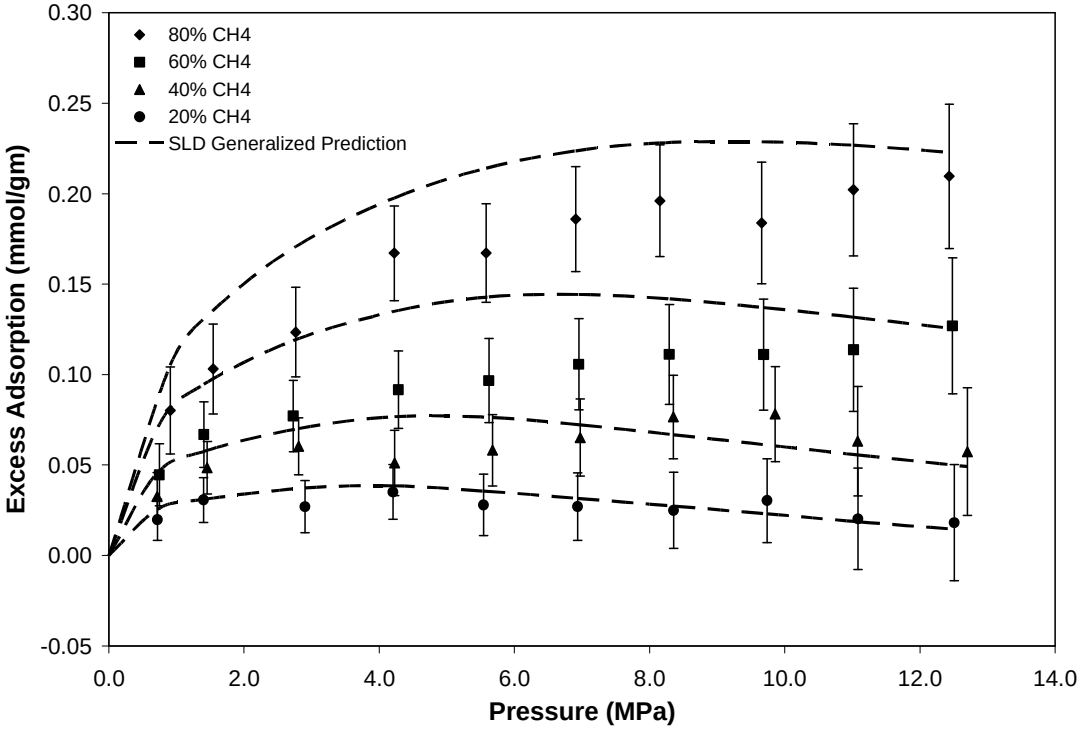

Figure 6.25 Generalized SLD-PR Model Predictions for Methane Component Adsorption in Methane/CO_2 Mixtures on Wet Illinois #6 Coal at 319.3 K

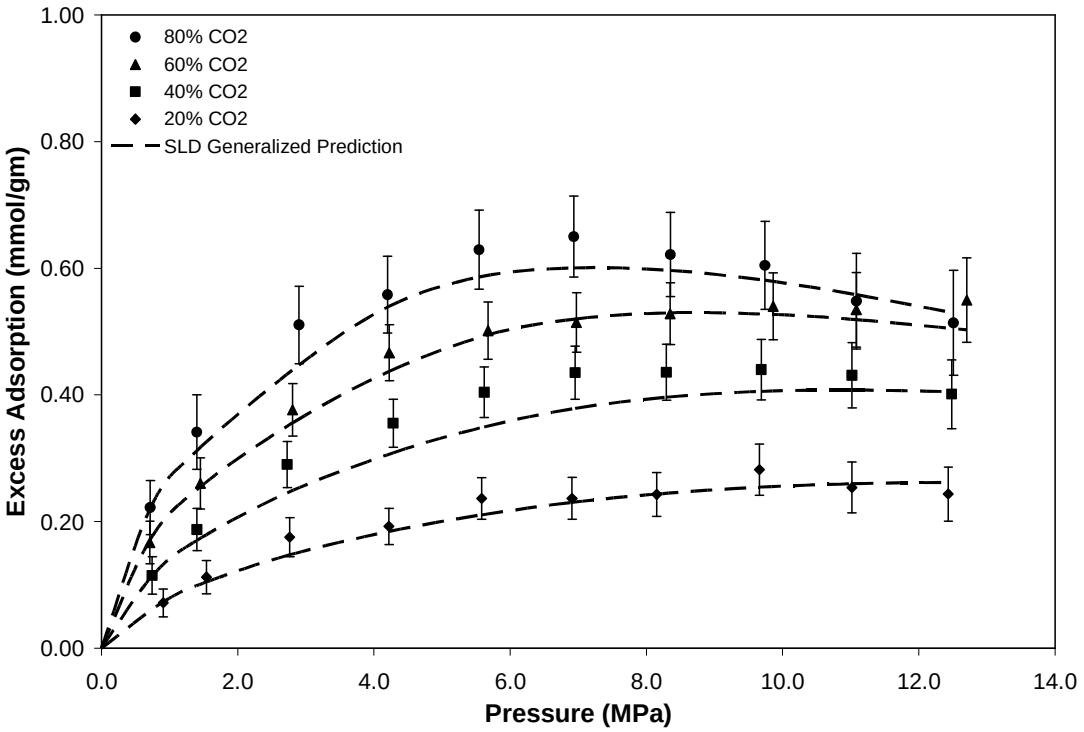

Figure 6.26 Generalized SLD-PR Model Predictions for CO_2 Component Adsorption in Methane/CO_2 Mixtures on Wet Illinois #6 Coal at 319.3 K

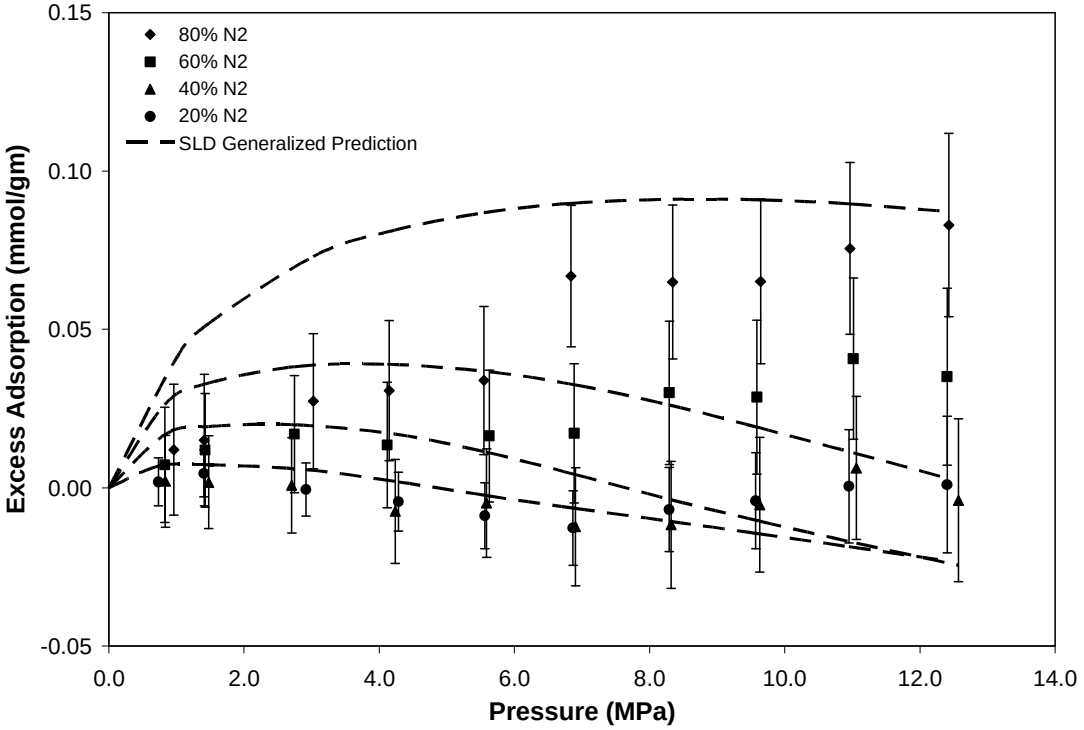

Figure 6.27 Generalized SLD-PR Model Predictions for Nitrogen Component Adsorption in Nitrogen/CO_2 Mixtures on Wet Illinois #6 Coal at 319.3 K

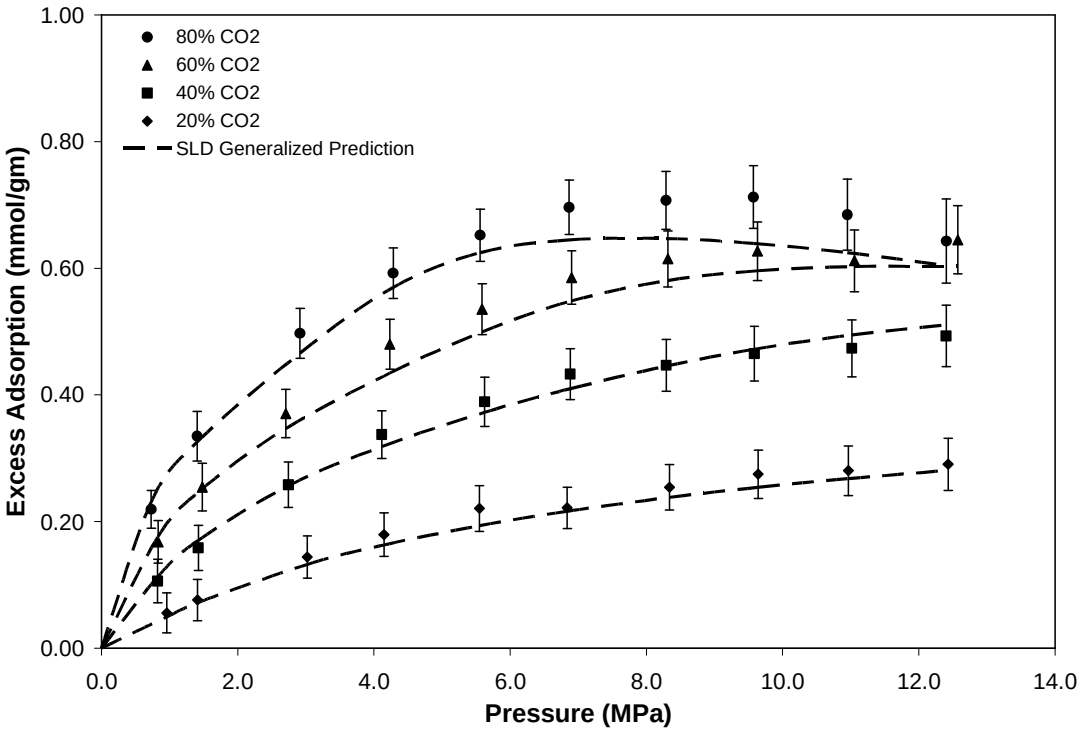

Figure 6.28 Generalized SLD-PR Model Predictions for CO_2 Component Adsorption in Nitrogen/CO_2 Mixtures on Wet Illinois #6 Coal at 319.3 K

Figures 6.29-6.31 present the prediction results for methane/nitrogen, methane/CO_2 and nitrogen/CO_2 binary gas mixtures on wet Tiffany coal, respectively. The methane component adsorption was considerably under-predicted beyond 4 MPa. In fact, the methane adsorption predictions for wet Tiffany coal provided the least satisfactory fit in mixed-gas generalized predictions. As documented in Table 6.10, the methane predictions in methane/nitrogen and methane/CO_2 binary mixtures of wet Tiffany coal yielded WAADs of 2.87 and 3.92, respectively. Fitzgerald[25] also obtained similar results in non-generalized predictions of these systems. In comparison, the second component in the above mixtures was reasonably well predicted. Further, the nitrogen/CO_2 binary mixture on the same coal was predicted within two times the experimental uncertainties.

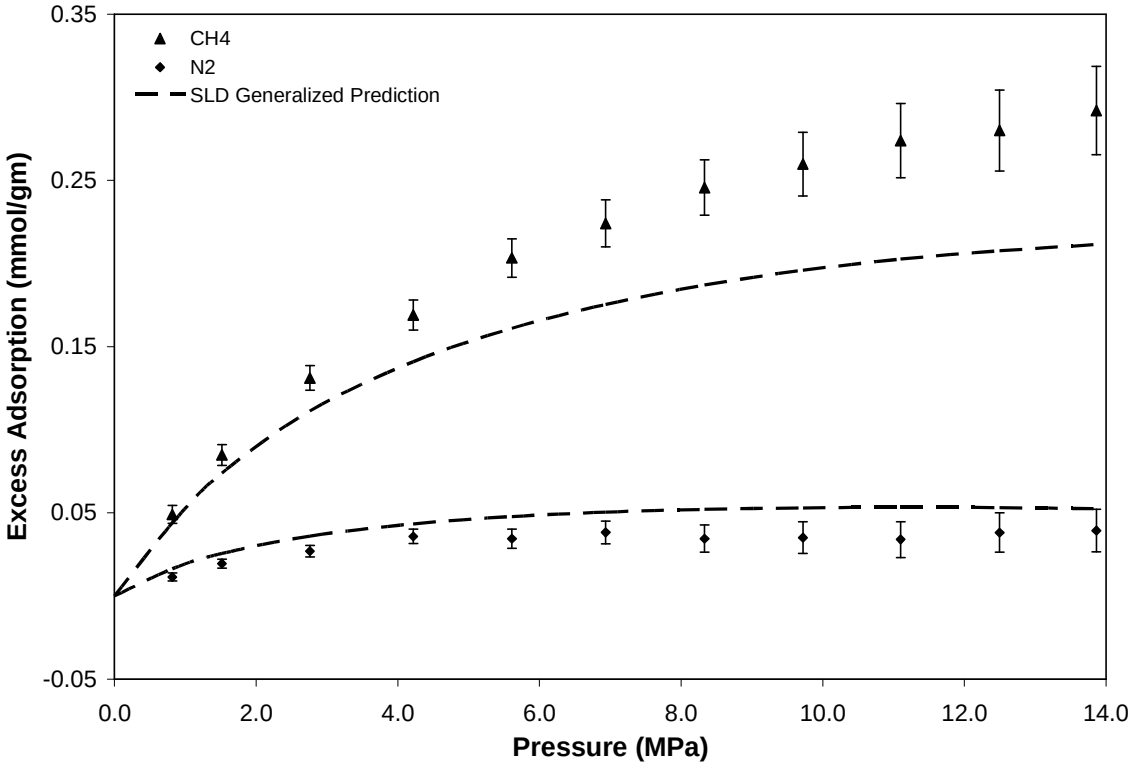

Figure 6.29 Generalized SLD-PR Model Predictions for Methane/Nitrogen Mixture on Wet Tiffany Coal at 327.6 K

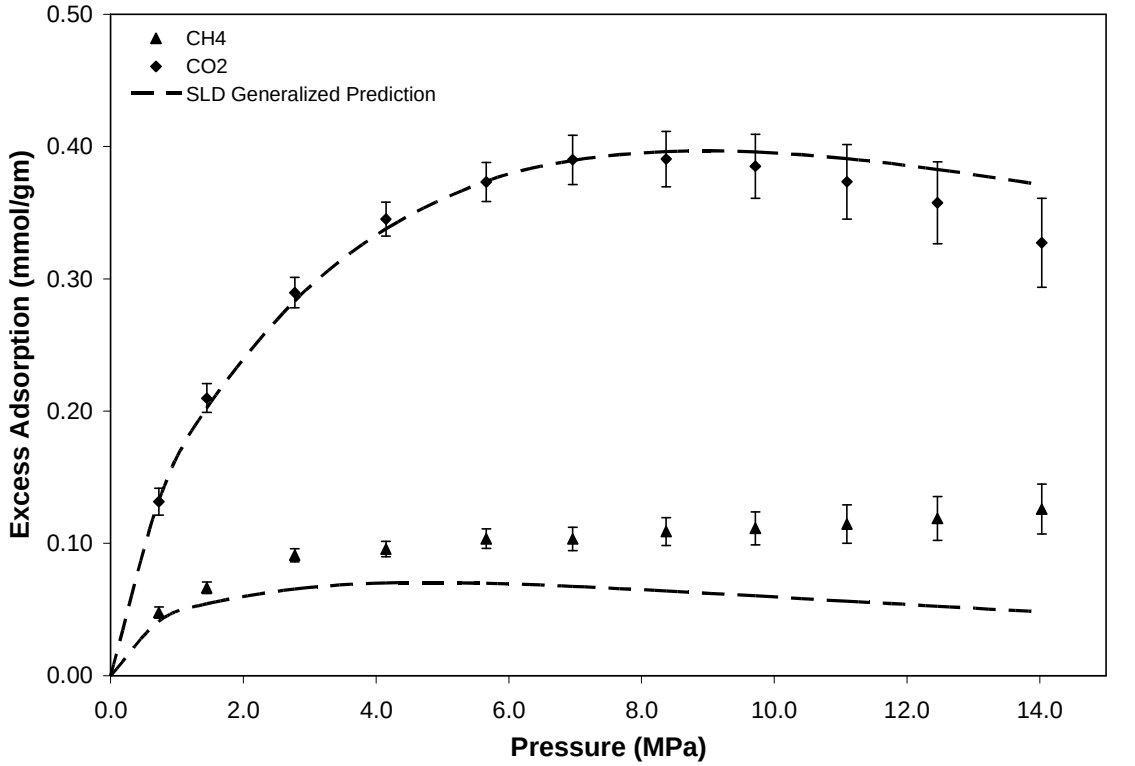

Figure 6.30 Generalized SLD-PR Model Predictions for Methane/CO_2 Mixture on Wet Tiffany Coal at 327.6 K

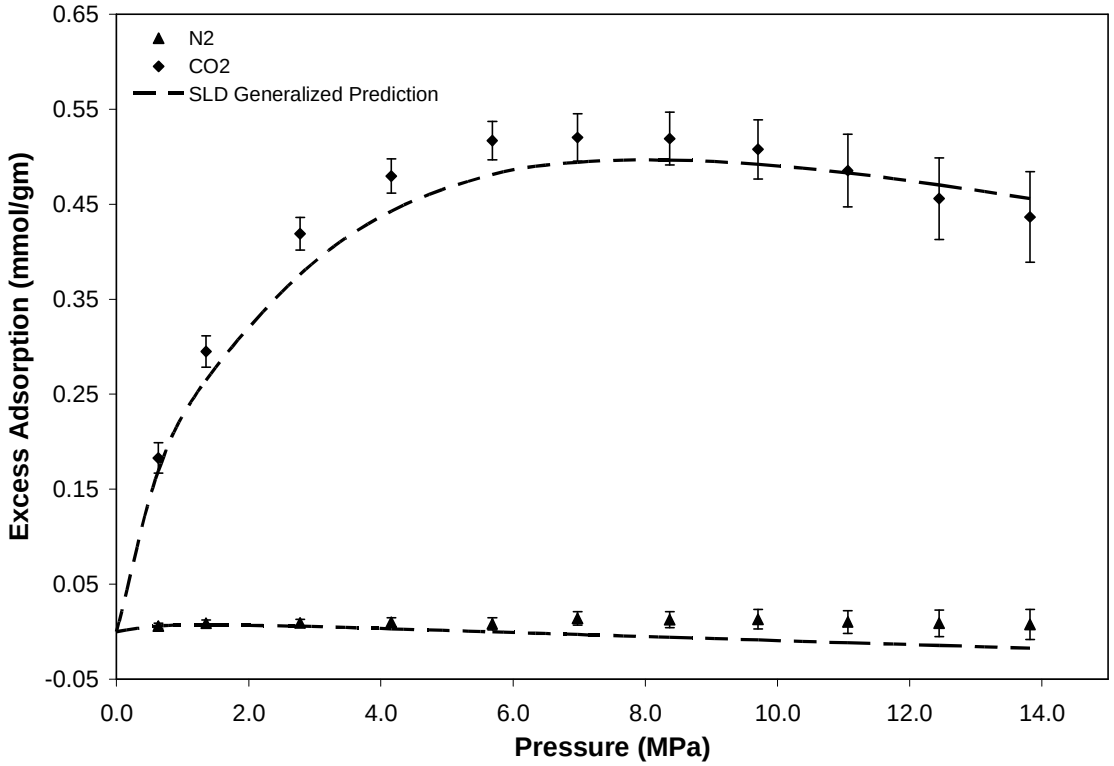

Figure 6.31 Generalized SLD-PR Model Predictions for Nitrogen/CO_2 Mixture on Wet Tiffany Coal at 327.6 K

Figure 6.32 presents the generalized prediction results for ternary gas adsorption on wet Tiffany coal. The feed gas composition was 10/40/50 for $CH_4/N_2/CO_2$ mixture. The model under-predicted the component adsorption of nitrogen at moderate to higher pressures. The WAAD for nitrogen adsorption prediction for the ternary mixture was 2.31 (Table 6.10). In contrast, the predictions for methane and CO_2 component adsorption for the ternary gas adsorption were within the experimental uncertainties, as documented in Table 6.10.

Figure 6.33 presents the deviation plot of mixed-gas adsorption generalized predictions. Overall, about 93% of the adsorption data was predicted within two times the experimental uncertainties.

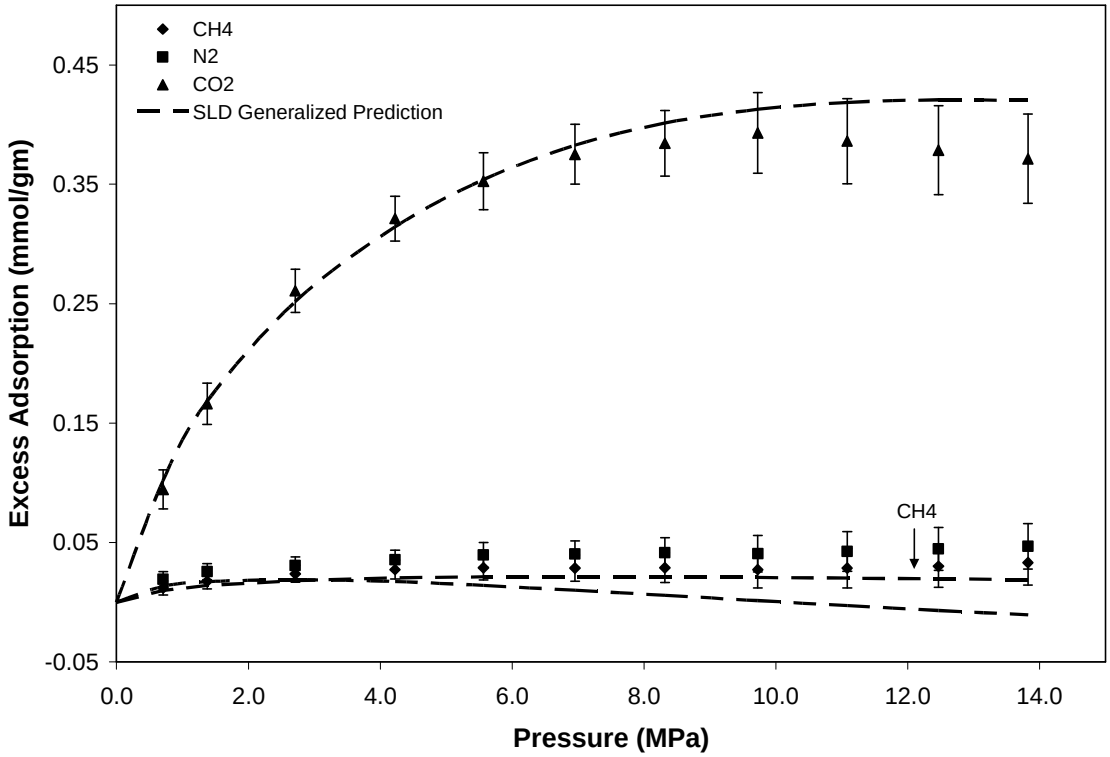

Figure 6.32 Generalized SLD-PR Model Predictions for Methane/Nitrogen/CO_2 Ternary Mixture on Wet Tiffany Coal at 327.6 K

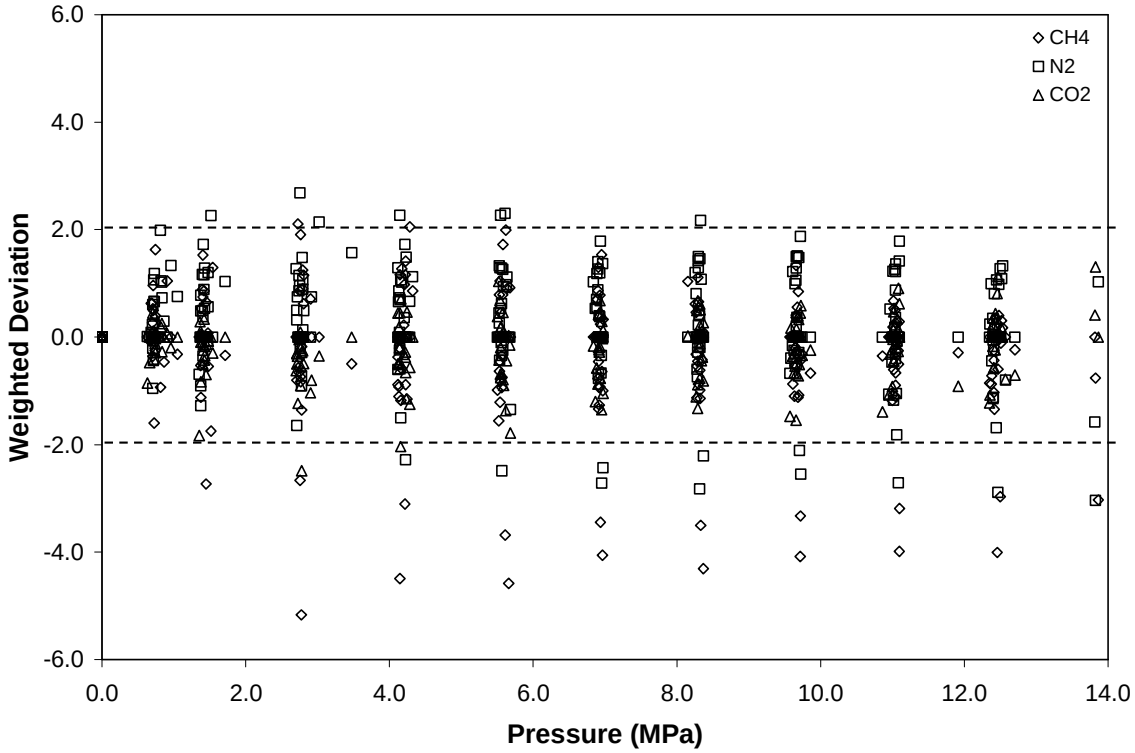

Figure 6.33 Deviation Plot for the Generalized SLD-PR Model Predictions for Mixed-Gas Adsorption on Coals

The results above for mixed-gas adsorption demonstrate that the generalized SLD-PR model is capable of *a priori* predictions of binary and ternary gas adsorption within three times the experimental uncertainties, on average.

6.9 Validation of the SLD-PR Generalized Model

The generalized SLD-PR model was further validated using an external data set involving CO_2 adsorption on twenty-seven diverse coals, published recently by Day et al.[71] They presented CO_2 adsorption data on coals varying in rank from lignite to low-volatile bituminous coal. The origin of these coals varied from Australia, New Zealand, Poland and USA.

The generalized SLD-PR model was utilized to predict *a priori* the CO_2 adsorption data on twenty-seven coals utilizing only the coal characterization information of these coals. The predictions obtained have been listed in Table 6.11 in terms of %AAD of each coal.

Table 6.11 Validation Results for the Generalized SLD-PR Model Predictions: CO_2 Adsorption on 27 Coals Reported by Day et al.[71]

Coals	%AAD	Coals	%AAD
NSW1	4.5	QLD8	7.4
NSW3	7.2	QLD9	13.2
NSW4	7.6	QLD10	3.3
NSW5	16.1	QLD11	6.3
NSW6	19.7	NZ	20.3
NSW7	18.8	Poland1	5.8
NSW8	14.1	Poland2	7.8
NSW9	22.3	USA1	11.5
NSW10	11.1	USA2	19.5
QLD1	20.8	USA3	9.7
QLD2	10.5	Beulah Zap	11.9
QLD3	6.3	Illinois-6	9.0
QLD6	14.9	Pocahontas	3.9
QLD7	11.9		
Average			**11.7**

As evident from Table 6.11, the generalized SLD-PR model was capable of predicting CO_2 adsorption on these diverse coals with an overall error of about 12% AAD. This is within the claimed accuracy of the model; estimated to be about 24%, on average.

Figure 6.34 presents the deviation plot for the model predictions on these coals. Overall, about 85% of the adsorption data was predicted within %AAD of 20%. Moreover, the error distribution appears to be fairly uniform about the center line in Figure 6.34.

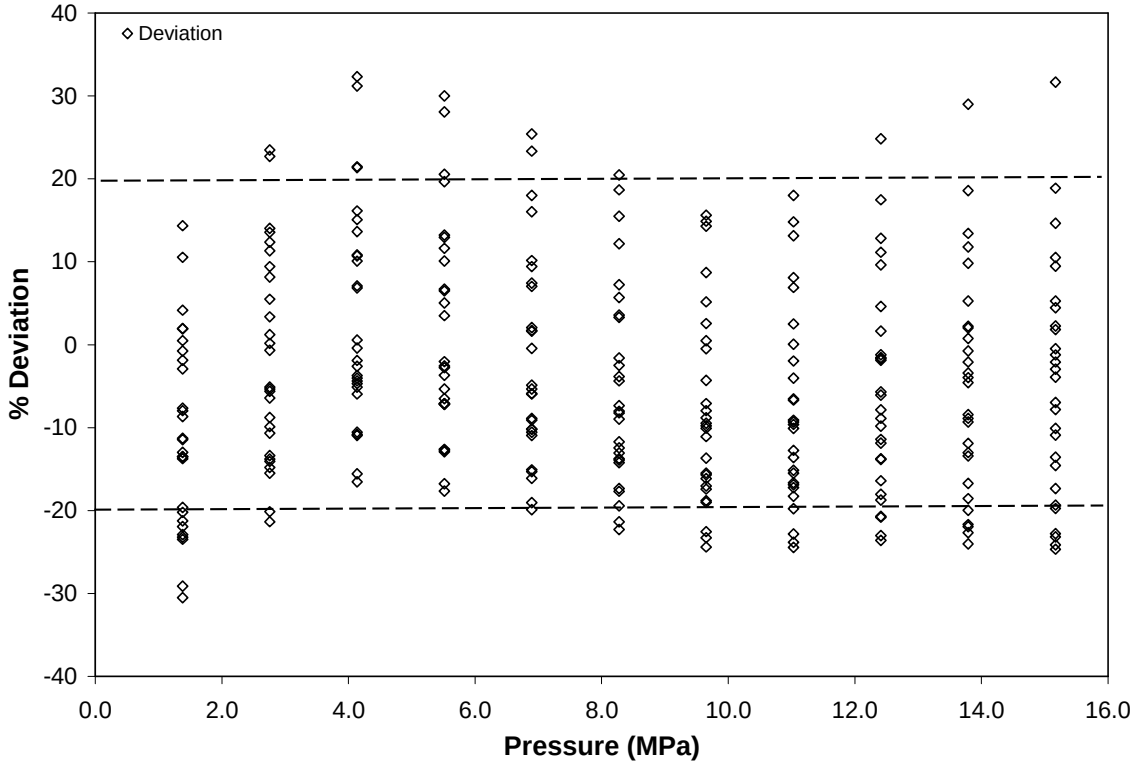

Figure 6.34 Deviation Plot for the Generalized SLD-PR Model Predictions for CO_2 Adsorption on 27 Coals Reported by Day et al.[71]

Figure 6.35 presents a "pie chart" depicting the distribution of errors in the prediction among the twenty-seven coals. Out of the twenty-seven coals, the predictions for twelve coals yielded %AAD of less than 10%. Further, twenty-four coals yielded

%AAD within 20%, whereas %AAD of more than 20% was observed for only three coals.

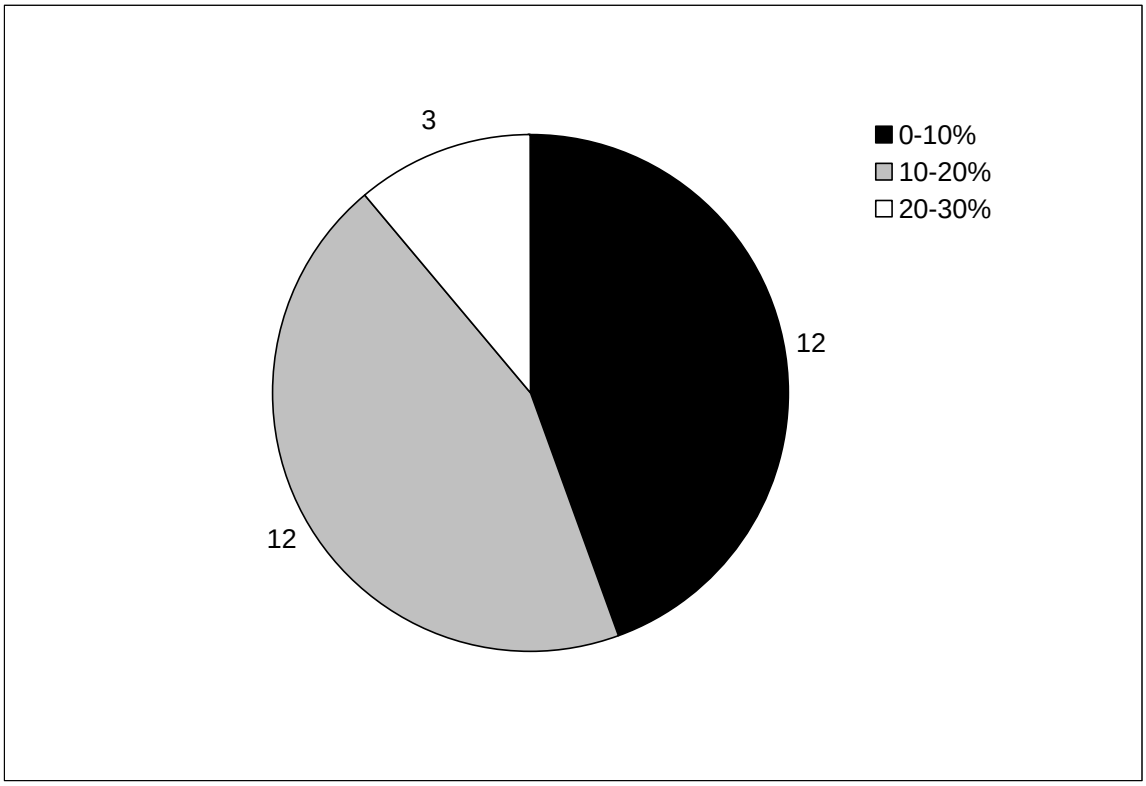

Figure 6.35 %AAD Distribution of the Generalized SLD-PR Model Predictions for CO_2 Adsorption Data Reported by Day et al.[71]

These results strongly indicate that the generalized SLD-PR model can predict reliably the gas adsorption on coals for CBM systems based solely on readily-available coal characterization information. Therefore, the SLD-PR model generalization appears to be sufficiently robust for simulations of enhanced coalbed methane recovery and CO_2 sequestration.

Notwithstanding these results, additional work will be required to account more rigorously for the presence of water on coals and develop even more realistic generalized models for CBM adsorption modeling.

6.10 Generalization Conclusions

Based on the results discussed above, the following important conclusions can be drawn from this chapter:

1. The coal-structure-based generalization of the SLD-PR model is capable of useful *a priori* predictions of gas adsorption on dry and wet coals.
2. The generalized SLD-PR model can predict the adsorption of pure methane, nitrogen and CO_2 within three times the experimental uncertainties.
3. The generalized SLD-PR model can predict, *a priori*, the mixed-gas adsorption of methane, nitrogen and CO_2 within three times the experimental uncertainties, on average.
4. The successful validation of the generalized model indicates that the model is sufficiently robust for use in simulations of enhanced CBM production and CO_2 sequestration.

CHAPTER 7

CONCLUSIONS AND RECOMMENDATIONS

This work addressed two important aspects of CBM adsorption research. Specifically, it sought to:

A. Delineate the fluid-fluid and fluid-solid molecular interactions of water, coalbed gases and carbonaceous adsorbents and propose rigorous accounting procedures for the effects of moisture in water-coalbed gas mixture adsorption on wet coals.

B. Develop a coal-structure-based generalized adsorption model that would be useful in simulations of coalbed methane recovery and CO_2 sequestration.

To meet the objectives of the study, the SLD-PR model was first modified to account for the polar and electrostatic interactions of water in the adsorbed phase. Then, new CO_2-water mixture adsorption data on wet Argonne coals were used to test the efficacy of the modified SLD-PR model to describe the adsorption behavior of this mixture. Finally, a coal-structure-based generalized adsorption model was developed that can facilitate accurate *a priori* gas adsorption predictions that are often necessary in CBM recovery and CO_2 sequestration operations.

Specific conclusions and recommendations based on this work are listed below.

7.1 Conclusions

A. Effects of Water in Coals on CO_2 Adsorption

(1) Review of water adsorption on carbons and coals showed that the adsorption of water occurs mainly through the formation of (a) hydrogen bonds between water

and active surface groups on the carbon surface, and (b) molecular clusters near previously adsorbed water molecules.

(2) The polar and electrostatic interactions of water play a significant role in the adsorption of water on activated carbons and coals.

(3) The SLD-PR model, when modified with the polar and electrostatic interactions of water, appears capable of describing the simultaneous adsorption of water and CO_2 mixture on wet Argonne coals.

(4) The SLD-PR model *represents* the CO_2-water mixture adsorption on five wet Argonne coals with a weighted average absolute deviation (WAAD) of 0.5 and 1.0 for CO_2 and water, respectively.

(5) The new data reduction method showed that substantial differences in the estimated gas adsorption capacity of wet coals can result if the conventional approach of treating water as a "pacifier" of the coal matrix is used in the data reduction of coals with large amounts of moisture.

B. Coal-Characterization-Based SLD-PR Generalized Model

(6) The coal-characterization-based generalization of SLD-PR model is capable of accurate *a priori* predictions of gas adsorption on dry and wet coals.

(7) The generalized SLD-PR model can *predict* adsorption of pure methane, nitrogen and CO_2 on nine coals within three times the expected experimental uncertainties.

(8) The generalized model can predict, *a priori*, the adsorption of mixtures formed by methane, nitrogen and CO_2 within three times the expected experimental

uncertainties, on average. The only exception to this occurred for gas mixtures on wet Tiffany coal.

(9) The generalized model was validated with a set of external data on CO_2 adsorption on 27 diverse coals. The model appears capable of predicting these adsorption data with an average absolute deviation (%AAD) of 12%, on average. These predictions were based solely on available coal characterization information of these coals.

(10) The phase analysis of CO_2-water mixture adsorption on wet Argonne coals using the SLD-PR model indicates the potential for an aqueous phase formation when dealing with coals that contain large amounts of moisture (with the exception of Beulah Zap lignite).

7.2 Recommendations

Based on the results of this work, the following recommendations are made for future studies:

(1) Develop an accurate equation-of-state (EOS) that is capable of reliable predictions of vapor-liquid equilibria of coalbed gases (including water) at conditions encountered in coalbed methane recovery and CO_2 sequestration operations.

(2) Utilize a density-measuring apparatus to obtain precise measurements of gas-phase densities of mixtures of coalbed gases and water to facilitate the development of the EOS.

(3) Develop a robust adsorption algorithm to perform three-phase equilibrium calculations.

(4) Utilize spectroscopic techniques such as the X-ray diffraction and small angle neutron-scattering experiments to investigate the growth and size of clusters of water molecules in water adsorption on carbons and coals.

(5) Implement the new data reduction method for gas adsorption on wet coals wherein the adsorbed water is excluded from gas solubility calculations and the presence of water in the gas phase is accurately accounted.

REFERENCES

1. Energy Information Administration, Annual Energy Outlook Early Release Overview, http://www.eia.doe.gov/oiaf/aeo/overview.html (March 9, 2009).

2. Clayton, J. L., Geochemistry of Coalbed Gas – A Review. *Int. J. Coal Geol.* **1998,** 35, 159-173.

3. Stevens, S.; Spector, D.; Reimer, P., Enhanced Coalbed Methane Recovery Using CO_2 Injection: Worldwide Resource and CO_2 Sequestration Potential. In *Sixth International Oil and Gas Conference and Exhibition, SPE 48881*, China, 1998; Vol. 1.

4. Energy Information Administration, U.S. Coalbed Methane: Past, Present and Future. http://www.eia.doe.gov/oil_gas/rpd/cbmusa2.pdf (April, 2008).

5. White, C. M.; Smith, D. H.; Jones, K. L.; Goodman, A. L.; Jikich, S. A.; LaCount, R. B.; DuBose, S. B.; Ozdemir, E.; Morsi, B. I.; Schroeder, K. T., Sequestration of Carbon Dioxide in Coal with Enhanced Coalbed Methane Recovery-A Review. *Energy Fuels* **2005,** 19, (3), 659-724.

6. Hall, F.; Zhou, C.; Gasem, K. A. M.; Robinson, R. L., Jr. , Adsorption of Pure Methane, Nitrogen, and Carbon Dioxide and Their Binary Mixtures on Wet Fruitland Coal. In *SPE Eastern Regional Conference & Exhibition, SPE Paper 29194*, Charleston, S.C., 1994.

7. Sudibandriyo, M.; Pan, Z.; Fitzgerald, J. E.; Robinson, R. L.; Gasem, K. A. M., Adsorption of Methane, Nitrogen, Carbon Dioxide, and Their Binary Mixtures on Dry Activated Carbon at 318.2 K and Pressures up to 13.6 MPa. *Langmuir* **2003,** 19, (13), 5323-5331.

8. Gasem, K. A. M.; Robinson, R. L., Jr.; Fitzgerald, J. E.; Pan, Z.; Sudibandriyo, M. *Sequestering Carbon Dioxide in Coalbeds*; DE-FC26-98FT40426; Prepared for the U.S. Department of Energy: 2003.

9. Pan, Z.; Sudibandriyo, M.; Fitzgerald, J. E.; Robinson, R. L., Jr.; Gasem, K. A. M., Equilibrium Models for Coalbed Methane Production and Carbon Dioxide Sequestration. In *International Petroleum Environmental Consortium (IPEC) Conference*, Albuquerque, NM, 2002.

10. Fitzgerald, J. E.; Pan, Z.; Sudibandriyo, M.; Robinson, R. L., Jr.; Gasem, K. A. M.; Reeves, S., Adsorption of Methane, Nitrogen, Carbon Dioxide and Their Mixtures on Wet Tiffany Coal. *Fuel* **2005,** 84, (18), 2351-2363.

11. Fitzgerald, J. E.; Robinson, R. L.; Gasem, K. A. M., Modeling High-Pressure Adsorption of Gas Mixtures on Activated Carbon and Coal Using a Simplified Local-Density Model. *Langmuir* **2006,** 22, (23), 9610-9618.

12. Gasem, K. A. M.; Robinson, R. L., Jr.; Mohammad, S. A.; Chen, J. S.; Fitzgerald, J. E. *Improved Adsorption Models for Coalbed Methane Production and CO_2 Sequestration*;

Final Technical Report, 2005-2007; Prepared for Advanced Resources International: 2008.

13. Langmuir, I., The Adsorption of Gases on Plane Surfaces of Glass, Mica and Platinum. *J. Am. Chem. Soc.* **1918,** 40, (9), 1361-1403.
14. Brunauer, S.; Emmett, P. H.; Teller, E., Adsorption of Gases in Multimolecular Layers. *J. Am. Chem. Soc.* **1938,** 60, (2), 309-319.
15. Myers, A. L.; Prausnitz, J. M., Thermodynamics of Mixed-Gas Adsorption. *AIChE J.* **1965,** 11, (1), 121-127.
16. DeGance, A. E., Multicomponent High-Pressure Adsorption Equilibria on Carbon Substrates: Theory and Data. *Fluid Phase Equilibria* **1992,** 78, 99.
17. Zhou, C.; Hall, F.; Gasem, K. A. M.; Robinson, R. L., Jr., Predicting Gas Adsorption Using Two-Dimensional Equations of State. *Ind. Eng. Chem. Res.* **1994,** 33, (5), 1280-1289.
18. Pan, Z. Modeling of Gas Adsorption Using Two Dimensional Equations of State. Ph.D. Dissertation, Oklahoma State University, Stillwater, 2004.
19. Ono, S.; Kondo, S., *Molecular Theory of Surface Tension*. Springer: Berlin, 1960.
20. Sudibandriyo, M. A Generalized Ono-Kondo Lattice Model for High Pressure Adsorption of Gases on Carbon Adsorbents. Ph.D. Dissertation, Oklahoma State University, 2003.
21. Arumugam, A. High-Pressure Adsorption of Pure Coalbed Methane Gases on Dry Coals. M.S. Thesis, Oklahoma State University, Stillwater, 2004.
22. Rangarajan, B.; Lira, C. T.; Subramanian, R., Simplified Local Density Model for Adsorption over Large Pressure Ranges. *AIChE Journal* **1995,** 41, (4), 838-845.
23. Soule, A. D.; Smith, C. A.; Yang, X.; Lira, C. T., Adsorption Modeling with the ESD Equation of State. *Langmuir* **2001,** 17, (10), 2950-2957.
24. Puziy, A. M.; Herbst, A.; Poddubnaya, O. I.; Germanus, J.; Harting, P., Modeling of High-Pressure Adsorption Using the Bender Equation of State. *Langmuir* **2003,** 19, (2), 314-320.
25. Fitzgerald, J. E. Adsorption of Pure and Multi-Component Gases of Importance to Enhanced Coalbed Methane Recovery: Measurements and Simplified Local-Density Modeling. Ph.D. Dissertation, Oklahoma State University, Stillwater, Oklahoma 2005.
26. Yang, X.; Lira, C. T., Theoretical Study of Adsorption on Activated Carbon from a Supercritical Fluid by the SLD-ESD Approach. *Journal of Supercritical Fluids* **2006,** 37, (2), 191-200.
27. Chen, J. S. Simplified Local-Density Modeling of Pure and Multi-Component Gas Adsorption. M.S. Thesis, Oklahoma State University, Stillwater, 2007.
28. Muller, E. A.; Hung, F. R.; Gubbins, K. E., Adsorption of Water Vapor-Methane Mixtures on Activated Carbons. *Langmuir* **2000,** 16, (12), 5418-5424.

29. Joubert, J. I.; Grein, C. T.; Bienstock, D., Sorption of Methane in Moist Coal. *Fuel* **1973,** 52, (3), 181-185.

30. Clarkson, C. R.; Bustin, R. M., Binary Gas Adsorption/Desorption Isotherms: Effect of Moisture and Coal Composition Upon Carbon Dioxide Selectivity over Methane. *Int. J. Coal Geol.* **2000,** 42, (4), 241-271.

31. Levy, J. H.; Day, S. J.; Killingley, J. S., Methane Capacities of Bowen Basin Coals Related to Coal Properties. *Fuel* **1997,** 9, (76), 813-819.

32. McCallum, C. L.; Bandosz, T. J.; McGrother, S. C.; Muller, E. A.; Gubbins, K. E., A Molecular Model for Adsorption of Water on Activated Carbon: Comparison of Simulation and Experiment. *Langmuir* **1999,** 15, (2), 533-544.

33. Fitzgerald, J. E.; Sudibandriyo, M.; Pan, Z.; Robinson, R. L.; Gasem, K. A. M., Modeling the Adsorption of Pure Gases on Coals with the SLD Model. *Carbon* **2003,** 41, (12), 2203-2216.

34. Hall, F. E. Adsorption of Pure and Multicomponent Gases on Wet Fruitland Coal. M.S. Thesis, Oklahoma State University, Stillwater, 1993.

35. Angus, S.; Armstrong, B.; de Reuck, K. M., *International Thermodynamic Tables of the Fluid State-5: Methane*. Pergamon Press: New York 1978.

36. Angus, S.; de Reuck, K. M.; Armstrong, B., *International Thermodynamic Tables of the Fluid State-6: Nitrogen*. Pergamon Press: New York, 1979.

37. Span, R.; Wagner, W., A New Equation of State for Carbon Dioxide Covering the Fluid Region from the Triple Point Temperature to 1100 K at Pressures up to 800 MPa. *J. Phys. Chem. Ref. Data* **1996,** 25, 1509-1590.

38. McCarty, R. D. *Thermophysical Properties of Helium-4 from 2 to 1500 K with Pressures to 1000 Atmospheres*; NBS Technical Note 631; U.S. Dept of Commerce 1972.

39. Vorres, K. S., The Argonne Premium Coal Sample Program. *Energy Fuels* **1990,** 4, (5), 420-426.

40. Humayun, R.; Tomasko, D., High-Resolution Adsorption Isotherms of Supercritical Carbon Dioxide on Activated Carbon. *AIChE J.* **2000,** 46, (10), 2065-2075.

41. Standard Test Method for Equilibrium Moisture of Coal at 96 to 97 Percent Relative Humidity and 30 C. In Gaseous Fuels; Coal and Coke, ASTM, Ed. Pennsylvania, 2000; D1412, pp 99-102.

42. Joubert, J. I.; Grein, C. T.; Bienstock, D., Effect of Moisture on the Methane Capacity of American Coals. *Fuel* **1974,** 53, (3), 186-191.

43. King, A. D. J.; Coan, C. R., Solubility of Water in Compressed Carbon Dioxide, Nitrous Oxide and Ethane. Evidence for Hydration of Carbon Dioxide and Nitrous Oxide in the Gas Phase. *J. Am. Chem. Soc.* **1971,** 93, (8), 1857-1862.

44. Dhima, A.; de Hemptinne, J.; Jose, J., Solubility of Hydrocarbons and CO_2 Mixtures in Water under High Pressure. *Ind. & Eng. Chem. Res.* **1999,** 38, (8), 3144-3161.

45. Weibe, R.; Gaddy, V., The Solubility of Carbon Dioxide in Water at Various Temperatures from 12° to 40° and at Pressures to 500 Atmospheres, Critical Phenomena. *J. Amer. Chem. Soc.* **1940,** 62 815-817.

46. Ozdemir, E.; Morsi, B. I.; Schroeder, K., Importance of Volume Effects to Adsorption Isotherms of Carbon Dioxide on Coals. *Langmuir* **2003,** 19, (23), 9764-9773.

47. Dutta, P.; Harpalani, S.; Prusty, B., Modeling of CO_2 Sorption on Coal. *Fuel* **2008,** 87, (10-11), 2023-2036.

48. Romanov, V.; Soong, Y.; Schroeder, K., Volumetric Effects in Coal Sorption Capacity Measurements. *Chemical Engineering & Technology* **2006,** 29, (3), 368-374.

49. Pan, Z.; Connell, L. D., A Theoretical Model for Gas Adsorption-Induced Coal Swelling. *Int. J. Coal Geol.* **2007,** 69, (4), 243-252.

50. Day, S.; Fry, R.; Sakurovs, R., Swelling of Australian Coals in Supercritical CO_2. *Int. J. Coal Geol.* **2008,** 74, (1), 41-52.

51. Arri, L. E.; Yee, D. In *Modeling Coalbed Methane Production with Binary Gas Sorption, SPE Paper 24363*, SPE Rocky Mountain regional meeting, Casper, WY, 1992; Casper, WY, 1992.

52. Goodman, A. L.; Busch, A.; Bustin, R. M.; Chikatamarla, L.; Day, S.; Duffy, G. J.; Fitzgerald, J. E.; Gasem, K. A. M.; Gensterblum, Y.; Hartman, C.; Jing, C.; Krooss, B. M.; Mohammed, S.; Pratt, T.; Robinson Jr, R. L.; Romanov, V.; Sakurovs, R.; Schroeder, K.; White, C. M., Inter-Laboratory Comparison II: CO_2 Isotherms Measured on Moisture-Equilibrated Argonne Premium Coals at 55 C and up to 15 MPa. *International Journal of Coal Geology* **2007,** 72, (3-4), 153-164.

53. Zhou, L.; Li, M.; Sun, Y.; Zhou, Y., Effect of Moisture in Microporous Activated Carbon on the Adsorption of Methane. *Carbon* **2001,** 39, (5), 773-776.

54. Yaginuma, R.; Sato, Y.; Kodama, D.; Tanaka, H.; Kato, M., Saturated Densities of Carbon Dioxide+Water Mixture at 304.1 K and Pressures to 10 MPa. *Journal of the Japan Institute of Energy* **2000,** 79, (2), 144-146.

55. Morrison, D. F., *Multivariate Statistical Methods*. McGraw Hill: New York 1967.

56. Markham, E. D.; Benton, A. F., The Adsorption of Gas Mixtures by Silica. *J. Am. Chem. Soc.* **1931,** 53, 497.

57. Stevenson, M. D.; Pinczewski, W. V.; Somers, M. L.; Bagio, S. E., Adsorption/Desorption of Multicomponent Gas Mixtures at in-Seam Conditions. In *SPE Asia-Pacific conference, SPE paper 23026*, Perth, Australia, 1991.

58. Dubinin, M. M., *Chemistry and Physics of Carbon*. Marcel Dekker: New York, 1966; Vol. 2.

59. Clarkson, C. R., Application of a New Multicomponent Gas Adsorption Model to Coal Gas Adsorption Systems, SPE Paper 78146. *SPE Journal* **2003,** 8, (3), 236-251.

60. Clarkson, C. R.; Bustin, R. M.; Levy, J. H., Application of the Mono/Multilayer and Adsorption Potential Theories to Coal Methane Adsorption Isotherms at Elevated Temperature and Pressure. *Carbon* **1997,** 35, (12), 1689-1705.

61. Do, D. D., *Adsorption Analysis: Equilibria and Kinetics*. Imperial College Press: London, 1998.

62. Chaback, J. J.; Morgan, D.; Yee, D., Sorption Irreversibilities and Mixture Compositional Behavior During Enhanced Coal Bed Methane Recovery Processes. In *SPE Gas Technology Symposium, Paper 35622*, 1996.

63. Yang, R. T., *Gas Separation by Adsorption Processes*. Butterworth: Boston, 1987.

64. Valenzuela, D. P.; Myers, A. L.; Talu, O.; Zwiebel, I., Adsorption of Gas Mixtures: Effect of Energetic Heterogeneity. *AIChE J.* **1988,** 34, 397-402.

65. Manik, J., Development and Validation of a Compositional Coalbed Simulator. *Journal of Canadian Petroleum Technology* **2002,** 41, (4), 39-45.

66. Dubinin, M. M., Chemistry and Physics of Carbon. In Walker, P. L., Ed. Marcel Dekker: New York, 1966; Vol. 2, pp 51-120.

67. Polanyi, M., Theories of the Adsorption of Gases: A General Survey and Some Additional Remarks. *Transactions of the Faraday Society* **1932,** 28, 316.

68. Dubinin, M. M.; Astakhov, V. A., Description of Adsorption Equilibria of Vapors on Zeolites over Wide Ranges of Temperature and Pressure. *Advances in Chemistry Series* **1971,** 102, 69-85.

69. Wood, G. O., Affinity Coefficients of the Polanyi/Dubinin Adsorption Isotherm Equations - A Review with Compilations and Correlations. *Carbon* **2001,** 39, 343-356.

70. Harpalani, S.; Prusty, B. K.; Dutta, P., Methane/CO_2 Sorption Modeling for Coalbed Methane Production and CO_2 Sequestration. *Energy Fuels* **2006,** 20, (4), 1591-1599.

71. Day, S.; Duffy, G.; Sakurovs, R.; Weir, S., Effect of Coal Properties on CO_2 Sorption Capacity under Supercritical Conditions. *International Journal of Greenhouse Gas Control* **2008,** 2, (3), 342-352.

72. Hill, T. L., Theory of Multimolecular Adsorption from a Mixture of Gases. *J. Chem. Phys.* **1946,** 14, 268.

73. de Boer, J. H., *The Dynamical Character of Adsorption*. Oxford University Press: London, 1953.

74. Hoory, S. E.; Prausnitz, J. M., Monolayer Adsorption of Gas Mixtures on Homogeneous and Heterogeneous Solids. *Chemical Engineering Science* **1967,** 22, (7), 1025-1033.

75. Aranovich, G. L.; Donohue, M. D., Adsorption of Supercritical Fluids. *Journal of Colloid and Interface Science* **1996,** 180, (2), 537-541.

76. Aranovich, G. L.; Donohue, M. D., Predictions of Multilayer Adsorption Using Lattice Theory. *Journal of Colloid and Interface Science* **1997,** 189, (1), 101-108.

77. Aranovich, G. L.; Donohue, M. D., Surface Compression in Adsorption Systems. *Colloids and Surfaces A: Physicochemical and Engineering Aspects* **2001,** 187-188, 95-108.

78. Hocker, T.; Aranovich, G. L.; Donohue, M. D., Monolayer Adsorption for the Subcritical Lattice Gas and Partially Miscible Binary Mixtures. *Journal of Colloid and Interface Science* **1999,** 211, (1), 61-80.

79. Henderson, D., *Fundamentals of Inhomogeneous Fluids*. Marcel Dekker Inc.: New York 1992.

80. Lee, L. L., *Molecular Thermodynamics of Non-Ideal Fluids*. Butterworths: Stoneham, 1988.

81. Chen, J. H.; Wong, D. S. H.; Tan, C. S.; Subramanian, R.; Lira, C. T.; Orth, M., Adsorption and Desorption of Carbon Dioxide onto and from Activated Carbon at High Pressures. *Ind. Eng. Chem. Res.* **1997,** 36, (7), 2808-2815.

82. Subramanian, R.; Pyada, H.; Lira, C. T., Engineering Model for Adsorption of Gases onto Flat Surfaces and Clustering in Supercritical Fluids. *Ind. Eng. Chem. Res.* **1995,** 34, (11), 3830.

83. Peng, D. Y.; Robinson, D. B., A New Two-Constant Equation of State. *Ind. Eng. Chem. Fund.* **1976,** 15, (1), 59-64.

84. Brennan, J. K.; Bandosz, T. J.; Thomson, K. T.; Gubbins, K. E., Water in Porous Carbons. *Colloids and Surfaces A: Physicochemical and Engineering Aspects* **2001,** 187-188, 539-568.

85. Dubinin, M. M., Water Vapor Adsorption and the Microporous Structures of Carbonaceous Adsorbents. *Carbon* **1980,** 18, (5), 355-364.

86. Brennan, J. K.; Thomson, K. T.; Gubbins, K. E., Adsorption of Water in Activated Carbons: Effects of Pore Blocking and Connectivity. *Langmuir* **2002,** 18, (14), 5438-5447.

87. Bandosz, T. J.; Jagiello, J.; Schwarz, J. A.; Krzyzanowski, A., Effect of Surface Chemistry on Sorption of Water and Methanol on Activated Carbons. *Langmuir* **1996,** 12, (26), 6480-6486.

88. IUPAC Commission on Colloid and Surface Chemistry, Reporting Physisorption Data for Gas/Solid Systems with Special Reference to the Determination of Surface Area and Porosity. Pure & Appl. Chem 1985, 57, (4), 603-619.

89. Olivier, J. P.; Conklin, W. B., Determination of Pore Size Distributions from Density Functional Theoretical Models of Adsorption and Condensation with Porous Solids. In *7th International Conference on Surface and Colloid Science*, France, 1991.

90. Hagymassy, J.; Brunauer, S.; Mikhail, R. S., Pore Structure Analysis by Water Vapor Adsorption : I. T-Curves for Water Vapor. *Journal of Colloid and Interface Science* **1969,** 29, (3), 485-491.

91. Do, D. D.; Do, H. D., A Model for Water Adsorption in Activated Carbon. *Carbon* **2000,** 38, (5), 767-773.

92. Mahajan, O. P.; Walker, P. L., Water Adsorption on Coals. *Fuel* **1971,** 50, (3), 308-317.

93. Youssef, A. M., Moisture Sorption in Relation to Some Characteristics of Coal. *Carbon* **1974,** 12, (4), 433-438.

94. Barton, S. S.; Evans, M. J. B.; Holland, J.; Koresh, J. E., Water and Cyclohexane Vapour Adsorption on Oxidized Porous Carbon. *Carbon* **1984,** 22, (3), 265-272.

95. Stoeckli, F.; Jakubov, T.; Lavanchy, A., Water Adsorption in Active Carbons Described by the Dubinin–Astakhov Equation. *J. Chem. Soc. Faraday Trans.* **1994,** 90, 783 – 786.

96. Dimotakis, E.; Cal, M.; Economy, J.; Rood, M.; Larson, S., Water Vapor Adsorption on Chemically Treated Activated Carbon Cloths. *Chem. Mater.* **1995,** 7, (12), 2269-2272.

97. Dubinin, M. M.; Serpinsky, V. V., Isotherm Equation for Water Vapor Adsorption by Microporous Carbonaceous Adsorbents. *Carbon* **1981,** 19, (5), 402-403.

98. D'Arcy, R. L.; Watt, I. C., Analysis of Sorption Isotherms of Non-Homogeneous Sorbents. *Trans. Faraday Soc.* **1970,** 66, 1236 – 1245.

99. Evans, M. J. B., The Adsorption of Water by Oxidised Microporous Carbon. *Carbon* **1987,** 25, (1), 81-83.

100. Rodriguez-Reinoso, F.; Molina-Sabio, M.; Munecas, M. A., Effect of Microporosity and Oxygen Surface Groups of Activated Carbon in the Adsorption of Molecules of Different Polarity. *J. Phys. Chem.* **1992,** 96, (6), 2707-2713.

101. Salame, I. I.; Bandosz, T. J., Experimental Study of Water Adsorption on Activated Carbons. *Langmuir* **1999,** 15, (2), 587-593.

102. Slasli, A. M.; Jorge, M.; Stoeckli, F.; Seaton, N. A., Water Adsorption by Activated Carbons in Relation to Their Microporous Structure. *Carbon* **2003,** 41, (3), 479-486.

103. Slasli, A. M.; Jorge, M.; Stoeckli, F.; Seaton, N. A., Modelling of Water Adsorption by Activated Carbons: Effects of Microporous Structure and Oxygen Content. *Carbon* **2004,** 42, (10), 1947-1952.

104. Barton, S. S.; Evans, M. J. B.; MacDonald, J. A. F., The Adsorption of Water Vapor by Porous Carbon. *Carbon* **1991,** 29, (8), 1099-1105.

105. Sing, K., The Use of Nitrogen Adsorption for the Characterisation of Porous Materials. *Colloids and Surfaces A: Physicochemical and Engineering Aspects* **2001,** 187-188, 3-9.

106. Stoeckli, F.; Centeno, T. A., On the Determination of Surface Areas in Activated Carbons. *Carbon* **2005,** 43, (6), 1184-1190.

107. Mahajan, O. P., CO_2 Surface Area of Coals: The 25-Year Paradox. *Carbon* **1991,** 29, (6), 735-742.

108. Walker, P. L.; Kini, K. A., Measurement of the Ultrafine Surface Area of Coals. *Fuel* **1965,** 44, 453-459.

109. Mahajan, O. P., In *Sample Selection, Aging and Reactivity of Coal*, John Wiley: New York, 1989; pp 157-215.

110. Mahajan, O. P., Physical Characterization of Coal. *Powder Technology* **1984,** 40, (1-3), 1-15.

111. Standard Test method for Total Moisture in Coal. In Gaseous Fuels; Coal and Coke, ASTM, Pennsylvania, 2005; D3302.

112. Mannheimer, M., Determination of the Moisture Content of Coal and Similar Substances. *Ind. Eng. Chem. Anal. Ed.* **1929,** 1, (3), 154-156.

113. Allardice, D. J.; Evans, D. G., The Brown Coal/Water System: Part 2. Water Sorption Isotherms on Bed-Moist Yallourn Brown Coal. *Fuel* **1971,** 50, (3), 236-253.

114. Shaw, T. M., The Surface Area of Crystalline Egg Albumen. *J. Chem. Phys.* **1944,** 12, (9), 391-392.

115. Bull, H. B., Adsorption of Water Vapor by Proteins. *J. Am. Chem. Soc.* **1944,** 66, (9), 1499-1507.

116. Pauling, L., The Adsorption of Water by Proteins. *J. Am. Chem. Soc.* **1945,** 67, (4), 555-557.

117. Iyengar, M. S.; Lahiri, A., The Nature of Reactive Groups in Coal. *Fuel* **1957,** 36, 286.

118. Schafer, H. N. S., Factors Affecting the Equilibrium Moisture Contents of Low-Rank Coals. *Fuel* **1972,** 51, (1), 4-9.

119. Matsyna, V. D., Investigation and Analysis of the Forms and Energies of the Binding of Moisture with Coal. *Solid Fuel Chemistry* **1981,** 15, (5), 1-7.

120. Kaji, R.; Muranaka, Y.; Otsuka, K.; Hishinuma, Y., Water Absorption by Coals: Effects of Pore Structure and Surface Oxygen. *Fuel* **1986,** 65, (2), 288-291.

121. Unsworth, J. F.; Fowler, C. S.; Heard, N. A.; Weldon, V. L.; McBrierty, V. J., Moisture in Coal : 1. Differentiation between Forms of Moisture by N.M.R. and Microwave Attenuation Techniques. *Fuel* **1988,** 67, (8), 1111-1119.

122. Boyle, N. G.; McBrierty, V. J.; Douglass, D. C., A Study of the Behavior of Water in Nafion Membranes. *Macromolecules* **1983,** 16, (1), 75.

123. Suuberg, E. M.; Otake, Y.; Yun, Y.; Deevi, S. C., Role of Moisture in Coal Structure and the Effects of Drying Upon the Accessibility of Coal Structure. *Energy Fuels* **1993,** 7, (3), 384-392.

124. Mraw, S. C.; Naas-O'Rourke, D. F., Water in Coal Pores: Low-Temperature Heat Capacity Behavior of the Moisture in Wyodak Coal. *Science* **1979,** 205, (4409), 901-902.

125. Mraw, S. C.; O'Rourke, D. F., Water in Coal Pores: The Enthalpy of Fusion Reflects Pore Size Distribution. *Journal of Colloid and Interface Science* **1982,** 89, (1), 268-271.

126. Allardice, D. J.; Clemow, L. M.; Favas, G.; Jackson, W. R.; Marshall, M.; Sakurovs, R., The Characterisation of Different Forms of Water in Low Rank Coals and Some Hydrothermally Dried Products*. *Fuel* **2003,** 82, (6), 661-667.

127. Norinaga, K.; Kumagai, H.; Hayashi, J. I.; Chiba, T., Classification of Water Sorbed in Coal on the Basis of Congelation Characteristics. *Energy Fuels* **1998,** 12, (3), 574-579.

128. Norinaga, K.; Hayashi, J. I.; Kudo, N.; Chiba, T., Evaluation of Effect of Pre-drying on the Porous Structure of Water-Swollen Coal Based on the Freezing Property of Pore Condensed Water. *Energy Fuels* **1999,** 13, (5), 1058-1066.

129. Lynch, L. J.; Barton, W. A.; Webster, D. S., Determination and Nature of Water in Low Rank Coals. In *Proceedings of the Sixteenth Biennial Low-Rank Fuels Symposium Montana*, 1991; pp 187-198.

130. Iiyama, T.; Nishikawa, K.; Suzuki, T.; Kaneko, K., Study of the Structure of a Water Molecular Assembly in a Hydrophobic Nanospace at Low Temperature with in Situ X-Ray Diffraction. *Chemical Physics Letters* **1997,** 274, (1-3), 152-158.

131. Iiyama, T.; Ruike, M.; Kaneko, K., Structural Mechanism of Water Adsorption in Hydrophobic Micropores from in Situ Small Angle X-Ray Scattering. *Chemical Physics Letters* **2000,** 331, (5-6), 359-364.

132. Bellissent-Funel, M.-C.; Sridi-Dorbez, R.; Bosio, L., X-Ray and Neutron Scattering Studies of the Structure of Water at a Hydrophobic Surface. *J. Chem. Phys.* **1996,** 104, (24), 10023-10029.

133. Luppens, J. A., The Equilibrium Moisture Problem. *Journal of Coal Quality* **1988,** 7, (2), 39-44.

134. Luppens, J. A.; Hoeft, A. P., Relationship between Inherent and Equilibrium Moisture Contents in Coals by Rank. *Journal of Coal Quality* **1991,** 10, (4), 133-141.

135. Gan, H.; Nandi, S. P.; Walker, P. L., Nature of the Porosity in American Coals. *Fuel* **1972,** 51, (4), 272-277.

136. Moisture Reduction, OSM Payer Handbook, Office of Surface Mining, http://ismdfmnt5.osmre.gov/payerhb/6_moist.htmlMining, (October 24, 2007).

137. Brown, G. M., The Determination of Moisture in Coals. *National Gas Bulletin, Australia* **1953,** 17, 14-21.

138. Lynch, L. J.; Webster, D. S., An N.M.R. Study of the Water Associated with Brown Coal. *Fuel* **1979,** 58, (6), 429-432.

139. Sircar, S., New Adsorption-Condensation Theory for Adsorption of Vapors on Porous Activated Carbons. *Carbon* **1987,** 25, (1), 39-48.

140. Talu, O.; Meunier, F., Adsorption of Associating Molecules in Micropores and Application to Water on Carbon. *AIChE J.* **1996,** 42, (3), 809-819.

141. Rutherford, S. W., Modeling Water Adsorption in Carbon Micropores: Study of Water in Carbon Molecular Sieves. *Langmuir* **2006,** 22, (2), 702-708.

142. Striolo, A.; Chialvo, A. A.; Cummings, P. T.; Gubbins, K. E., Water Adsorption in Carbon-Slit Nanopores. *Langmuir* **2003,** 19, (20), 8583-8591.

143. Striolo, A.; Gubbins, K. E.; Chialvo, A. A.; Cummings, P. T., Simulated Water Adsorption Isotherms in Carbon Nanopores. *Molecular Physics* **2004,** 102, (3), 243-251.

144. Segarra, E. I.; Glandt, E. D., Model Microporous Carbons: Microstructure, Surface Polarity and Gas Adsorption. *Chemical Engineering Science* **1994,** 49, (17), 2953-2965.

145. Ulberg, D. E.; Gubbins, K. E., Water Adsorption in Microporous Graphitic Carbons. *Molecular Physics* **1995,** 84, (6), 1139 - 1153.

146. Jorgensen, W. L.; Chandrasekhar, J.; Madura, J. D.; Impey, R. W.; Klein, M. L., Comparison of Simple Potential Functions for Simulating Liquid Water. *J. Chem. Phys.* **1983,** 79, (2), 926-935.

147. Maddox, M.; Ulberg, D.; Gubbins, K. E., Molecular Simulation of Simple Fluids and Water in Porous Carbons. *Fluid Phase Equilibria* **1995,** 104, 145-158.

148. Briggs, J. M.; Nguyen, T. B.; Jorgensen, W. L., Monte Carlo Simulations of Liquid Acetic Acid and Methyl Acetate with the OPLS Potential Functions. *J. Phys. Chem.* **1991,** 95, (8), 3315-3322.

149. Gao, J., Comparison of the Hybrid AM1/TIP3P and the OPLS Functions through Monte Carlo Simulations of Acetic Acid in Water. *J. Phys. Chem.* **1992,** 96, (15), 6432-6439.

150. Muller, E. A.; Rull, L. F.; Vega, L. F.; Gubbins, K. E., Adsorption of Water on Activated Carbons: A Molecular Simulation Study. *J. Phys. Chem.* **1996,** 100, (4), 1189-1196.

151. Postorino, P., The Interatomic Structure of Water at Supercritical Temperatures. *Nature* **1993,** 366, (6456), 668.

152. Postorino, P.; Ricci, M. A.; Soper, A. K., Water above Its Boiling Point: Study of the Temperature and Density Dependence of the Partial Pair Correlation Functions. I. Neutron Diffraction Experiment *J. Chem. Phys.* **1994,** 101, 4123.

153. Luck, W. A. P., A Model of Hydrogen-Bonded Liquids. *Angewandte Chemie International Edition in English* **1980,** 19, (1), 28-41.

154. Steele, W. A., *The Interaction of Gases with Solid Surfaces*. Pergamon Press: Oxford, 1974.

155. Berendsen, H. J. C.; Grigera, J. R.; Straatsma, T. P., The Missing Term in Effective Pair Potentials. *J. Phys. Chem.* **1987,** 91, (24), 6269-6271.

156. Kotdawala, R.; Kazantzis, N.; Thompson, R., An Application of Mean-Field Perturbation Theory for the Adsorption of Polar Molecules in Nanoslit-Pores. *Journal of Mathematical Chemistry* **2005,** 38, (3), 325-344.

157. Smith, C. A. Adsorption of Water on Carbon: A Study Using the ESD Equation of State. M.S. Thesis, Michigan State University, East Lansing, 1997.

158. Elliott, J. R.; Suresh, S. J.; Donohue, M. D., A Simple Equation of State for Non-spherical and Associating Molecules. *Ind. Eng. Chem. Res.* **1990,** 29, (7), 1476-1485.

159. Reid, R. C.; Prausnitz, J. M.; Poling, B. E., *The Properties of Gases and Liquids*. McGraw-Hill New York, 1987.

160. Gasem, K. A. M.; Gao, W.; Pan, Z.; Robinson, R. L., Jr., A Modified Temperature Dependence for the Peng-Robinson Equation of State. *Fluid Phase Equilibria* **2001,** 181, (1-2), 113-125.

161. Tester, J. W.; Modell, M., *Thermodynamics and Its Applications*. 3rd ed.; Prentice-Hall: New Jersey, 1997; p 936.

162. Prausnitz, J. M.; Lichtenthaler, R. N.; Azevedo, E. G., *Molecular Thermodynamics of Fluid-Phase Equilibria*. 3rd ed.; Prentice-Hall: New Jersey, 1999; p 860.

163. Riggs, J. B., *An Introduction to Numerical Methods for Chemical Engineers*. 2nd ed.; Texas Tech University Press: Lubbock, 1994; p 472.

164. Chen, J. S.; Gasem, K. A. M. A Case Study on SLD-PR Adsorption Modeling of CO2-Water Binary Mixed-Gas Adsorption on Wet Argonne Coals. Unpublished work, 2007.

165. Golla, S. Virtual Design of Chemical Penetration Enhancers. M.S. Thesis, Oklahoma State University, Stillwater, 2008.

166. Reeves, S.; Gasem, K. A. M.; Sudibandriyo, M.; Fitzgerald, J. E.; Pan, Z.; Robinson, R. L., Jr., Measurement and Prediction of Single- and Multi-Component Methane, Carbon Dioxide and Nitrogen Isotherms for U.S. Coals, Paper 527. In *2005 International Coalbed Methane Symposium*, Tuscaloosa, AL, 2005.

VITA

Sayeed Ahmed Mohammad

Candidate for the Degree of

Doctor of Philosophy

Dissertation: ADSORPTION MODELING OF COALBED GASES AND THE EFFECTS OF WATER ON THEIR ADSORPTION BEHAVIOR

Major Field: Chemical Engineering

Biographical:

Education:

Received Bachelor of Science in Chemical Engineering from Osmania University, Hyderabad, India in July 2003.

Completed the requirements for the Doctor of Philosophy in Chemical Engineering at Oklahoma State University, Stillwater, Oklahoma in May, 2009.

Experience:

Employed by the School of Chemical Engineering, Oklahoma State University as a Research Assistant from August 2004 to May 2009. Worked as a Teaching Assistant for Thermodynamics in the same department from August 2004 to December 2005.

Professional Memberships:

American Institute of Chemical Engineers (AIChE)

Phi Kappa Phi National Honor Society

Name: Sayeed Ahmed Mohammad Date of Degree: May, 2009

Institution: Oklahoma State University Location: Stillwater, Oklahoma

Title of Study: ADSORPTION MODELING OF COALBED GASES AND THE EFFECTS OF WATER ON THEIR ADSORPTION BEHAVIOR

Pages in Study: 231 Candidate for the Degree of Doctor of Philosophy

Major Field: Chemical Engineering

Scope and Method of Study:

The simplified local-density/Peng-Robinson (SLD-PR) adsorption model was utilized to investigate the adsorption behavior of coalbed gases on coals of varying rank. The model parameters were generalized in terms of readily-accessible coal properties such as the ultimate and proximate analyses of the coals. Further, the effects of water present in coals on the gas adsorption behavior were studied. In particular, the SLD-PR model was used to investigate this effect wherein water was treated as a separate adsorbed component in a binary mixture. To conduct this study, new high-pressure gas adsorption measurements were acquired for CO_2 on wet Argonne coals and for methane, nitrogen and CO_2 on dry and wet activated carbon using a volumetric technique.

Findings and Conclusions:

The generalized SLD-PR model was found to be capable of accurate predictions of the adsorption of coalbed gases and their mixtures on dry and wet coals. Specifically, the generalized model was capable of (a) predicting the pure-gas isotherms for methane, nitrogen and CO_2 on coals within two times the expected experimental uncertainties and (b) predicting, *a priori*, the adsorption of mixtures formed by these gases within three times the expected experimental uncertainties, on average. The generalized model was validated with an external data set which comprised of CO_2 adsorption isotherms on 27 diverse coals.

CO_2-water binary mixed gas adsorption modeling results on wet coals indicated that the SLD-PR model is capable of representing the adsorption of this highly asymmetric mixture within the experimental uncertainties, on average. The model parameterization used and the molecular interactions accounted for in describing water adsorption behavior on coals illustrated a viable method to obtain precise representations of this adsorbed mixture. The phase-check analysis of the same mixture indicated that there is a potential for the formation of an aqueous phase in these systems for coals that contain large amounts of moisture, with the exception of Beulah Zap lignite coal.

ADVISER'S APPROVAL: Khaled A. M. Gasem